GEOCHEMICAL EFFECTS OF ALTERATION IN A SECTION OF LOWER OCEAN CRUST; ODP HOLE 735B, SOUTHWEST INDIAN RIDGE

by

Neil R. Banerjee

Submitted in partial fulfilment of the requirements
for the degree of Master of Science

at

Dalhousie University
Halifax, Nova Scotia
June, 1996

DALHOUSIE UNIVERSITY

DEPARTMENT OF EARTH SCIENCES

The undersigned hereby certify that they have read and recommend to the Faculty of Graduate Studies for acceptance a thesis entitled "Geochemical Effects of Alteration in a Section of Lower Ocean Crust; ODP Hole 735B, Southwest Indian Ridge"

by Neil R. Banerjee

in partial fulfilment of the requirements for the degree of Master of Science

Dated 16 June 1996

External Examiner:

Supervisor:

Readers:

DALHOUSIE UNIVERSITY

DATE: July 3, 1996

AUTHOR: Neil R. Banerjee

TITLE: Geochemical effects of alteration in a section of lower ocean crust; ODP Hole 735B, Southwest Indian Ridge.

DEPARTMENT OR SCHOOL: Earth Sciences

DEGREE: M.Sc. CONVOCATION: October YEAR: 1996

Permission is herewith granted to Dalhousie University to circulate and to have copied for non-commercial purposes, at its discretion, the above title upon the request of individuals or institutions.

Signature of Author

TABLE OF CONTENTS

LIST OF FIGURES

LIST OF TABLES

ABSTRACT

The 500 metres of gabbro drilled in ODP Hole 735B provide a unique opportunity to study the chemical effects of hydrothermal alteration resulting from seawater penetration into the lower ocean crust. Previous studies identified five major styles of alteration / metamorphism ranging from anhydrous granulite facies assemblages accompanying brittle-ductile deformation to lower greenschist and zeolite facies assemblages resulting from circulation of cold oxygenated seawater. Many veins contain sequential mineral assemblages indicating progressive alteration.

This study focuses on the geochemical effects of alteration in and around inclined veins on a variety of scales: within minerals; between minerals; in thin sections; and in altered whole-rock samples a few centimetres from veins. Microprobe traverses from primary clinopyroxene to secondary amphibole are characterized by abrupt decreases in CaO and less abrupt, variable changes in other oxides. A traverse from primary plagioclase to secondary sodic plagioclase is characterized by an abrupt increase in SiO_2 and Na_2O, and an abrupt decrease in Al_2O_3 and CaO. A similar traverse from primary plagioclase to secondary epidote is characterized by an abrupt decrease in SiO_2 and Na_2O, and an abrupt increase in FeO and CaO. Primary minerals, secondary plagioclase, and secondary epidote have relatively constant compositions but secondary amphibole is more variable. Overall, the mineral traverses suggest that CaO and MgO were lost, FeO and Na_2O were gained, Al_2O_3 remained relatively constant, and SiO_2 was variable during alteration.

Element mobility was determined by comparison of major and trace element bulk-rock compositions of altered host rock adjacent to veins and fresh equivalents. Element fluxes based on constant aluminum indicate element mobility within a few centimetres of each vein. Calculated volume factors are used to explain different element-flux trends in the same lithology and suggests that alteration probably occurred under conditions of constant volume. Modal mineralogy is used to explain element-flux variations between lithologies. Element-flux trends, particularly observed discrepancies in CaO and MgO

fluxes reflect vein mineral assemblages. Qualitative comparison of element fluxes from Hole 735B samples with similar studies of oceanic Layer 2, indicate that for Si and Na, trends appear to be similar; however, Rb and Mg trends are reversed.

Gridded electron microprobe traverses provide chemical data for entire thin sections. Equivalent fresh mineral compositions are subtracted to produce residual chemical maps of alteration. These show chemical gradients near veins resulting from chemical exchange between the vein and host rock which are interpreted as alteration halos. Gradients are only observed in certain oxide residual maps, namely SiO_2, CaO, and Na_2O, suggesting that alteration affected different elements by different amounts. In general, alteration halos are restricted to areas within a few millimetres of veins suggesting limited chemical modification of the host rock. Residual maps show very similar trends to microprobe traverses for alteration of both clinopyroxene and plagioclase. In addition, estimates of chemical changes in the host rock from residual maps are almost the same in direction and magnitude as calculated element fluxes for the same samples. However, residual maps also provide spatial information on alteration trends which whole-rock analyses do not. Residual chemical maps, therefore, provide a new method to quantify the effects of alteration in samples at the thin section scale.

ACKNOWLEDGMENTS

I wish to thank Dr. Paul Robinson for his support and encouragement while supervising this thesis. Dr. Gunter Muecke helped create the idea for the chemical mapping technique and his comments and interest made it possible. Initial drafts of the thesis benefitted from critical comments by Dr. Paul Robinson, Dr. Gunter Muecke, Dr. Deborah Kelley, and Scott Anderson. Comments by Dr. Becky Jamieson and Dr. Jarda Dostal greatly improved the final draft. The patience and insight of Bob MacKay helped make the chemical maps possible and many long hours on the microprobe pleasant. The high quality thin sections produced by Gordon Brown from difficult samples were especially appreciated. Thank you to Dr. John Malpas (Memorial University) for providing trace-element data and Sally Stanford (St. Mary's University) for providing major-element data. The interest shown by Dr. Henry Dick and Dr. Kathryn Gillis helped encourage me during preparation of this thesis. Dr. Pat Ryall and Dr. Peter Reynolds provided guidance whenever asked. Special thanks to Stephanie Laurence and Renée Cheng who drafted many of the figures in this thesis. Thank you also to Jane Barrett, Norma Keeping, and Darlene Van De Rijt who never tired from my constant questions.

Thank you to my friends and fellow students, graduate and undergraduate, who made my stay at Dal most enjoyable and who provided necessary moral support. I will miss their company and friendship. I could not have completed this thesis without the constant encouragement of my family.

This study was supported by NSERC grants to Dr. Paul Robinson and by a Dalhousie Graduate Scholarship.

Chapter 1

Introduction

1.0 GENERAL STATEMENT

Hydrothermal circulation is a ubiquitous process operating at mid-ocean ridges. The interaction between circulating fluids and ocean crust dissipates thermal energy stored in the crust, affects seawater chemistry, results in the formation of massive sulphide deposits, and causes large scale geochemical alteration of the crust. Fluid circulation at spreading centres, therefore, plays an important role in oceanic crustal evolution.

Three seismically defined layers are recognized in the ocean crust (Figure 1.1). Based on the geophysical properties of rocks dredged from the seafloor and from studies of ophiolites (fossil sections of ocean crust), layer 1 is composed of chert, limestone, and/or clay, layer 2 is a sequence of volcanic rocks including pillow basalts and basalt flows that grade downward to rocks dominated by sheeted basalt dykes and metabasalts, and layer 3 consists of plutonic material, dominated by gabbro, that crystallized in some sort of magma chamber beneath the ridge crest. It should be noted, however, that this simple stratigraphy does not take into account dynamic processes such as alteration and tectonism which are now believed to play an important part in governing the internal stratigraphy of ocean crust (Dick *et al.*, 1992).

Alteration of oceanic rocks results from chemical exchange between circulating hydrothermal fluids and the surrounding host rocks (Figure 1.2). The hydrothermal fluid has traditionally been thought of as superheated sea water reaching temperatures up to 400°C (Delaney *et al.*, 1984). This fluid can penetrate to depths of several kilometres beneath the sea-floor *via* fractures resulting from tectonic stresses induced by ocean ridge tectonics and cooling of the section (Cronan, 1992). In addition, vesiculation in lavas reaching 20-40 volume per cent, drained pillows, lobes and lava lakes, as well as buried talus and volcanic breccia, can increase the shallow permeability and ease of hydrothermal circulation through rocks in axial regions and seamounts (Scott, 1992). It is believed the

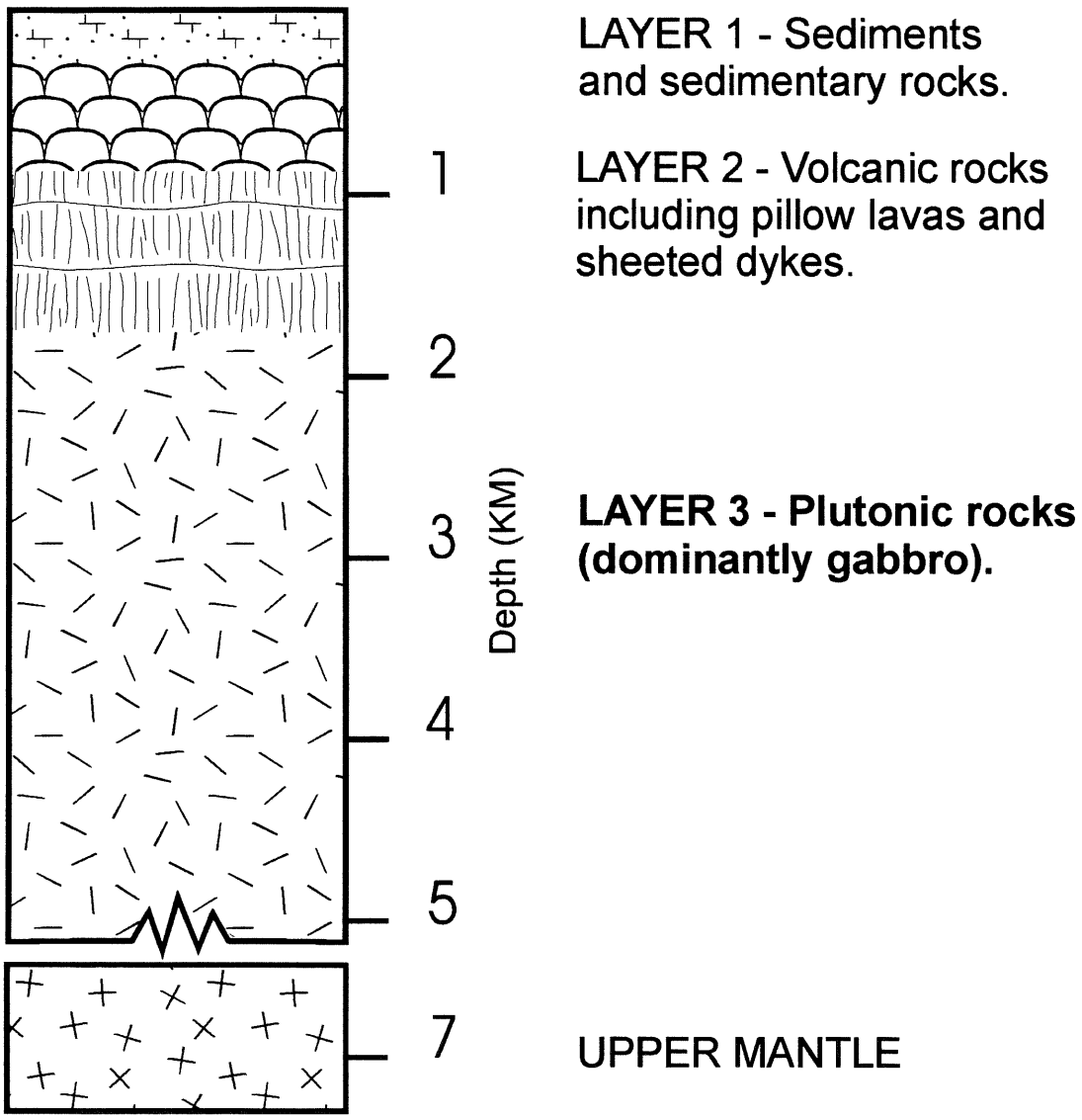

Figure 1.1 Idealized three-layer oceanic crustal section.

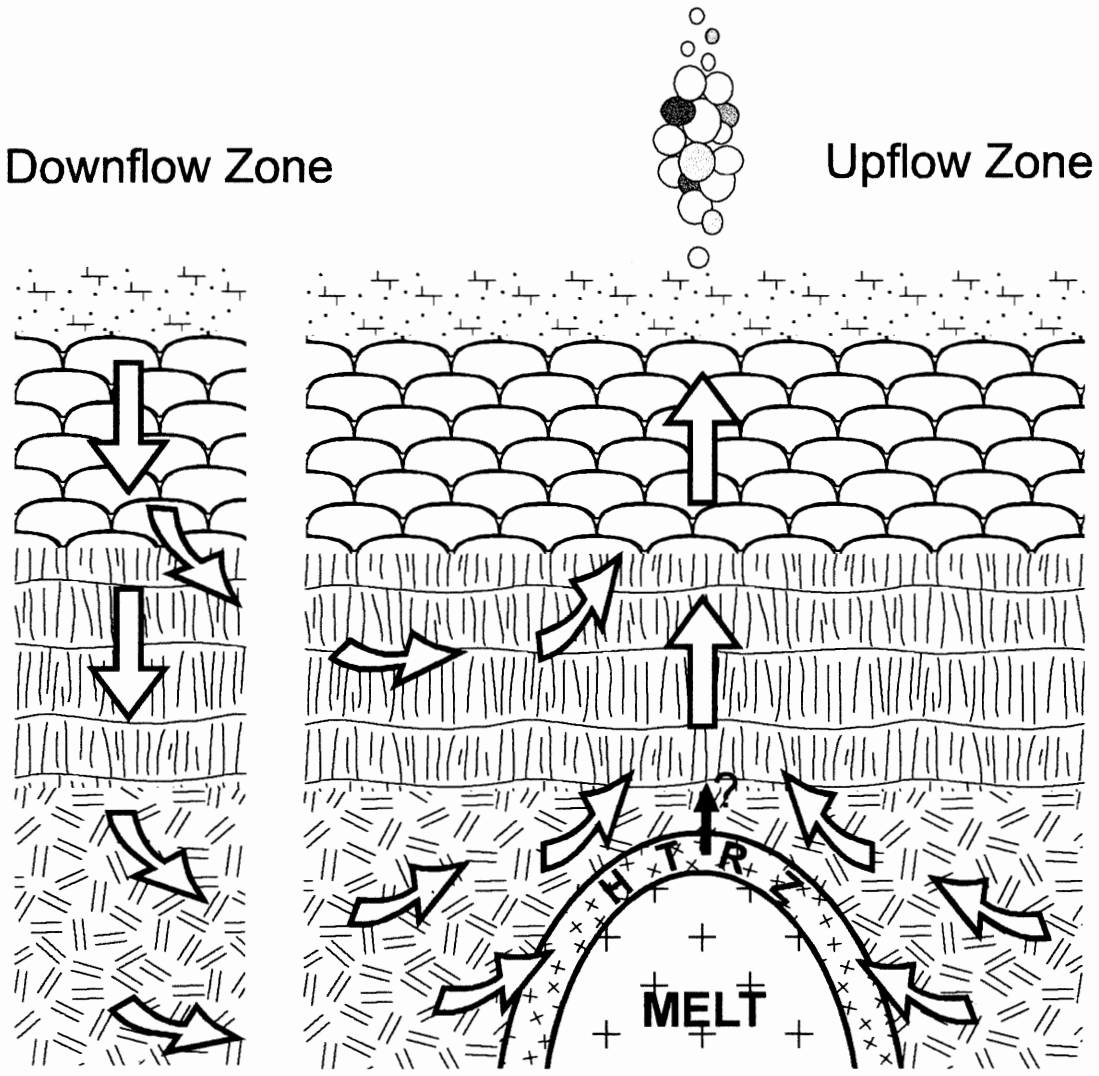

Figure 1.2 Simplified model of hydrothermal circulation in the ocean crust
HTRZ = high temperature reaction zone.

fluid becomes heated at depths of 2-4 km by relatively shallow magma chambers which provide the heat source necessary to drive circulation. Evidence for this process has come through seismic imaging of active ridge systems that has identified magma chambers within 2 km of the ocean-floor in fast-spreading environments (Detrick *et al.*, 1987). Evidence is also provided by studies of ophiolites where synvolcanic intrusions and associated altered rock zones, which result from the upward migration of hydrothermal fluids, are exposed on land (Gillis, 1986; Gillis and Robinson, 1988).

Numerous studies have documented the circulation of fluids and their geochemistry in the upper portions of ocean crust (layer 2) (eg. Rona *et al.*, 1986; Von Damm, 1988; Gillis and Robinson, 1988). These studies focus on the circulation of seawater in the upper 1-2 kilometres of crust and the associated effects of hydrothermal alteration. Few studies have documented the effects of hydrothermal alteration on plutonic rocks which make up layer 3.

Until recently most studies on the alteration of layer 3 focused on ophiolites or samples recovered from tectonically exposed sections on the seafloor, an approach which presents certain problems. It is believed that most ophiolites were formed in supra-subduction zone environments, and were disrupted by tectonic processes during their emplacement (eg. Miyashiro, 1973; Robinson *et al.*, 1983; Robinson *et al.*, 1991; Bai *et al.*, 1993; and others). These sections, therefore, probably do not represent "typical" oceanic crust. In addition, samples of lower crust obtained from dredge hauls or by submersible do not provide continuous stratigraphic sections (Fox and Stroup, 1981). Most plutonic samples come from fault zone environments where alteration and tectonic processes are likely to be greater than in non-fault zone environments (Robinson *et al.*, 1991). Petrologic studies of samples from the lower ocean crust have shown that alteration is commonly related to sub-solidus, predominantly brittle deformation and/or interaction with hydrothermal fluids during the progressive cooling of the plutonic sequence (Gillis *et al.*, 1993; Kelley *et al.*, 1993; Vanko, 1988; Stakes *et al.*, 1991; Mevel, 1987, 1988). In order to understand and constrain the chemical evolution of the oceanic crust, it is important to characterize the chemical changes responsible for the formation of

secondary minerals during the alteration process.

Previous studies on the alteration of lower ocean crust have focused on secondary mineralogy and whole rock analyses (Robinson *et al.*, 1991; Stakes *et al.*, 1991). These studies provide a good qualitative estimate of alteration in the form of down-hole profiles and they characterize the secondary mineralogy, however, they do not address quantitative chemical changes resulting from alteration of host rock on a variety of scales. Many studies have concentrated on alteration products in veins (Madge *et al.*, 1995). Veins dominate the permeability structure of the lower ocean crust and represent an important pathway for hydrothermal fluids causing alteration. Generally, veins represent only a small proportion of the ocean crust as a whole and do not provide information on chemical changes to the host rock. In order to accurately document the effects of hydrothermal alteration on the ocean crust it is necessary to determine the chemical changes associated with both host rock and vein assemblages and the extent to which they affect the bulk composition of the ocean crust.

The main goal of this study is to provide a quantitative estimate of the chemical effects of hydrothermal alteration in samples of lower ocean crust at different scales. This study involves a step by step approach which is broken into four parts: 1) geochemical variability in primary minerals; 2) geochemical changes between primary minerals and secondary minerals; 3) geochemical changes in the host rock proximal to veins; and 4) element fluxes between altered and fresh whole-rock equivalents. This approach provides a systematic study of chemical effects of alteration at different scales, from changes in minerals to changes in whole-rock samples. The work involves four main approaches: 1) petrographic description; 2) detailed description of the alteration styles and mineralogy; 3) detailed geochemical analysis; and 4) interpretation.

Fresh and altered plutonic samples of layer 3 were recovered from Hole 735B during Leg 118 of the Ocean Drilling Program (ODP). Due to unprecedented recovery (87%), these samples represent the most complete stratigraphically controlled suite of *in-situ* plutonic rocks ever recovered from a submarine environment. Studies of these gabbroic samples have documented a variety of progressive styles and stages of alteration

(Robinson *et al.*, 1991). These samples provide a unique opportunity to study the chemical effects of alteration on *in situ* samples of oceanic layer 3.

Over 100 samples from various stratigraphic positions in the core, which display varying degrees of alteration, were available to document the chemical effects of alteration. Petrographic analyses are used to distinguish between fresh and altered samples, determine primary and secondary mineralogy, and determine the various styles of alteration associated with various mineral assemblages and distributions. Electron microprobe analyses are used to characterize representative compositions of primary and secondary minerals, including the chemical variability in mineral grains that optically display partial alteration. A unique and important aspect of this study involves the use of residual chemical maps which provide quantitaive estimates of chemical changes in the groundmass within a few centimetres of veins. Whole-rock geochemical analyses for major (XRF) and trace elements (ICP-MS) have been performed on a number of samples. Samples were chosen in order to document the chemical effects of alteration near different types of veins. These data are supplemented by analyses of fresh rocks. Immobile element geochemistry is used to normalize altered samples to fresh samples and mobile trace element variations document the geochemical effects of alteration. By comparing altered and fresh sample analyses element fluxes have been calculated which suggest element mobility within a few centimetres of veins.

1.1 PREVIOUS WORK

Plutonic rocks recovered from Hole 735B represent the first stratigraphically controlled, nearly continuous section of oceanic layer 3 recovered in a submarine environment. The initial work on these rocks documented the internal stratigraphy, mineralogy and physical properties of the lower oceanic crustal rocks (Shipboard Scientific Party, 1989 and references therein). Geochemical analyses were performed on various samples of the core but most of the analyzed samples were chosen from unaltered or weakly altered sections in order to provide a baseline for further studies of the lower ocean crust (Shipboard

Scientific Party, 1989). Subsequent work has expanded on the initial studies of Hole 735B to include information on metamorphism and deformation (eg. Stakes *et al.*, 1991; Cannat, 1991; Cannat *et al.*, 1991), geochemistry of hydrothermal fluids (Vanko and Stakes, 1991; Kelley, *et al.*, 1994; Kelley, 1996) and studies of alteration (Robinson *et al.*, 1991; Stakes *et al.*, 1991). These studies provide a useful reference from which to determine the geochemical effects of alteration of lower ocean crust formed in a slow-spreading environment.

Several contributions by previous authors are relevent to this study. These include documentation of the deformation, secondary minerals, vein filling assemblages and down-hole chemical profiles for core recovered from Hole 735B (Dick *et al*, 1991; Robinson *et al*, 1991; Stakes *et al.*, 1991). Extensive petrographic studies have identified a variety of textures, mineral assemblages and alteration patterns (Stakes *et al.*, 1991; Robinson *et al.*, 1991). In addition, microprobe data are available for primary and secondary minerals from various lithologies (eg. Dick *et al.*, 1991a; Stakes *et al.*, 1991; Hébert *et al.*, 1991; Natland *et al.*, 1991). These data have been used to characterize general trends of alteration which are commonly visible petrographically or in hand sample. Again, emphasis has been placed on vein mineral assemblages. These data do not characterize chemical changes between minerals in the host rock which appear to have undergone variable amounts of recrystallization, or changes within a few centimetres of veins. This study, therefore, focuses on these types of chemical changes.

Initial studies of whole-rock compositions were designed to establish a chemical stratigraphy of the recovered gabbro section and samples were chosen from major sections of the drilled sequence and macroscopically different lithologies (Shipboad Scientific Party, 1989). As a result, whole-rock geochemical data for both major and trace elements are available for almost 100 fresh samples collected from Hole 735B (Shipboad Scientific Party, 1989). As a rule, only the freshest samples were selected and little data are available for altered material. In order to better understand the geochemical effects of alteration on whole-rock geochemistry, altered whole-rock samples have been analyzed. Through comparison with data for fresh samples, element fluxes have been calculated for

samples from Hole 735B.

Stable isotope and fluid inclusion data have been collected for plutonic rocks, from Hole 735B and other localities, which reveal varying degrees of interaction with hydrothermal fluids (Vanko and Stakes, 1991; Stakes and O'Neil, 1982; Vanko, 1988; Kelley & Delaney, 1987; Kelley *et al.*, 1993; Kelley, 1996; Gillis *et al.*, 1993). In rocks from Hole 735B, fluid inclusions record a range of temperatures and compositions from early high-temperature fluids composed of varying amounts of seawater and magmatic fluids to low-temperature seawater-derived fluids (Vanko and Stakes, 1991; Kelley *et al.*, 1994; Kelley, 1996). A diagnostic shift in oxygen isotopes to low values in samples from Hole 735B suggests the presence of seawater as an alteration agent (Vanko and Stakes, 1991). Fluid inclusion and stable isotope data suggest that conditions varied during alteration in Hole 735B (Vanko and Stakes, 1991; Stakes *et al.*, 1991; Kelley *et al.*, 1994; Kelley, 1996). In this study, a variety of samples from Hole 735B, including various lithologies and vein assemblages, are investigated to account for the variable nature of alteration in the core. In addiditon, analyses are performed at a variety of scales to investigate microscopic and macroscopic chemical changes. Finally, comparison of fresh and altered equivalents provides a quantitative estimate of the geochemical effects of alteration at different scales in a section of lower ocean crust.

Chapter 2
Geology

2.0 INTRODUCTION

Gabbros recovered from Hole 735B represent samples of the lower ocean crust that are believed to dominate seismic layer 3 (Shipboard Scientific Party, 1989; Hébert *et al.*, 1991). Study of these rocks has documented formation of the lower ocean crust through the complex interplay of processes that include intrusion, brittle-ductile deformation, and hydrothermal alteration (Shipboard Scientific Party, 1989; Robinson *et al.*, 1991; Stakes at al., 1991; Vanko and Stakes, 1991; Cannat *et al.*, 1991; Dick *et al.*, 1991a; 1991b; 1992). The following chapter summarizes previous work regarding the geology and tectonic setting of Hole 735B and provides background for studying the geochemical effects of alteration presented in this dissertation.

2.1 TECTONIC SETTING

ODP Site 735 (32°43.395'S, 57°15.959'E) is located on a shallow platform 731 m below sea level on the eastern rim of the Atlantis II Transform (Figures 2.1 & 2.2). The Atlantis II Fracture Zone is one of several transform faults that offset the Southwest Indian Ridge (SWIR), which is one of the slowest spreading ridges in the modern oceans (0.8 cm/yr half-rate) (Dick *et al.*, 1991a). Fracture zones commonly exhibit extreme topographic relief as a result of tectonic processes, and mantle and lower crustal rocks are commonly exposed on the floors and walls of many fracture zones (Dick *et al.*, 1991b).

Site 735B is situated between magnetic anomalies 5 and 5a approximately 93 km south of the present day axis of the SWIR (Dick *et al.*, 1991b). Crustal reconstruction, based on constant spreading direction over the last 11 Ma, suggests that the crust sampled at 735B formed beneath the median valley of the SWIR, 15-19 km from the ridge-transform intersection (Dick *et al.*, 1991b). This age has been confirmed by a single Pb-

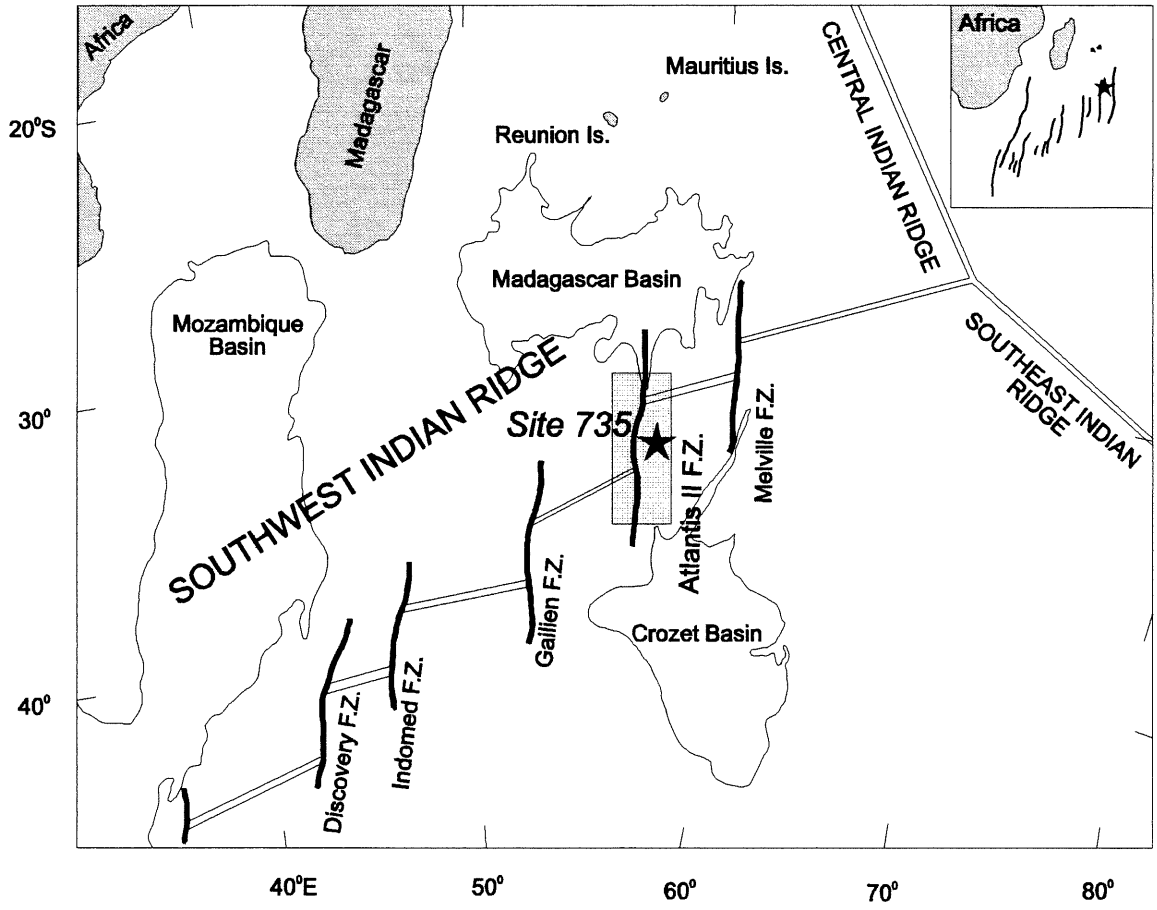

Figure 2.1 Location of ODP Site 735, Atlantis II Fracture Zone, Southwest Indian Ridge. Detail of the shaded box is shown in Figure 2.2.

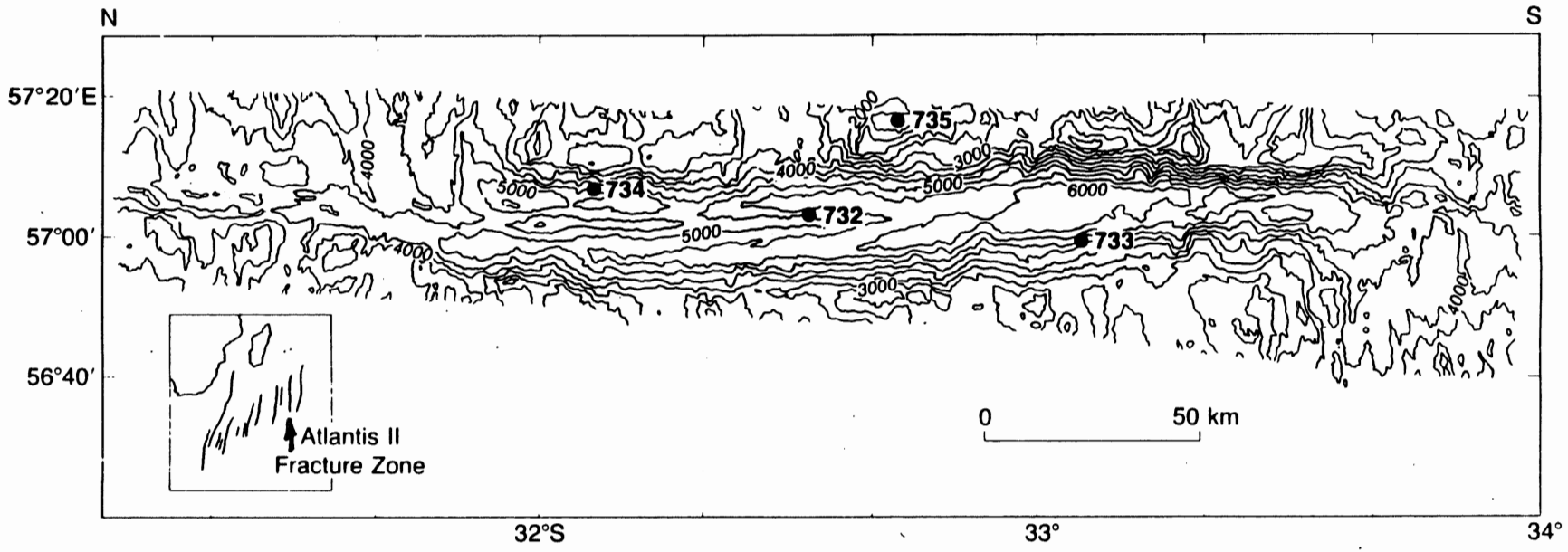

Figure 2.2 Bathymetric map at 500-m contour intervals of the Atlantis II Fracture Zone, Southwest Indian Ridge, showing Leg 118 drill sites (from Dick *et al.*, 1991b).

zircon age of 11.3 Ma from a trondhjemite vein near the top of the plutonic section (Stakes *et al.*, 1991). Subsequent uplift has exposed the plutonic section along an extensive horst block on the transverse ridge.

2.2 LITHOSTRATIGRAPHY

Core from Hole 735B consists of 434.81 m of olivine gabbro, olivine-bearing gabbro, two-pyroxene gabbro, gabbronorite, iron-titanium oxide gabbro, troctolite, and microgabbro, with rare basalt and trondjhemite, representing an average recovery of 87% over a penetration depth of 500.1 m (Shipboard Scientific Party, 1989). Three principal classes of rocks have been documented from Hole 735B which represent individual intrusive events: 1) primary gabbro, 2) late intrusive microgabbro, and 3) synkinematic oxide-bearing gabbros (Dick *et al.*, 1991a). The rocks are interpreted to represent a middle layer 3 assemblage (Robinson, pers. comm.). Six major lithologic units have been identified based on igneous mineralogy, mineral compositions, and style of deformation (Figure 2.3) (Dick *et al.*, 1991a; 1992). This section summarizes the major lithological units from Hole 735B. For a complete stratigraphic description see Dick *et al.* (1991a and 1992), Robinson *et al.* (1991), and Stakes *et al.* (1991).

2.2.1 Unit I - Gabbronorite (0-37.41 mbsf)

Unit I is predominantly composed of gabbronorite which is subdivided into two units: Subunit IA - deformed gabbronorite; and Subunit IB - mixed gabbronorite and olivine gabbro. Textures present in the rocks include poorly foliated metagabbro, porphyroclastic metagabbro, foliated metagabbronorite, mylonite, gneissic metagabbro and augen metagabbro. For the most part the unit is highly deformed with well developed foliation marked by alternating bands of plagioclase and amphibole or pyroxene. Primary igneous textures are generally not preserved in this unit. Common porphyroclastic textures consist of deformed and rounded plagioclase, clinopyroxene, and rare orthopyroxene grains in a neoblastic matrix of the same minerals. Partial replacement of pyroxene by green and

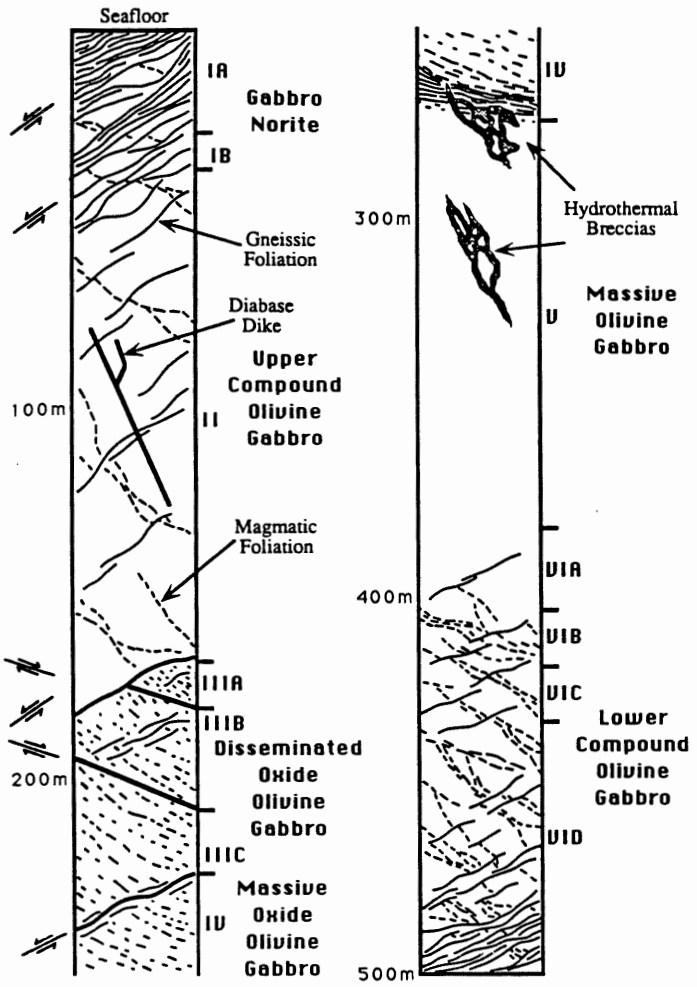

Legend: Hole 735B Igneous Lithostratigraphy

Unit I = Gabbronorite
- Subunit 1A = Massive gabbronorite
- Subunit 1B = Olivine gabbro and gabbronorite

Unit II = Upper compound olivine gabbro
- Minor: intrusive microgabbro and olivine microgabbro synkinematic oxide and oxide-olivine gabbro

Unit III = Disseminated oxide-olivine gabbro
- Subunit IIIA = Disseminated-oxide-olivine and olivine gabbro
- Subunit IIIB = Massive disseminated-oxide-olivine gabbro
- Subunit IIIC = Disseminated-oxide-olivine and olivine gabbro

Unit IV = Massive oxide olivine gabbro

Unit V = Massive olivine gabbro

Unit VI = Lower compound olivine gabbro
- Subunit VIA = Compound olivine gabbro
- Minor: Intrusive oxide microgabbronorite and olivine microgabbro synkinematic oxide and oxide-olivine gabbro
- Subunit VIB = Compound olivine, oxide-olivine, and disseminated oxide-olivine gabbro
- Minor: Intrusive olivine and oxide-olivine microgabbro
- Subunit VIC = Compound troctolitic and olivine gabbro
- Minor = Synkinematic oxide-olivine gabbro and oxide-olivine microgabbro intrusive troctolite and troctolitic microgabbro
- Subunit VID = Compound olivine and oxide-olivine gabbro
- Minor = Intrusive troctolite, diopsidic-olivine and troctolitic gabbro synkinematic disseminated-oxide-olivine and oxide gabbro

Figure 2.3 Summary lithologic column for Hole 735B. Short dashed lines in all units indicate approximate orientation of magmatic foliation in oxide-bearing gabbros, while long wavy lines indicate the locus of sub-solidus amphibolite facies ductile deformation. The strike and dip-direction of the subsolidus and late magmatic ductile deformations are assumed constant, though this might not be the case. Approximate location of several hydrothermal breccias shown for reference - note crosscutting relationship at the base of Unit IV. Approximate locations of major subunit boundaries deduced from microfaults in the core are shown for Units III and VI. Contacts within Unit I and II are presumed to lie in the foliation plane. (From Dick *et al.*, 1991a)

sometimes brown amphibole is common and in some highly altered metagabbros, pyroxene has been completely pseudomorphed. Pseudomorphs of olivine and orthopyroxene reflect replacement by talc, magnesian amphibole, and Fe-oxide minerals. Rare mylonitic bands in this unit contain abundant Fe-Ti oxide minerals, which typically fill fractures. Veins filled with fibrous green amphibole are also present.

2.2.2 Unit II - Upper Compound Olivine Gabbro (37.41-170.22 mbsf)

Unit II is predominantly composed of compound olivine gabbro with intervals of oxide olivine gabbro, microgabbro, and olivine gabbro. The word compound reflects the complex relationship between different rock types in this unit which produces an igneous layering unlike any in layered intrusions studied on land (Dick *et al.*, 1991a). The rocks typically exhibit anhedral to subhedral granular and mesocumulate textures with modal and grain size layering. Subtle modal layering is defined by olivine-rich and olivine-poor regions. Rocks contain olivine, generally less than 5%, clinopyroxene, plagioclase, and orthopyroxene, up to 5% (Robinson *et al.*, 1991). Clinopyroxene averages 5 mm but also occurs as large oikocrysts enclosing plagioclase. Olivine is commonly replaced, to varying degrees, by colourless amphibole, talc, secondary magnetite, and brown clay. Pyroxene is variably altered to green and brown amphibole.

Unit II is generally less deformed than Unit I but is intruded by several intervals of nearly oxide-free gabbro. These intervals are cross-cut by layers of oxide gabbro, consisting predominantly of clinopyroxene and plagioclase, with minor amounts of inverted pigeonite, along shear zones. Oxide minerals, in oxide gabbros, are intimately intergrown with pyroxene and the rocks are pyroxene rich, with olivine-bearing varieties being rare, suggesting reaction with late magmatic liquids in the deformed zones (Dick *et al.*, 1991a). Also contained in this unit are a basalt dyke, a microgabbro dyke and narrow troctolite intervals. Similar to Unit I, this unit is also cut by fractures that are commonly filled with fibrous green amphibole.

2.2.3 Unit III - Disseminated Oxide Olivine Gabbro (170.22-223.57 mbsf)

Unit III is predominantly composed of disseminated oxide olivine gabbro which is subdivided into three subunits: Subunit IIIA - disseminated oxide olivine and olivine gabbro; Subunit IIIB - massive disseminated oxide olivine gabbro; and Subunit IIIC - disseminated oxide olivine and olivine gabbro. Unit III is somewhat more compositionally evolved than Unit II and is characterized by an overall increase in disseminated oxide olivine gabbro and a sharp decrease in the abundance of olivine gabbro. The gabbroic rocks in this unit are coarse- to very coarse-grained, displaying mesocumulate textures and magmatic foliations. Unit III generally exhibits less deformation than Units I and II, however, rare Fe-Ti oxide-rich bands coincide with small shear zones and display porphyroclastic and mylonitic textures. Plagioclase and clinopyroxene with variable amounts of olivine are the principal minerals, accompanied by minor disseminated Fe-Ti oxide minerals (1 modal percent average) and small amounts of inverted pigeonite. Minor layers of troctolitic microgabbro, olivine microgabbro and microgabbro intrude Unit III. Most rocks are petrographically relatively fresh although some alteration is apparent especially along veins. Pyroxenes are typically rimmed by green amphibole, and olivine, where present, is replaced by talc-tremolite. Unit III contains several trondhjemitic veins, as well as small veins containing variable amounts of sodic plagioclase (An_{10-20}), hornblende, sphene and chlorite (Robinson *et al.*, 1991).

2.2.4 Unit IV - Massive Oxide Olivine Gabbro (223.57-274.06 mbsf)

Unit IV consists predominantly of massive oxide olivine gabbro which marks a transition from disseminated oxide olivine gabbro to oxide olivine gabbro in which the average modal oxide content is relatively high (10.1%) (Dick *et al.*, 1991a). As a result, these rocks are believed to be more compositionally evolved than the other units. Olivine is less abundant (less than 2%) and more iron-rich (Fo_{35-45}) than that in Unit III, and plagioclase is typically sodic (An_{35-50}) (Robinson *et al.*, 1991). Augite and inverted pigeonite are also present.

The unit is composed of coarse-grained oxide olivine gabbro that overlies olivine-rich oxide gabbro which contains a few layers of olivine gabbro. Olivine gabbro in this unit has a higher modal olivine content and more primitive mineral compositions than olivine gabbro from other units. Oxide-rich gabbros are coarse-grained with subhedral mesocumulate textures in which plagioclase and clinopyroxene define a subhorizontal igneous layering. Oxide minerals appear to be primary and are post-cumulus or late-magmatic phases which fill spaces between plagioclase and pyroxene grains or which appear as oikocrysts enclosing silicate minerals (Robinson *et al.*, 1991). Deformed sections displaying porphyroclastic to submylonitic textures in which secondary ilmenite fills cracks and small shear zones suggest Fe-Ti oxide mobility. Shear zones also contain variable assemblages of secondary minerals that include green amphibole, epidote, and sphene, with minor chlorite. Trondhjemite veins and intrusion breccias similar to those in Unit III are also present.

2.2.5 Unit V - Massive Olivine Gabbro (274.06-382.40 mbsf)

Unit V consists predominantly of massive olivine gabbro. This unit exhibits little deformation and is characterized by the almost ubiquitous presence of olivine and the lack of Fe-Ti oxide minerals and pigeonite. Plagioclase (45%-55%), clinopyroxene (40-45%), olivine (5-10%), and minor orthopyroxene constitute the main minerals, all of which display rather uniform compositions (olivine, Fo_{75-80} and plagioclase, An_{60-65}) (Robinson *et al.*, 1991).

The plutonic rocks display coarse-grained, equigranular, mesocumulate textures with some primary grain size layering. Ophitic to subophitic textures are common in which pyroxene (up to 16 mm long and 6.5 mm wide) encloses euhedral to subhedral plagioclase laths (Dick *et al.*, 1991a). Olivine is not found as chadacrysts, but instead forms intergranular to granular aggregates with plagioclase between oikocrysts. Throughout this unit, there are thin troctolite layers, plagioclase-rich zones, and breccia zones with felsic veins containing assemblages of diopside, green amphibole, sodic plagioclase, epidote, and sometimes chlorite. Although the overall modal oxide content in

this unit is low (average 0.05%), narrow oxide-rich shear zones are locally present (Dick *et al.*, 1991a).

2.2.6 Unit VI - Lower Compound Olivine Gabbro (382.40-500.70 mbsf)

Unit VI consists predominantly of compound olivine gabbro, divided into four subunits: Subunit VIA - compound olivine gabbro with minor intervals of intrusive oxide microgabbronorite, olivine microgabbro, and oxide olivine gabbro; Subunit VIB - compound olivine, oxide olivine, and disseminated oxide olivine gabbro, with minor intrusive olivine and oxide olivine microgabbro; Subunit VIC - compound troctolite and olivine gabbro, with minor oxide olivine gabbro, oxide olivine microgabbro, intrusive troctolite, and troctolitic microgabbro; and Subunit VID - compound olivine, oxide olivine, and troctolitic gabbro, with disseminated oxide olivine and oxide gabbro. For the most part, olivine gabbro (>10% olivine), exhibiting cumulate textures, is cross-cut by layers of troctolite and microgabbro. Numerous thin shear zones rich in Fe-Ti oxide minerals, primarily ilmenite, criss-cross the intrusive microgabbros. Igneous layering is defined by grain size variations, however, phase layering is also present.

The rocks in this unit have variable modal mineralogy with olivine, plagioclase, pyroxene and minor spinel as the main mineral phases. Olivine commonly has compositions between Fo_{65-85} and typically exceeds 10 modal percent, although values up to 60 modal percent are common in the troctolites (Robinson *et al.*, 1991). Plagioclase typically has compositions around An_{65} but varies from An_{35} in ferrogabbros to An_{75} in troctolites (Robinson *et al.*, 1991). Coarse-grained subhedral pyroxene oikocrysts commonly enclose plagioclase laths. Alteration assemblages reflecting amphibolite facies conditions and associated with subsolidus brittle-ductile shear zone fabrics overprint earlier high-temperature intrusive and late magmatic deformation. These shear zones commonly contain veins filled with diopside, epidote, sodic plagioclase, green amphibole and chlorite. Olivine is also commonly replaced by Fe oxide minerals.

2.3 ALTERATION AND METAMORPHISM

This section is summarized from previous studies and briefly describes the alteration and metamorphic history that has been documented in core from Hole 735B. For a more detailed discussion see Robinson *et al.* (1991), Stakes *et al.* (1991), Vanko and Stakes (1991), Shipboard Scientific Party (1989), Cannat *et al.* (1991), and Dick *et al.* (1992).

Rocks from Hole 735B have undergone varying degrees of alteration and metamorphism. Five major styles of alteration have been identified in samples from Hole 735B which are summarized in Table 2.1 (Robinson *et al.*, 1991; Dick *et al.*, 1992). These are, from early to late: 1) high temperature metamorphism associated with brittle-ductile deformation; 2) static alteration during which olivine and some orthopyroxene were partly to completely replaced by Fe-Mg amphiboles, talc, and secondary magnetite; 3) infilling of inclined veins during brittle deformation; 4) deposition of smectite in subvertical cracks; and 5) late-stage replacement of olivine and pyroxene by reddish Fe-oxides, carbonate, and clay minerals (Robinson *et al.*, 1991). The following sections are based on previous studies (Robinson *et al.*, 1991; Dick *et al.*, 1992) and briefly summarize the distribution, secondary mineralogy, temperature and water/rock ratios associated with each of the documented alteration styles. Particular attention is paid to the filling of inclined veins since this study focuses on host rock alteration near inclined veins.

2.3.1 High Temperature Metamorphism

Two stages of brittle-ductile deformation have been recognized in rocks from Hole 735B - a late magmatic stage associated with the formation of oxide gabbros which is concentrated in Units III and IV, and a subsolidus stage associated with granulite and amphibolite facies metamorphism - the latter of which is most important to this study (Cannat *et al.*, 1991; Stakes *et al.*, 1991; Dick *et al.*, 1991a). High temperature granulite to amphibolite facies metamorphism, related to subsolidus deformation during the formation of thin shear zones throughout the core, is best preserved in Unit I, where the rocks exhibit well-developed porphyroclastic and mylonitic fabrics. Two major mineral

Table 2.1 Styles of alteration in Hole 735B

Type of alteration	Distribution	Secondary mineralogy	Temperature range (°C)	Water/rock ratios
1. Granulite and amphibolite facies metamorphism	Chiefly lithologic Units I and II	(a) Recrystallized pyroxene and feldspar with minor olivine, amphibole, and Fe-Ti oxides	(a) 640°-720°	(a) Low
		(b) Green and brown hornblende, plagioclase and minor Fe-Ti oxides and brown mica	(b) 590°-640°	(b) High
2. Static recplacement of olivine units	All olivine-bearing	Talc, tremolite, secondary magnetite, and cummingtonite	?	Moderate?
3. Filling of inclined veins	Throughout core	(a) Early veins are filled with diopside, hornblende, feldspar, epidote, sphene, magnetite, and zircon	(a) Amphibole-plagioclase 640° Diopside-Plagioclase 200°-420° Trondhjemite 225°-360°	(a) High
		(b) Late veins are filled with zeolite, chlorite, clay minerals, and calcite	(b) <100°(?)	(b) High
4. Filling of vertical cracks	Scattered through core	Smectite	<100°(?)	Moderate?
5. Oxidative replacement of olivine	Cores 118-735B-1-8, 9-10, 31-39, 57, 63-67, 70-73	Clay minerals, Fe oxides, and calcite	<25°(?)	Moderate to high

From Robinson *et al.* (1991)

assemblages have been documented in these rocks based on water/rock ratios (Cannat *et al.*, 1991; Stakes *et al.*, 1991). In rocks altered at low water/rock ratios, mineral assemblages consist of recrystallized primary igneous minerals which have re-equilibrated to somewhat lower P-T conditions. Mineral assemblages reflect protolith compositions (e.g. gabbronorite in Unit I), and common minerals include plagioclase, clinopyroxene, and orthopyroxene with minor olivine, brown amphibole, and Fe-Ti oxides. Where present, porphyroclasts are enclosed by neoblasts of the same minerals, except in the case of orthopyroxene which forms small brecciated grains rather than neoblasts. Neoblast compositions differ slightly from nearby porphyroclasts with clinopyroxene being more diopsidic and plagioclase being more sodic (Robinson *et al.*, 1991).

Rocks exposed to higher water/rock ratios exhibit progressive replacement of pyroxene by amphibole, forming an amphibolite gneiss (Robinson *et al.*, 1991). Igneous porphyroclasts are rare in these rocks and are commonly totally replaced. Common mineral assemblages include plagioclase, Fe-Ti oxides, green and brown amphibole, and minor brown mica. Rocks often contain amphibole veins which cut, are cut by, and are parallel to, gneissic foliation. Matrix amphibole is chemically similar to that occurring in veins and some grains contain significant amounts of chlorine suggesting influence by seawater (Ito and Anderson, 1983; Vanko, 1986; Mevel, 1988; Vanko and Stakes, 1991). Amphiboles are chiefly Mg-rich hornblendes with Fe-rich hornblendes restricted to more evolved trondhjemitic patches (Robinson *et al.*, 1991). Actinolitic hornblende replaces porphyroclasts and forms rims around earlier Mg hornblende.

High temperature metamorphism in the granulite facies under anhydrous conditions is indicated by primary magmatic oxygen isotope compositions in augite porphyroclasts ($\delta^{18}O$ values between 5.08 and 5.4‰) (Vanko and Stakes, 1991). Subsequent cooling to amphibolite metamorphic conditions is believed to have occurred as seawater penetrated into the system and water/rock ratios increased. This is marked by a depletion in oxygen isotope values in actinolitic hornblende and actinolite to 1.6‰ and a shift to low values in plagioclase (Vanko and Stakes, 1991). Estimated temperatures

associated with amphibolite metamorphic conditions range from 590° to 720°C (Vanko and Stakes, 1991).

2.3.2 Static Alteration

Static alteration, chiefly in undeformed zones, resulted in variable replacement of olivine, and to a lesser extent orthopyroxene, by colourless amphibole, talc, and secondary magnetite. Many pseudomorphs are zoned with mixtures of tremolite and talc in the cores, which are rimmed by tremolite, cummingtonite, or anthophyllite. Very fine secondary magnetite grains commonly form concentric bands parallel to the original grain boundary. Minor pargasitic amphibole and phlogopite occur along olivine-plagioclase grain boundaries and clinozoisite locally replaces feldspar grains. Minor chlorite and actinolite rim plagioclase and clinopyroxene porphyroclasts in amphibolite gneiss.

The origin and timing of static alteration is problematic. Because it affects olivine and, to a lesser extent, orthopyroxene, its distribution is largely related to variations in primary mineralogy and not vein proximity or density (Robinson *et al.*, 1991) (see Appendix 2, Sample 63R-6 98-106 cm). Static alteration may be deuteric and reflect reaction with late-stage magmatic fluids at high temperatures because there appear to be no channel ways in undeformed rock along which fluids could have migrated. Conversely, it may reflect interaction with seawater along small cracks and at grain boundaries which may have occurred in deformed zones which locally acted as seawater conduits. Timing may have been penecontemporaneous with brittle-ductile deformation and amphibolite facies metamorphism. Pseudomorphed porphyroclasts in foliated rocks contain unoriented secondary minerals formed by static alteration which clearly post-date deformation. However, if static alteration occured earlier, it may have been overprinted by the amphibolite facies metamorphism.

2.3.3 Filling of Inclined Veins

Hydrothermal and late-stage magmatic veins make up 2.4% of the core in Hole 735B (Dick *et al.*, 1992). Veins are uniformly distributed down the hole although specific vein

types have restricted stratigraphic distributions (Figure 2.4). The relative proportions of common vein types are shown in Figure 2.5. Recent studies of fluid inclusions, in samples from Hole 735B indicate that certain veins have magmatic origins (Kelley *et al.*, 1994; Kelley, 1996). Veins with a magmatic origin acted as pathways for later hydrothermal fluids. This is suggested by felsic veins that exhibit sequential assemblages that formed at successively lower temperatures as the hydrothermal fluids cooled. For example, some felsic veins are observed which contain narrow bands of zeolite, carbonate or clay at their centres (Figure 2.6). As a result, all veins in this study are treated as having a hydrothermal component.

2.3.3.1 Amphibole veins

Monomineralic amphibole veins are most abundant in the upper portion of the core and are commonly restricted to zones of brittle-ductile deformation and amphibolite facies metamorphism. Amphibole veins appear to be rotated into the plane of the foliation in the more deformed zones in the upper 40 m of the core, however, veins also cut, and are cut by, the gneissic to mylonitic foliation (Figure 2.7a). Cracks 1-3 mm wide, oriented perpendicular to the foliation, may continue into porphyroclasts as microcracks in less deformed zones (Figure 2.7b). Amphibole veins typically consist of green to green-brown, pleochroic, magnesio-hornblende, that commonly exhibits fibrous textures oriented both perpendicular and parallel to the vein (Figure 2.8a). Some coarse-grained, euhedral crystals exhibit compositional zoning, however, vein amphibole is chemically similar to amphibole replacing primary phases (Robinson *et al.*, 1991). Temperature estimates for metamorphic amphibole and vein hornblende overlap, suggesting an intimate association between brittle-ductile deformation and associated amphibolite facies metamorphism (Vanko and Stakes, 1991). Numerous veins in the lower parts of the core also contain amphibole although amphibole is only a minor component and usually occur as rims on other minerals (Figure 2.8b).

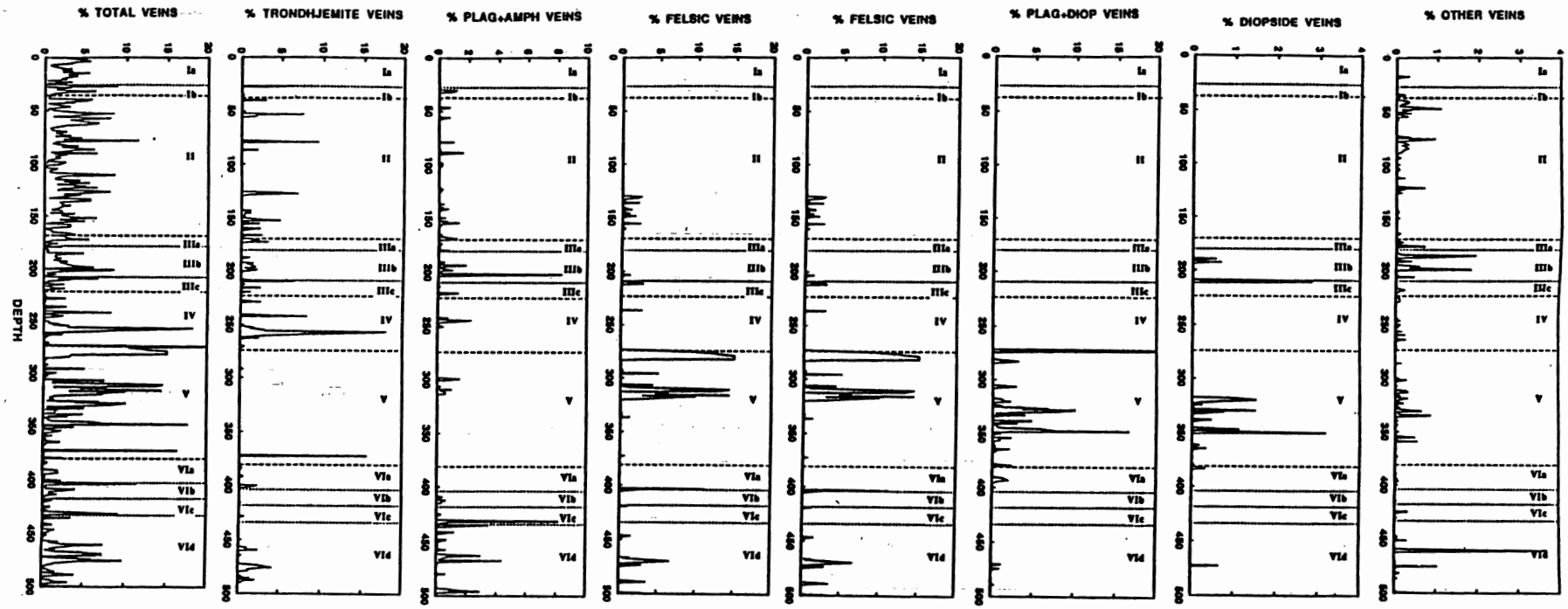

Figure 2.4 Downhole log of Hole 735B showing 1 metre average density for Hole 735B vein assemblages. Horizontal lines show the divisions between major lithostratigraphic units. "Other" refers to low-temperature veins including carbonate, clay, and zeolites. (From Dick *et al.*, 1992)

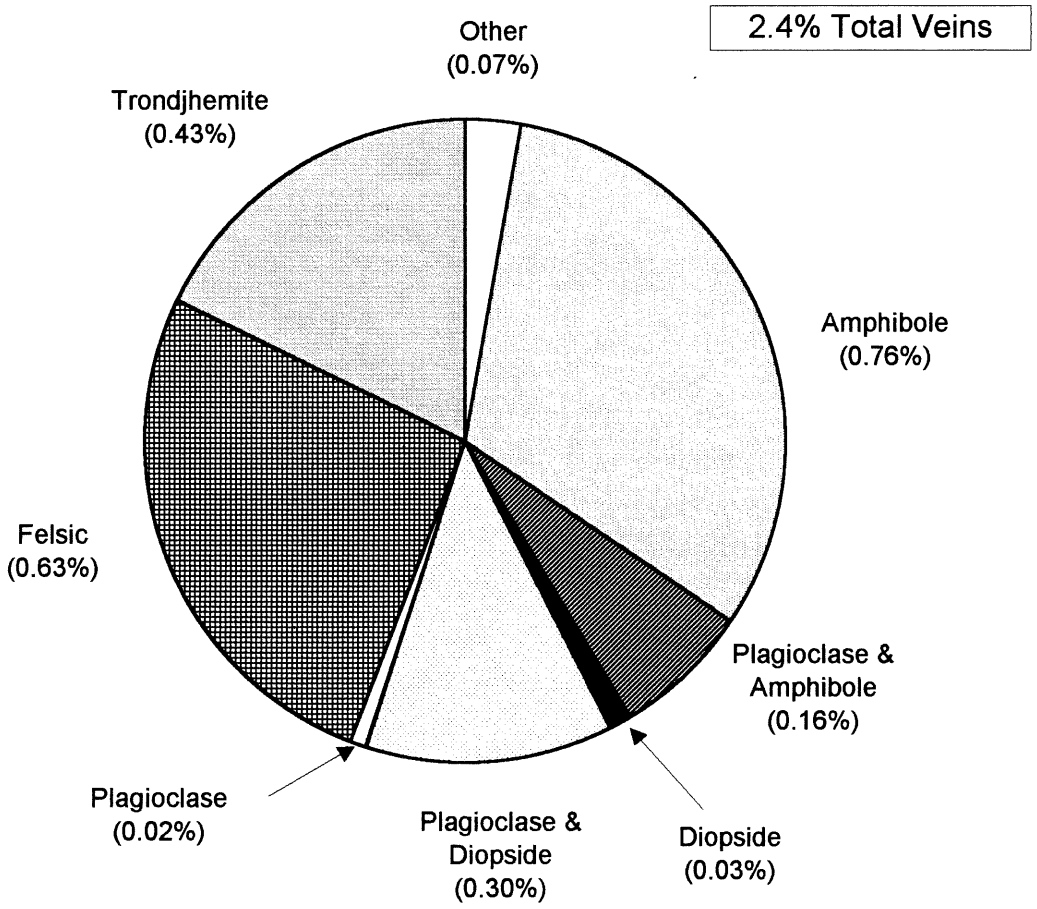

Figure 2.5 Relative vein proportions, Hole 735B, visually estimated on a fragment by fragment basis for the entire core at the ODP Core Repository and then summed (from Dick *et al*., 1991a).

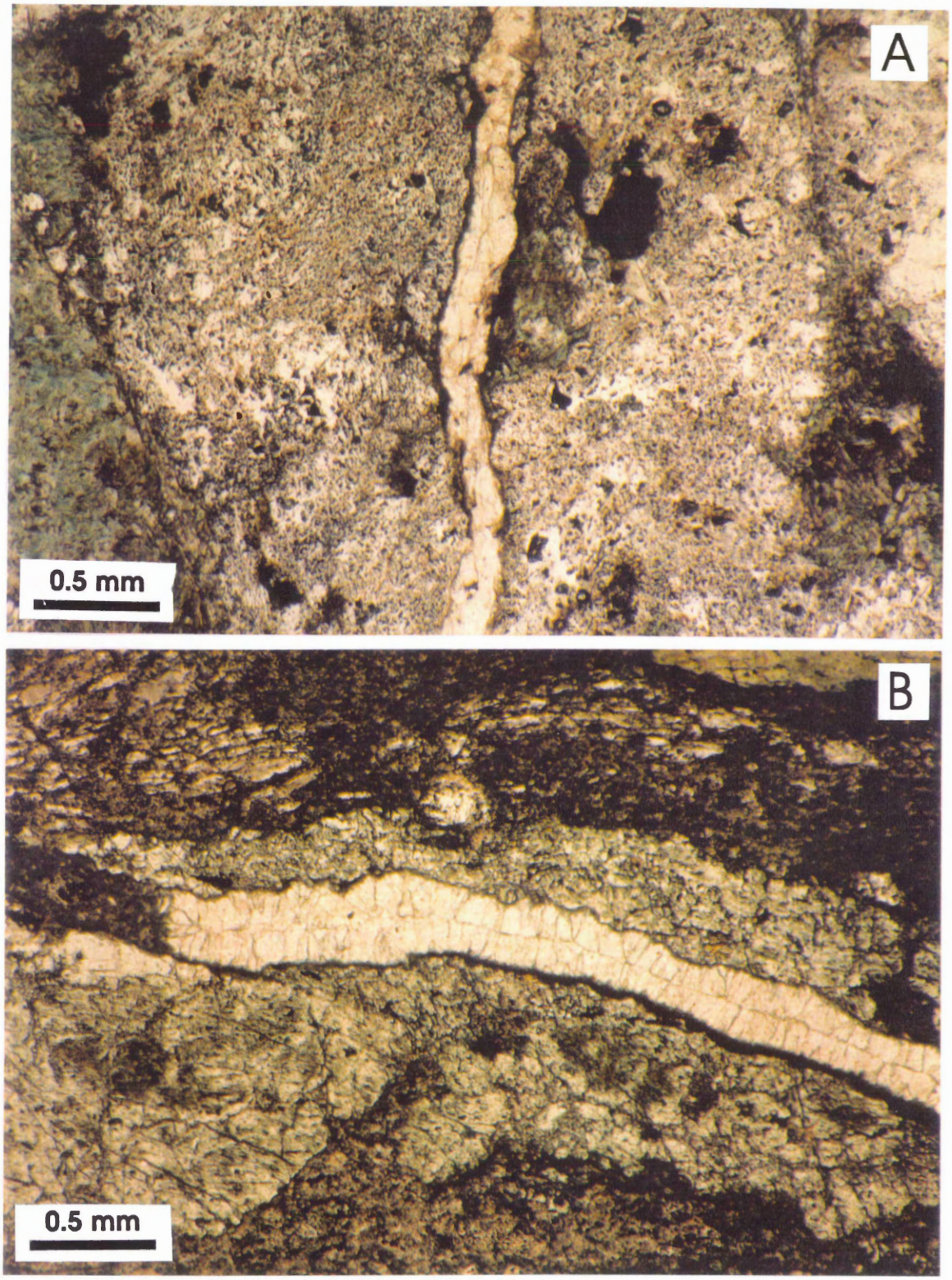

Figure 2.6 A. Narrow zeolite vein cutting through centre of felsic vein (Sample 84R-6 31-41 cm). B. Narrow carbonate vein cutting through centre of plagioclase-hornblende vein (Sample 67R-1 88-93 cm). Both after Robinson *et al.* (1991).

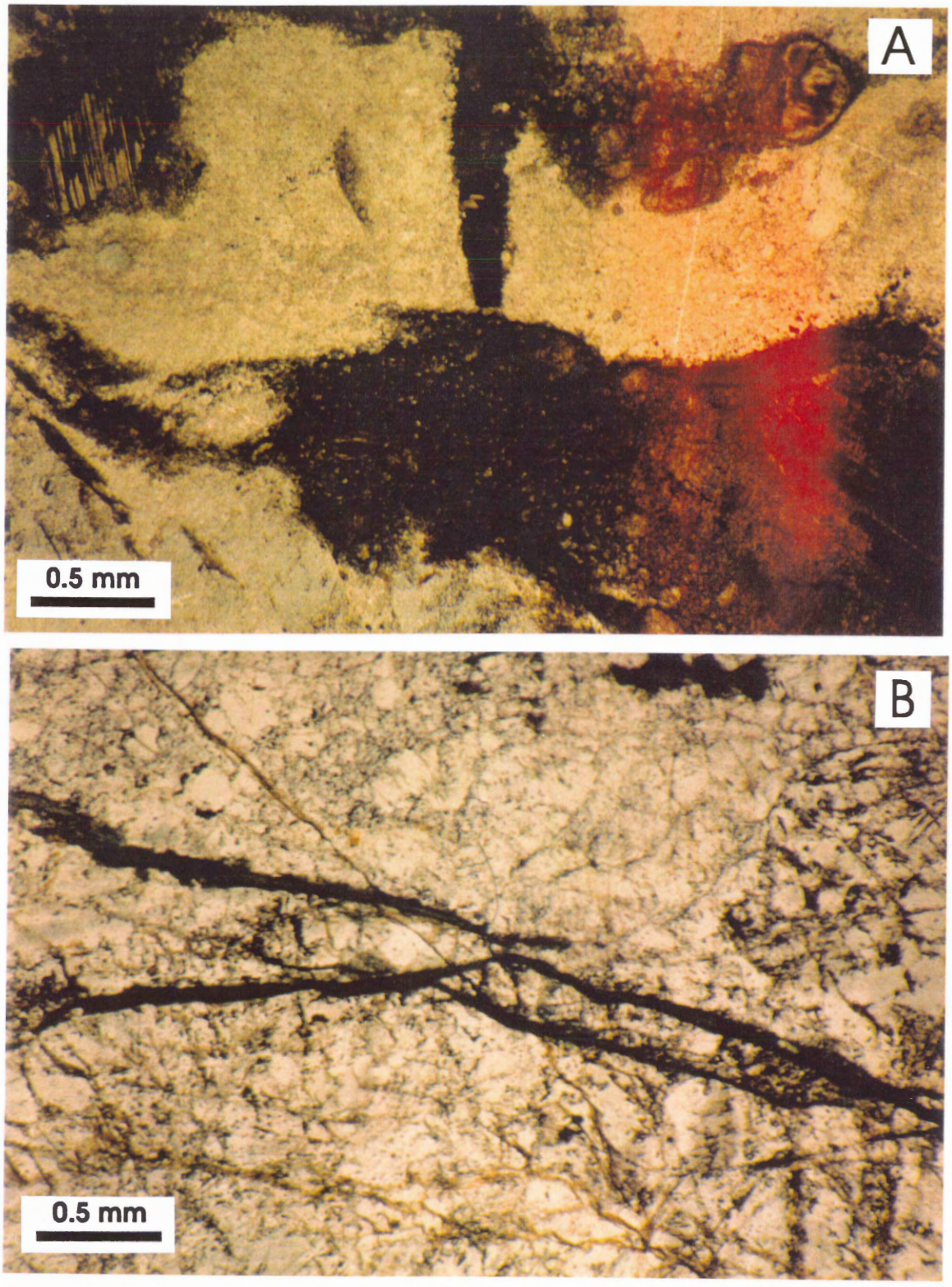

Figure 2.7 A. Narrow amphibole vein cut by foliation in deformed gabbro. Foliation is defined by plagioclase (light bands) and amphibole (dark bands) (Sample 2D-1 123-127 cm). After Robinson *et al.* (1991). B. Narrow amphibole veinlets cutting plagioclase pophyroclast (Sample 18R-1 139-147 cm).

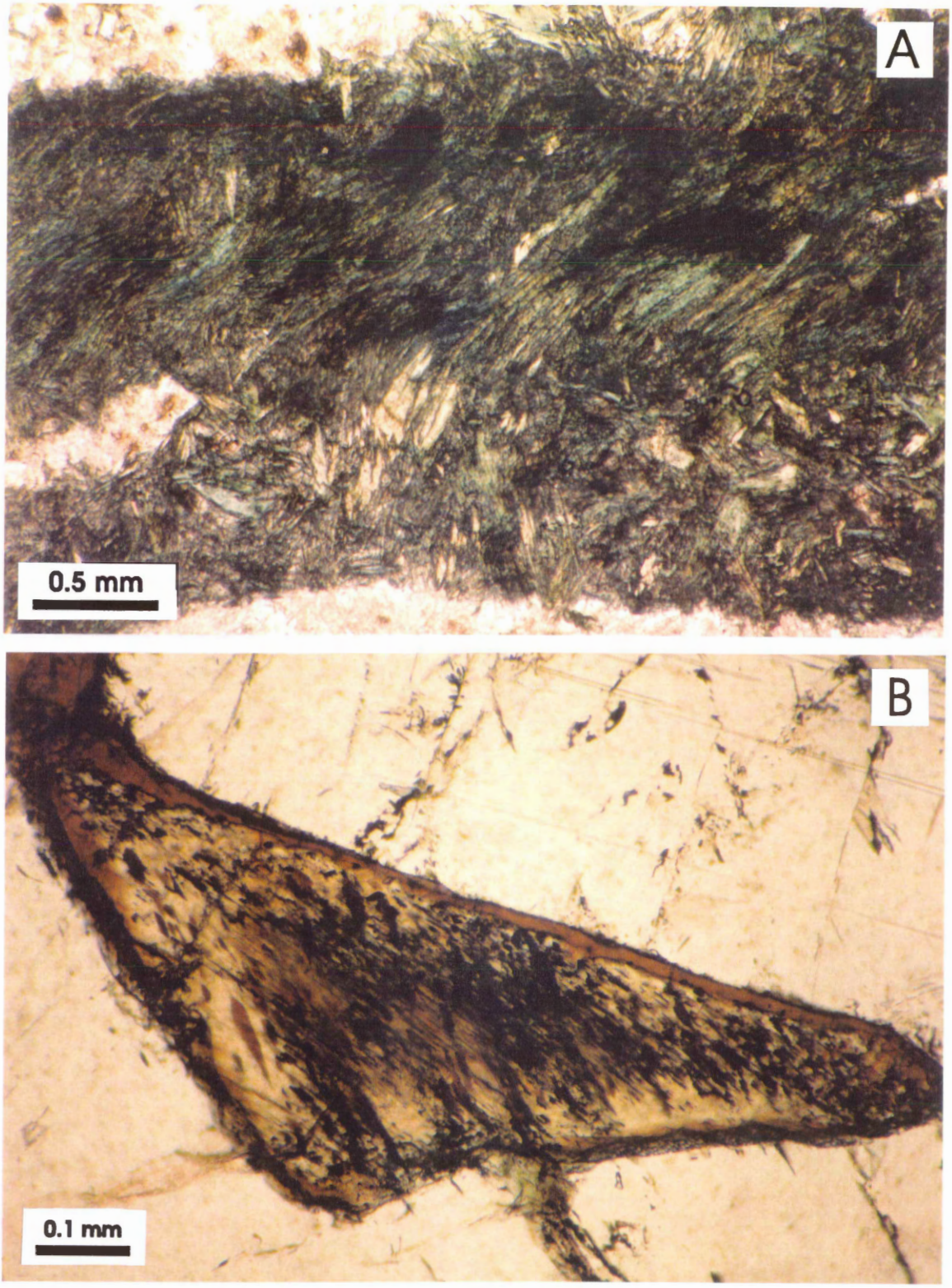

Figure 2.8 A. Vein filled with green amphibole displaying fibrous texture. Most of the amphibole is oriented oblique to the vein margin (Sample 32R-2 86-95 cm). B. Brown amphibole rim on clinopyroxene grain (Sample 84R-6 31-41 cm).

2.3.3.2 Trondhjemite veins

Trondhjemite veins, typically 1 to 2 cm wide, occur in discrete zones but are most abundant in Fe-Ti oxide gabbros. The veins have been deformed during subsolidus brittle-ductile deformation, resulting in some veins being completely transported into the plane of the foliation, making them difficult to distinguish from other felsic layers. The veins contain trondhjemitic mineral assemblages including euhedral plagioclase, quartz, minor brown amphibole or biotite, and trace amounts of zircon (Figure 2.9b). Although these veins appear to be igneous in origin, many have undergone subsequent hydrothermal alteration. These veins are believed to have formed from highly-evolved late magmatic liquids which penetrated the Fe-Ti oxide gabbros (Dick *et al.*, 1991). Temperature estimates from fluid inclusions in quartz and feldspar yield low values (227^0 to 358^0C) that seem to indicate interaction with hydrothermal, or substantially cooled, magmatic fluids (Vanko and Stakes, 1991).

2.3.3.3 Felsic veins

Many felsic veins exhibit variable mineralogy associated with sequential growth inward from fracture walls, as well as replacement of primary minerals. Typical vein mineral assemblages include sodic plagioclase, diopside, amphibole, epidote, sphene, magnetite and zircon (Figure 2.9). Monomineralic veins also occur (see Appendix 2, Sample 32R-2 86-95 cm), however, zoned assemblages are more common (see Appendix 2, Sample 31R-3 4-10 cm). Typical vein growth patterns include diopside at the vein margin, followed by tabular epidote crystals, with fine grained plagioclase in the centre. Progressive alteration produces rims of amphibole on diopside and Fe-Mg zoning in diopside is also common (Figure 2.10a). Primary clinopyroxene cut by veins commonly shows epitaxial growth of diopside in veins (Figure 2.10b). Vein diopside is more abundant in the lower portion of the core, possibly reflecting the changing chemistry of the hydrothermal fluids (Robinson *et al.*, 1991; Bird *et al.*, 1988). The centres of veins commonly contain variable mineralogies, which may include sphene, ilmenite, pyrite, allanite, and biotite. Lower temperature mineral assemblages that include zeolites, carbonate, and clay minerals, form

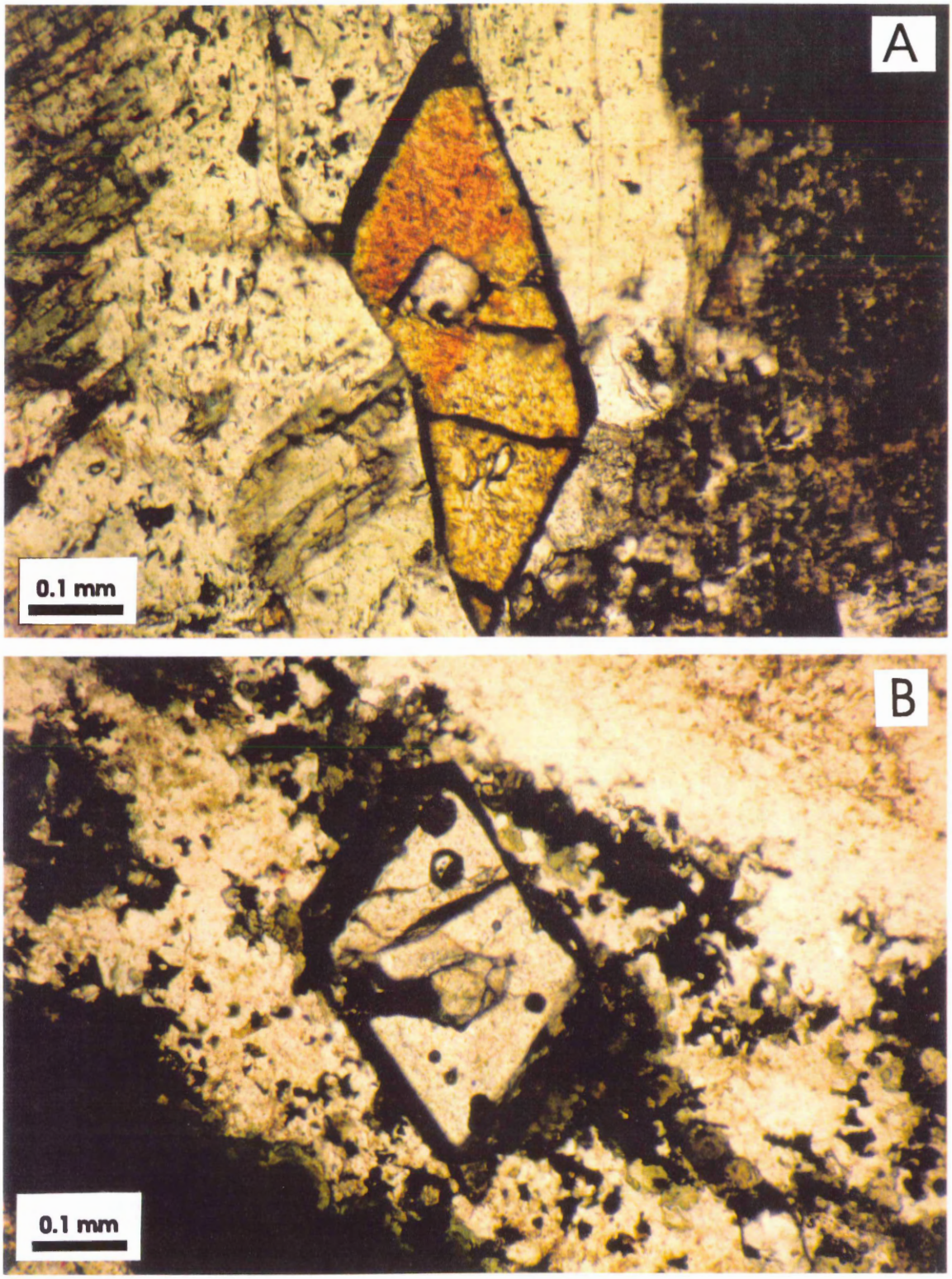

Figure 2.9 A. Euhedral sphene in felsic vein (Sample 66R-2 25-31 cm). After Robinson *et al.* (1991). B. Euhedral zircon in felsic vein. Foliation is defined by plagioclase (light bands) and amphibole (dark bands) (Sample 12R-3 29-34 cm).

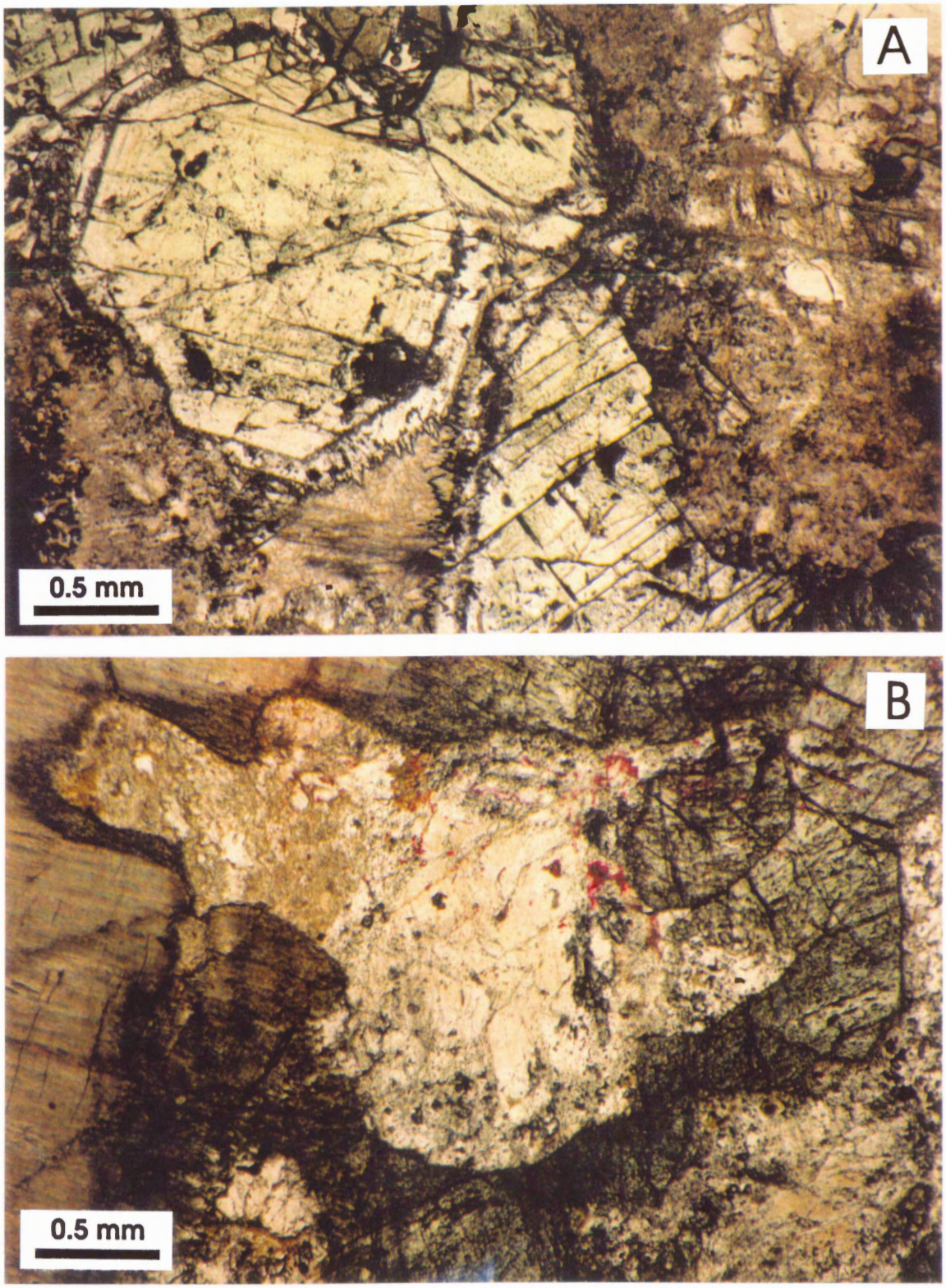

Figure 2.10 A. Large, euhedral, zoned diopside crystals in felsic vein. Zoning is in iron and magnesium. After Robinson *et al.* (1991) (Sample 69R-5 31-41 cm). B. Epitaxial growth of green diopside on primary clinopyroxene at the margin of a vein (Sample 70R-1 39-49 cm).

as patches that replace primary plagioclase, and fill cracks at the centres of pre-existing veins (Figure 2.6).

Fluid inclusions in diopside from felsic veins homogenize at temperatures between 370° and 400°C (Vanko and Stakes, 1991). Fluid inclusions in plagioclase from the same samples are slightly less saline than those in diopside and homogenize at lower temperatures, generally between 207° and 285°C (Vanko and Stakes, 1991). However, oxygen isotope values from felsic veins range from near-magmatic to hydrothermal (Stakes *et al.*, 1991). Textural evidence suggests some veins formed from late-magmatic liquids, particularly those which contain euhedral plagioclase, quartz, and zircon (Robinson *et al.*, 1991). Stakes *et al.* (1991) suggests that there is a complete gradation from magmatic trondhjemites to hydrothermal veins, including later modification of magmatic veins by hydrothermal processes.

2.3.4 Smectite-Lined Fractures

Late-stage subvertical fractures lined with green smectite commonly cut inclined veins. The fractures are common in less deformed, coarse-grained rocks and rarely extend for more than 1 metre along the core axis. They contain only green smectite, which indicates formation at temperatures less than 50°C (cf. Kristmannsdottir, 1979). The fractures are easily distinguished from other veins by their high mean dip angle (70°) (Dick *et al.*, 1991a). The walls of these fractures break around mineral grains instead of through them suggesting formation by release of stored elastic thermal stress during uplift (Dick *et al.*, 1991a).

2.3.5 Late-Stage Oxidation

Red to reddish-brown clots replacing olivine, and to a lesser extent orthopyroxene, represent the last stage of alteration. Oxidative alteration is found in discrete sections of the core probably indicating the introduction of oxygenated seawater along cracks and fractures. Pyroxene is still recognizable and exhibits partial replacement and associated reddening (Figure 2.11a). However, olivine is commonly completely pseudomorphed

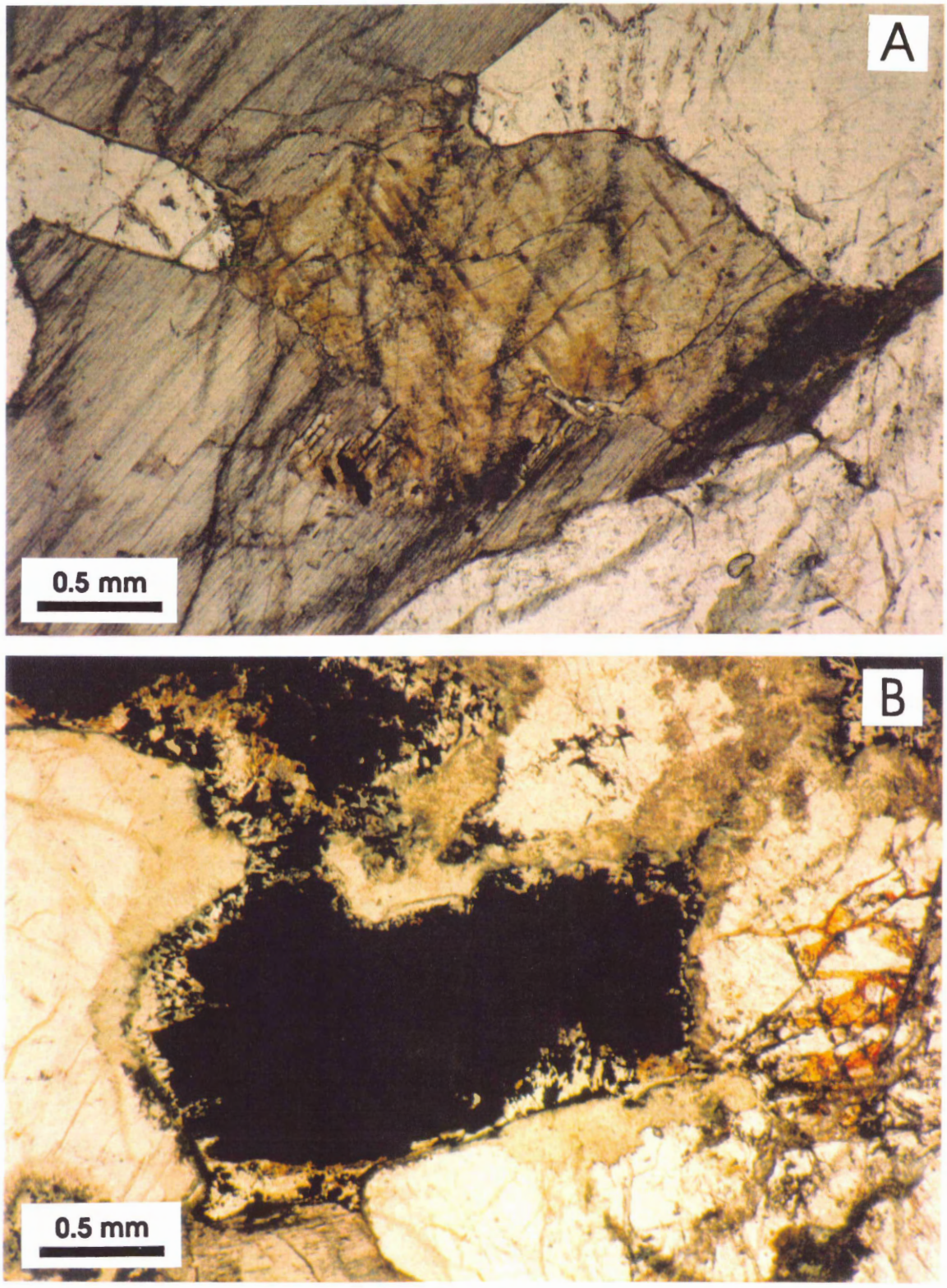

Figure 2.11 A. Clinopyroxene grain exhibiting partial replacement and associated reddening (Sample 63R-6 98-106 cm). B. Olivine grain replaced by red, opaque oxides during oxidative alteration. Corona contains talc and tremolite that formed during earlier static alteration (Sample 63R-6 98-106 cm).

resulting in opaque clots. Some of these clots have coronas of talc, tremolite, and secondary magnetite resulting from previous static alteration of olivine (Figure 2.11b). Other minerals replacing olivine include green-brown clay minerals (smectite), calcite, and/or ferric oxides (Robinson *et al.*, 1991). Calcite is found in veinlets and at the centres of altered felsic veins. This latest stage of alteration is believed to have occurred at temperatures near those of ambient seawater (Robinson *et al.*, 1991).

2.4 SUMMARY

Plutonic rocks recovered from ODP Hole 735B represent the only significant stratigraphically controlled *in situ* samples of oceanic layer 3 presently available. These rocks are believed to have formed under the very slow-spreading median valley of the SWIR approximately 11 Ma and record a complex history of intrusion, brittle-ductile deformation, and successive penetration by hydrothermal fluids. Six major lithologic units have been identified in the core that are believed to represent at least 3 main intrusive events. Alteration and metamorphism are believed to have initiated under anhydrous granulite metamorphic conditions, followed by amphibolite and greenschist facies conditions concomitant with cooling and increased water/rock ratios. Continued subsolidus brittle deformation under amphibolite facies conditions produced monomineralic amphibole veins. Increased penetration and circulation of seawater along zones of relative permeability, such as felsic veins, led to the formation of zoned assemblages reflecting hydrothermal modification of magmatic veins. Late-stage, smectite-lined, subvertical fractures cross-cut previous veins and probably formed from release of stored elastic thermal stress associated with cooling and uplift of the plutonic sequence onto the rift-valley walls (Dick *et al.*, 1991). Late oxidation is characterized by red-brown opaque clots that are observed throughout the core, and which are most obvious in brecciated zones. Re-opening of previous fractures has produced calcite veins which indicate circulation of cold oxygenated seawater (Robinson *et al.*, 1991).

Chapter 3

Mineral Traverses

3.0 INTRODUCTION

In this chapter chemical changes in primary minerals adjacent to hydrothermal veins are investigated using microprobe traverses across vein boundaries from primary to secondary minerals. Each traverse contains between 4 and 7 points. Twelve microprobe traverses were performed in 6 olivine gabbro samples. Each of these samples was chosen because it displays distinct veins exhibiting petrographic signs of alteration along the vein margins. Three main primary minerals are present in these samples: clinopyroxene, plagioclase, and olivine. Most of the traverses extend from primary clinopyroxene to secondary amphibole, however, two traverses go from primary calcic plagioclase to secondary sodic plagioclase and secondary epidote, respectively. Olivine was not analyzed because no fresh olivine was found near veins. Full petrographic descriptions and thin section photos of the samples can be found in Appendix 2.

3.1 METHODS

Microprobe traverse data were collected from six polished thin sections using the analytical methods described in Appendix 1. Samples were analyzed for nine oxides: SiO_2, TiO_2, Al_2O_3, FeO, MnO, MgO, CaO, Na_2O, and K_2O. Traverses vary from 4 to 7 points, although most contain 5 points. Additional points were needed in areas of highly variable alteration. Spacing between points was not kept constant but instead was varied to incorporate the broadest range of primary minerals and alteration products in a single traverse, in order to determine chemical variability between minerals. In most cases, each mineral phase contains multiple points so that chemical variability within individual grains could be determined.

3.1.1 Sample Selection

Thin sections containing distinct veins exhibiting petrographic evidence of alteration were selected for the microprobe traverses. Three of these samples were further analyzed for chemical mapping (Chapter 5) and determination of element flux (Chapter 4) to allow comparison of chemical variability at different scales. Areas showing a progression of secondary minerals were chosen to determine if chemical changes were gradual or abrupt. Replacement of primary clinopyroxene by amphibole is common in samples from Hole 735B and these minerals were the targets of several microprobe traverses. Two traverses in primary plagioclase have also been included.

3.2 RESULTS

Microprobe traverse data are summarized in Appendix 4 and plotted in Figures 3.1 and 3.2. Only elements which show variations greater than a few weight percent are plotted because of the limited vertical exaggeration of the plots. SiO_2 was not included on altered clinopyroxene plots because extrapolation of the scale to include SiO_2 decreases vertical exaggeration in the other elements. Traverse points are marked on thin section photographs in Figures 3.1 and 3.2 and the location of traverses are marked on thin section photos in Appendix 2. Traverses involve fresh clinopyroxene and plagioclase and are grouped together based on the nature of the primary mineral.

3.2.1 Replacement of Clinopyroxene by Amphibole

The most pronounced chemical changes in traverses between clinopyroxene and amphibole occur at the pyroxene-amphibole transition. This transition is characterized by an abrupt decrease in CaO from above 20 wt% (in clinopyroxene) to below 15 wt % (in amphibole) in all samples except 60R-4 (112-120) Spot 1 which displays a more gradual loss of CaO. The abrupt loss of CaO at the pyroxene-amphibole transition appears to be initially compensated by three factors: an increase in FeO [35R-4 (117-124) Spot 2 Point

Figure 3.1 Microprobe traverse plots and thin section photographs for alteration of primary clinopyroxene. Traverse points are marked on thin section photographs below each plot. The inferred mineralogy of each traverse point from petrography is indicated in *italics* on each plot. The distance between traverse points varies. Symbols are the same for all plots. The location of microprobe traverses is indicated on thin section photographs in Appendix 2. See text for explanation.

35R-4 117-124 cm Spot 2

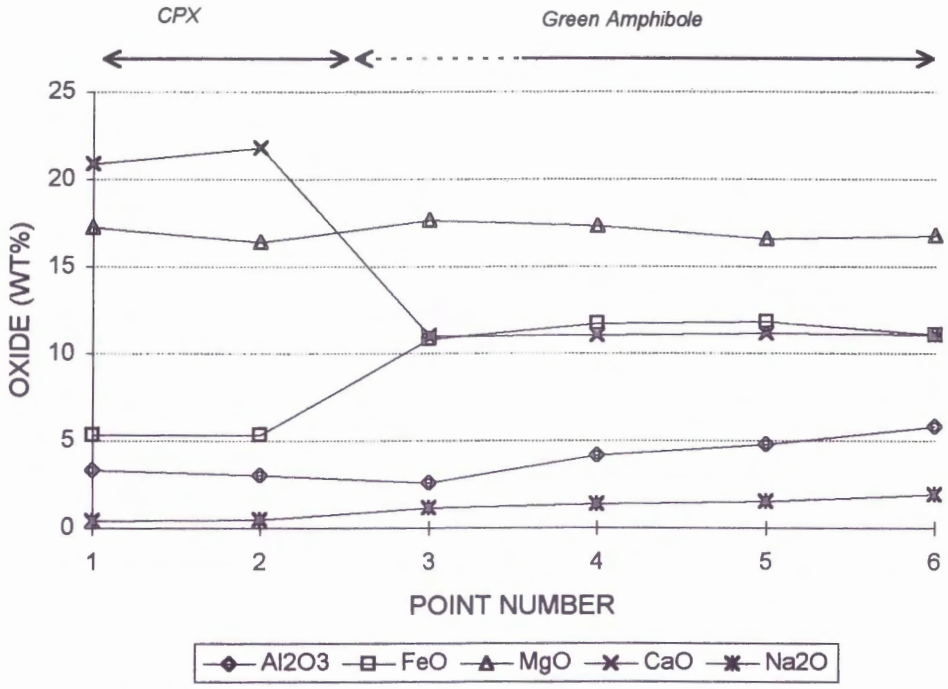

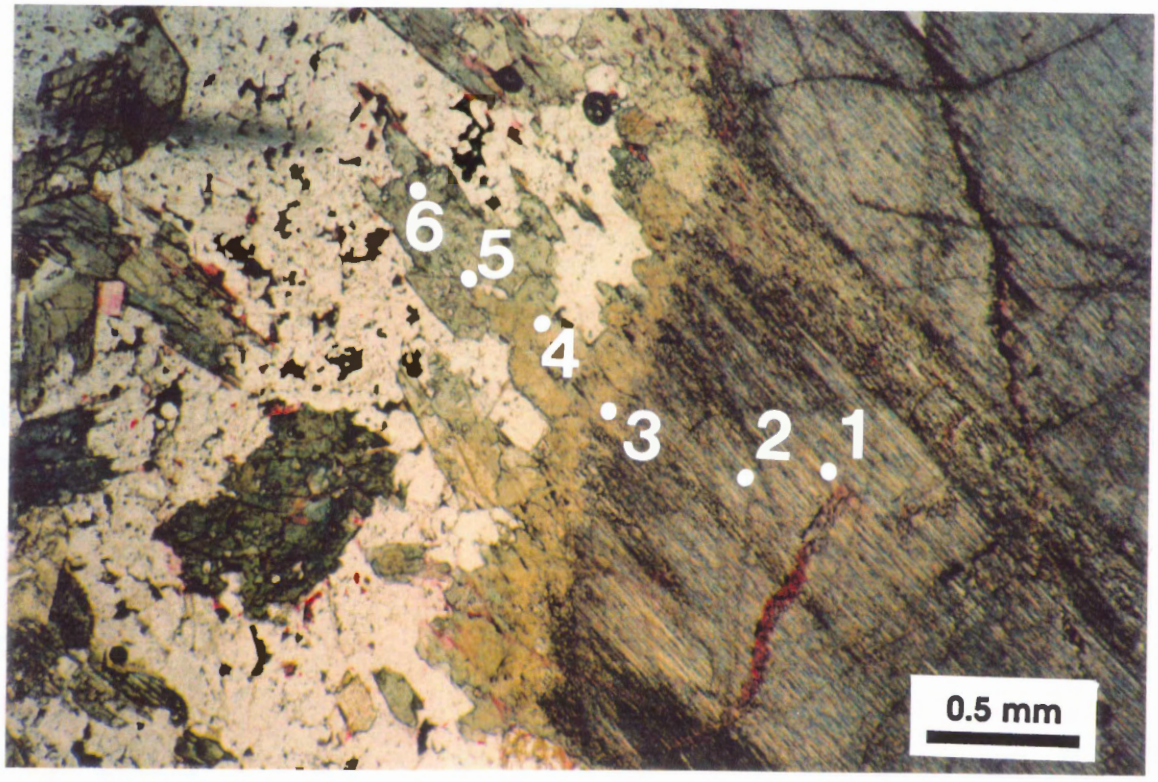

Figure 3.1a

44R-1 35-47 cm Spot 1

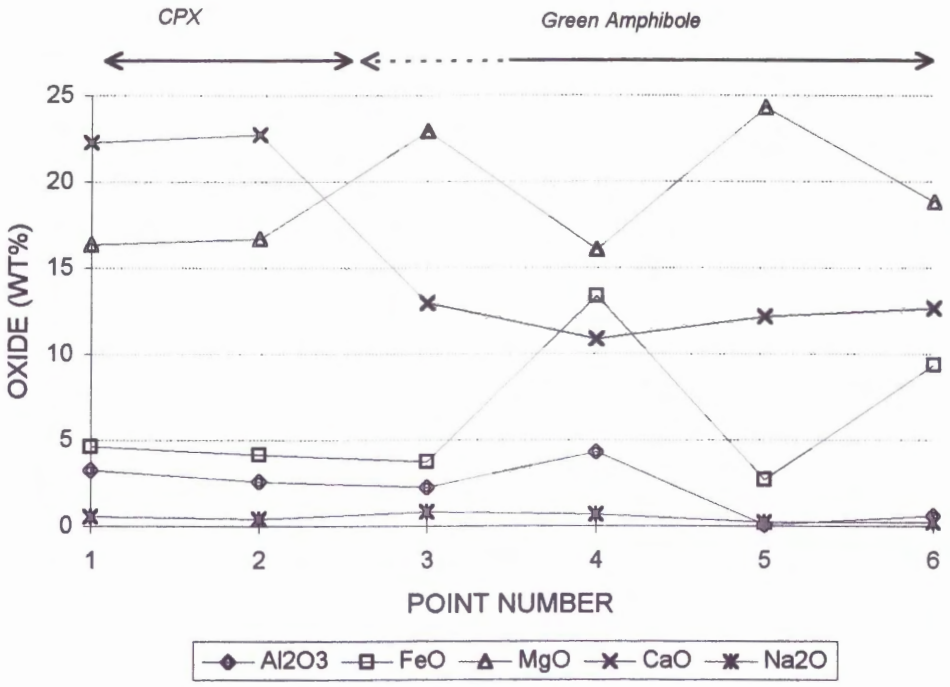

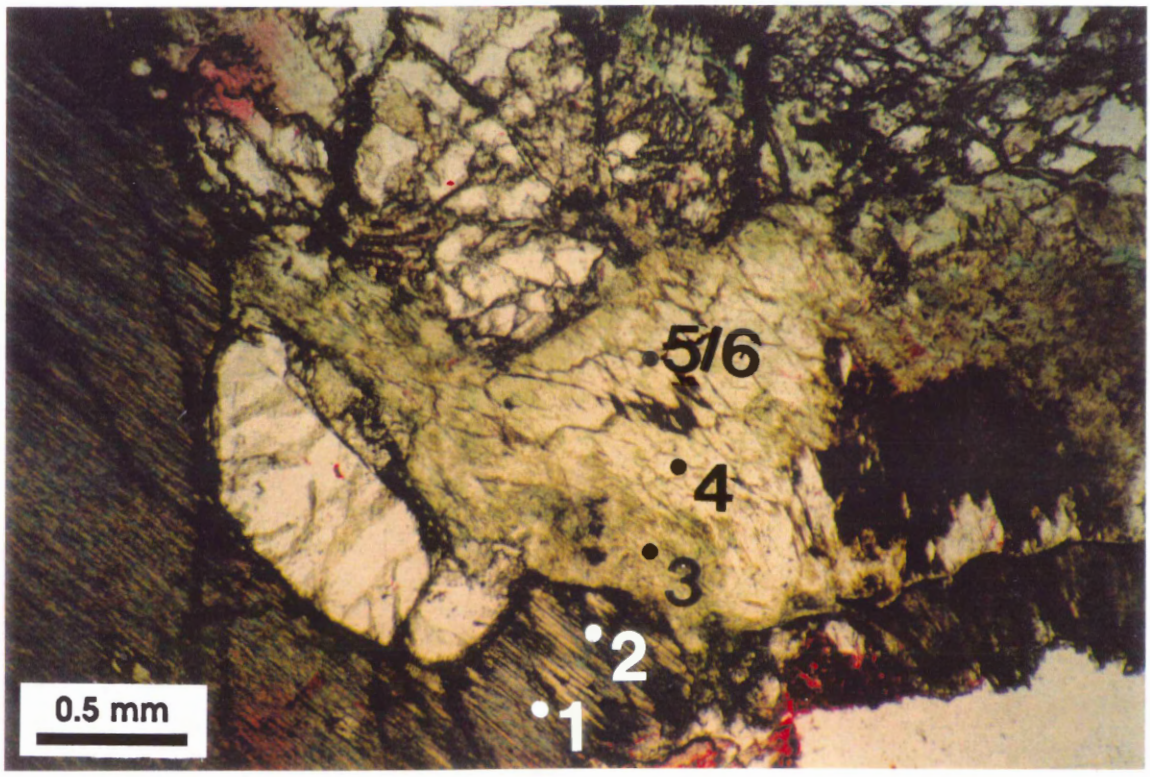

Figure 3.1b

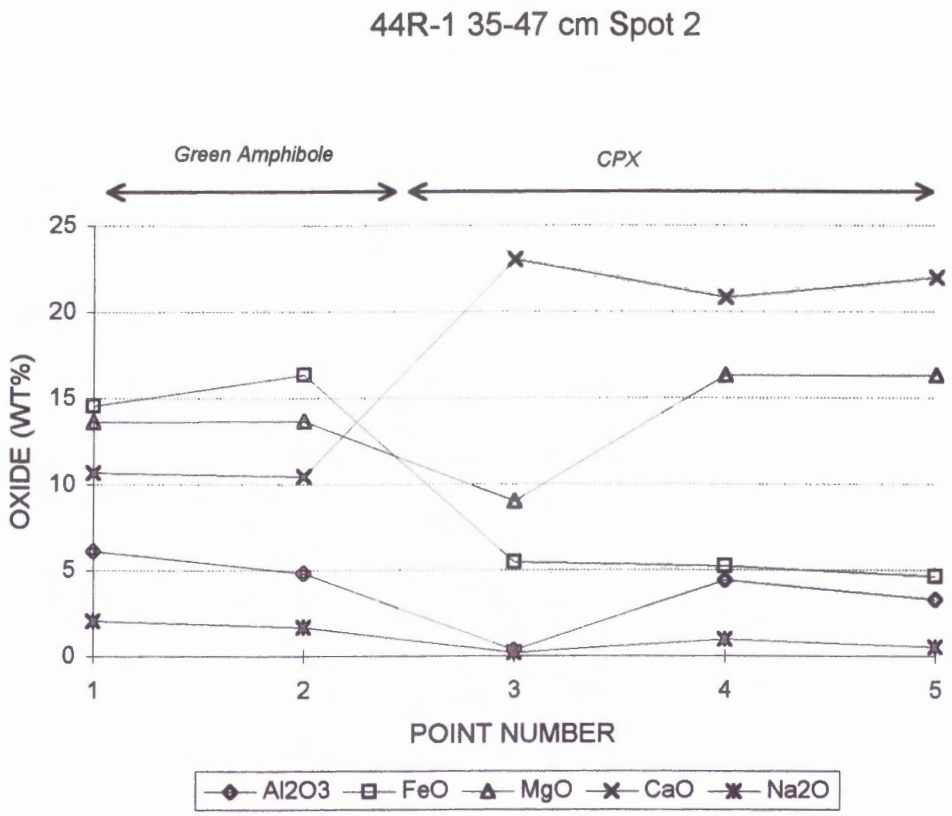
44R-1 35-47 cm Spot 2
Green Amphibole
CPX
25
20
15
10
5
0
OXIDE (WT%)
1
2
3
4
5
POINT NUMBER
Al2O3
FeO
MgO
CaO
Na2O

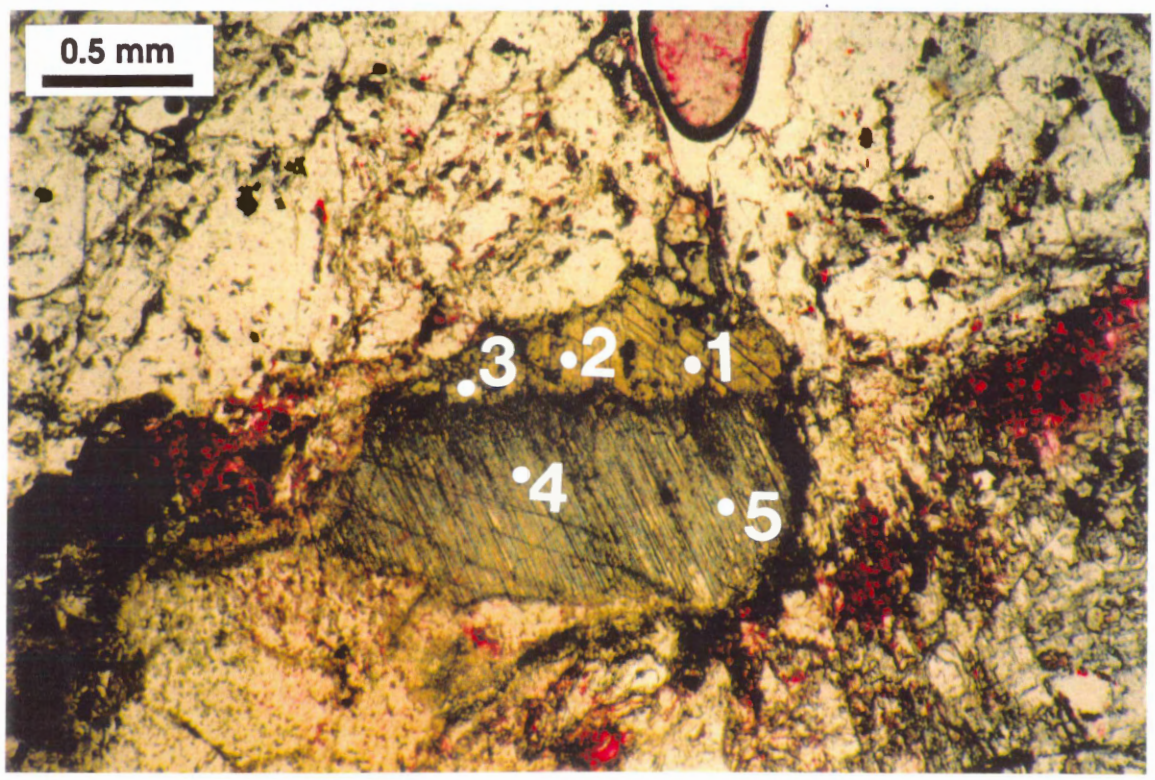
0.5 mm
3
2
1
4
5

Figure 3.1c

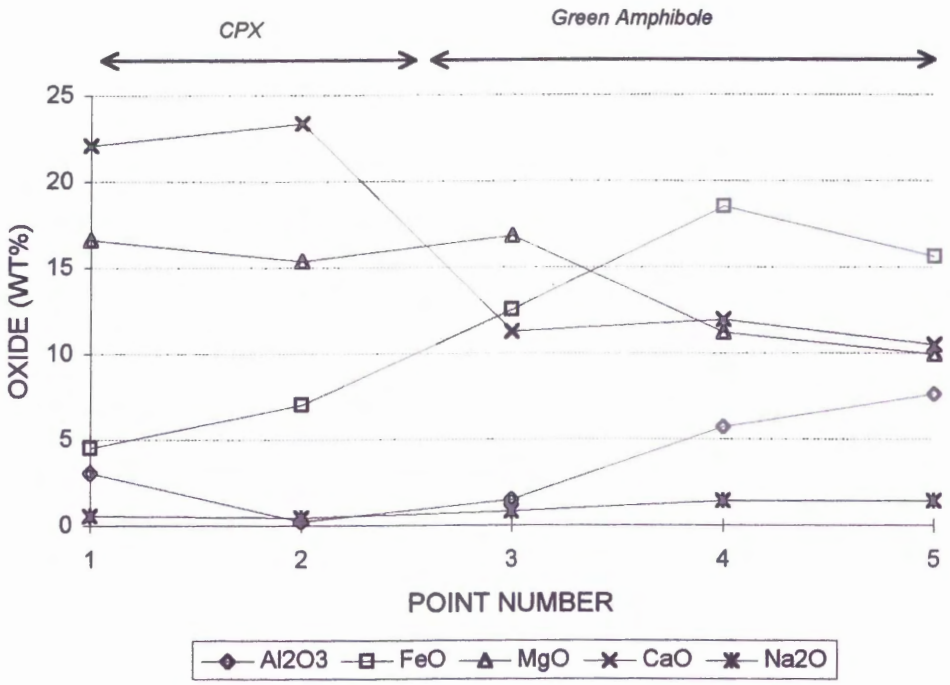
44R-1 35-47 cm Spot 3
CPX
Green Amphibole
25
20
15
10
5
0
OXIDE (WT%)
1
2
3
4
5
POINT NUMBER
Al2O3
FeO
MgO
CaO
Na2O

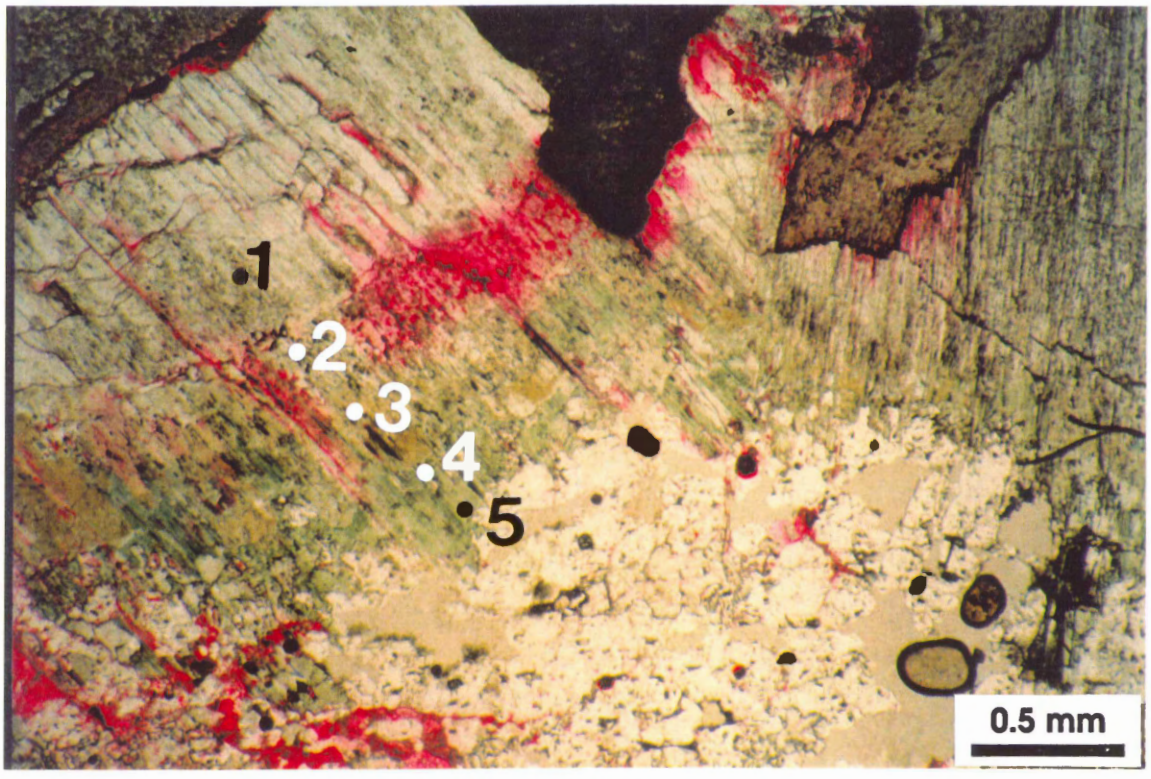
1
2
3
4
5
0.5 mm

Figure 3.1d

58R-3 0-8 cm Spot 1

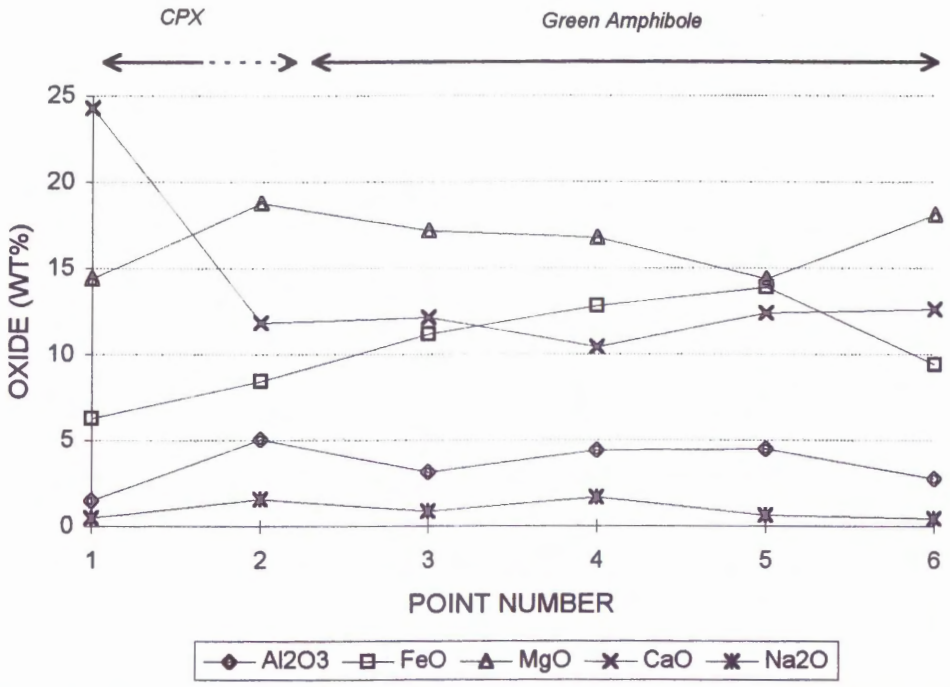

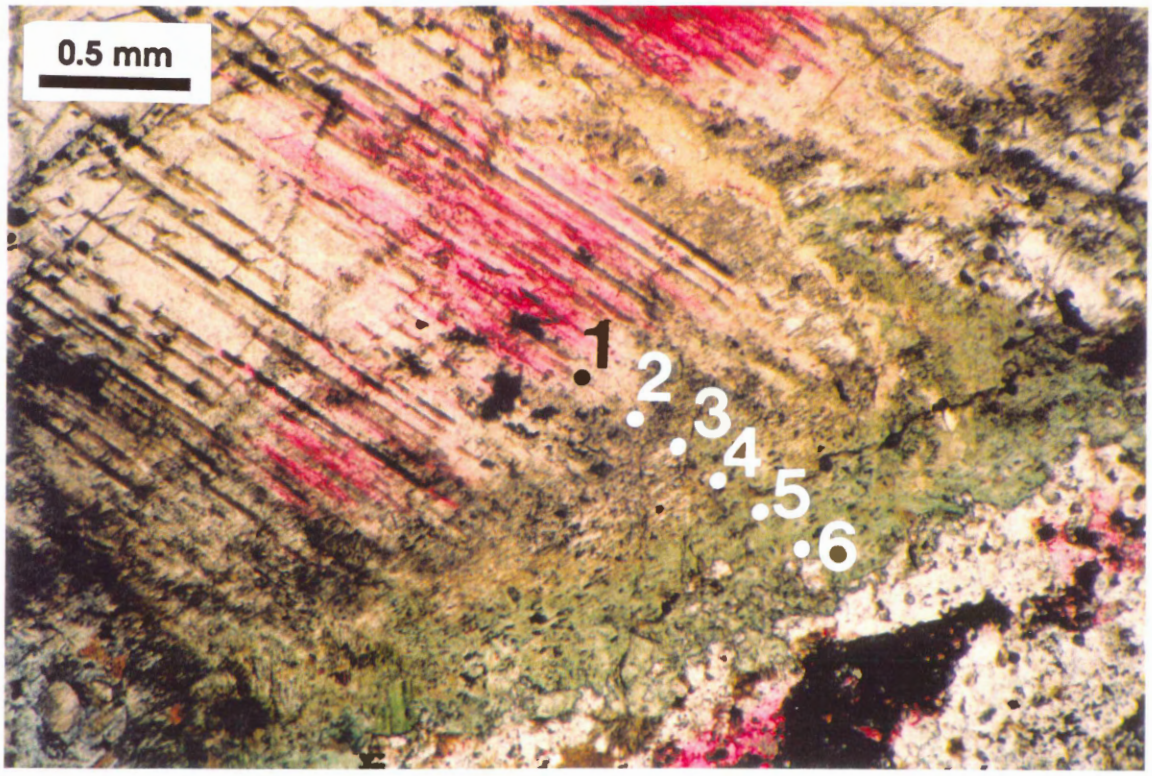

Figure 3.1e

58R-3 0-8 cm Spot 2

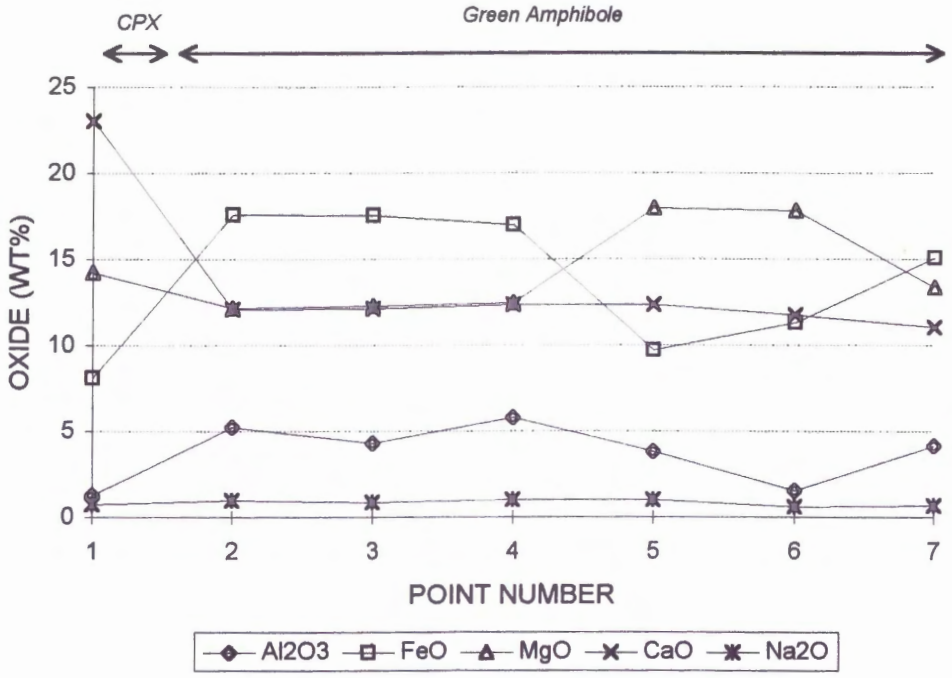

Figure 3.1f

60R-4 112-120 cm Spot 1

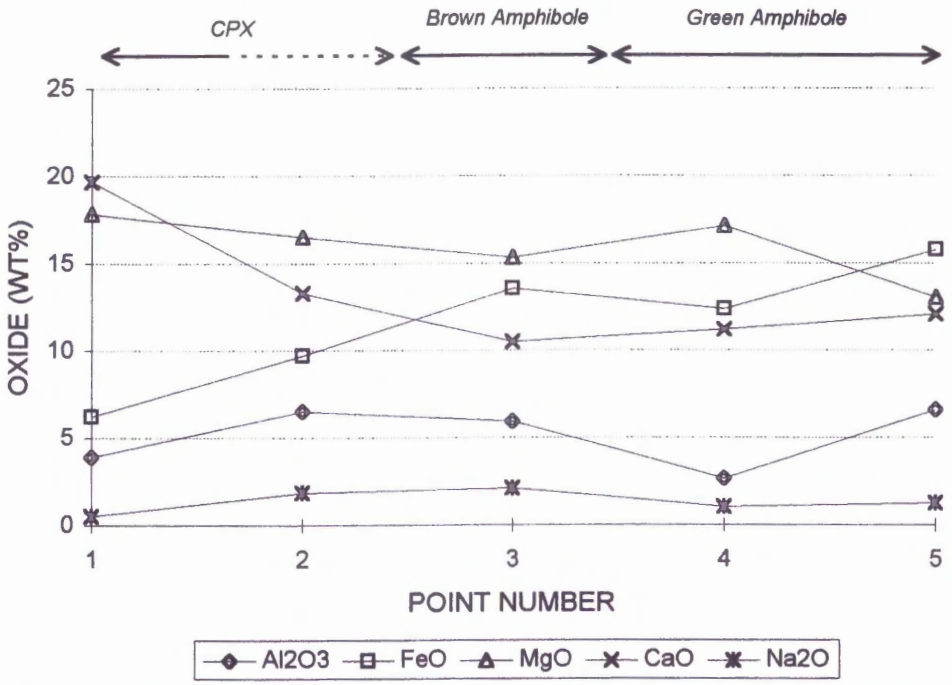

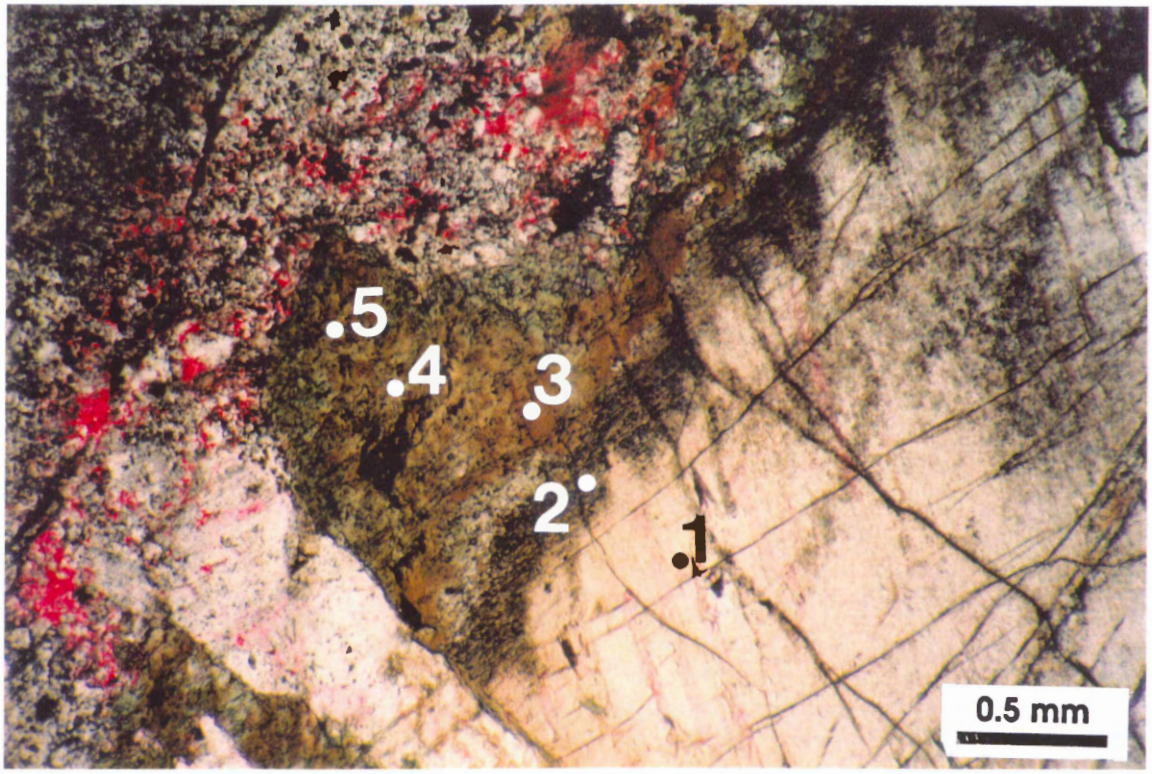

Figure 3.1g

60R-4 112-120 cm Spot 2

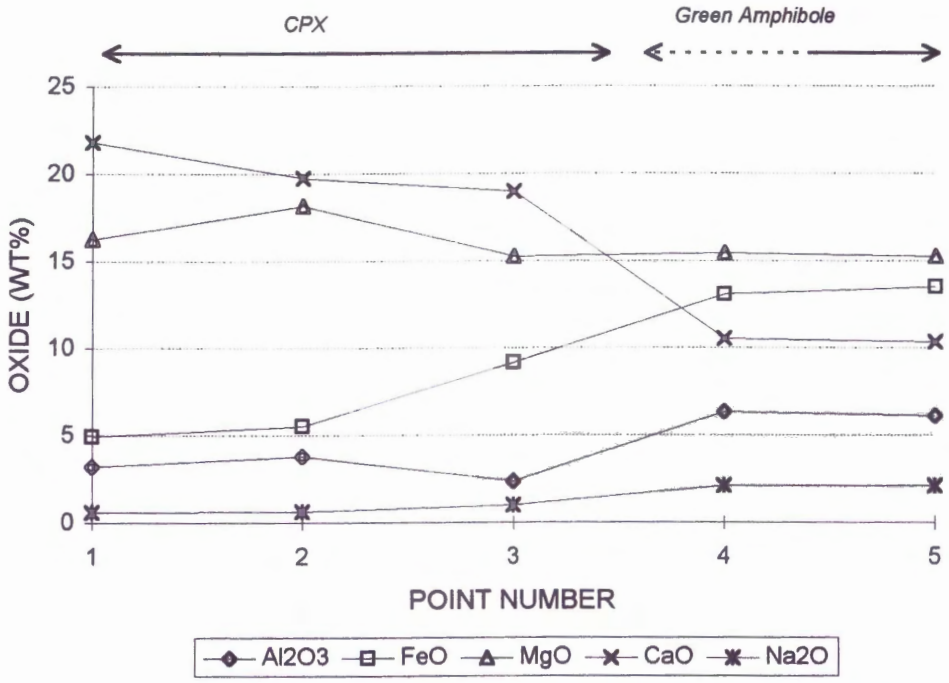

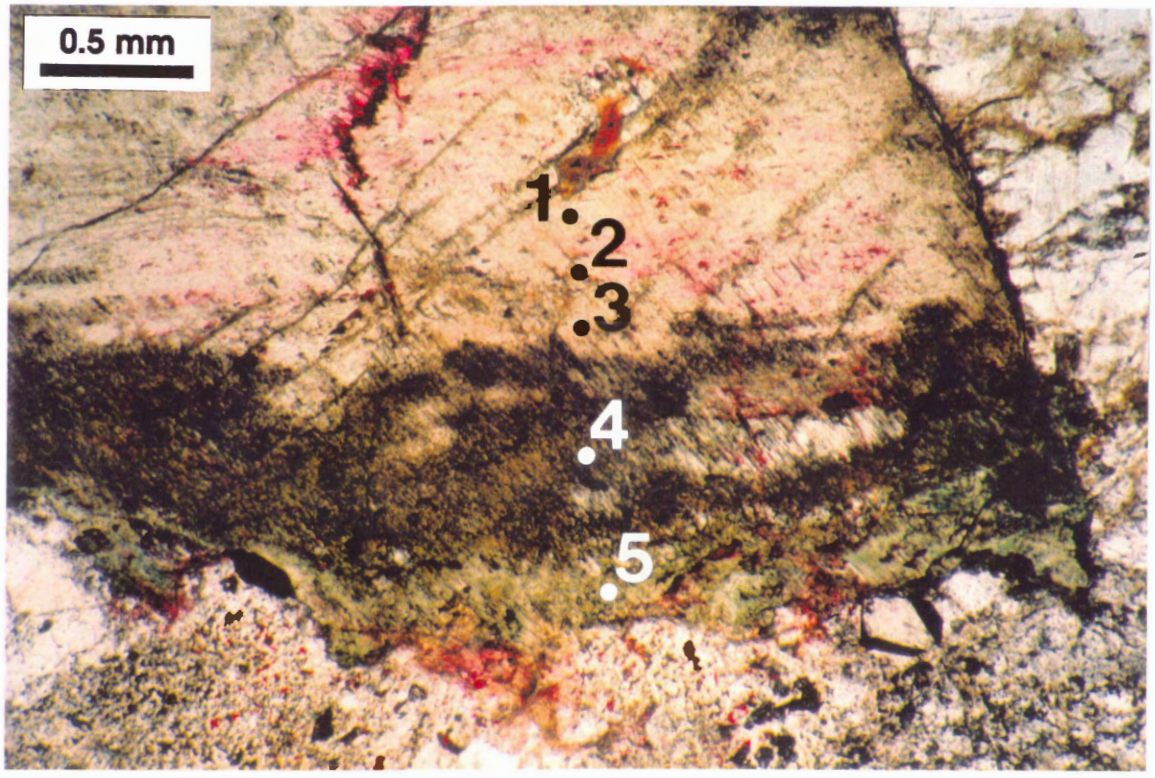

Figure 3.1h

60R-4 112-120 cm Spot 3

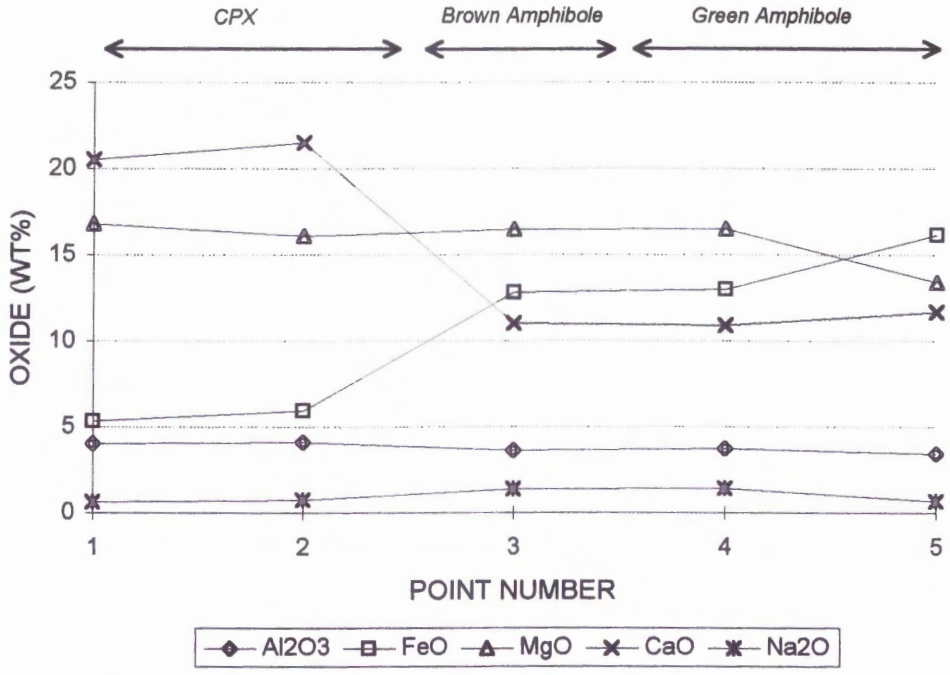

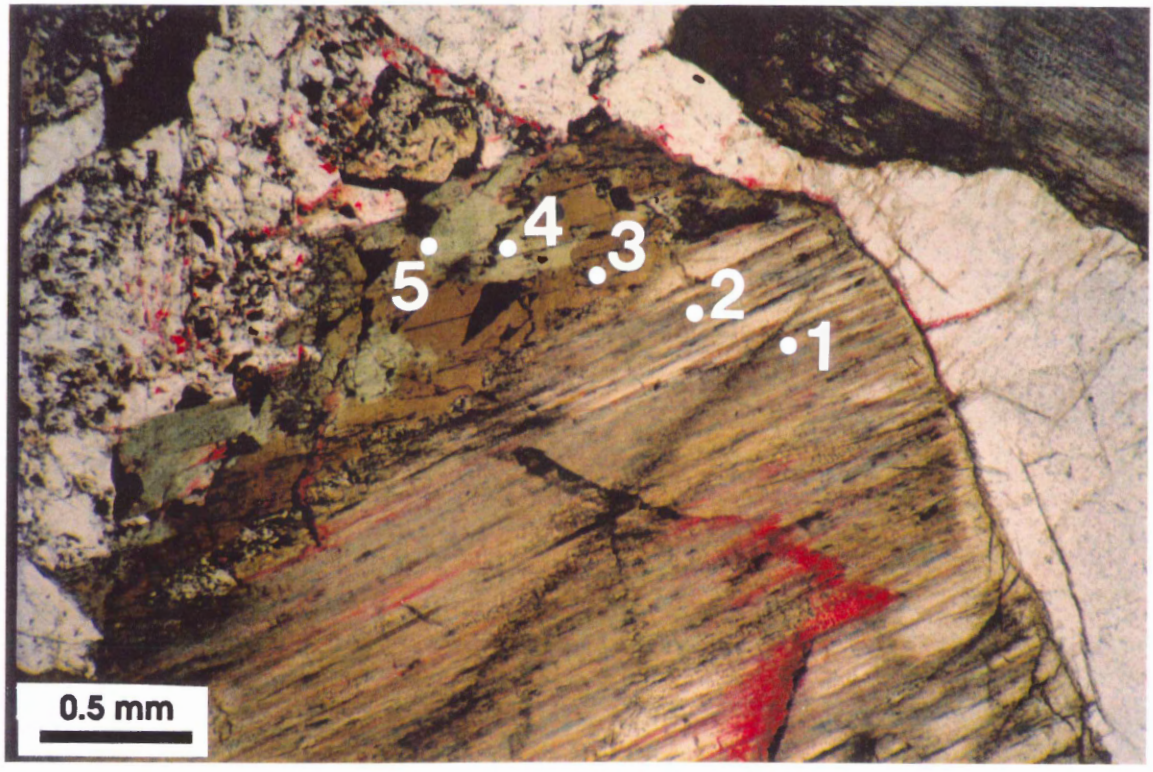

Figure 3.1i

60R-4 112-120 cm Spot 5

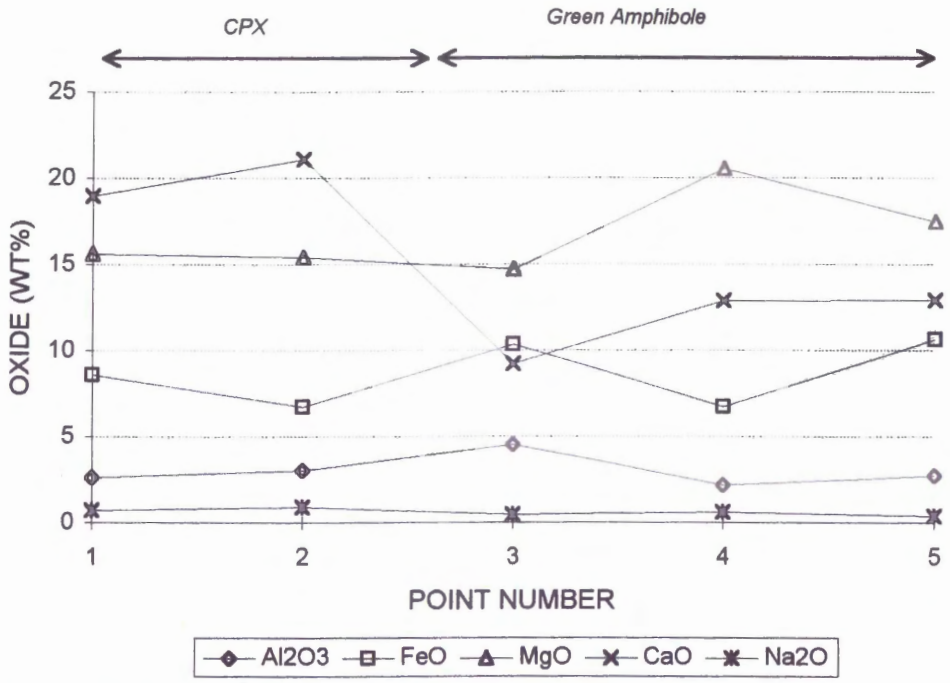

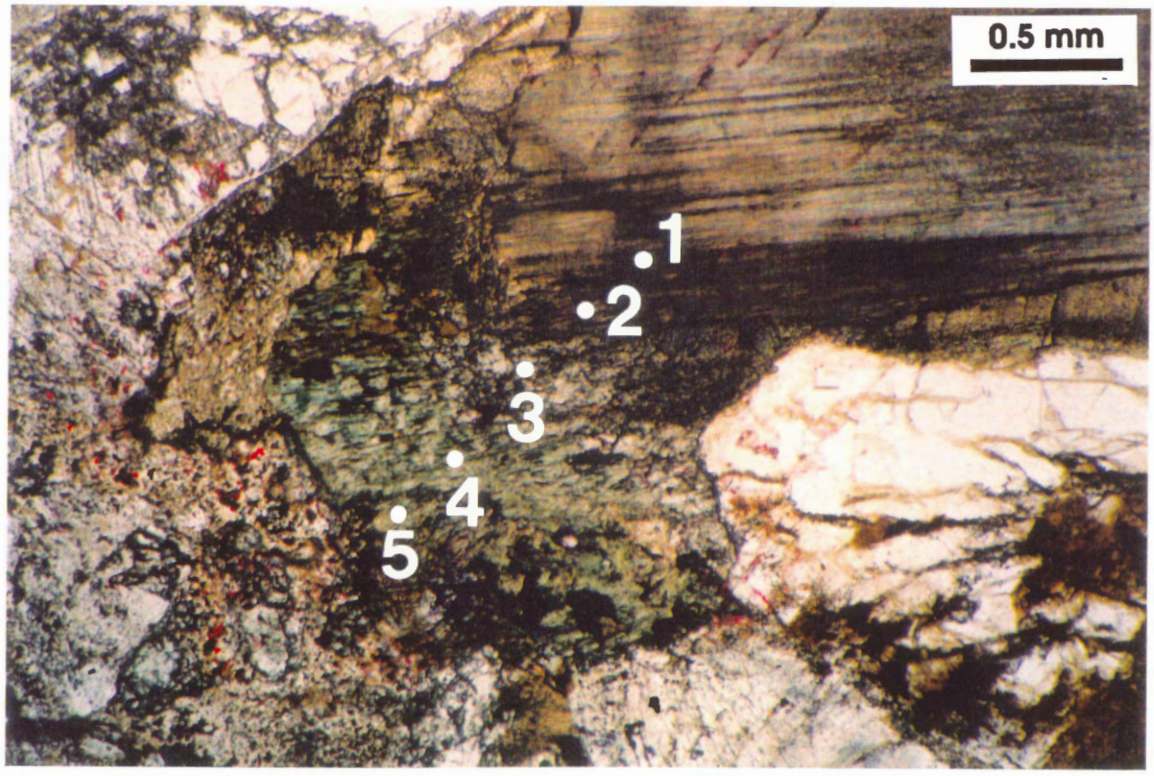

Figure 3.1j

Figure 3.2 Microprobe traverse plots and thin section photographs for alteration of primary plagioclase. Traverse points are marked on thin section photographs below each plot. The inferred mineralogy of each traverse point from petrography is indicated in *italics* on each plot. The distance between traverse points varies. Symbols are the same for all plots. The location of microprobe traverses is indicated on thin section photographs in Appendix 2. See text for explanation.

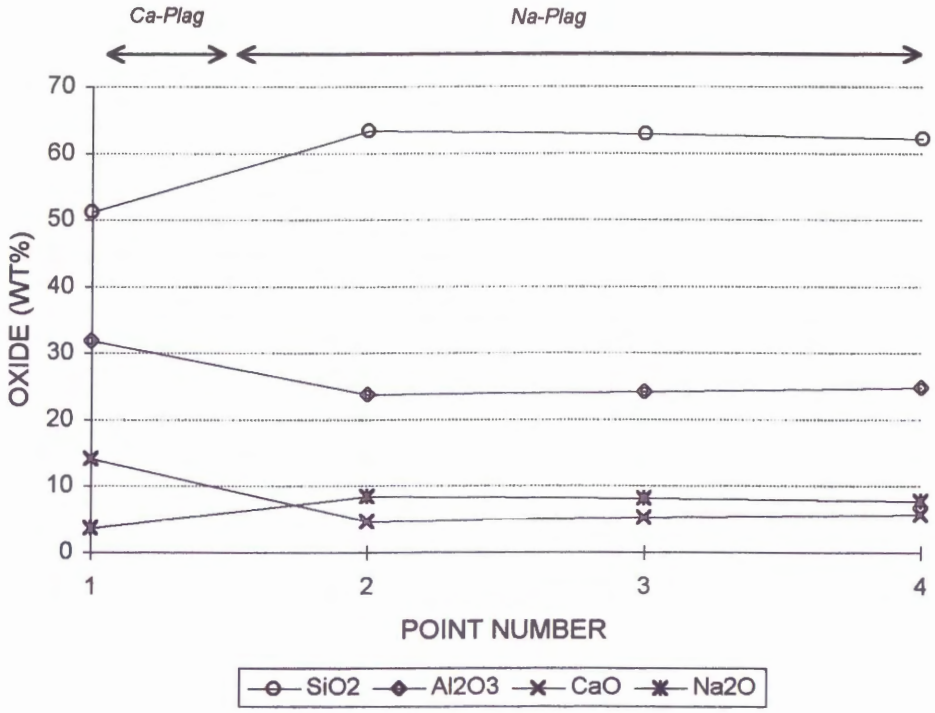
Ca-Plag
Na-Plag
70
60
50
40
30
20
10
0
OXIDE (WT%)
1
2
3
4
POINT NUMBER
SiO2
Al2O3
CaO
Na2O

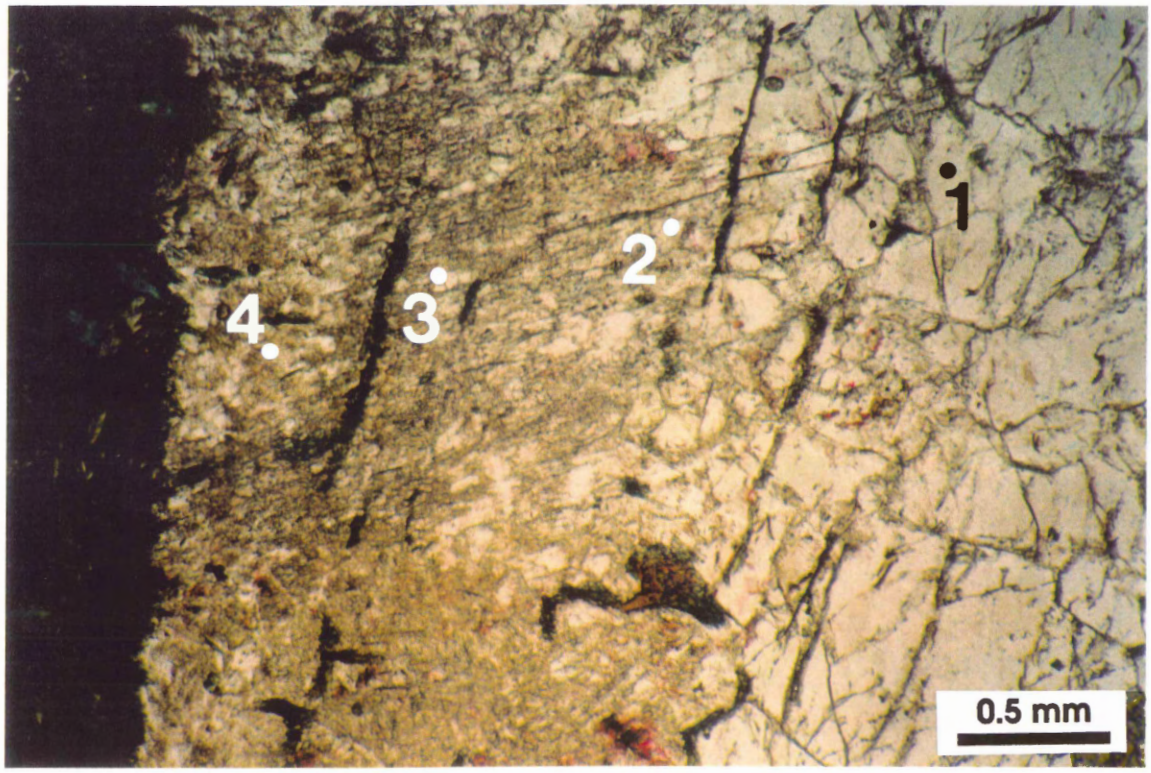
1
2
3
4
0.5 mm

Figure 3.2a

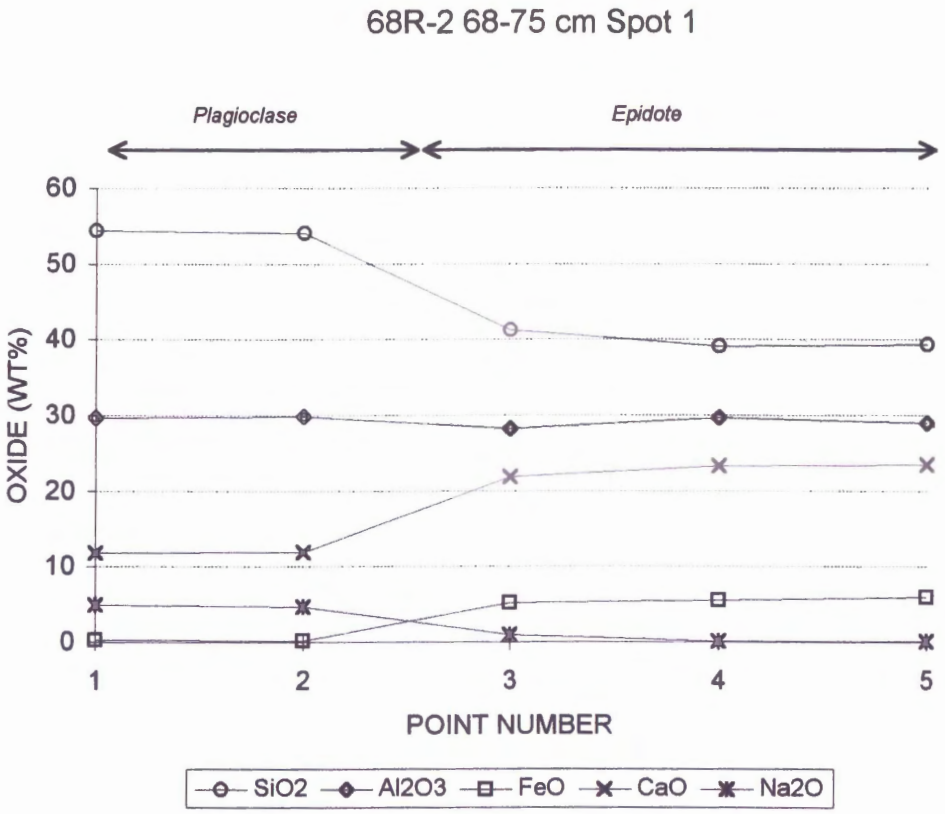
68R-2 68-75 cm Spot 1
Plagioclase
Epidote
60
50
40
30
20
10
0
OXIDE (WT%)
1
2
3
4
5
POINT NUMBER
SiO2
Al2O3
FeO
CaO
Na2O

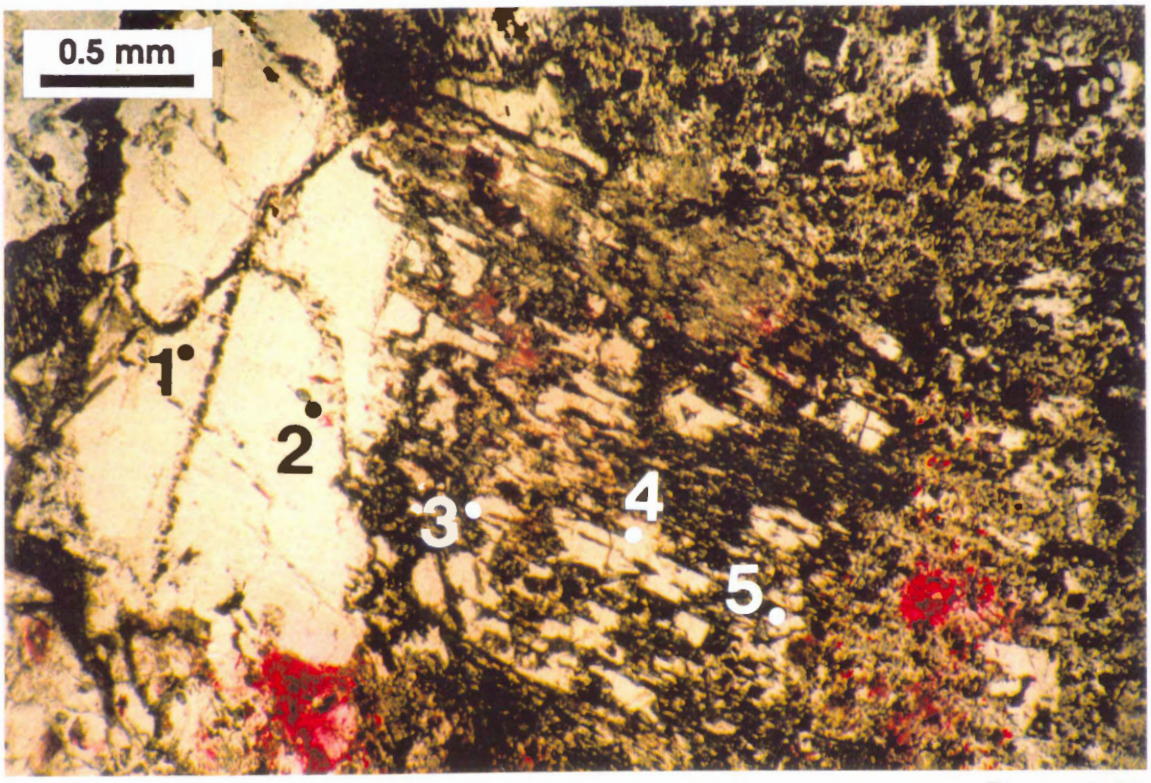
0.5 mm
1
2
3
4
5

Figure 3.2b

3 , 44R-1 (35-47) Spot 3 Point 3, 60R-4 (112-120) Spot 2 Point 4, and 60R-4 (112-120) Spot 3 Point 3]; an increase in MgO [44R-1 (35-47) Spot 1 Point 3]; or changes in both FeO and MgO [44R-1 (35-47) Spot 2 Point 3, 58R-3 (0-8) Spot 1 Point 2, 58R-3 (0-8) Spot 2 Point 2, and 60R-4 (112-120) Spot 5 Point 3].

Several traverses contain multiple analyses in primary clinopyroxene and/or secondary amphibole. Most traverses which contain multiple analyses in primary clinopyroxene display relatively constant chemistry [35R-4 (117-124) Spot 2 Points 1 & 2, 44R-1 (35-47) Spot 1 Points 1 & 2, 44R-1 (35-47) Spot 2 Points 4 &5 , 60R-4 (112-120) Spot 3 Points 1 & 2, and 60R-4 (112-120) Spot 5 Points 1 & 2] although some traverses show slight chemical variation, particularly in CaO, MgO, and FeO [60R-4 (112-120) Spot 2 Points 1 to 3 and 44R-1 (35-47) Spot 3 Points 1 & 2]. Multiple analyses in amphibole are generally more variable than those in primary clinopyroxene, however, three cases also display relatively constant chemistry [35R-4 (117-124) Spot 2 Points 1 & 2, 44R-1 (35-47) Spot 2 Points 3 to 6, and 60R-4 (112-120) Spot 2 Points 4 & 5]. Relatively constant chemistry is also observed in sample 60R-4 (112-120) Spot 3 Points 3 & 4 even though these points are in brown and green amphibole, respectively.

General chemical trends in traverses between primary clinopyroxene and secondary amphibole are also observed. Although CaO values drop at the pyroxene-amphibole transition, they remain relatively constant with only minor variations (less than 5 wt%) in either primary clinopyroxene or secondary amphibole. MgO generally exhibits minor variations (less than 5 wt%) between clinopyroxene and amphibole in traverses . For example, sample 35R-4 (117-124) Spot 2 exhibits almost no change in MgO, however, larger variations (> 5 wt%) are observed in some samples [44R-1 (35-47) Spot 1 and 44R-1 (35-47) Spot 2]. FeO is considerably more varied than MgO in the same traverses. FeO variability is characterized by gradual decreases [58R-3 (0-8) Spot 1], gradual increases [44R-1 (35-47) Spot 3, 60R-4 (112-120) Spot 1, 60R-4 (112-120) Spot 2, and 60R-4 (112-120) Spot 3], variable changes [44R-1 (35-47) Spot 1, 58R-3 (0-8) Spot 2 , and 60R-4 (112-120) Spot 5], and relatively constant values in either primary clinopyroxene or secondary amphibole [35R-4 (117-124) Spot 2 and 44R-1 (35-47) Spot

2]. Al_2O_3 and Na_2O exhibit only small (< 5 wt%) changes in most traverses, although the variability of Al_2O_3 is somewhat larger in sample 44R-1 (35-47) Spot 3. Also, Na_2O is somewhat greater in amphibole analyses than in clinopyroxene analyses, although the increase is not very large (< 2 wt%). In several samples, it is observed that where Al_2O_3 increases, Na_2O also increases, and where Al_2O_3 decreases, Na_2O also decreases [35R-4 (117-124) Spot 2, 44R-1 (35-47) Spot 2, 44R-1 (35-47) Spot 3, 58R-3 (0-8) Spot 1, 60R-4 (112-120) Spot 1, and 60R-4 (112-120) Spot 2]. Changes in SiO_2 are not consistent between pyroxene-amphibole traverses.

3.2.2 Alteration of Plagioclase

A microprobe traverse in sample 32R-2 (86-95) Spot 1 from primary plagioclase to more sodic (altered) plagioclase is characterized by an abrupt increase in SiO_2 and Na_2O and an abrupt decrease in Al_2O_3 and CaO. Multiple analyses in calcic plagioclase were not performed for this sample; however, those in sodic plagioclase exhibit very uniform chemistry [32R-2 (86-95) Spot 1 Points 2 to 4].

A microprobe traverse in sample 68R-2 (68-75) Spot 1 from primary plagioclase to epidote is characterized by an abrupt decrease in SiO_2 and Na_2O and an abrupt increase in FeO and CaO. Multiple analyses in calcic plagioclase [68R-2 (68-75) Spot 1 Points 1 & 2] and epidote [68R-2 (68-75) Spot 1 Points 3 to 5] both exhibit very uniform chemistry. Al_2O_3 remains relatively constant, around 30 wt%, throughout the traverse between primary plagioclase and epidote [68R-2 (68-75) Spot 1].

3.3 DISCUSSION

One reason for performing mineral traverses was to determine if chemical changes between primary and secondary minerals are gradual or abrupt. Mineral traverses between primary plagioclase and secondary minerals (sodic plagioclase and epidote) suggest that this transition is abrupt for oxides with a concentration greater than a few weight percent. Mineral traverses between primary pyroxene and secondary amphibole, however, suggest

that both gradual and abrupt transitions can occur and that the type of transition is different for each individual oxide.

The nature of the chemical change , abrupt or gradual, for various oxides in pyroxene-amphibole traverses, can be explained by certain crystal-chemical limitations. For example, CaO exhibits an abrupt decrease in most pyroxene-amphibole traverses. The abrupt change in CaO is probably due to crystal-chemical limits in the amphibole structure which cannot accommodate the same amount of CaO as clinopyroxene (see Robinson *et al.*, 1982 for a detailed discussion of amphibole chemistry). FeO and MgO, however, are less restricted by the amphibole structure and are observed, in certain traverses, to vary somewhat more gradually from pyroxene to amphibole than CaO. The similarity in variability of Al_2O_3 and Na_2O can also be explained by crystal-chemical limitations. During the replacement of Si by Al in hornblende, charge balance is maintained by the entry of Na (Deer *et al.*, 1992). In addition, the relatively small increase of Na_2O in amphibole over clinopyroxene can be explained by the ability of the amphibole structure to accommodate more Na than clinopyroxene with the observed compositions.

Another goal of the mineral traverses was to determine the chemical variability of individual mineral grains. Multiple microprobe analyses in individual mineral grains suggest that primary minerals such as clinopyroxene and calcic plagioclase have rather constant compositions. Multiple analyses in secondary sodic plagioclase and epidote also exhibit rather constant chemistry. Secondary amphibole, however, is more variable. The variability in amphibole composition is evident in sample 44R-1 35-47 cm Spot 1 in which Points 5 and 6 show distinctly different compositions and yet are taken only microns apart. Some of the variation in amphibole composition could be due to the presence of relict primary clinopyroxene in areas that appear to be altered. However, most of the variability is probably due to the highly variable chemistry of naturally occurring metamorphic amphiboles (Robinson *et al.*, 1982).

Amphibole is the most abundant secondary phase in Hole 735B (Vanko and Stakes, 1991). Amphibole compositions from mineral traverses include tremolite, actinolite, actinolitic hornblende, magnesio-hornblende, and edenitic hornblende, and are

illustrated in Figure 3.3. Amphibole from this study was recalculated using procedures outlined in Stakes *et al.* (1991) who document a similar range of compositions for amphibole replacing pyroxene (Figure 3.4). Previous studies have documented both homogeneous and variable amphibole compositions (Vanko and Stakes, 1991). Variable amphibole compositions probably result from progressive replacement resulting from fluctuations in hydrothermal fluid parameters (such as temperature, pressure, and individual component activities) (Vanko and Stakes, 1991).

The chemical changes documented by the mineral traverses suggest that several oxides were mobile during alteration. The absence of secondary mineral phases near altered primary minerals to balance the observed chemical changes, indicates that alteration probably took place under open system conditions. For example, CaO-rich phases are not found near clinopyroxene grains replaced by amphibole. Some epidote is present which could have taken up excess CaO, however, epidote is only a minor component in these samples (Appendix 2). As a result, CaO was probably lost from the host rock and taken up by the hydrothermal fluid. Similarly, MgO decreases in most pyroxene-amphibole traverses and was probably lost from the host rock. Conversely, Na_2O and FeO were probably gained by the host rock, as indicated by sample 32R-2 (86-95) Spot 1 and pyroxene-amphibole traverses. SiO_2 is variable and was probably both lost and gained by the host rock, depending on the sample. Al_2O_3, however, does not vary substantially (< 5 wt%) and does not increase or decrease consistently in the observed traverses, suggesting Al_2O_3 remained relatively constant during alteration of primary clinopyroxene and plagioclase. The low concentrations (< 1 wt%) of several oxides, including TiO_2, MnO, Cr_2O_3, and K_2O, in mineral traverses preclude determination of trends for these oxides.

Chlorine values in amphibole are somewhat higher in sample 35R-4 (117-124) Spot 2 than the other samples which are from lower in the core (Appendix 5). Magnesio-hornblende in samples from Units I, II, and III commonly contains a few tenths of a percent of chlorine, however, magnesio-hornblende from samples in Units IV, V, and VI contains noticeably less chlorine (Vanko and Stakes, 1991). This could indicate that the

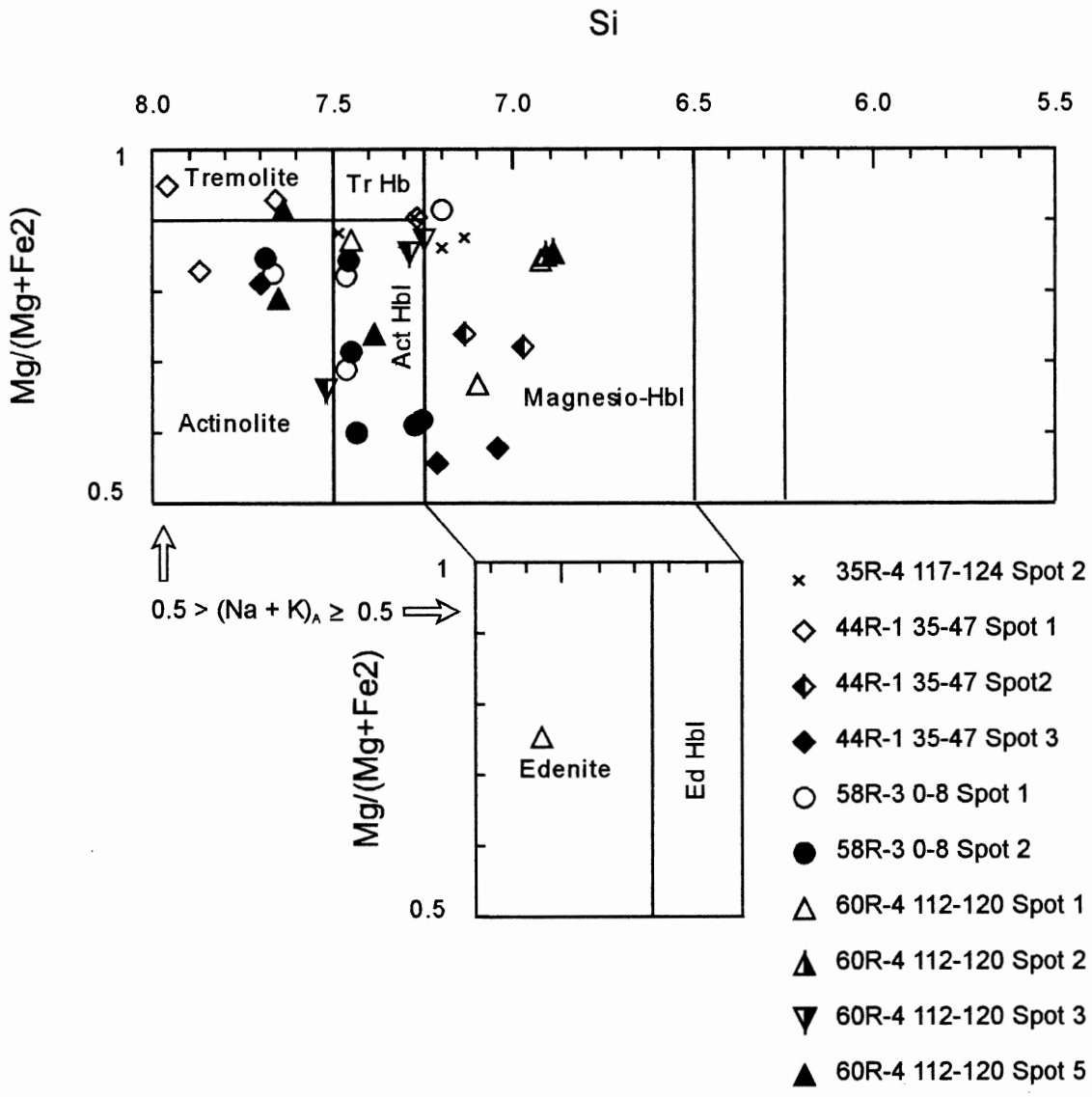

Figure 3.3 Plot of amphibole compositions from mineral traverses. Amphibole recalculations follow procedures used in Stakes *et al.* (1991). Amphibole nomenclature is after Robinson *et al.* (1982). Recalculated amphibole analyses are listed in Appendix 5.

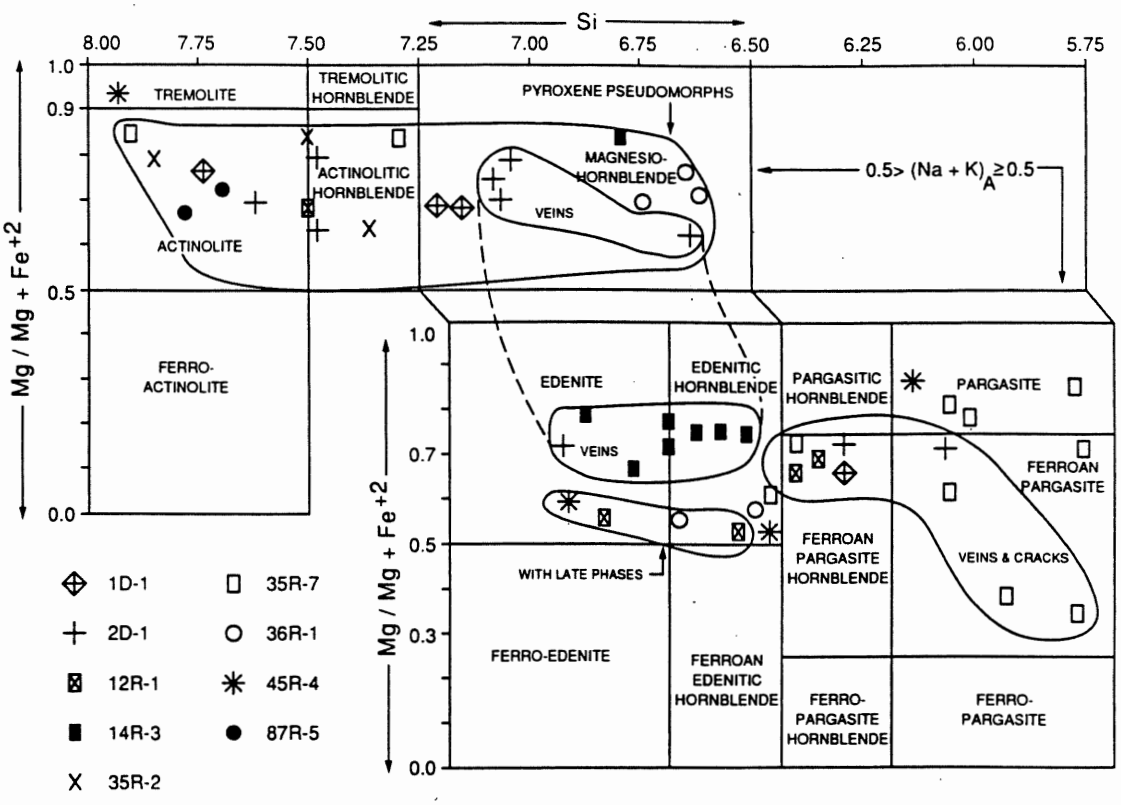

Figure 3.4 Distribution of calcic amphibole compositions from Hole 735B. Amphibole nomenclature is after Robinson *et al.* (1982). Most aluminous pargasite and pargasitic hornblende was found in cracks, veins, and replacing deformed igneous phases in gneissic gabbros. Large vein amphiboles compositions vary from edenitic to magnesio-hornblende, depending on assumptions for recalculation of formula. Actinolite and actinolitic hornblende were common replacements of cores of clinopyroxene porphyroclasts and foliation planes of secondary pyroxene. Hornblendes "with late phases" were observed with apatite and zircon in ferrogabbro. (From Stakes *et al.*, 1991)

fluids from which amphibole formed deep in Hole 735B were less saline (Vanko and Stakes, 1991).

3.4 SUMMARY

Microprobe traverses from primary minerals to secondary minerals along vein boundaries were performed in 6 olivine gabbro samples in order to determine the chemical changes within minerals and between minerals as a result of alteration. Microprobe traverses from primary clinopyroxene to secondary amphibole are characterized by abrupt decreases in CaO and less abrupt, variable changes in other oxides. Microprobe traverses from primary plagioclase to secondary sodic plagioclase and secondary epidote are characterized by abrupt chemical changes. The nature of the chemical changes, abrupt or gradual, can be explained by the crystal-chemical limitations of the primary and secondary mineral structures. Multiple analyses in primary and secondary minerals indicate that primary minerals, secondary plagioclase, and secondary epidote have relatively constant compositions. Secondary amphibole, however, commonly exhibits more varied compositions. The chemical changes documented by mineral traverses suggest that CaO and MgO were lost, FeO and Na_2O were gained, and Al_2O_3 remained relatively constant during alteration. SiO_2 was probably both lost and gained, depending on the sample. Finally, chlorine values in sample 35R-4 (117-124) Spot 2 are higher than those in other samples which could indicate that the salinity of fluids from which amphibole formed decreased with depth in Hole 735B.

Chapter 4

Element Fluxes

4.0 INTRODUCTION

This chapter documents the chemical effects of alteration on host rock adjacent to hydrothermal veins in gabbroic samples recovered from ODP Hole 735B. This is accomplished through a comparison of analyses for fresh and altered whole-rock samples that provides a semi-quantitative estimate of element fluxes. Analyses of 10 altered samples (Table 4.1) are compared with analyses of equivalent fresh samples to determine the mobility of elements within a few centimetres of veins. Three different lithologies are represented: olivine gabbro, oxide olivine gabbro, and disseminated oxide olivine gabbro. A variety of vein types has been specifically chosen in order to determine if element mobility is dependent on lithology or vein type. Full petrographic descriptions and thin section photos of the samples analyzed are presented in Appendix 2.

4.1 ASSUMPTIONS

To calculate element fluxes it is necessary to make certain assumptions regarding the conditions during alteration and what constitutes the fresh equivalent of an altered rock. For example, it is commonly assumed that replacement occurs under conditions of constant volume (Alt and Emmermann, 1985; Thompson, 1983), that certain elements remain immobile, or that ratios of elements are constant during alteration (Gillis, 1986; Appleyard, 1980; Gresens, 1967; Bednarz and Schmincke, 1989). It would be inappropriate to assume that alteration took place under conditions of constant volume for the samples used in this study. Although primary igneous textures are preserved and pseudomorphic replacement of phenocryst phases might suggest little or no changes in volume, the presence of veins in altered samples indicate that small, but significant changes in volume must have taken place. It is therefore necessary to choose a different method

Table 4.1 Recalculated altered whole-rock analyses.

Lithology:	Olivine Gabbro							Disseminated Oxide Olivine Gabbro		Oxide Olivine Gabbro
Sample Number:	22R-1 82-90 cm	31R-3 4-10 cm	35R-4 117-124 cm	44R-1 35-47 cm	58R-3 0-8 cm	63R-6 98-106 cm	72R-3 10-19 cm	41R-1 26-31 cm	41R-3 43-49 cm	54R-4 69-78 cm
SiO_2	51.66	52.71	51.49	51.45	52.35	51.35	52.31	50.84	52.36	46.67
Al_2O_3	14.86	17.40	19.36	19.58	16.13	16.44	16.33	15.57	16.42	12.32
Fe_2O_3	5.72	5.76	3.75	3.67	6.15	5.30	8.77	6.31	8.17	18.79
MgO	11.14	7.86	7.99	8.84	9.13	9.64	7.98	11.56	7.71	4.31
CaO	14.20	12.64	14.56	13.85	13.14	14.77	10.53	13.17	11.40	8.26
Na_2O	1.91	2.95	2.47	2.27	2.53	2.04	3.38	2.05	3.25	4.09
K_2O	0.05	0.07	0.05	0.03	0.04	0.05	0.07	0.03	0.05	0.27
TiO_2	0.31	0.48	0.21	0.22	0.40	0.29	0.46	0.33	0.48	5.02
MnO	0.12	0.10	0.11	0.08	0.12	0.10	0.16	0.12	0.16	0.25
P_2O_5	0.01	0.03	0.01	0.02	0.01	0.01	0.01	0.02	0.01	0.04
Rb	0.2	0.2	0.2	0.2	0.2	0.4	0.4	0.1	0.2	1.4
Sr	127	173	176	172	163	145	161	144	164	167
Y	9	10	6	5	13	7	16	8	13	33
Zr	11	15	6	5	14	8	12	13	16	70
Nb	0.3	0.4	0.2	0.1	0.4	0.1	0.4	0.1	0.2	6.5
LOI	0.90	0.70	1.80	1.00	0.70	1.50	1.50	0.30	1.30	0.00
Total:	100	100	100	100	100	100	100	100	100	100

Analyses have been recalculated on a volatile-free basis. Major oxides are in weight percent, trace elements are in ppm, and LOI is in weight percent.

for the present study. Whatever method is chosen, it is necessary to ensure that validation of the selected procedure is based on independent observations or on geochemical evidence comparing several possible models (Appleyard, 1980). The following sections describe the assumptions made during calculation of element fluxes in this study.

4.1.1 Definition of Fresh Rock

When calculating element fluxes it is critical to define what constitutes the 'fresh' equivalent of an altered rock. Studies of seafloor systems commonly use glass compositions (Gillis, 1986; Alt and Emmermann, 1985); however, this is not possible for the plutonic rocks used in this study. Another method is to use samples that display few or no petrographic signs of alteration. These criteria are problematic because the samples available (for this study) were selected originally to document alteration in core from Hole 735B. Analyses of fresh samples from published data are available (Shipboard Scientific Party, 1989; Dick *et al.*, 1991a), however, they do not always correspond to the same lithological interval from which altered samples have been selected. Where corresponding analyses of fresh and altered samples are available, variability in grain size and textures commonly affect modal mineralogy, which further complicates direct comparison.

In this study, the average of several analyses from 'fresh' samples is used for each of the three represented lithologies (Table 4.2). These include values from the original shipboard XRF analyses (Shipboard Scientific Party, 1989) which have been supplemented by additional analyses conducted at Woods Hole Oceanographic Institution (Dick et al., 1991a). In both cases the main objective was to establish a chemical stratigraphy for the 735B core from representative lithologies (Shipboard Scientific Party, 1989; Dick et al., 1991a). As a rule, the freshest samples were chosen to minimize effects of alteration (Shipboard Scientific Party, 1989).

For each lithology, the number of samples analyzed and standard deviation for each element are given (Table 4.2). The number of samples analyzed, ranging from 9 to 54 for the given lithologies, allows calculation of standard deviations of element analyses. Because of the small sample populations for each lithology, only one standard deviation

Table 4.2 Recalculated average fresh whole-rock analyses

Lithology:	Olivine Gabbro		Disseminated Oxide Olivine Gabbro		Oxide Olivine Gabbro	
		1σ		1σ		1σ
SiO_2	50.87	0.93	52.14	0.99	42.22	3.95
Al_2O_3	17.08	2.20	15.65	1.40	10.79	2.20
Fe_2O_3	5.47	0.70	8.72	0.60	22.89	1.60
MgO	10.14	2.20	8.33	1.10	5.97	1.30
CaO	13.43	1.30	11.00	0.70	8.93	1.10
Na_2O	2.51	0.50	3.31	0.30	2.70	0.70
K_2O	0.04	0.00	0.05	0.00	0.06	0.00
TiO_2	0.34	0.10	0.61	0.20	6.00	2.40
MnO	0.11	0.00	0.17	0.00	0.30	0.10
P_2O_5	0.01	0.00	0.01	0.00	0.15	0.40
Rb	1.4	1.1	1.2	0.1	0.9	0.1
Sr	161	27	179	23	162	26
Y	11	7	14	3	28	19
Zr	22	30	19	10	54	25
Nb	1.0	0.5	0.7	0.2	4.2	1.7
LOI	0.7	0.4	0.3	0.2	0.4	0.2
N	54		10		9	
Total	100		100		100	

Whole-rock analyses are from Dick et al. (1991a). Oxides are in weight percent; trace elements are in ppm. Values have been recalculated on a volatile free basis. 1σ = one standard deviation; N = number of samples.

from the mean is used as a measure of variability. Values within one standard deviation of the mean represent a 67% probability that they are the result of natural variability, such as changes in modal mineralogy and texture. For most elements the standard deviation is low and demonstrates relatively homogeneous whole-rock compositions. However, elements like Ti, Fe, Mg, and the trace elements, particularly in the oxide and disseminated oxide olivine gabbros, show higher standard deviations due to variable modal mineralogy.

This estimate of fresh rock composition was chosen over those discussed earlier for several reasons. Each value is an average of several analyses that incorporate possible compositional variation due to changes in modal mineralogy and texture. Multiple analyses from the same lithology make it possible to determine the chemical variability (standard deviation) in each lithology and to place limits on this variation. Small standard deviations in element analyses indicate that the 'fresh' composition of each lithology is relatively homogeneous. Thus, the values used in this study are believed to closely represent the best approximation of the 'fresh' equivalent of the altered samples analyzed.

4.1.2 Al_2O_3 Immobility

In this study, altered and fresh samples were normalized assuming Al was immobile during alteration. This method was chosen because Al has been shown to be immobile during alteration of mafic rocks by seawater in a number of studies (Gillis, 1986; Alt and Emmermann, 1985; Humphris and Thompson, 1978). TiO_2 versus Al_2O_3 trends for fresh and altered whole-rock analyses from samples used in this study also indicate that TiO_2/Al_2O_3 ratios do not change significantly during alteration (Figure 4.1).

Element-flux calculations based on several elements which are believed to be immobile (Gillis, 1986; Alt and Emmermann, 1985; Humphris and Thompson, 1978; Bednarz and Schmincke, 1989), such as Ti, Al, and Zr, are summarized in Tables 4.3 and 4.4a. Comparison of these calculations shows that fluxes are similar in direction and magnitude for Ti and Al (Figure 4.2). Although titanium has been shown to be immobile during hydrothermal alteration of some oceanic rocks (Gillis, 1986), Ti was not used because Ti mobility is suspected in samples from Hole 735B due to anomalous

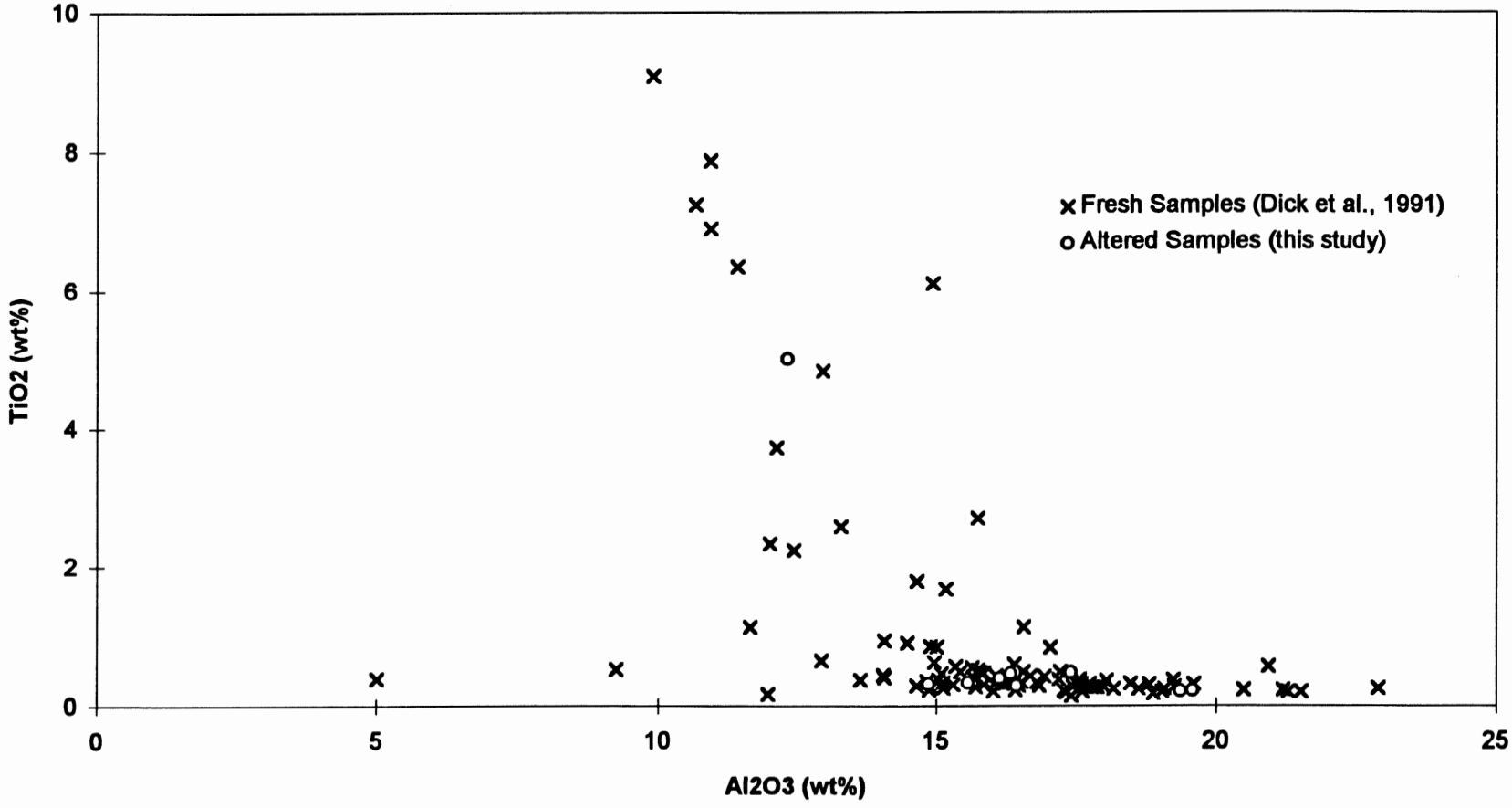

Figure 4.1 Comparison of TiO2 vs Al2O3 for Fresh and Altered Samples.

Table 4.3 Element fluxes normalized to constant Ti and Zr for Hole 735B samples

Lithology:	Olivine Gabbro														Disseminated Oxide Olivine Gabbro				Oxide Olivine Gabbro	
Sample Number:	22R-1 82-90 cm		31R-3 4-10 cm		35R-4 117-124 cm		44R-1 35-47 cm		58R-3 0-8 cm		63R-6 98-106 cm		72R-3 10-19 cm		41R-1 26-31 cm		41R-3 43-49 cm		54R-4 69-78 cm	
Norm:	Ti	Zr	Ti	Zr	Ti	Zr	Ti	Zr	Ti	Zr	Ti	Zr	Ti	Zr	Ti	Zr	Ti	Zr	Ti	Zr
Fv	1.10	2.04	0.71	1.52	1.64	3.64	1.59	4.01	0.87	1.56	1.19	2.63	0.74	1.88	1.88	1.45	1.27	1.18	1.20	0.77
SiO_2	6.11	54.34	-13.20	29.05	33.81	136.75	30.94	155.21	-5.50	31.00	10.35	84.11	-12.11	47.58	43.62	21.44	14.48	9.51	13.64	-6.06
Al_2O_3	-0.68	13.20	-4.64	9.31	14.76	53.46	14.06	61.36	-3.09	8.16	2.52	26.13	-4.97	13.66	13.67	6.88	5.24	3.68	3.96	-1.24
Fe_2O_3	0.85	6.19	-1.35	3.27	0.70	8.19	0.37	9.24	-0.13	4.16	0.86	8.48	1.03	11.04	3.17	0.41	1.67	0.89	-0.40	-8.33
MgO	2.14	12.54	-4.53	1.77	2.99	18.96	3.91	25.27	-2.23	4.14	1.35	15.21	-4.23	4.88	13.45	8.40	1.48	0.75	-0.82	-2.64
CaO	2.24	15.49	-4.39	5.74	10.51	39.61	8.59	42.04	-2.04	7.13	4.17	25.38	-5.63	6.39	13.80	8.06	3.50	2.42	0.96	-2.53
Na_2O	-0.40	1.39	-0.40	1.96	1.55	6.48	1.10	6.57	-0.31	1.45	-0.07	2.86	0.00	3.85	0.56	-0.33	0.83	0.52	2.20	0.47
K_2O	0.02	0.07	0.01	0.07	0.05	0.15	0.01	0.08	-0.01	0.02	0.02	0.09	0.01	0.10	0.01	-0.01	0.01	0.01	0.26	0.15
TiO_2	0.00	0.29	0.00	0.38	0.00	0.42	0.00	0.52	0.00	0.28	0.00	0.41	0.00	0.53	0.00	-0.14	0.00	-0.05	0.00	-2.12
MnO	0.03	0.14	-0.04	0.04	0.08	0.31	0.02	0.22	-0.01	0.08	0.01	0.16	0.01	0.20	0.06	0.01	0.04	0.02	0.00	-0.10
P_2O_5	0.00	0.01	0.01	0.04	0.01	0.03	0.02	0.07	0.00	0.01	0.00	0.02	0.00	0.01	0.03	0.02	0.00	0.00	-0.10	-0.12
Rb	-1.2	-1.1	-1.3	-1.2	-1.1	-0.8	-1.2	-0.8	-1.3	-1.2	-1.0	-0.4	-1.1	-0.6	-0.9	-1.0	-1.0	-1.0	0.7	0.2
Sr	-21	98	-38	101	129	481	112	527	-20	94	12	220	-42	142	92	29	29	14	38	-33
Y	-1	8	-4	4	-2	10	-4	8	0	9	-2	9	1	20	1	-2	3	2	11	-3
Zr	-10	0	-12	0	-12	0	-13	0	-10	0	-12	0	-13	0	6	0	2	0	29	0
Nb	-0.7	-0.4	-0.7	-0.4	-0.8	-0.4	-0.9	-0.8	-0.6	-0.4	-0.9	-0.8	-0.7	-0.2	-0.4	-0.5	-0.5	-0.5	3.6	0.8

Major oxides are in g/100g and trace elements ar in ppm. - is a relative loss; + is a relative gain. Fv is the calculated volume factor. Norm refers to the element used to normalize the data.

Figure 4.2 Comparison of major-element fluxes for samples from Hole 735B (in g/100g). Values are from Table 4.3 and Table 4.4a. Fluxes have been calculated assuming constant Al (black), Ti (stippled), and Zr (white). Open bars indicate values greater than the limits of the Y-axis. Patterns are the same for all plots.

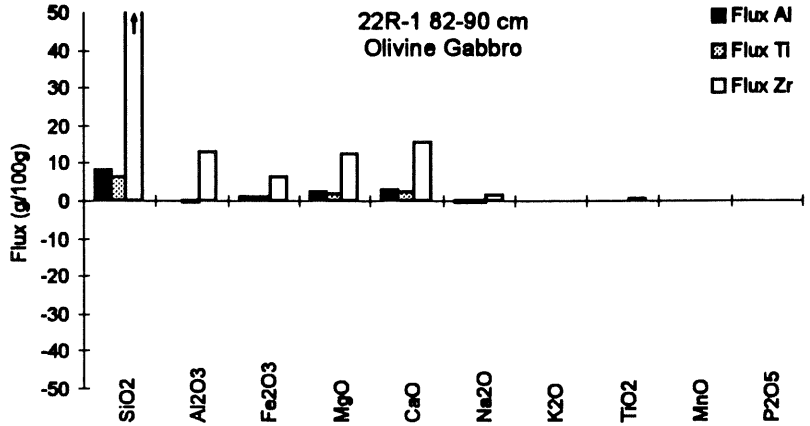

Figure 4.2a

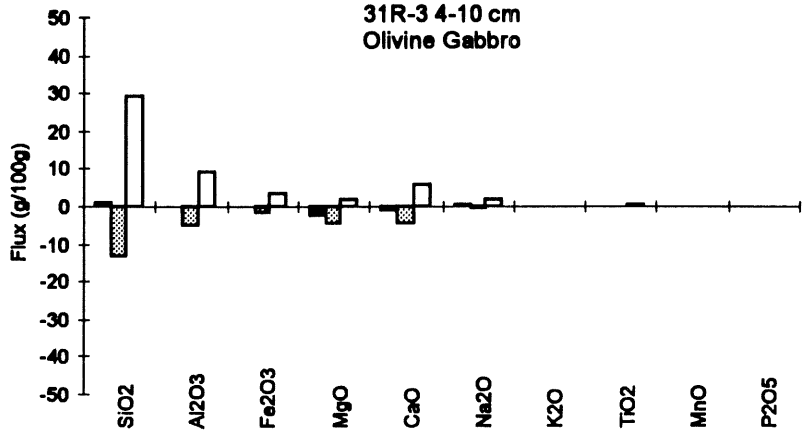

Figure 4.2b

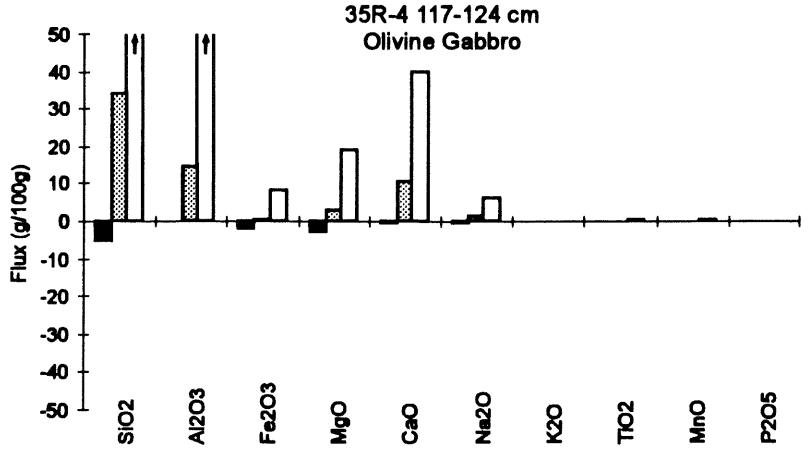

Figure 4.2c

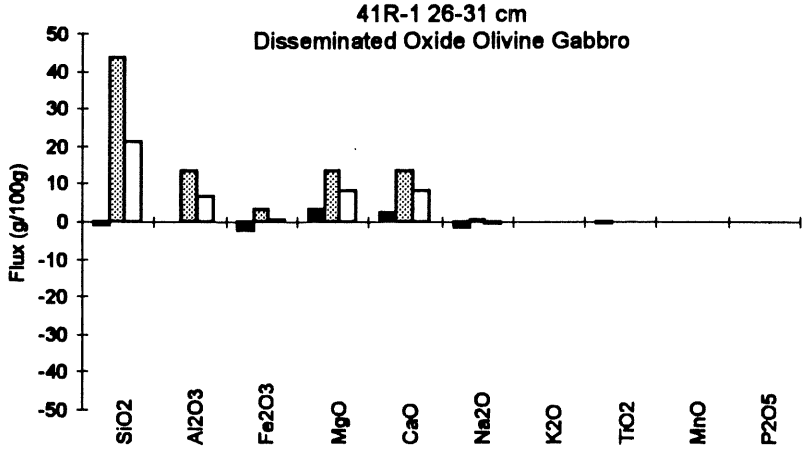

Figure 4.2d

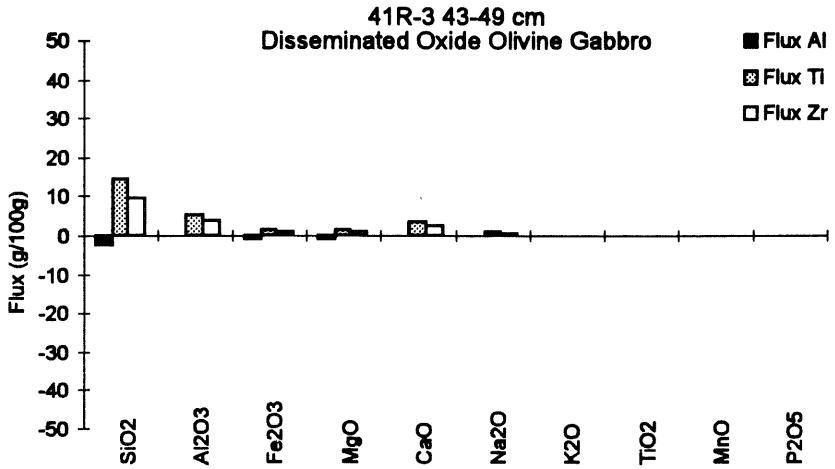

Figure 4.2e

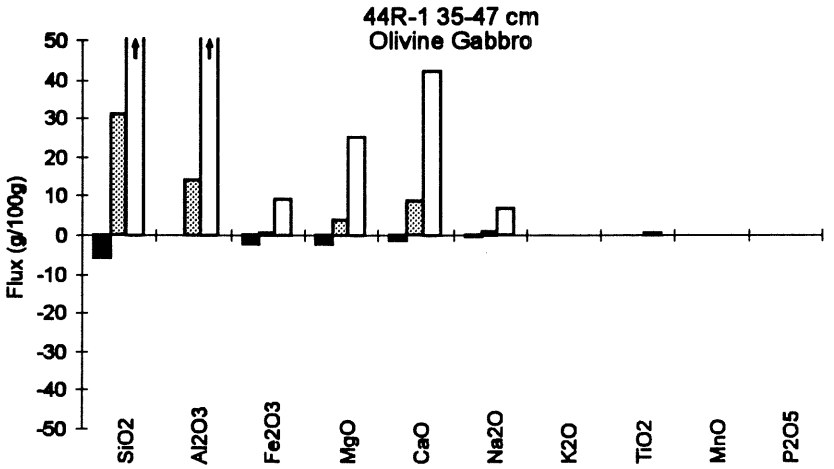

Figure 4.2f

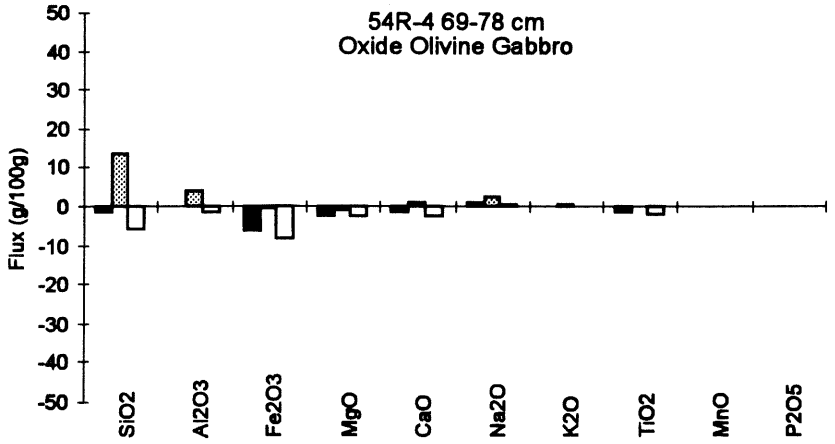

Figure 4.2g

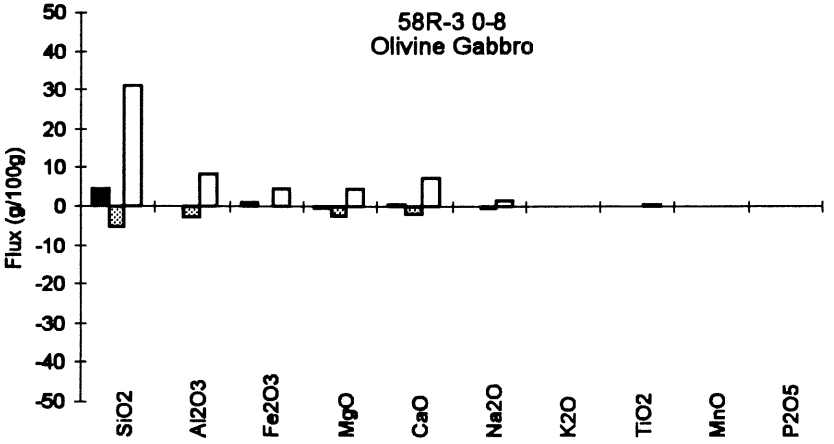

Figure 4.2h

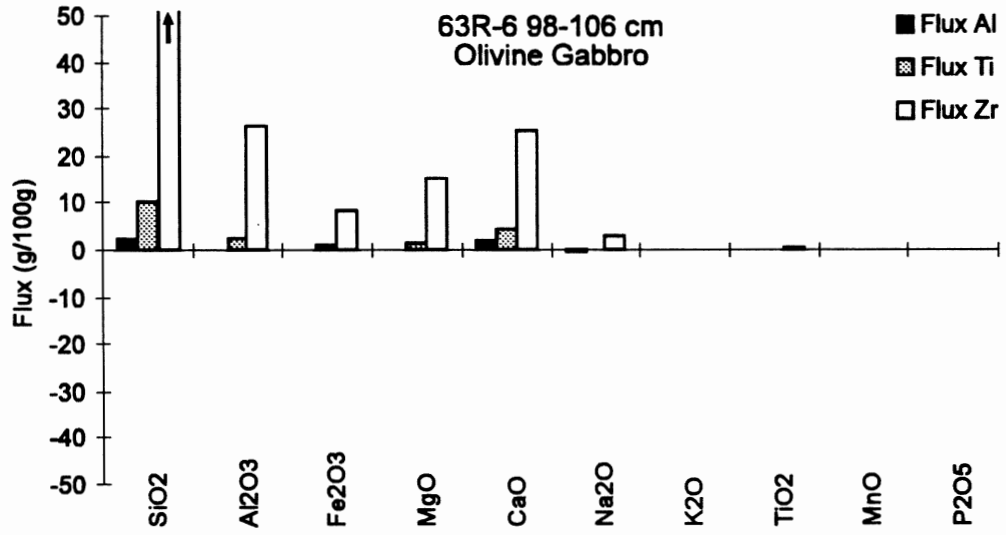

Figure 4.2i

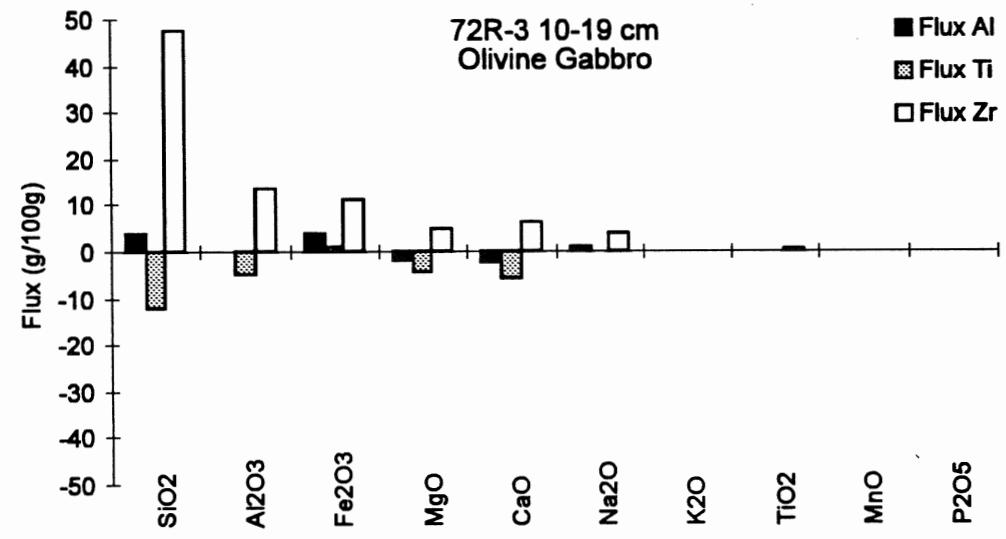

Figure 4.2j

concentrations of Fe-Ti oxides in shear zones (Dick et al., 1991a). Ti concentrations are also relatively small and highly dependent on modal oxide content, so that small variations in chemistry could introduce errors in calculated fluxes. Zr is another element which is believed to be immobile (Bednarz and Schmincke, 1989). However, this element was not used because of the variable modal abundance of zircon in samples from Hole 735B.

Element fluxes calculated assuming constant Al agree with independent petrological observations and analyses of the altered samples. Mineral traverses from primary minerals (pyroxene and plagioclase) to secondary minerals (amphibole, sodic plagioclase, and epidote) along vein boundaries indicate that Al remains relatively constant (see Chapter 3). It should be noted that centimetre-scale Al mobilization has been documented in several studies (Anderson and Burnham, 1983; Baumgartner and Eugster, 1988; Dipple et al., 1990). Local Al mobilization in samples from Hole 735B is suggested by the presence of aluminous phases such as clays and zeolites (see Appendix 2). This, however, is believed to be minor for the reasons outlined above.

4.2 METHODS

Ten altered whole-rock samples were analyzed using X-ray fluorescence (XRF) for major oxide compositions and inductively coupled plasma mass spectrometry (ICP-MS) for trace element abundances (Table 4.1). XRF analyses were performed at the Regional Geochemical Centre, St. Mary's University, and ICP-MS analyses were performed at the Memorial University of Newfoundland. A brief description of analytical procedures are outlined in Appendix 1.

4.2.1 Sample Selection

The main objective of the sampling strategy was to determine the chemical effects of alteration on host rock samples adjacent to various vein types. The samples used in this study are comprised of core slabs of various sizes from the 735B core (Figure 4.3). In order to minimize the problem of representative sampling of medium to coarse-grained

Figure 4.3 Element flux sample photographs. Each sample represents a slab cut from the 735B core. Veins were removed from each sample and the remaining host-rock was analyzed using the procedures outlined in Appendix 1. Some samples show evidence of host-rock alteration proximal to veins. Rock types and vein assemblages are summarized in Table 4.5. Sample numbers and scales appear in each photograph.

Figure 4.3a

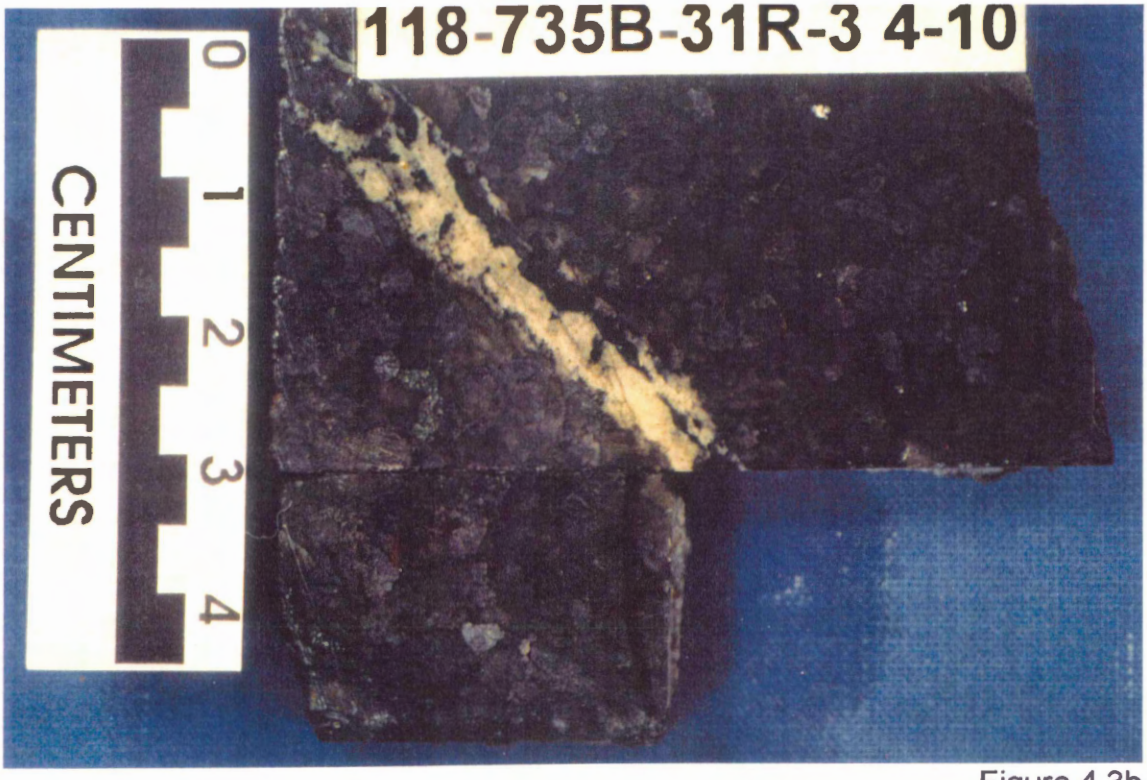

Figure 4.3b

Figure 4.3c

Figure 4.3d

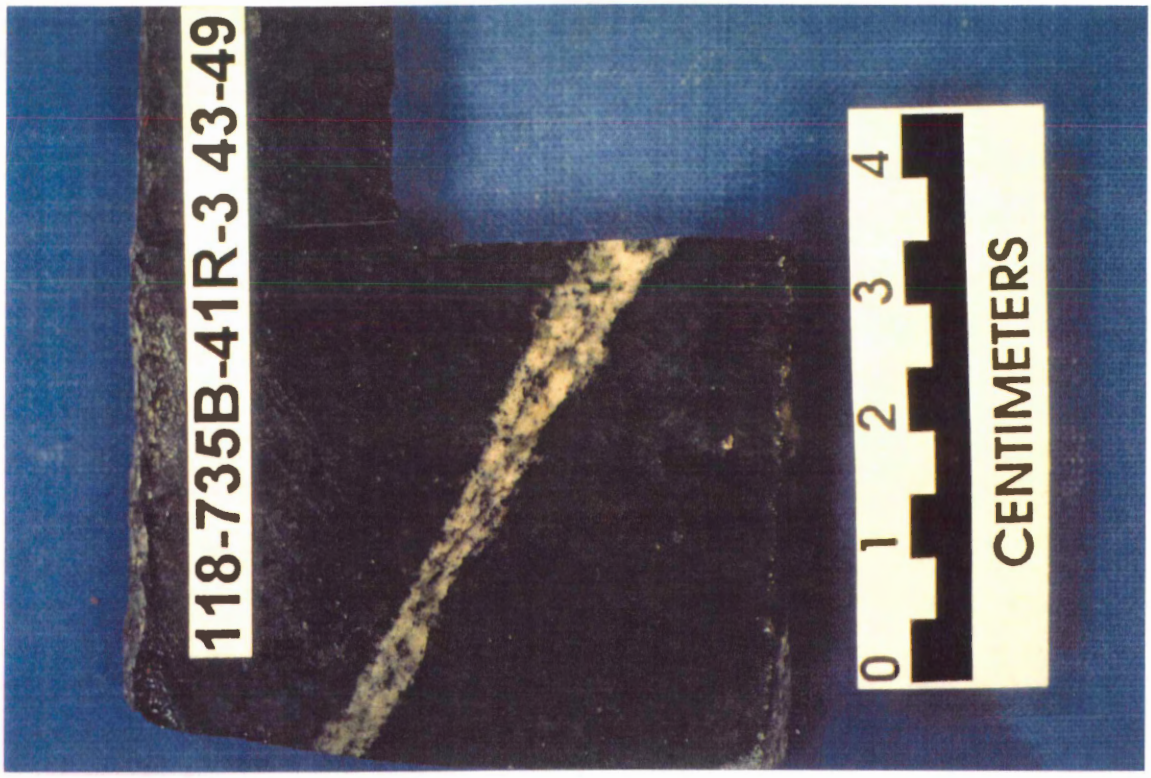

Figure 4.3e

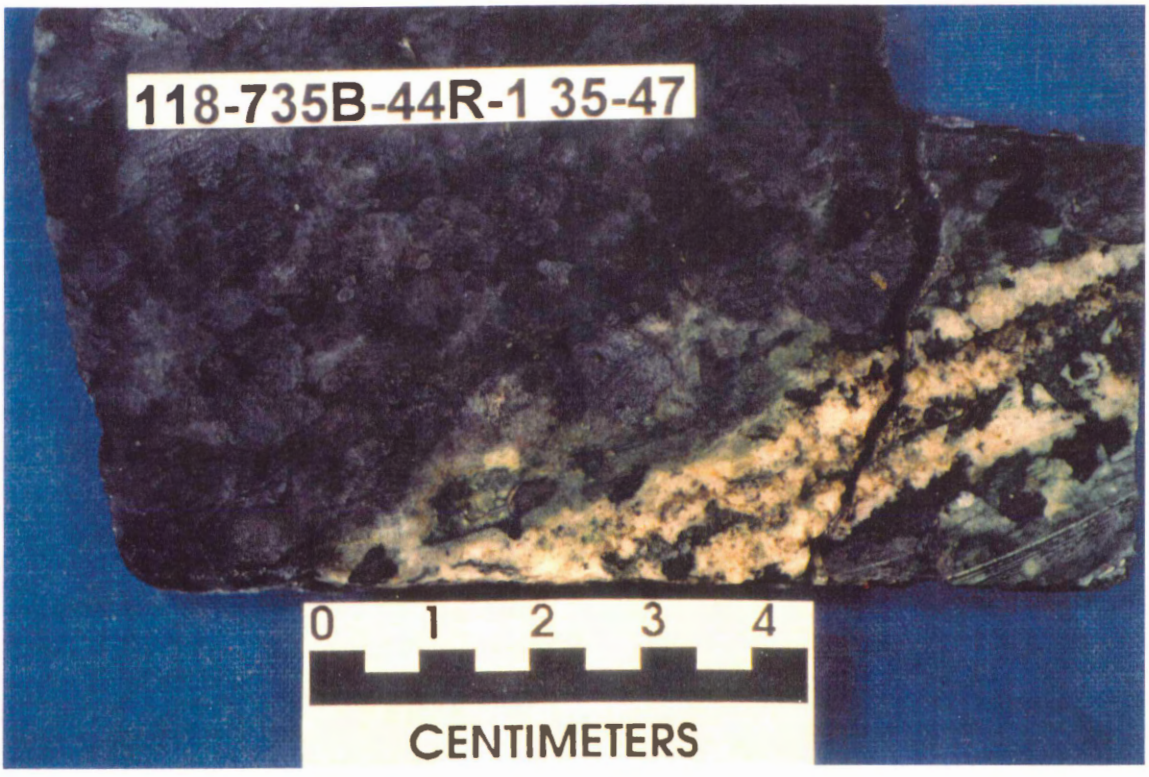

Figure 4.3f

Figure 4.3g

Figure 4.3h

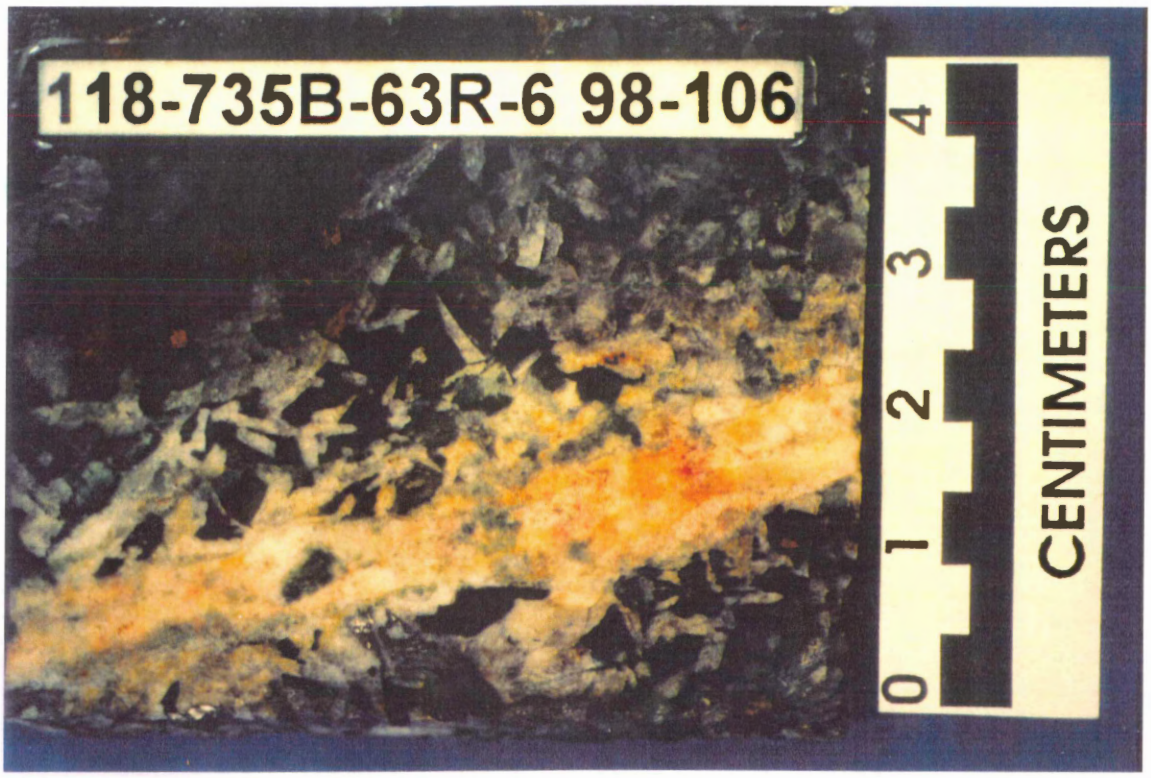

Figure 4.3i

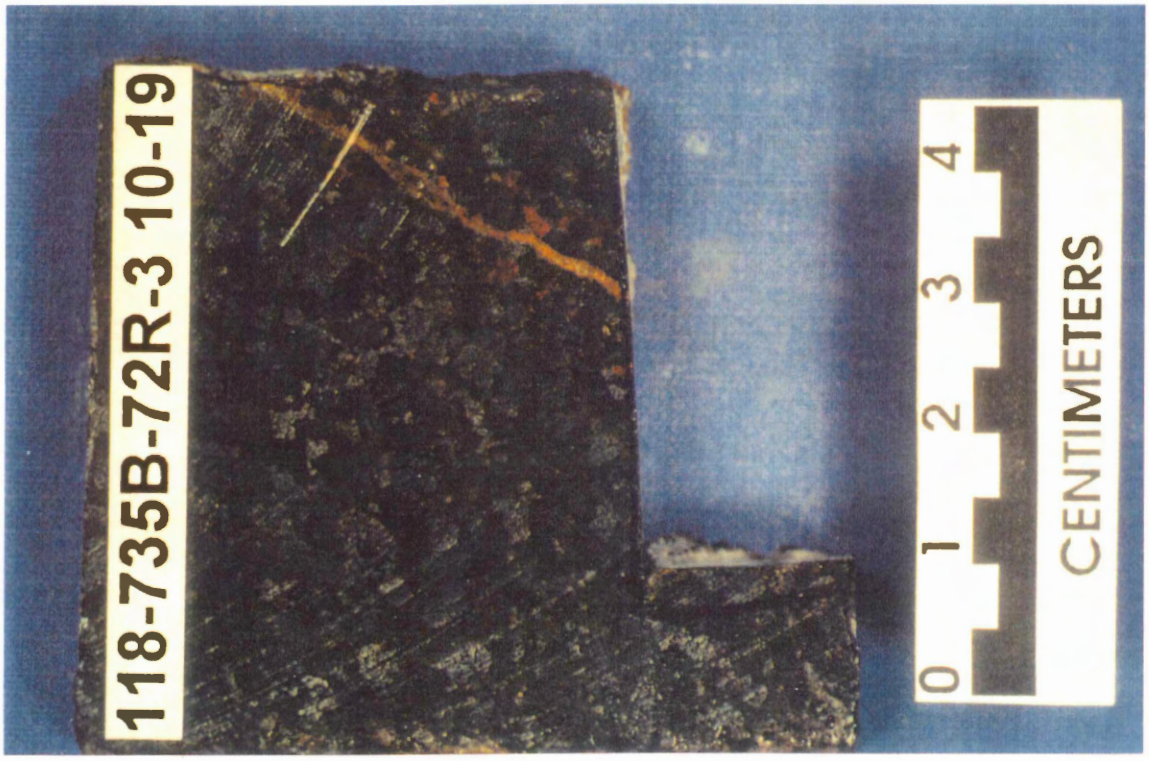

Figure 4.3j

plutonic rocks, only the largest samples with clearly defined veins were selected for whole-rock analysis. As a result, only three different lithologies are represented: olivine gabbro, oxide olivine gabbro, and disseminated oxide olivine gabbro. Some of the samples are coarse- to very coarse-grained, which may preclude representative sampling given the relatively small sample sizes allowed by ODP. Samples ranged from 25 to 50 grams.

4.2.2 Sampling Method

In order to analyze the chemical effects of alteration on host rock near veins, it was necessary to remove the veins from the samples (Figure 4.3). Before the vein was removed, a small strip, which included a portion of the vein, was removed and saved. The vein was then removed from the remaining sample. Care was taken to sample as close to the vein as possible without including vein material. The remaining sample was prepared according to the methods outlined in Appendix 1. Each sample contains material within a few centimetres of the vein. It was not possible to sample the same distance away from individual veins in every case because of the small sample sizes. Instead, the amount of host rock is different for each sample.

4.3 CALCULATIONS

Element fluxes were calculated using the method of Gresens (1967). The following formula (Gresens, 1967 - equation 14) was used:

$$100\left[fv \times \left(\frac{g_B}{g_A}\right) \times c_n^B - c_n^A\right] = x_n \qquad 4.1$$

In this equation, rock A is altered to rock B with specific gravities g_A and g_B, respectively. fv is the volume factor by which the volume of the fresh rock must be multiplied in order to obtain the volume of the altered rock. If $fv > 1$ then alteration takes place with a

volume increase. If $fv < 1$ then alteration takes place with a volume decrease. $fv = 1$ describes a special case when alteration is volume for volume. c_n^Z is the weight fraction of component n in rock Z which is known from chemical analysis. Finally, x_n is the amount of component n lost or gained which is termed the flux.

Equation 4.1 has two unknowns. Since it is assumed that Al is immobile, the value of $x_{Al_2O_3}$ can be set to zero and the equation can then be reduced to solve for fv. Equation 4.1 becomes:

$$fv = \frac{c^A_{Al_2O_3}}{c^B_{Al_2O_3} \times \left(\frac{g_B}{g_A}\right)} \qquad 4.2$$

By combining equation 4.2 and equation 4.1 the specific gravity terms cancel and the equation reduces to:

$$100\left[\left(\frac{c^A_{Al_2O_3}}{c^B_{Al_2O_3}}\right) \times c^B_n - c^A_n\right] = x_n \qquad 4.3$$

4.4 RESULTS

Element fluxes calculated using Equation 4.3 for 735B samples are summarized in Table 4.4 which includes element fluxes calculated from mean primary values (Table 4.4a), mean primary values plus one standard deviation (Table 4.4b), and mean primary values minus one standard deviation (Table 4.4c). Each of these calculated values of element flux is identified by a different pattern in Figure 4.4. This provides a quick way of estimating the variation in element flux values with changes in primary composition. Of the ten samples

Table 4.4a Element fluxes for Hole 735B samples calculated from mean primary values

Lithology:	Olivine Gabbro							Disseminated Oxide Olivine Gabbro		Oxide Olivine Gabbro
Sample Number:	22R-1 82-90 cm	31R-3 4-10 cm	35R-4 117-124 cm	44R-1 35-47 cm	58R-3 0-8 cm	63R-6 98-106 cm	72R-3 10-19 cm	41R-1 26-31 cm	41R-3 43-49 cm	54R-4 69-78 cm
Fv	1.15	0.98	0.88	0.87	1.06	1.04	1.05	1.01	0.95	0.88
SiO_2	8.47	0.84	-5.45	-6.01	4.54	2.47	3.82	-1.02	-2.22	-1.35
Fe_2O_3	1.11	0.19	-2.16	-2.26	1.05	0.05	3.71	-2.38	-0.94	-6.44
MgO	2.65	-2.43	-3.10	-2.43	-0.48	-0.13	-1.80	3.30	-0.98	-2.20
CaO	2.89	-1.02	-0.59	-1.35	0.48	1.91	-2.42	2.24	-0.14	-1.70
Na_2O	-0.31	0.38	-0.33	-0.53	0.17	-0.39	1.02	-1.24	-0.21	0.88
K_2O	0.02	0.03	0.01	-0.01	0.00	0.01	0.03	-0.02	0.00	0.17
TiO_2	0.01	0.13	-0.16	-0.15	0.08	-0.04	0.14	-0.29	-0.15	-1.61
MnO	0.03	-0.01	-0.01	-0.04	0.02	0.00	0.06	-0.05	-0.01	-0.08
P_2O_5	0.00	0.02	0.00	0.01	0.00	0.00	0.00	0.01	0.00	-0.11
Rb	-1.2	-1.2	-1.3	-1.3	-1.2	-1.0	-0.9	-1.1	-1.0	0.3
Sr	-15	8	-6	-11	12	-11	7	-34	-23	-16
Y	0	-1	-6	-7	3	-3	6	-6	-1	1
Zr	-10	-8	-17	-17	-7	-13	-10	-6	-4	7
Nb	-0.7	-0.6	-0.9	-0.9	-0.6	-0.9	-0.5	-0.6	-0.5	1.5

Element fluxes are calculated assuming constant aluminum. Major oxides are in g/100g and trace elements are in ppm. Fv is the calculated volume factor.
- is a relative loss; + is a relative gain. See text for discussion.

Table 4.4b Element fluxes for Hole 735B samples calculated from mean primary values plus 1 standard deviation

Lithology:	Olivine Gabbro							Disseminated Oxide Olivine Gabbro		Oxide Olivine Gabbro
Sample Number:	22R-1 82-90 cm	31R-3 4-10 cm	35R-4 117-124 cm	44R-1 35-47 cm	58R-3 0-8 cm	63R-6 98-106 cm	72R-3 10-19 cm	41R-1 26-31 cm	41R-3 43-49 cm	54R-4 69-78 cm
Fv	1.30	1.11	1.00	0.98	1.19	1.17	1.18	1.10	1.04	1.05
SiO_2	15.19	6.58	-0.53	-1.16	10.74	8.42	9.94	2.56	1.25	3.03
Fe_2O_3	-0.08	-1.12	-3.77	-3.89	-0.15	-1.28	2.85	-3.52	-1.95	-11.69
MgO	2.10	-3.64	-4.39	-3.64	-1.44	-1.03	-2.93	3.24	-1.42	-2.73
CaO	3.69	-0.73	-0.23	-1.10	0.98	2.59	-2.30	2.72	0.14	-1.32
Na_2O	-0.53	0.25	-0.55	-0.78	0.02	-0.61	0.98	-1.36	-0.23	0.91
K_2O	0.03	0.04	0.01	-0.01	0.01	0.02	0.04	-0.02	0.00	0.22
TiO_2	-0.04	0.09	-0.24	-0.23	0.03	-0.11	0.10	-0.46	-0.31	-3.12
MnO	0.05	0.00	0.00	-0.03	0.03	0.01	0.08	-0.04	0.00	-0.14
P_2O_5	0.00	0.02	0.00	0.01	0.00	0.00	0.00	0.01	0.00	-0.51
Rb	-2.3	-2.3	-2.3	-2.4	-2.3	-2.1	-2.0	-1.1	-1.1	0.4
Sr	-23	4	-12	-18	7	-18	2	-44	-32	-12
Y	-6	-7	-12	-13	-3	-9	1	-8	-3	-13
Zr	-38	-36	-46	-47	-35	-42	-38	-14	-12	-5
Nb	-1.1	-1.0	-1.3	-1.4	-1.0	-1.4	-1.0	-0.7	-0.7	0.9

Element fluxes are calculated assuming constant aluminum. Major oxides are in g/100g and trace elements are in ppm. Fv is the calculated volume factor.
- is a relative loss; + is a relative gain. See text for discussion.

Table 4.4c Element fluxes for Hole 735B samples calculated from mean primary values minus 1 standard deviation

Lithology:	Olivine Gabbro							Disseminated Oxide Olivine Gabbro		Oxide Olivine Gabbro
Sample Number:	22R-1 82-90 cm	31R-3 4-10 cm	35R-4 117-124 cm	44R-1 35-47 cm	58R-3 0-8 cm	63R-6 98-106 cm	72R-3 10-19 cm	41R-1 26-31 cm	41R-3 43-49 cm	54R-4 69-78 cm
Fv	1.00	0.85	0.77	0.76	0.92	0.90	0.91	0.92	0.87	0.70
SiO_2	1.76	-4.89	-10.37	-10.86	-1.67	-3.47	-2.30	-4.61	-5.70	-5.74
Fe_2O_3	2.30	1.49	-0.55	-0.64	2.24	1.37	4.56	-1.23	0.08	-1.18
MgO	3.20	-1.23	-1.81	-1.23	0.47	0.78	-0.68	3.36	-0.54	-1.67
CaO	2.08	-1.32	-0.94	-1.61	-0.01	1.23	-2.54	1.75	-0.41	-2.07
Na_2O	-0.09	0.51	-0.11	-0.29	0.33	-0.16	1.07	-1.12	-0.19	0.85
K_2O	0.01	0.02	0.00	-0.02	0.00	0.01	0.03	-0.02	-0.01	0.13
TiO_2	0.07	0.17	-0.08	-0.08	0.12	0.02	0.18	-0.11	0.01	-0.11
MnO	0.01	-0.02	-0.02	-0.05	0.00	-0.02	0.04	-0.06	-0.03	-0.02
P_2O_5	0.00	0.02	0.00	0.01	0.00	0.00	0.00	0.01	0.00	0.28
Rb	-0.1	-0.2	-0.2	-0.2	-0.2	0.0	0.1	-1.0	-0.9	0.2
Sr	-7	13	1	-4	16	-3	12	-25	-14	-19
Y	5	4	0	-1	8	3	11	-3	1	14
Zr	19	21	13	12	21	16	19	3	5	19
Nb	-0.2	-0.1	-0.4	-0.5	-0.1	-0.4	-0.1	-0.4	-0.4	2.0

Element fluxes are calculated assuming constant aluminum. Major oxides are in g/100g and trace elements are in ppm. Fv is the calculated volume factor.
- is a relative loss; + is a relative gain. See text for discussion.

Figure 4.4 Element fluxes calculated assuming constant aluminum for samples from Hole 735B (values are from Table 4.4). Major-element fluxes are in g/100g and trace-element fluxes are in ppm. Values have been calculated for mean fresh analyses (stippled), mean minus one standard deviation (black), and mean plus one standard deviation (white). Open bars indicate values greater than the limit of the Y-axis. Patterns are the same for all plots.

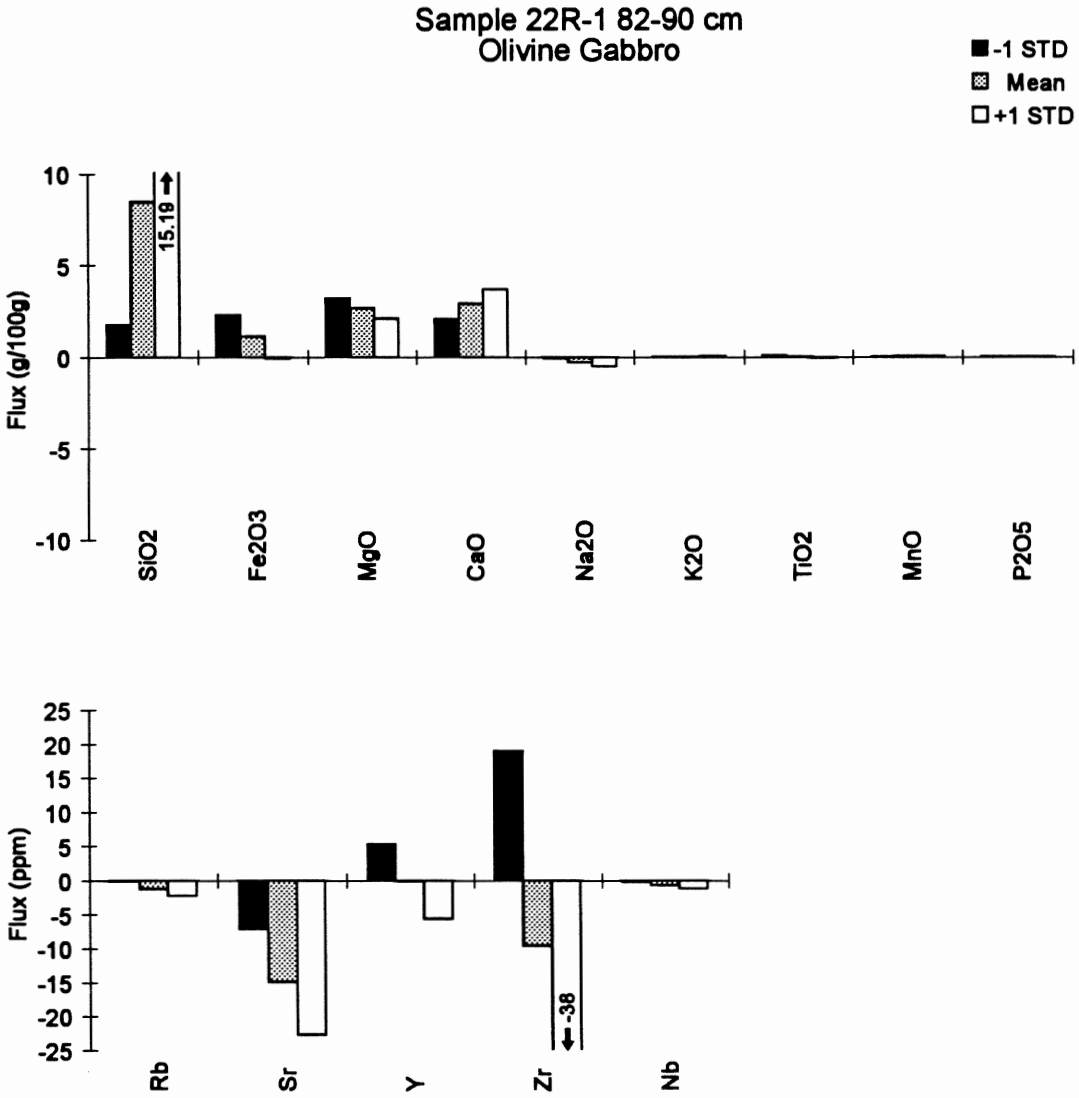
Sample 22R-1 82-90 cm
Olivine Gabbro
-1 STD
Mean
+1 STD
Flux (g/100g)
10
5
0
-5
-10
15.19
SiO2
Fe2O3
MgO
CaO
Na2O
K2O
TiO2
MnO
P2O5
Flux (ppm)
25
20
15
10
5
0
-5
-10
-15
-20
-25
-38
Rb
Sr
Y
Zr
Nb

Figure 4.4a

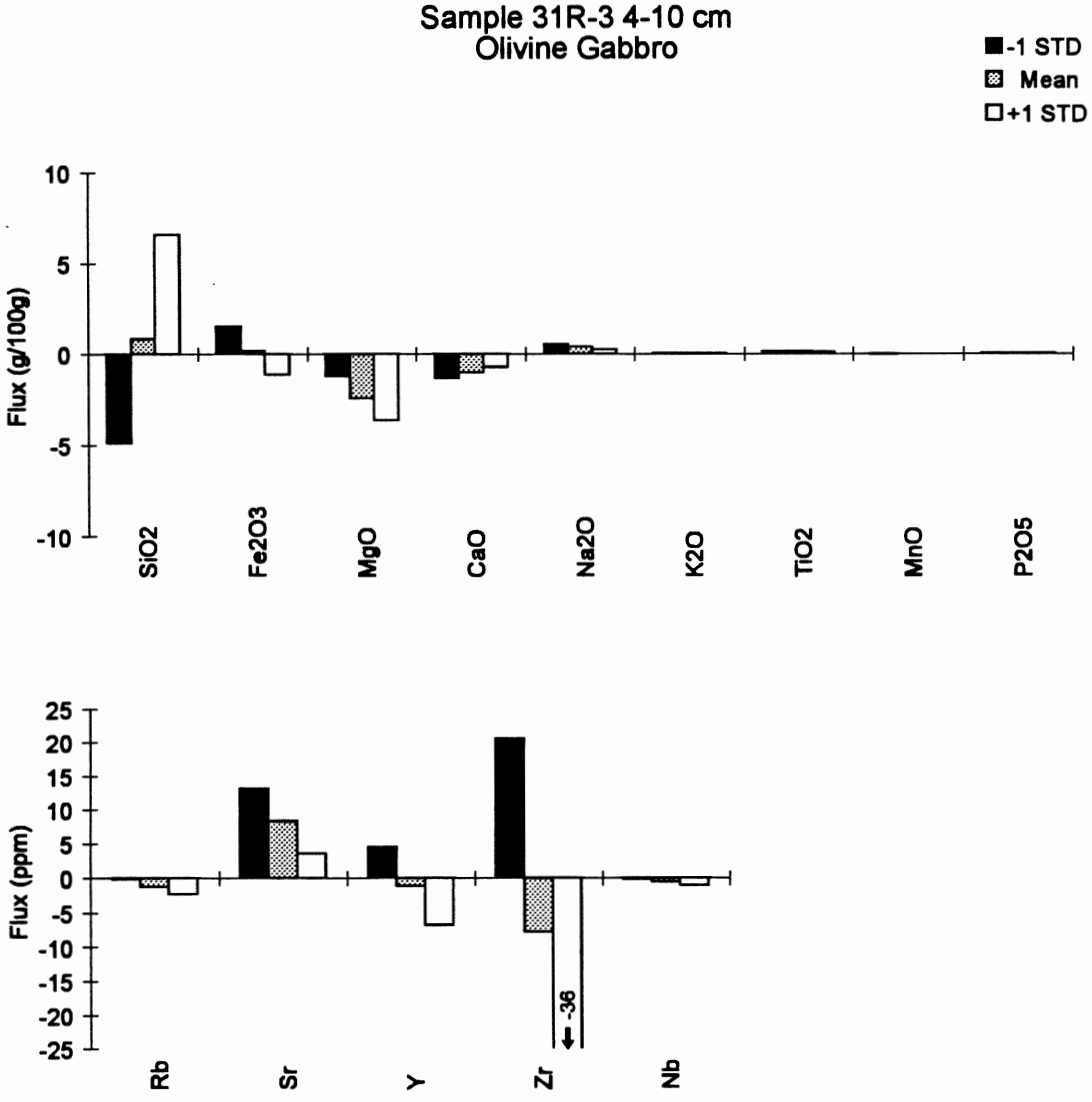
Sample 31R-3 4-10 cm
Olivine Gabbro
-1 STD
Mean
+1 STD
Flux (g/100g)
10
5
0
-5
-10
SiO2
Fe2O3
MgO
CaO
Na2O
K2O
TiO2
MnO
P2O5
Flux (ppm)
25
20
15
10
5
0
-5
-10
-15
-20
-25
-36
Rb
Sr
Y
Zr
Nb

Figure 4.4b

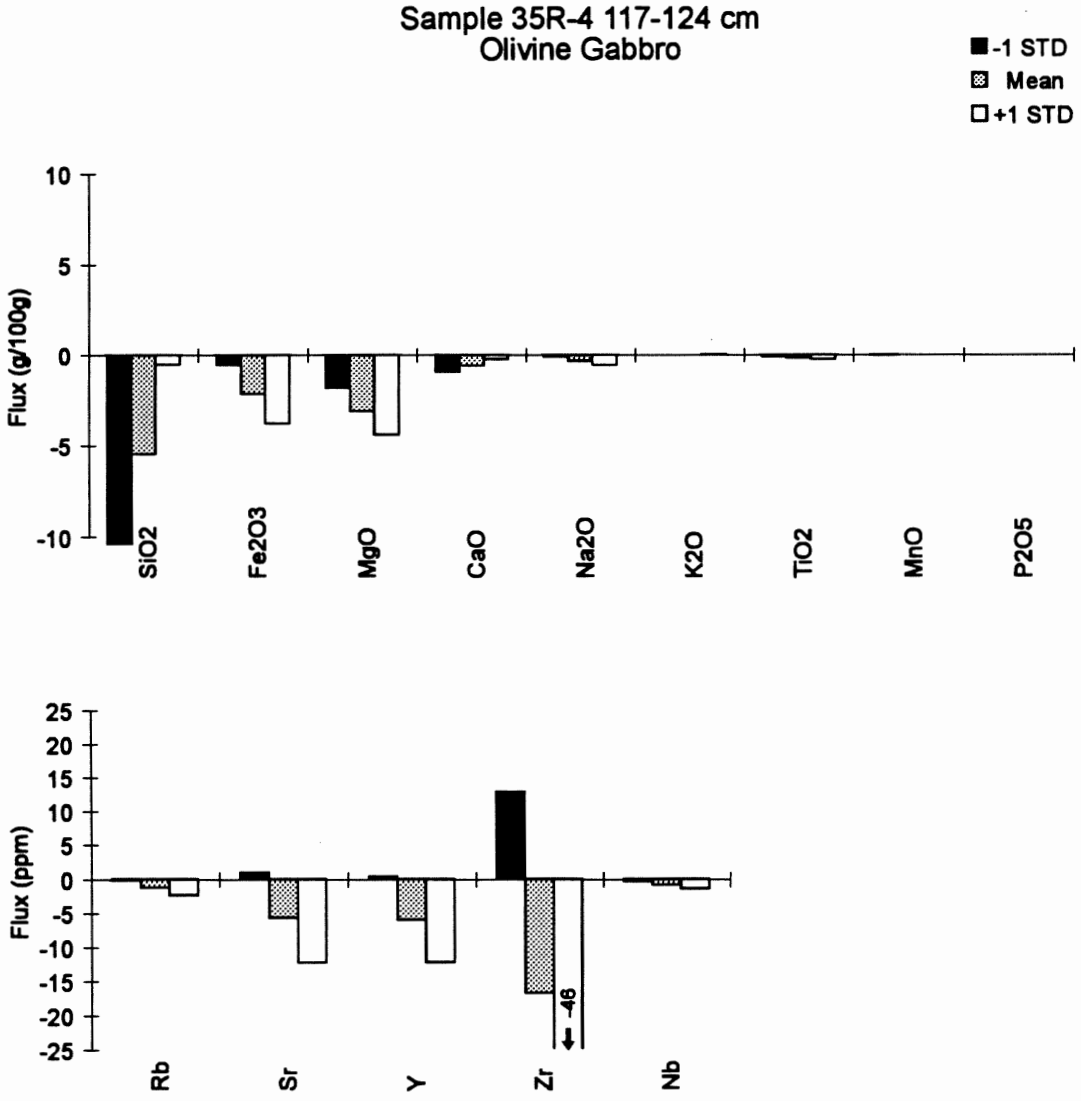
Sample 35R-4 117-124 cm
Olivine Gabbro
-1 STD
Mean
+1 STD
Flux (g/100g)
10
5
0
-5
-10
SiO2
Fe2O3
MgO
CaO
Na2O
K2O
TiO2
MnO
P2O5
Flux (ppm)
25
20
15
10
5
0
-5
-10
-15
-20
-25
-46
Rb
Sr
Y
Zr
Nb

Figure 4.4c

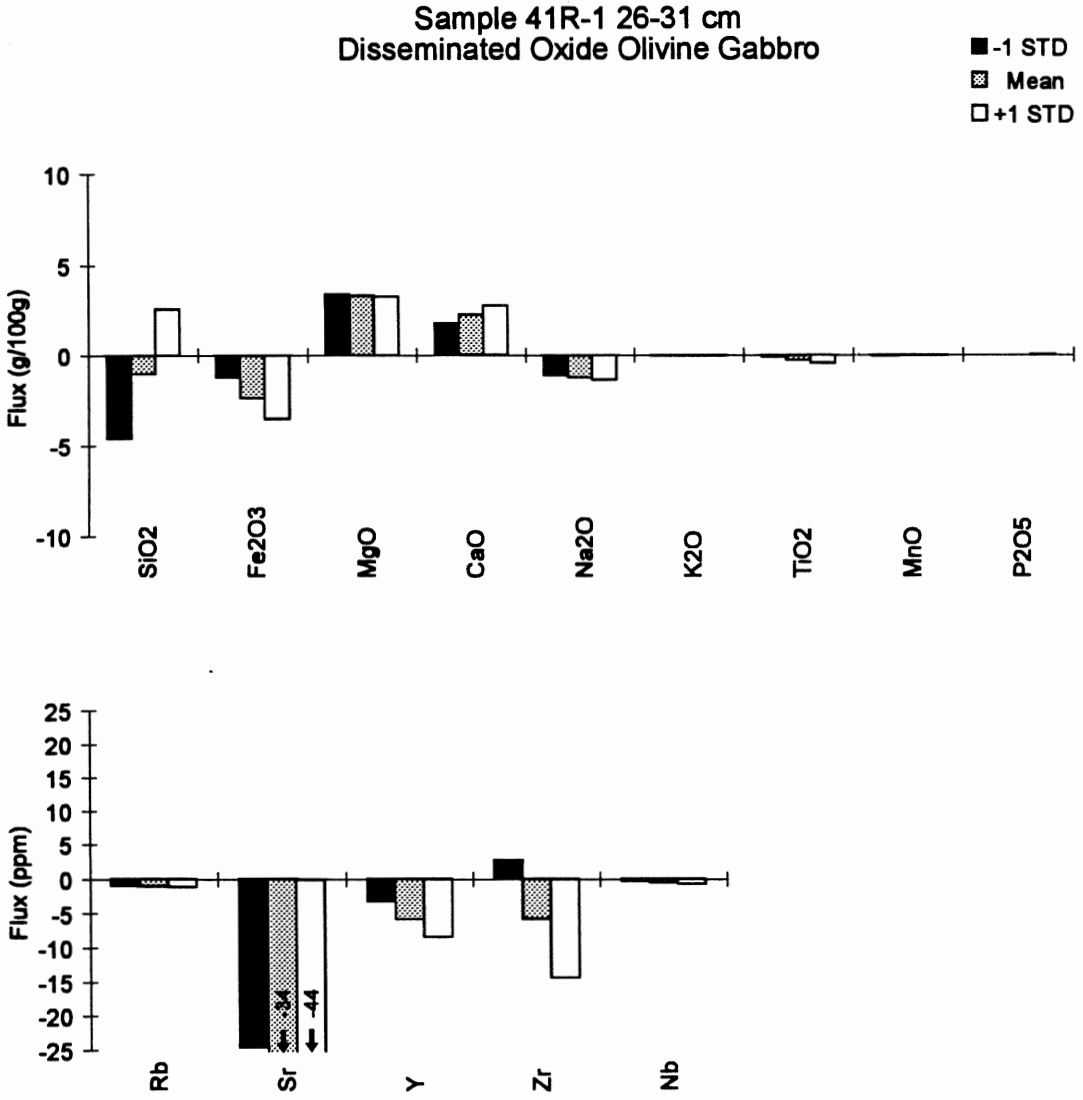
Sample 41R-1 26-31 cm
Disseminated Oxide Olivine Gabbro
-1 STD
Mean
+1 STD
Flux (g/100g)
10
5
0
-5
-10
SiO2
Fe2O3
MgO
CaO
Na2O
K2O
TiO2
MnO
P2O5
Flux (ppm)
25
20
15
10
5
0
-5
-10
-15
-20
-25
-34
-44
Rb
Sr
Y
Zr
Nb

Figure 4.4d

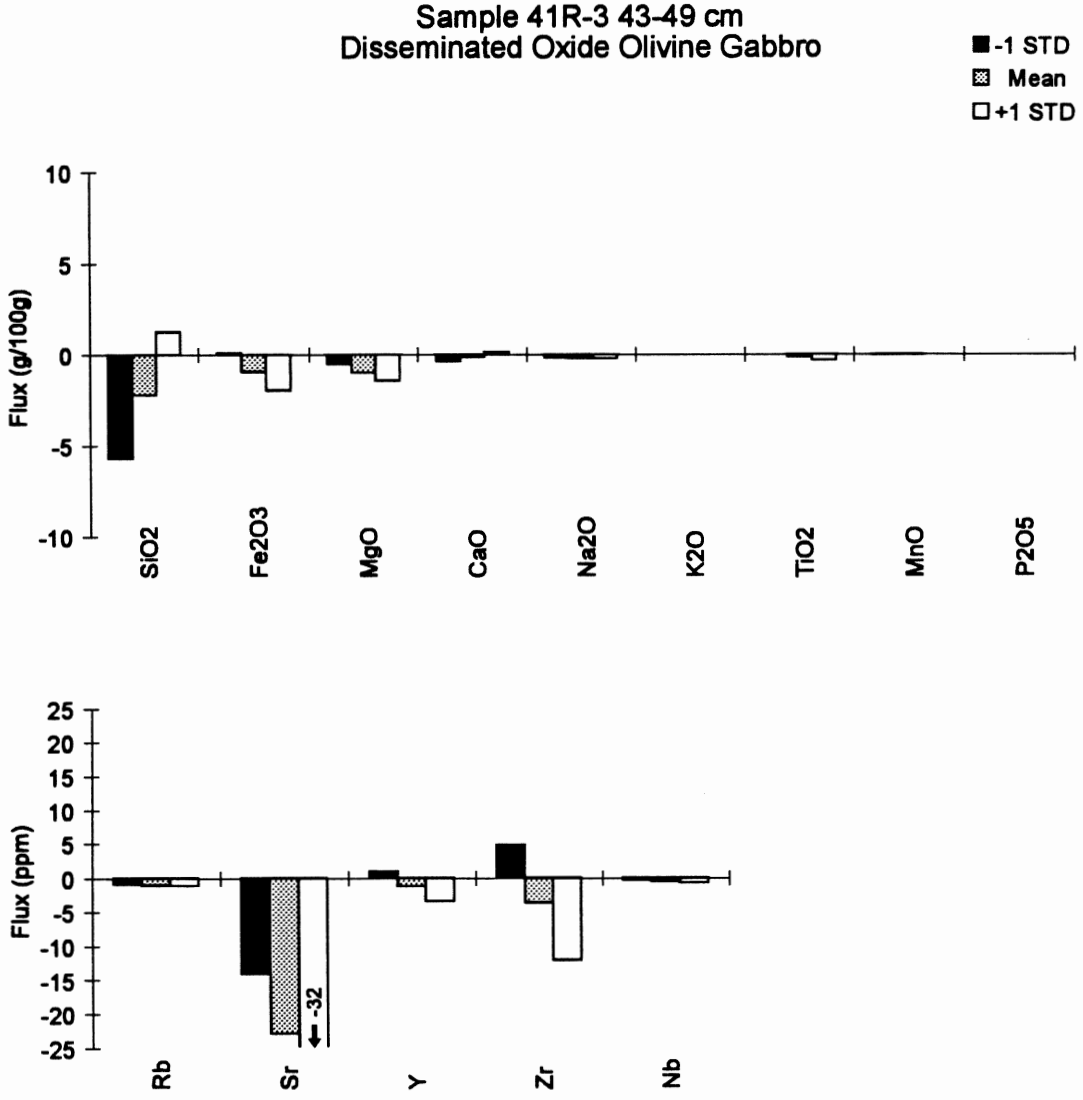
Sample 41R-3 43-49 cm
Disseminated Oxide Olivine Gabbro
-1 STD
Mean
+1 STD
Flux (g/100g)
10
5
0
-5
-10
SiO2
Fe2O3
MgO
CaO
Na2O
K2O
TiO2
MnO
P2O5
Flux (ppm)
25
20
15
10
5
0
-5
-10
-15
-20
-25
-32
Rb
Sr
Y
Zr
Nb

Figure 4.4e

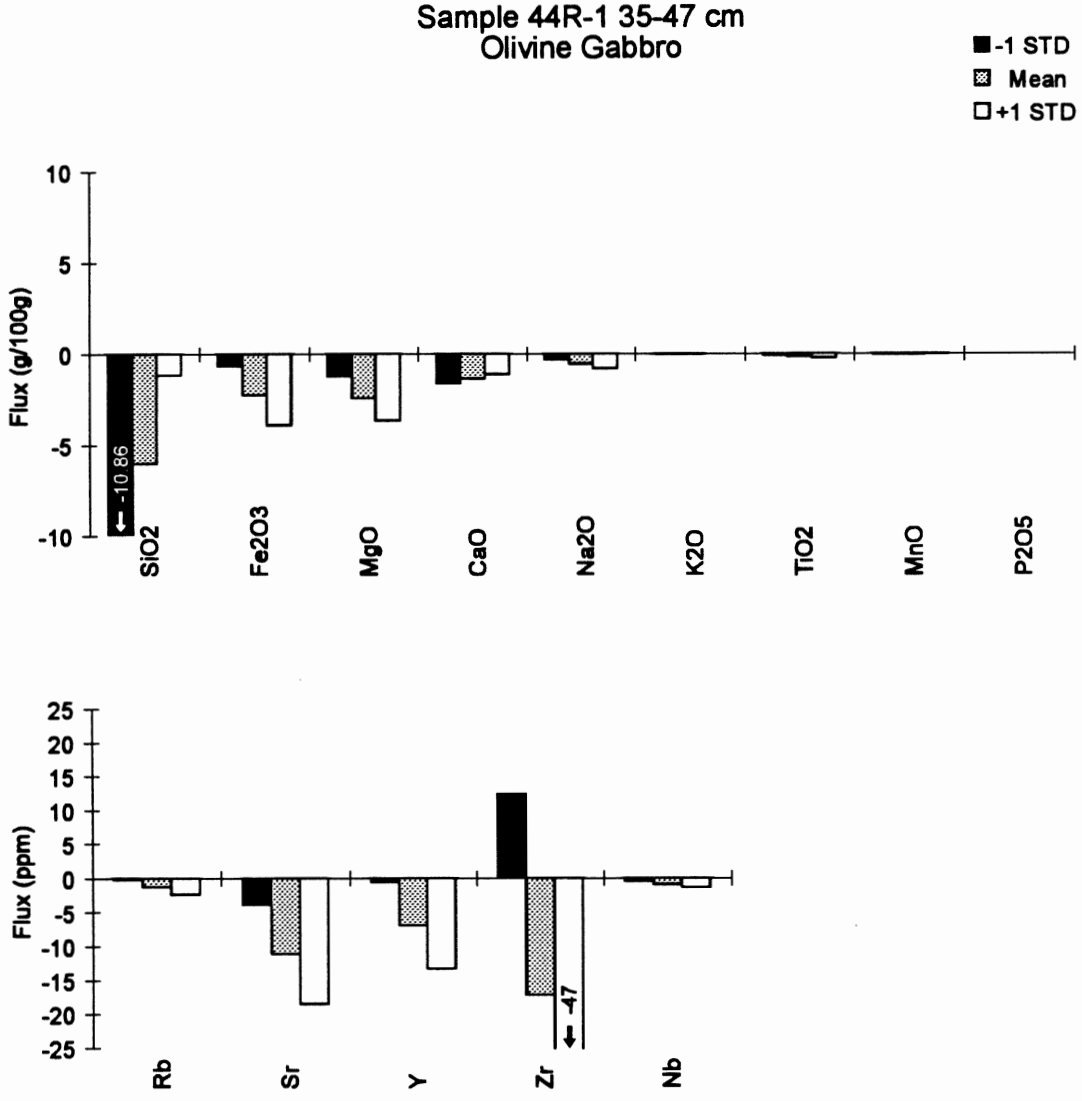
Sample 44R-1 35-47 cm
Olivine Gabbro
-1 STD
Mean
+1 STD
Flux (g/100g)
10
5
0
-5
-10
-10.86
SiO2
Fe2O3
MgO
CaO
Na2O
K2O
TiO2
MnO
P2O5
Flux (ppm)
25
20
15
10
5
0
-5
-10
-15
-20
-25
-47
Rb
Sr
Y
Zr
Nb

Figure 4.4f

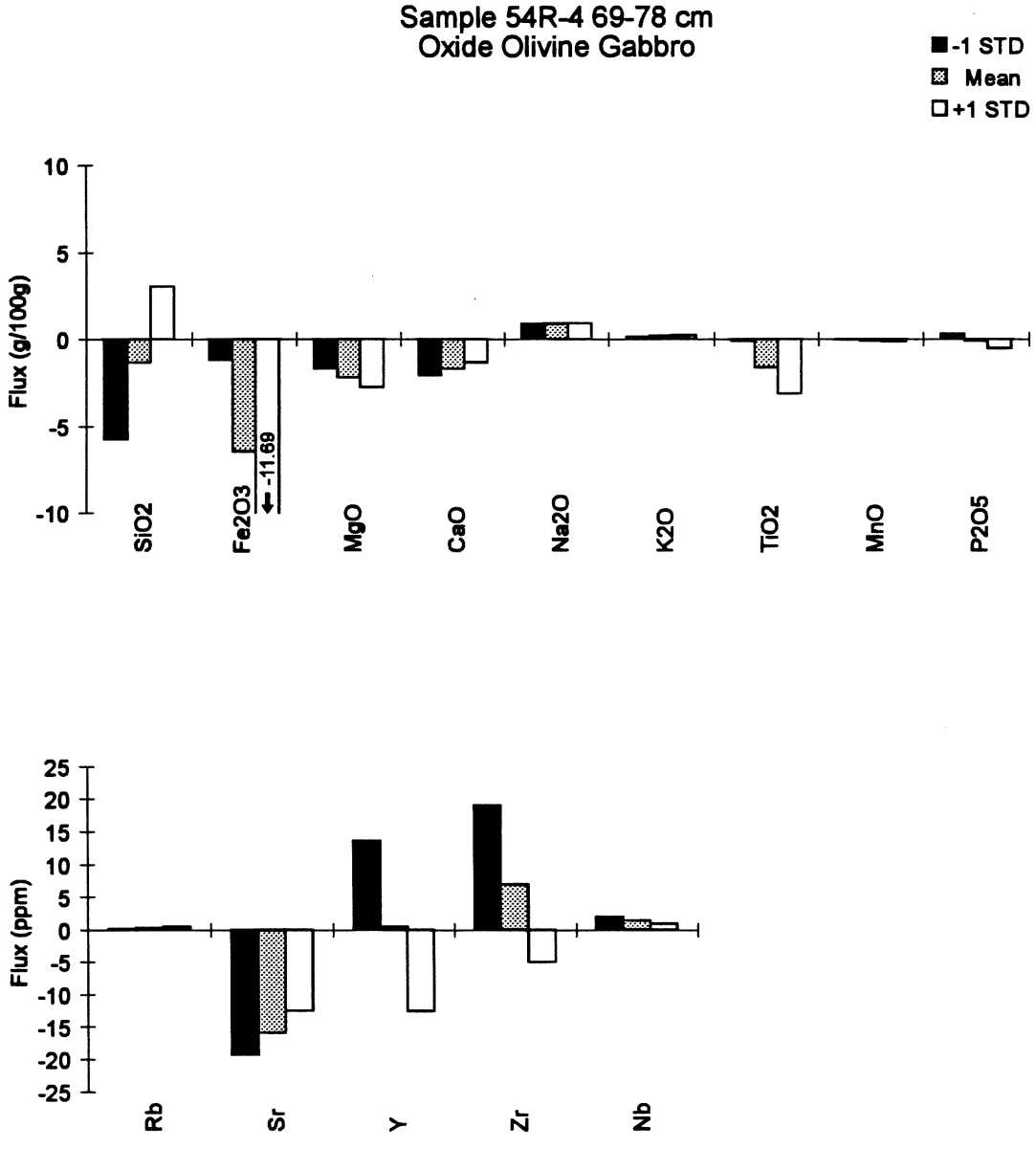
Sample 54R-4 69-78 cm
Oxide Olivine Gabbro
-1 STD
Mean
+1 STD
Flux (g/100g)
10
5
0
-5
-10
-11.69
SiO2
Fe2O3
MgO
CaO
Na2O
K2O
TiO2
MnO
P2O5
Flux (ppm)
25
20
15
10
5
0
-5
-10
-15
-20
-25
Rb
Sr
Y
Zr
Nb

Figure 4.4g

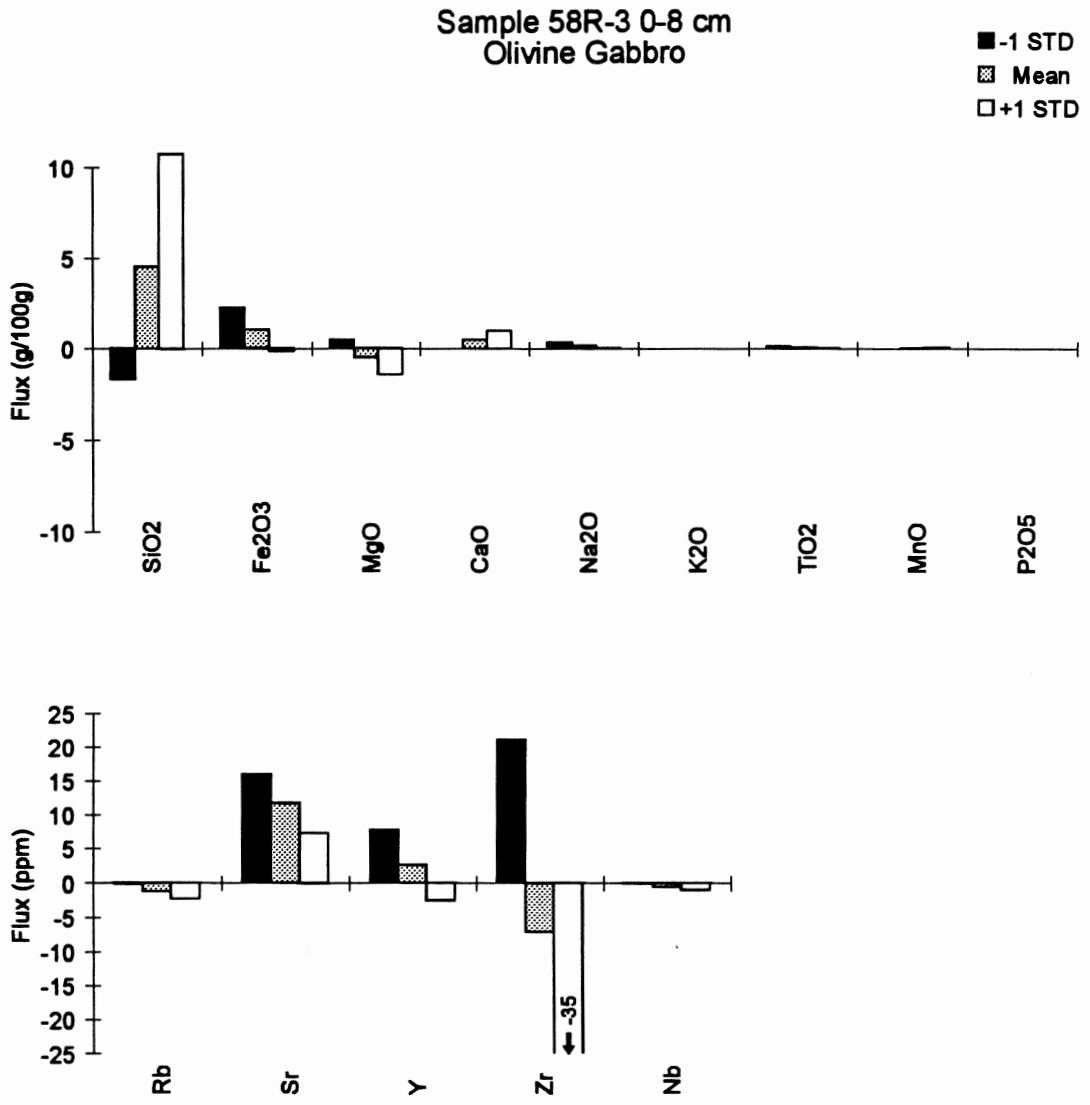
Sample 58R-3 0-8 cm
Olivine Gabbro
-1 STD
Mean
+1 STD
Flux (g/100g)
10
5
0
-5
-10
SiO2
Fe2O3
MgO
CaO
Na2O
K2O
TiO2
MnO
P2O5
Flux (ppm)
25
20
15
10
5
0
-5
-10
-15
-20
-25
-35
Rb
Sr
Y
Zr
Nb

Figure 4.4h

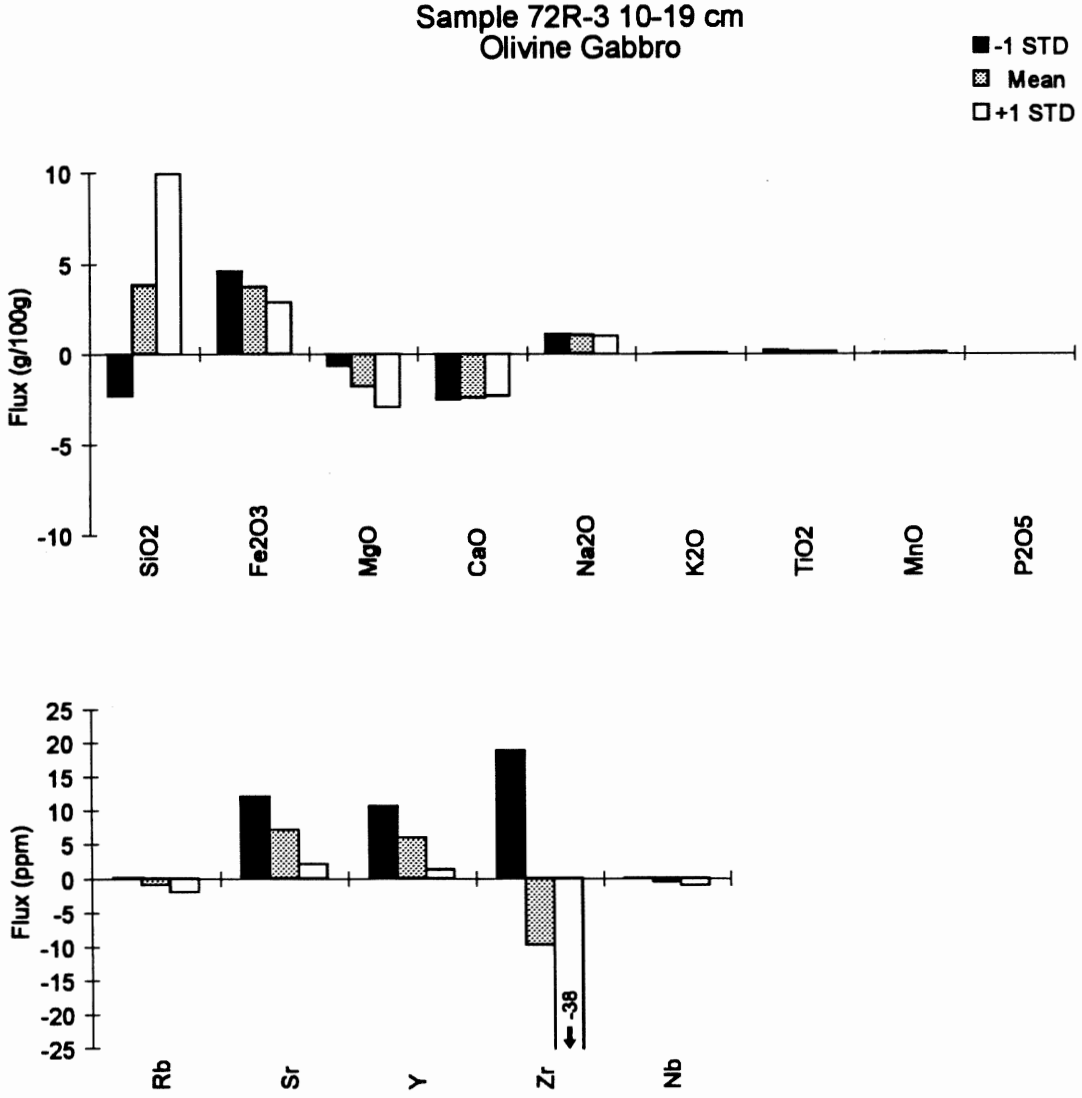
Sample 72R-3 10-19 cm
Olivine Gabbro
-1 STD
Mean
+1 STD
Flux (g/100g)
10
5
0
-5
-10
SiO2
Fe2O3
MgO
CaO
Na2O
K2O
TiO2
MnO
P2O5
Flux (ppm)
25
20
15
10
5
0
-5
-10
-15
-20
-25
-38
Rb
Sr
Y
Zr
Nb

Figure 4.4j

analyzed, seven are olivine gabbro, two are disseminated oxide olivine gabbro and one is an oxide olivine gabbro. Element flux trends are grouped based on the these three lithologies.

4.4.1 Olivine Gabbro Element Fluxes

Element fluxes for olivine gabbro samples are plotted in Figure 4.5. SiO_2 and Fe_2O_3 fluxes are consistent in magnitude and increase in all samples except for 35R-4 117-124 cm and 44R-1 35-47 cm which show decreases. MgO decreases in all samples except 22R-1 82-90 cm which exhibits an increase. All samples exhibit a decrease in CaO except for samples 22R-1 82-90 cm, 58R-3 0-8 cm, and 63R-6 98-106 cm which exhibit an increase. There is no consistent trend for Na_2O although the range of values (-0.53 to 1.02 g/100g) suggests mobility. K_2O, TiO_2, MnO, and P_2O_5 all exhibit very small fluxes with no consistent trends suggesting little or no change. Sr, Y, and Zr vary in both direction and magnitude between samples and do not exhibit a consistent trend. Nb and Rb are consistently lost in all samples.

4.4.2 Disseminated Oxide Olivine Gabbro Element Fluxes

Element fluxes for disseminated oxide olivine gabbro samples are plotted in Figure 4.6. Trends for SiO_2, Fe_2O_3, Na_2O, TiO_2, Rb, Sr, Y, Zr, and Nb are consistent in magnitude and exhibit decreases in two disseminated oxide olivine gabbro samples. K_2O, MnO, and P_2O_5 are consistent in magnitude and direction but exhibit only small flux values suggesting little or no change. MgO and CaO decrease in sample 41R-3 43-49 cm and increase in sample 41R-1 26-31 cm.

4.4.3 Oxide Olivine Gabbro Element Fluxes

SiO_2, Fe_2O_3, MgO, CaO, TiO_2, MnO, P_2O_5, and Sr decrease in sample 54R-4 69-78 cm whereas Na_2O, K_2O, Zr and Nb increase. Rb and Y flux values are small which indicates limited mobility.

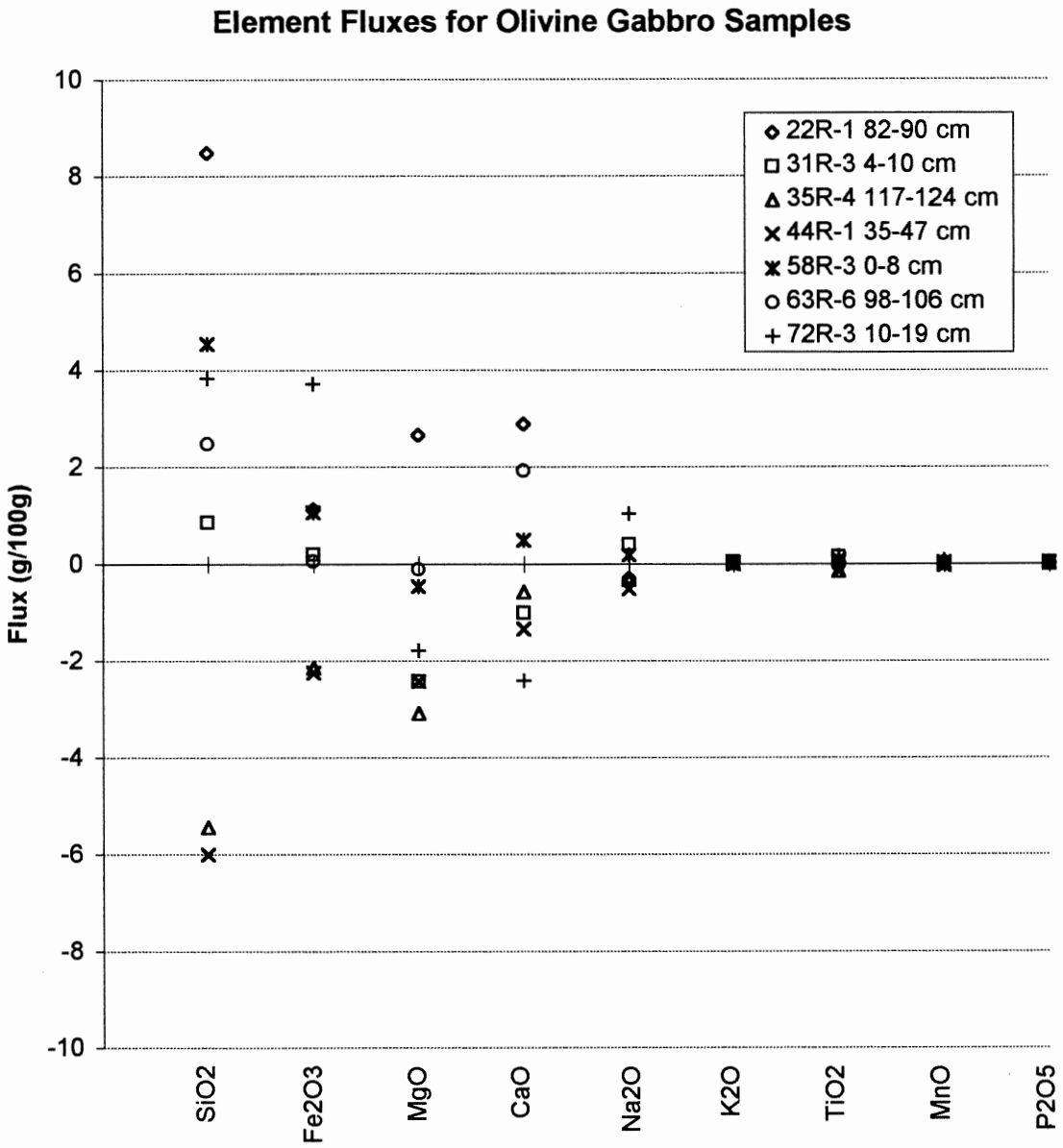

Figure 4.5 Plot of major-element fluxes for olivine gabbro samples. All values are from Table 4.4a. Values have been calculated assuming constant aluminum and mean values for fresh analyses.

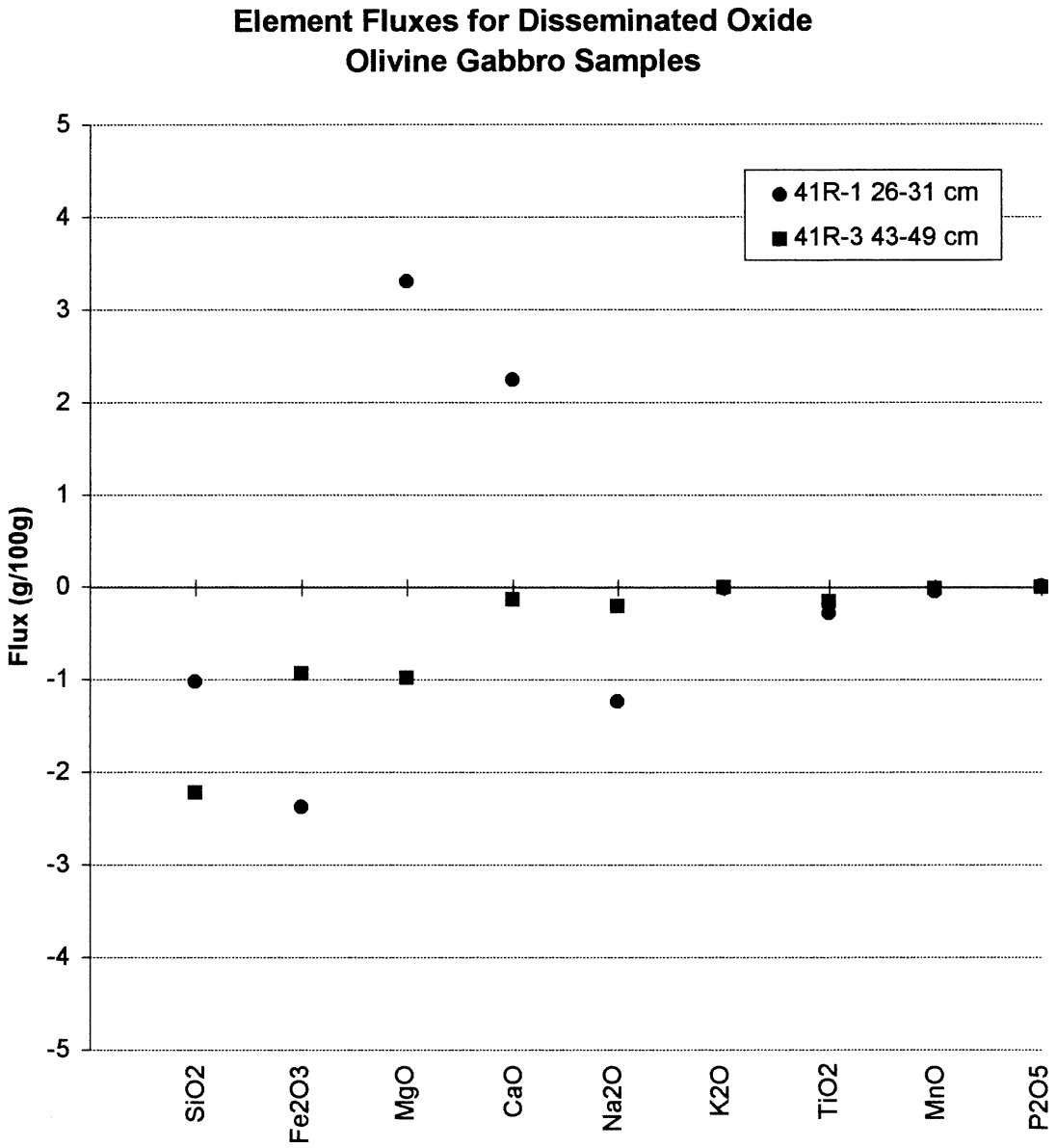

Figure 4.6 Plot of major-element fluxes for disseminated oxide olivine gabbro samples. All values are from Table 4.4a. Values have been calculated assuming constant aluminum and mean values for fresh analyses.

4.5 DISCUSSION

Zr is the only element that shows similar behaviour in all samples. Zr fluxes are characterized by high variability within one standard deviation of the mean suggesting no systematic variation. This is probably due to primary variations in Zr rather than changes due to alteration. No other systematic trends are observed when all samples are considered together.

4.5.1 Comparison of Sample Lithology and Element-Flux Trends

Examination of element fluxes based on lithology can be used to partially explain the observed trends. For example, both sample 35R-4 117-124 cm and 44R-1 35-47 cm (olivine gabbro) show volume decreases as indicated by calculated volume factors of 0.88 and 0.87 (Table 4.4a). This could account for observed losses in SiO_2 and Fe_2O_3 for olivine gabbro samples. However, volume decreases are not what is expected during alteration of the crystalline rocks used in this study. Most calculated volume factors are very near 1 (see Table 4.4), particularly when 1 standard deviation from the mean for the primary values are considered suggesting alteration took place under conditions of constant volume. Since the vein was removed from all samples, it would be reasonable to duplicate the calculation using constant volume. However, the densities of the altered and primary equivalents are necessary for the calculation. Due to the variable grain sizes and modal mineralogy of the samples studied, variation in specific densities would have increased the error in the calculation since adjacent altered and primary equivalents were not used. As a result, the assumption of constant Al was chosen.

It is observed that both TiO_2 and Fe_2O_3 increase in most olivine gabbro samples, but decrease in disseminated oxide olivine and oxide olivine gabbro samples. This is probably related to the higher modal proportion of Fe-Ti oxides in the oxide-bearing samples, which when altered release TiO_2 and Fe_2O_3. In addition, the relatively large TiO_2 fluxes in disseminated oxide olivine gabbro (-0.15 and -0.29 g/100g) and oxide olivine gabbro (-1.61 g/100g) samples indicates that TiO_2 is mobile, particularly in samples with

high modal oxide content. Similarly, both MnO and P_2O_5 exhibit relatively large decreases from oxide-bearing gabbro, which may also be due to different modal mineralogy from olivine gabbro and disseminated oxide olivine gabbro.

4.5.2 Comparison of Vein Assemblage and Element-Flux Trends

Many of the observed element-flux trends can be correlated with vein assemblages, assuming that different vein assemblages crystallized from fluids exhibiting different parameters (such as temperature, pressure, and individual component activities). Table 4.5 summarizes the lithology and vein assemblage of each sample. Disseminated oxide olivine gabbro samples have similar major and trace element-flux trends, both in direction and magnitude, except for CaO and MgO. Sample 41R-1 26-31 cm, however, contains a plagioclase-diopside vein and sample 41R-3 43-49 cm contains a plagioclase-amphibole vein. The presence of diopside in the vein from sample 41R-1 26-31 cm probably reflects higher Ca and Mg concentrations in the initial fluid relative to 41R-3 43-49 cm. This probably resulted in elevated CaO and MgO fluxes in 41R-1 26-31 cm relative to 41R-3 43-49 cm.

MgO and CaO element-flux trends in olivine gabbro can also be interpreted based on vein assemblages. MgO uniformly decreases in all olivine gabbro samples except 22R-1 82-90 cm which contains a monomineralic amphibole vein. All other veins cutting olivine gabbro samples have more complex assemblages containing more than two minerals. This may have resulted from lower Mg concentrations in initial fluids relative to 22R-1 82-90 cm, resulting in negative Mg fluxes. CaO decreases in all samples except 22R-1 82-90 cm, 58R-3 0-8 cm, and 63R-6 98-106 cm. The positive CaO flux in 22R-1 82-90 cm can be explained in a similar way as Mg. The complex vein mineralogies in samples 58R-3 0-8 cm and 63R-6 98-106 cm include Ca-bearing minerals, such as sphene and epidote, which suggests Ca may have been elevated in these fluids, resulting in positive CaO fluxes.

Finally, although K_2O shows no discernable trends based on lithology, the relatively high K_2O value in sample 54R-4 69-78 cm may be due to high K in fluids from

Table 4.5 Comparison of lithology and vein assemblage for element-flux samples.

	Lithology		
Sample	Olivine Gabbro	Disseminated Oxide Olivine Gabbro	Oxide Olivine Gabbro
22R-1 (82-90cm)	Amphibole (minor Plag)		
31R-3 (4-10cm)	Plagioclase + Amphibole		
35R-4 (117-124cm)	Plagioclase + Amphibole		
44R-1 (35-47cm)	Plagioclase + Amphibole		
58R-3 (0-8cm)	Plagioclase + Amphibole		
41R-3 (43-49cm)		Plagioclase + Amphibole	
41R-1 (26-31cm)		Plagioclase + Diopside	
63R-6 (98-106cm)	Plagioclase + Diopside		
54R-4 (69-78cm)			Plagiogranite
72R-3 (10-19cm)	Carbonate + Clay		

Vein assemblages have been simplified for comparison. For a complete description see Appendix 2.

which the plagiogranite vein crystallized. Subsequent hydrothermal alteration of host-rock plagioclase may have resulted in formation of K-feldspar although this is difficult to determine petrographically (see Appendix 2).

4.5.3 Element Fluxes Relative to Original Compositions

Another method of interpreting the element fluxes calculated for 735B samples is to express them relative to their starting (fresh) compositions. These data are summarized in terms of percent relative to starting composition in Table 4.6.

It is apparent that most of the trace-element fluxes exhibit large variations relative to their starting compositions, except for possibly Sr. Many trace-element fluxes vary as much as 100% from their original concentrations, and several vary by even greater values. This could be due to three factors. First, the variability could be the result of elevated mobility, which is suggested by elements showing distinct trends described in the previous sections. Second, the variability could be related to primary variation rather than secondary affects, which is probably the case for Zr which does not show any discernable trends. Third, because of the low concentrations of many trace-elements, the variability could be due to analytical uncertainty, which can vary as much as 7% for trace-elements.

Many major-element fluxes also exhibit large percentage variations. TiO_2 exhibits high percentage fluxes relative to starting compositions, particularly in olivine gabbro. This trend is most likely due to primary variations in TiO_2 and is probably further complicated by some Ti mobility, particularly in oxide-bearing gabbros. MgO and CaO percentage fluxes are also high, however, their magnitude is similar in most samples, suggesting variation related to mobilization. Other oxides show smaller, yet significant, fluxes relative to starting composition which are consistent with varying degrees of mobility.

4.5.4 Comparison of Hole 735B Element Fluxes with Previous Studies

Element fluxes and estimates of element mobility during alteration of oceanic rocks have been determined for dredged pillow basalt (e.g. Humphris and Thompson, 1978), core

Table 4.6a Element fluxes relative to starting compositions calculated from mean primary values

Lithology:	Olivine Gabbro							Disseminated Oxide Olivine Gabbro		Oxide Olivine Gabbro
Sample Number:	22R-1 82-90 cm	31R-3 4-10 cm	35R-4 117-124 cm	44R-1 35-47 cm	58R-3 0-8 cm	63R-6 98-106 cm	72R-3 10-19 cm	41R-1 26-31 cm	41R-3 43-49 cm	54R-4 69-78 cm
SiO_2	16.40	1.60	-10.59	-11.68	8.66	4.82	7.31	-2.01	-4.25	-2.90
Fe_2O_3	7.47	1.07	-11.15	-11.56	6.48	0.28	22.70	-15.26	-5.71	-52.24
MgO	46.30	-42.22	-82.68	-66.29	-7.81	-2.36	-20.52	52.20	-12.01	-11.72
CaO	25.91	-13.04	-7.36	-15.31	5.29	19.80	-30.34	19.37	-1.77	-39.36
Na_2O	-2.17	3.03	-2.28	-3.84	1.32	-2.62	9.74	-9.42	-1.83	10.71
K_2O	1.00	1.01	0.23	-0.59	0.10	0.64	1.03	-0.95	-0.04	4.25
TiO_2	27.46	178.85	-305.01	-502.70	186.99	-85.90	195.79	-936.58	-299.81	-605.56
MnO	10.27	-2.25	-4.69	-18.23	4.53	-1.47	13.20	-14.79	-3.00	-1.59
P_2O_5	1.46	19.55	-0.78	9.53	0.54	0.57	0.40	8.52	-0.17	-45.91
Rb	-723.4	-771.4	-755.2	-839.9	-774.7	-271.5	-215.8	-775.4	-590.4	22.1
Sr	-12	5	-3	-7	7	-7	4	-24	-14	-10
Y	-2	-11	-103	-150	20	-44	37	-72	-9	2
Zr	-89	-54	-276	-313	-51	-159	-84	-44	-22	10
Nb	-250.1	-137.7	-574.0	-1579.5	-136.9	-1130.7	-124.8	-406.7	-314.0	22.8

Note: Values are in per cent relative to starting compositions. Fluxes are calculated assuming constant aluminum and mean primary values.

Table 4.6b Element fluxes relative to starting compositions calculated from mean primary values plus 1 standard deviation

Lithology:	Olivine Gabbro							Disseminated Oxide Olivine Gabbro		Oxide Olivine Gabbro
Sample Number:	22R-1 82-90 cm	31R-3 4-10 cm	35R-4 117-124 cm	44R-1 35-47 cm	58R-3 0-8 cm	63R-6 98-106 cm	72R-3 10-19 cm	41R-1 26-31 cm	41R-3 43-49 cm	54R-4 69-78 cm
SiO_2	29.40	12.48	-1.03	-2.25	20.53	16.39	19.00	5.03	2.39	6.50
Fe_2O_3	-0.52	-6.44	-19.46	-19.85	-0.94	-7.79	17.47	-22.62	-11.90	-94.91
MgO	36.66	-63.17	-117.15	-99.16	-23.34	-19.50	-33.35	51.24	-17.43	-14.55
CaO	33.11	-9.24	-2.92	-12.41	10.68	26.81	-28.86	23.55	1.76	-30.66
Na_2O	-3.70	2.02	-3.79	-5.61	0.14	-4.16	9.31	-10.29	-2.03	11.08
K_2O	1.40	1.32	0.47	-0.44	0.32	0.97	1.32	-0.82	0.09	5.42
TiO_2	-76.95	123.60	-451.61	-749.05	73.24	-205.87	143.29	-1496.31	-609.97	-1170.90
MnO	16.19	0.44	1.56	-13.95	8.72	3.31	17.99	-11.41	-0.10	-2.70
P_2O_5	2.70	23.35	0.26	12.33	1.67	1.91	1.25	10.02	0.36	-205.42
Rb	-1367.3	-1442.0	-1406.5	-1557.2	-1452.8	-553.0	-454.0	-839.4	-639.0	32.7
Sr	-18	2	-7	-11	4	-12	1	-31	-19	-7
Y	-60	-68	-211	-288	-19	-123	8	-104	-25	-39
Zr	-354	-249	-765	-852	-252	-506	-329	-110	-75	-7
Nb	-417.8	-243.0	-893.8	-2401.6	-244.6	-1734.6	-226.0	-542.6	-422.4	14.5

Note: Values are in per cent relative to starting compositions. Fluxes are calculated assuming constant aluminum.

Table 4.6c Element fluxes relative to starting compositions calculated from mean primary values minus 1 standard deviation

Lithology:	Olivine Gabbro							Disseminated Oxide Olivine Gabbro		Oxide Olivine Gabbro
Sample Number:	22R-1 82-90 cm	31R-3 4-10 cm	35R-4 117-124 cm	44R-1 35-47 cm	58R-3 0-8 cm	63R-6 98-106 cm	72R-3 10-19 cm	41R-1 26-31 cm	41R-3 43-49 cm	54R-4 69-78 cm
SiO_2	3.40	-9.28	-20.15	-21.11	-3.20	-6.76	-4.39	-9.06	-10.88	-12.30
Fe_2O_3	15.47	8.58	-2.84	-3.27	13.90	8.34	27.93	-7.91	0.48	-9.58
MgO	55.93	-21.28	-48.20	-33.43	7.71	14.78	-7.70	53.15	-6.59	-8.90
CaO	18.71	-16.83	-11.79	-18.20	-0.11	12.79	-31.82	15.18	-5.29	-48.07
Na_2O	-0.65	4.03	-0.77	-2.07	2.49	-1.09	10.16	-8.54	-1.62	10.34
K_2O	0.60	0.70	-0.01	-0.75	-0.12	0.30	0.75	-1.09	-0.18	3.09
TiO_2	131.88	234.10	-158.41	-256.36	300.75	34.07	248.28	-376.84	10.35	-40.22
MnO	4.35	-4.94	-10.94	-22.51	0.33	-6.25	8.41	-18.16	-5.91	-0.47
P_2O_5	0.23	15.76	-1.81	6.72	-0.60	-0.77	-0.44	7.03	-0.70	113.60
Rb	-79.6	-100.9	-103.9	-122.7	-96.5	10.1	22.4	-711.4	-541.8	11.5
Sr	-6	8	1	-2	10	-2	7	-17	-9	-12
Y	57	45	6	-12	60	35	66	-40	7	42
Zr	176	142	213	225	151	188	161	21	30	27
Nb	-82.4	-32.4	-254.3	-757.4	-29.1	-526.8	-23.6	-270.8	-205.6	31.2

Note: Values are in per cent relative to starting compositions. Fluxes are calculated assuming constant aluminum.

recovered from ophiolites (e.g. Bednarz and Schmincke, 1989), core recovered from *in situ* ocean crust (e.g. Bach *et al.*, 1996), lab experiments reproducing conditions during basalt-seawater interactions (e.g. Mottl and Holland, 1978; Mottl *et al.*, 1979), and various combinations of these (e.g. Thompson, 1983). Most of these studies focused on volcanic rocks which make up Layer 2, such as pillow basalt and sheeted dikes (Figure 1.1). Comparison of element fluxes from previous studies with those from 735B samples, therefore, provides a measure of the variability of element fluxes between oceanic Layers 2 and 3.

A summary of element fluxes for Hole 735B samples is given in Table 4.7. Gains and losses are based on trends displayed by the majority of samples for each lithology. Elements which displayed relatively equal gains and losses, for the same lithology, were termed variable. Elements which showed small or no changes were also identified. A similar classification was used for previous studies of element fluxes (Table 4.8). Each summary does not attempt to quantify the amount of change associated with gains and losses and is only qualitative.

Previous studies of alteration in Layer 2 document a consistent gain of Mg and loss of Ca from rocks as a result of hydrothermal alteration. Other trends are less consistent between studies, however, Na and Rb appear to be gained and Si appears to be lost in most studies. Fe, K, Ti, Mn, and Sr are either variable or not documented in multiple studies.

Consideration of Ca and Mg element fluxes in terms of steady-state geochemical mass balances for the oceans suggest that hydrothermal alteration may have a significant impact on the geochemical budget of these, and possibly other, elements (Humphris and Thompson, 1978). Mg gains in basalt during chemical exchange with seawater at low water/rock ratios are explained by the formation of secondary minerals such as smectite, tremolite-actinolite, and talc (Mottl and Holland, 1978). Na gains are similarly explained by the formation of sodic feldspar and possibly analcime (Mottl and Holland, 1978). Despite an overall loss from altered basalt, secondary Ca-bearing phases are also observed, including anhydrite and tremolite-actinolite (Mottl and Holland, 1978).

Table 4.7 Summary of element fluxes for Hole 735B samples

Lithology:	Olivine Gabbro	Disseminated Oxide Olivine Gabbro	Oxide Olivine Gabbro
SiO_2	+	-	-
Fe_2O_3	+	-	-
MgO	-	+/-	-
CaO	+/-	+/-	-
Na_2O	+/-	-	+
K_2O	nc	nc	+
TiO_2	nc	-	-
MnO	nc	nc	nc
P_2O_5	nc	nc	nc
Rb	-	-	nc
Sr	+/-	-	-
Y	+/-	-	nc
Zr	+/-	-	+
Nb	-	-	+
N=	7	2	1

Gains and losses are relative to primary whole-rock compositions. + = gain; - = loss ;+/- = variable changes between samples; nc = small or no change. N = number of samples. See text for explanation.

Table 4.8 Summary of element fluxes from previous studies

	Humphris & Thompson, 1978	Mottl & Holland, 1978; 1979	Thompson, 1983	Bednarz & Schmincke, 1989	Bach *et al.*, 1996
Si	-	-	-	+/-	-
Fe		+	-		
Mg	+	+	+	+	+
Ca	-	-	-	-	-
Na	+/-	+		+	
K	+/-	-		+	
Ti			+		-
Mn			-		
Rb			+	+	
Sr		+/-			

Gains and losses reflect whole-rock changes relative to starting compositions. + = gain; - = loss ; +/- = variable changes. See text for explanation.

Element-flux trends for Si and Na in samples from Hole 735B are similar to those in previous studies. Element-flux trends for Mg, Ca, and Rb from previous studies, however, do not seem to be the same as those in samples from Hole 735B. MgO and CaO tend to be lost and Rb gained by 735B samples although there is some variability, especially in CaO. The loss of MgO and gain of Rb by Hole 735B samples is the opposite of what is observed in previous studies. This may be due to different conditions during alteration of Layer 3 than Layer 2. For example, alteration of Layer 2 rocks are often dominated by alteration assemblages characteristic of greenschist metamorphic conditions, such as chlorite, actinolite, epidote, and sodic plagioclase (Humphris and Thompson, 1978). Layer 3 rocks from Hole 735B are characterized by amphibolite and granulite metamorphic assemblages (see Chapter 2). Amphibole is the dominant secondary mineral in Hole 735B rocks (Stakes *et al.*, 1991). The differences in common secondary minerals between Layer 2 and 3 suggests that the fluids from which they crystallized were probably different. This possibly resulted in the observed differences in element fluxes. The starting compositions of the rocks (basalt from Layer 2 and gabbro from Layer 3) may also have influenced element fluxes. Finally, Mottl and Holland (1978) have documented that the crystallinity of the starting rock in basalt-seawater experiments affects the amount of secondary minerals which form. The plutonic rocks from in this study are much coarser-grained than the basalt and diabase from previous studies and do not contain glass which may have resulted in the observed differences. Element fluxes for Fe, K, Ti, Mn, and Sr from previous studies are difficult to compare with those from Hole 735B because they are variable or are not available from multiple studies.

4.6 SUMMARY

Semi-quantitative estimates of whole-rock element flux have been determined for 10 altered samples from ODP Hole 735B. Fluxes were calculated using equations from Gresens (1967) assuming conservation of aluminum. Samples were chosen to include a variety of lithologies and several contained different vein assemblages. Average analyses

of 'fresh' samples from published data are used to approximate the unaltered equivalent of the altered samples. Zr is the only element with similar trends in all samples and is characterized by high variability. This is interpreted to reflect primary rather than secondary variation. Calculated volume factors are used to explain different element-flux trends in the same lithology and suggests that alteration probably occurred under conditions of constant volume. Modal mineralogy is used to explain element-flux variations between lithologies. Vein assemblages are also used to interpret element-flux trends, particularly observed discrepancies in CaO and MgO fluxes. For example, the presence of amphibole, or alternatively, diopside in vein assemblages is believed to reflect differences in fluid composition which may have affected CaO and MgO fluxes. This suggests that element fluxes are related to the composition of the hydrothermal fluid as well as the primary composition of the rock. Element fluxes have been expressed relative to starting compositions which provides an estimate of the degree of element mobility. Elements fluxes that exhibit consistent variation relative to starting compositions are believed to represent secondary mobility, however, more variable element fluxes relative to starting compositions are believed to reflect primary variations. Qualitative comparison of element fluxes from Hole 735B samples with similar studies of oceanic Layer 2 samples provides an estimate of the differences in chemical effects of alteration at different levels in the ocean crust. Element-flux trends for Si and Na appear to be similar for 735B samples and Layer 2 samples, however, Mg and Rb fluxes appear to be opposite in direction. This could be due to differences in fluid factors (such as temperature, pressure, or individual component activities), composition of the rocks, degree of crystallinity of the rocks, or any combination of these factors. Element fluxes in samples from Hole 735B indicate that there is some variation between the chemical effect of alteration in the lower and upper ocean crust. This could have a significant impact on the geochemical budget of elements which become mobile during hydrothermal alteration.

Chapter 5

Chemical Mapping

5.0 INTRODUCTION

In this chapter the chemical effects of alteration on host rock adjacent to hydrothermal veins, at thin section scale, is investigated. This was accomplished by the creation of residual chemical maps which were produced from gridded microprobe data. Residual chemical maps were created by subtracting primary mineral chemistry from altered analyses to determine what chemical changes had occurred in the host rock as a result of alteration. Gridded microprobe data were collected for nine major oxides, from five samples, representing two different lithologies: olivine gabbro and oxide olivine gabbro. These samples were also analyzed for whole-rock element fluxes in order to compare directly chemical changes at different scales. These chemical maps provide a new method for quantifying chemical changes at thin section scale.

5.1 ASSUMPTIONS

Calculation of residual chemistry requires assumptions which are very similar to those necessary to calculate element fluxes (Chapter 4). First, it is necessary to determine what constitutes the 'fresh' equivalent of the altered samples. Second, it is necessary to normalize the data from altered samples to account for the passive accumulation of elements. The differences in techniques (mineral analyses versus whole-rock), however, do result in some variations.

It is also necesary to make certain assumptions regarding alteration mineralogy. In order to calculate residuals, the primary minerals from which secondary minerals have formed must be known. In many cases, a given secondary mineral can form from more than one primary mineral. Alteration trends, therefore, must be known to pair secondary minerals accurately with their primary equivalents.

5.1.1 Definition of Primary Minerals

Unlike element-flux calculations, residual calculations require multiple fresh equivalents. These fresh equivalents are required for each of the mineral phases analyzed. In this study five mineral phases are recognized as primary: plagioclase, olivine, pyroxene, ilmenite, and magnetite. Analyses of fresh minerals from Hébert *et al.* (1991) and Natland *et al.* (1991) for both lithologies were averaged to produce an estimate of unaltered compositions (Table 5.1). Average values for primary ilmenite and magnetite were not available for olivine gabbro. Silicate analyses are from least altered samples (Hébert *et al.*, 1991) and oxide analyses are from samples representing the full range of oxide proportions (Natland *et al.*, 1991). Averages include multiple analyses of individual mineral grains which provides an estimate of chemical variablity within individual grains (Hébert *et al.*, 1991; Natland *et al.*, 1991). In addititon, because of the small sample population, one standard deviation from the mean is quoted for each element in order to estimate variability between samples.

5.1.2 Normalization to Al_2O_3

Microprobe analyses were normalized to Al_2O_3 for two reasons. First, normalization corrects for the passive accumulation of other elements during residual calculation. Second, normalization to Al_2O_3 for chemical map data allows direct comparison with element fluxes. There are, however, certain differences between normalization to Al_2O_3 for whole-rock analyses and mineral analyses. Unlike whole-rock analyses, some mineral analyses do not contain Al_2O_3. This is true for minerals such as olivine, quartz, magnetite, and ilmenite which are common in the samples analyzed. As a result, microprobe analyses identified as olivine, quartz, magnetite, or ilmenite were not normalized to Al_2O_3. Calculation of residuals is discussed later in this chapter (section 5.3.8).

5.1.3 Recognition of Parent Minerals

Alteration patterns in samples from Hole 735B have already been discussed (Chapter 2). On the basis of these observations, the following assumptions were made: 1) secondary

Table 5.1a Microprobe analyses of primary plagioclase

	Olivine Gabbro Samples																	
Core/Section:	13R-1	14R-1	14R-1	44R-3	44R-3	57R-3	57R-3	64R-2	64R-2	69R-2	69R-2	69R-2	69R-2	74R-5	83R-6	86R-4		N=	16
Interval (cm):	102-105	26-29	26-29	37-40	37-40	37-43	37-43	74-84	74-84	55-67	55-67	55-67	55-67	84-92	53-59	64-70			
Piece:	11B	2A	2A	5D	5D	1C	1C	1E	1E	2B	2B	2B	2B	3B	3	3B			
Unit:	II	II	II	III	III	V	V	V	V	V	V	V	V	V	VI	VI		Mean	1σ
SiO_2	53.79	54.10	54.09	51.69	51.34	54.51	54.34	51.70	51.78	51.27	51.27	51.92	52.23	52.20	49.06	54.20		52.47	1.54
TiO_2	0.00	0.00	0.00	0.00	0.00	0.00	0.00	0.00	0.00	0.00	0.00	0.00	0.00	0.00	0.00	0.00		0.00	0.00
Al_2O_3	29.01	29.63	29.70	30.45	30.73	28.44	28.26	30.56	31.10	30.03	29.96	30.25	30.06	30.69	32.38	29.35		30.04	1.02
FeO	0.13	0.10	0.21	0.18	0.16	0.26	0.26	0.33	0.36	0.27	0.31	0.27	0.20	0.25	0.06	0.12		0.22	0.09
MnO	0.00	0.00	0.00	0.00	0.00	0.00	0.00	0.00	0.00	0.00	0.00	0.00	0.00	0.00	0.00	0.00		0.00	0.00
MgO	0.06	0.30	0.03	0.04	0.07	0.06	0.05	0.11	0.11	0.09	0.11	0.11	0.08	0.09	0.14	0.06		0.09	0.06
CaO	11.79	11.57	11.75	13.56	13.73	10.73	10.75	13.87	13.80	13.45	13.42	13.45	13.07	13.02	15.31	11.87		12.82	1.27
Na_2O	4.58	5.16	4.95	3.76	3.48	5.21	5.27	4.10	3.94	4.42	4.34	4.37	4.49	4.43	3.26	4.90		4.42	0.60
K_2O	0.90	0.02	0.04	0.00	0.00	0.03	0.03	0.03	0.03	0.08	0.03	0.03	0.03	0.02	0.00	0.03		0.08	0.22
Total:	99.45	100.61	100.77	99.68	99.51	99.24	98.96	100.70	101.12	99.61	99.44	100.40	100.16	100.70	100.21	100.53		100.07	0.65

	Oxide Olivine Gabbro Samples															
Core/Section:	38R-3	47R-2	47R-2	52R-4	52R-4	54R-4	54R-4	54R-4	54R-4	80R-6	80R-6	81R-1	86R-1	86R-1	N=	14
Interval (cm):	58-64	5-10	5-10	12-25	12-25	0-9	0-9	0-9	0-9	121-129	121-129	130-132	94-101	94-101		
Piece:	2	1	1	1	1	1	1	1	1	14	14	1	8A	8A		
Unit:	III	IV	IV	IV	IV	IV	IV	IV	IV	VI	VI	VI	VI	VI	Mean	1σ
SiO_2	58.53	58.35	58.15	58.88	59.35	60.22	59.93	60.50	59.92	60.22	59.96	52.16	60.53	59.90	59.04	2.14
TiO_2	0.00	0.00	0.00	0.00	0.00	0.00	0.00	0.00	0.00	0.00	0.00	0.00	0.00	0.00	0.00	0.00
Al_2O_3	26.82	26.38	26.43	25.45	26.20	25.89	25.92	25.32	25.55	24.61	24.70	30.29	25.79	25.47	26.06	1.37
FeO	0.25	0.18	0.16	0.32	0.10	0.15	0.32	0.15	0.16	0.20	0.21	0.08	0.20	0.20	0.19	0.07
MnO	0.00	0.00	0.00	0.00	0.00	0.00	0.00	0.00	0.00	0.00	0.00	0.00	0.00	0.00	0.00	0.00
MgO	0.02	0.01	0.01	0.06	0.06	0.06	0.04	0.04	0.04	0.02	0.02	0.06	0.00	0.00	0.03	0.02
CaO	8.29	7.93	7.91	7.51	7.76	7.12	7.40	6.45	6.77	6.15	6.29	12.93	7.04	6.84	7.60	1.67
Na_2O	6.47	7.66	7.40	7.86	7.39	7.33	7.49	8.56	8.37	8.05	8.44	4.24	6.66	7.15	7.36	1.09
K_2O	0.13	0.10	0.13	0.03	0.10	0.13	0.13	0.15	0.12	0.17	0.14	0.00	0.17	0.14	0.12	0.05
Total:	100.51	100.61	100.19	100.11	100.96	100.90	101.23	101.17	100.93	99.42	99.76	99.76	100.39	99.70	100.40	0.59

Values are from Hebert *et al.* (1991). 1σ = one standard deviation from the mean.

Table 5.1b Microprobe analyses of primary clinopyroxene

	Olivine Gabbro Samples																
Core/Section:	13R-1	14R-1	14R-1	25R-2	44R-3	57R-3	61R-1	64R-2	64R-4	69R-2	74R-5	75R-5	82R-4	83R-6	84R-7	N=	15
Interval (cm):	102-105	26-29	26-29	5-7	96-101	37-43	126-135	74-84	105-112	55-67	84-92	45-53	12-20	53-59	13-23		
Piece:	11B	2A	2A	1A	4	1C	5	1E	4	2B	3B	1B	1B	3	1D		
Unit:	II	II	II	II	III	V	V	V	V	V	V	V	VI	VI	VI	Mean	1σ
SiO_2	50.62	50.10	51.82	50.53	52.19	50.86	51.50	51.50	49.27	51.97	51.66	50.84	52.92	53.41	51.94	51.41	1.07
TiO_2	0.87	0.71	0.13	0.55	0.40	0.62	0.53	0.45	0.50	0.40	0.55	0.48	0.41	0.38	0.58	0.50	0.17
Al_2O_3	2.87	2.66	0.68	2.86	3.38	2.36	2.14	3.06	4.32	2.64	2.58	3.15	3.16	3.09	2.83	2.79	0.77
FeO	8.10	11.57	8.21	7.86	6.50	9.04	8.11	5.94	6.57	6.56	6.87	6.27	5.32	5.52	6.95	7.29	1.60
MnO	0.39	0.51	0.41	0.33	0.21	0.37	0.32	0.21	0.27	0.25	0.29	0.36	0.17	0.17	0.30	0.30	0.10
MgO	16.79	14.19	14.89	15.86	16.36	16.86	16.60	18.15	17.06	17.96	17.74	17.61	17.24	17.37	16.16	16.72	1.11
CaO	19.27	20.08	22.78	21.20	20.90	18.09	20.23	19.82	21.48	19.80	20.18	20.56	20.51	19.90	21.17	20.40	1.07
Na_2O	0.50	0.40	0.17	0.42	0.40	0.44	0.38	0.42	0.43	0.38	0.41	0.35	0.41	0.35	0.56	0.40	0.08
K_2O	0.02	0.00	0.00	0.01	0.00	0.00	0.00	0.00	0.00	0.00	0.00	0.00	0.00	0.00	0.00	0.00	0.01
Total:	99.51	100.22	99.09	99.62	100.69	98.68	99.91	99.81	100.11	100.13	100.39	99.74	100.52	100.44	100.24	99.94	0.55

	Oxide Olivine Gabbro Samples											
Core/Section:	38R-3	38R-3	47R-2	48R-3	51R-3	52R-4	54R-4	54R-4	80R-6	81R-1	N=	10
Interval (cm):	58-64	58-64	5-10	28-32	110-114	12-25	0-9	0-9	121-129	130-132		
Piece:	2	2	1	1C	1E	1	1	1	14	1		
Unit:	III	III	IV	IV	IV	IV	IV	IV	VI	VI	Mean	1σ
SiO_2	50.77	50.20	51.17	50.38	51.18	50.77	51.03	50.61	50.13	50.93	50.72	0.38
TiO_2	0.67	0.63	0.63	0.81	0.74	0.64	0.36	0.41	0.38	0.42	0.57	0.16
Al_2O_3	2.13	2.32	1.93	2.03	2.31	1.82	1.18	1.15	1.00	3.78	1.97	0.80
FeO	12.42	13.23	11.89	12.93	12.86	13.67	16.22	16.87	16.93	5.46	13.25	3.32
MnO	0.47	0.49	0.47	0.62	0.39	0.60	0.51	0.70	1.43	0.20	0.59	0.33
MgO	12.69	12.93	13.29	13.10	12.94	12.57	11.30	11.54	12.65	18.22	13.12	1.90
CaO	20.62	19.32	19.75	19.92	18.95	19.99	18.95	18.16	17.48	20.04	19.32	0.95
Na_2O	0.44	0.46	0.00	0.45	0.46	0.40	0.42	0.49	0.07	0.38	0.36	0.17
K_2O	0.00	0.00	0.00	0.00	0.00	0.00	0.00	0.00	0.00	0.00	0.00	0.00
Total:	100.21	99.58	99.13	100.24	99.83	100.48	99.97	99.93	100.07	99.72	99.92	0.38

Values are from Hebert *et al.* (1991). NiO and Cr_2O_3 data has been removed. 1σ = one standard deviation from the mean.

Table 5.1c Microprobe analyses of primary olivine

	Olivine Gabbro Samples													
Core/Section:	13R-1	44R-3	44R-3	61R-1	69R-2	74R-5	75R-5	81R-6	82R-4	83R-6	84R-7	86R-4	N=	12
Interval (cm):	102-105	37-40	37-40	126-135	55-67	84-92	27-30	77-86	12-20	53-59	13-23	64-70		
Piece:	11B	5D	5D	5	2B	3B	1A	4B	1B	3	1A	3B		
Unit:	II	III	III	V	V	V	V	VI	VI	VI	VI	VI	Mean	1σ
SiO_2	37.93	38.13	38.05	38.69	37.64	39.02	37.27	38.44	38.44	39.51	37.29	37.29	38.14	0.72
TiO_2	0.00	0.00	0.00	0.00	0.00	0.00	0.00	0.00	0.00	0.00	0.00	0.00	0.00	0.00
Al_2O_3	0.00	0.00	0.00	0.00	0.00	0.00	0.00	0.00	0.00	0.00	0.00	0.00	0.00	0.00
FeO	25.67	19.48	19.51	21.73	22.19	22.93	20.38	18.89	18.42	15.56	26.24	28.42	21.62	3.71
MnO	0.52	0.37	0.38	0.40	0.42	0.43	0.49	0.45	0.38	0.31	0.53	0.73	0.45	0.11
MgO	36.54	42.11	41.84	38.84	39.61	38.27	40.97	41.08	43.08	44.68	36.17	34.15	39.78	3.11
CaO	0.03	0.04	0.00	0.08	0.07	0.03	0.00	0.05	0.06	0.05	0.13	0.02	0.05	0.04
Na_2O	0.00	0.00	0.00	0.00	0.00	0.00	0.00	0.00	0.00	0.00	0.00	0.00	0.00	0.00
K_2O	0.00	0.00	0.00	0.00	0.00	0.00	0.00	0.00	0.00	0.00	0.00	0.00	0.00	0.00
Total:	100.69	100.13	99.87	99.80	100.09	100.71	99.11	99.35	100.41	100.14	100.38	100.62	100.11	0.51

	Oxide Olivine Gabbro Samples									
Core/Section:	51R-3	51R-3	54R-4	54R-4	54R-4	54R-4	80R-6	81R-1	N=	8
Interval (cm):	110-114	110-114	0-9	0-9	0-9	0-9	121-129	130-132		
Piece:	1E	1E	1	1	1	1	14	1		
Unit:	IV	IV	IV	IV	IV	IV	VI	VI	Mean	1σ
SiO_2	33.85	33.70	32.80	32.64	32.64	36.98	32.63	38.46	34.21	2.25
TiO_2	0.00	0.00	0.00	0.00	0.00	0.00	0.00	0.00	0.00	0.00
Al_2O_3	0.00	0.00	0.00	0.00	0.00	0.00	0.00	0.00	0.00	0.00
FeO	44.49	46.58	51.47	51.56	52.35	26.34	50.08	22.78	43.21	11.85
MnO	0.71	0.74	1.02	1.04	1.47	0.59	1.16	0.50	0.90	0.33
MgO	21.38	19.30	14.41	14.13	13.17	36.18	15.74	38.83	21.64	10.20
CaO	0.00	0.00	0.10	0.10	0.08	0.00	0.12	0.07	0.06	0.05
Na_2O	0.00	0.00	0.00	0.00	0.00	0.00	0.00	0.00	0.00	0.00
K_2O	0.00	0.00	0.00	0.00	0.00	0.00	0.00	0.00	0.00	0.00
Total:	100.43	100.32	99.80	99.47	99.76	100.09	99.73	100.67	100.03	0.41

Values are from Hebert *et al.* (1991). NiO and Cr_2O_3 data has been removed. 1σ = one standard deviation from the mean.

Table 5.1d Microprobe analyses of primary ilmenite from oxide olivine gabbro samples

Core/Section:	48R-3*	50R-3*	51R-1*	51R-3*	86R-1*	49R-2+	49R-3+	52R-4+	52R-4+	53R-4+	53R-4+	73R-5+	73R-5+	79R-2+	N=	14
Interval (cm):	28-32	91-98	79-84	110-114	94-101	89-91	89-91	69-71	69-71	68-78	68-78	74-78	74-78	64-67		
Piece:	1C	1D	1D	1E	8A	*na*	*na*	*na*	*na*	*na*	*na*	*na*	*na*	*na*		
Unit:	IV	IV	1V	IV	IV	*na*	*na*	*na*	*na*	*na*	*na*	*na*	*na*	*na*	Mean	1σ
TiO_2	50.07	51.23	49.67	51.08	50.24	51.57	51.04	49.57	50.02	49.15	50.19	49.78	48.29	50.36	50.16	0.88
Al_2O_3	0.00	0.00	0.00	0.00	0.00	0.00	0.00	0.00	0.00	0.00	0.00	0.02	0.00	0.00	0.00	0.01
FeO	45.73	45.98	48.93	46.56	45.90	47.03	47.82	46.61	46.77	48.34	48.28	48.50	48.83	46.64	47.28	1.13
MnO	1.45	1.24	1.05	0.66	1.19	1.28	0.73	0.77	0.78	1.30	0.79	1.21	1.43	0.71	1.04	0.29
MgO	1.84	2.06	1.13	1.45	1.21	0.41	0.37	0.93	0.93	0.03	0.21	0.29	0.12	0.57	0.83	0.65
Total:	99.09	100.51	100.78	99.75	98.54	100.29	99.96	97.88	98.50	98.82	99.47	99.80	98.67	98.28	99.31	0.90

Values are from: * = Hebert *et al*. (1991); + = Natland *et al*. (1991). FeO and Fe_2O_3 have been converted to FeO_t for samples from Natland *et al*. (1991). 1σ = one standard deviation from the mean; na = not available.

Table 5.1e Microprobe analyses of primary magnetite from oxide olivine gabbro samples

Core/Section:	49R-2	49R-3	52R-4	53R-4	53R-4	73R-5	73R-5	79R-2	79R-2	N=	9
Interval (cm):	89-91	89-91	69-71	68-78	68-78	74-78	74-78	64-67	64-67	Mean	1σ
TiO_2	4.94	6.06	6.54	4.42	5.50	0.78	2.77	13.14	3.08	5.25	3.47
Al_2O_3	2.85	2.90	2.03	0.45	0.88	0.74	0.93	0.90	11.85	2.61	3.58
FeO	85.10	83.26	82.63	85.19	84.75	91.09	91.26	78.63	79.74	84.63	4.36
MnO	0.22	0.19	0.27	0.17	0.23	0.11	0.23	1.44	0.16	0.34	0.42
MgO	0.34	0.17	0.08	0.02	0.00	0.01	0.05	0.33	0.75	0.19	0.25
Total:	93.45	92.58	91.55	90.25	91.36	92.73	95.24	94.44	95.58	93.02	1.82

Values are from Natland *et al.* (1991). 1σ = one standard deviation from the mean. FeO and Fe_2O_3 have been converted to FeOt.

amphibole formed from alteration of pyroxene; 2) sodic plagioclase formed from alteration of calcic plagioclase; and 3) altered ilmenite, magnetite, and olivine formed from alteration of fresh equivalents. Clearly all amphibole did not form by alteration of pyroxene; some is after olivine. However, amphibole that replaces olivine is commonly much more magnesium-rich than that after pyroxene and the two can be easily distinguished. Mineral classification is discussed later in this chapter (section 5.3.3).

5.2 METHODS

Gridded microprobe data were collected from five polished thin sections using the analytical methods described in Appendix 1. Samples were analyzed for nine oxides: SiO_2, TiO_2, Al_2O_3, FeO, MnO, MgO, CaO, Na_2O, and K_2O. The grid spacing was set at 0.5mm in both directions, in order to obtain a reasonable number of points per grain and reduce analysis time to a manageable level. Microprobe grids were manually configured using backscatter x-ray images. In all cases, the maximum possible area for each thin section was analyzed. Grid sizes (and the number of points) vary between samples because of differences in thin section sizes and shapes. The number of points analyzed per sample varied from 1215 to 2475. Once the microprobe grid file was created, stage control was automatic. Average microprobe runs lasted 7-8 hours.

Microprobe data were then imported into Microsoft® Excel® 5.0. An example of a data sheet is shown in Table 5.2. Residual chemistry (altered minus primary) was calculated using a program written in Visual Basic®. This program is discussed in detail later in this chapter. Grid files were created from the residual data in SURFER® for Windows™ based on the original microprobe grid geometry. For each sample, a contour map of residual chemistry was created from grid files for each of the eight oxides. Negative residuals represent losses and positive residuals represent gains in the host rock as a result of alteration. All maps are contoured at intervals of 5 wt% from -50 to 50 wt%. These values were chosen to convey the maximum amount of information possible while trimming outliers. As a result, residual values greater than 50 wt% or less than -50

Table 5.2 Example of microprobe data sheet.

Point	SiO2	TiO2	Al2O3	FeO	MnO	MgO	CaO	Na2O	K2O	Total	Beam current
1	-0.0826	0.1907	-0.1096	0.1478	0.0365	0.186	0.1203	0.0442	-0.0302	0	15.5
2	51.6733	0.2886	2.9235	6.2413	0.6891	21.1564	13.7784	0.9518	-0.0054	96.72	15.5
3	50.6937	0.5799	2.9372	7.7509	0.0062	18.7163	16.2455	0.4068	-0.0393	96.34	15.5
4	45.6888	-0.2531	3.9083	7.6788	0.8834	16.9636	17.3939	0.5632	0.198	91.63	15.5
5	7.9513	-0.3226	0.5303	64.9071	-0.1501	4.7666	-0.0609	0.6621	-0.0866	77.63	15.5
6	53.5595	-0.0411	2.4241	5.8532	0.3071	21.272	11.2154	0.5769	0.2721	94.32	15.5
7	50.0553	-0.2014	5.8302	7.4642	0.2454	19.086	12.0657	1.5252	-0.0721	96.03	15.5
8	52.642	0.0285	22.2739	2.1469	0.1087	3.3218	5.8789	6.4591	0.0517	92.72	15.5
9	53.0212	-0.2455	27.1196	0.3375	-0.6164	0.061	11.0001	5.124	0.0541	96.26	15.5
10	58.6687	0.2395	23.1193	-0.1546	0.1089	0.0746	5.9877	8.861	-0.0207	96.64	15.5
11	43.3984	0.104	23.9712	-0.2007	0.0936	0.2764	1.5187	12.7945	0.0098	81.68	15.5
12	54.8506	-0.3048	21.3551	0.5406	0.3304	-0.102	3.7379	10.3002	0.1972	90.24	15.5
13	52.4015	0.2597	27.0915	0.6992	-0.0633	-0.0261	11.6041	5.0472	-0.0872	96.14	15.5
14	52.6031	0.7029	28.629	1.0421	-0.0472	0.1159	10.487	5.5952	-0.0535	98.02	15.5
15	38.734	0.1687	19.1776	0.1919	-0.2508	0.78	8.205	3.2115	1.041	71.15	15.5
...continued											

Values are taken from sample 58R-3 and are actual values.

wt% are grouped into the >50 wt% and <-50 wt% contours, respectively. The contours were smoothed using a low pass simple cubic spline interpolation to provide a pleasing image, however, every attempt was made to preserve the original data.

5.2.1 Sample Selection

The main objective of the sampling strategy was to choose samples which contained distinct veins displaying petrographic signs of host rock alteration proximal to the vein. All samples selected were also chosen for element-flux calculations and three were chosen for mineral traverses to allow comparison of results at different scales. As a result five samples were selected. These include two lithologies: olivine gabbro (4 samples) and oxide olivine gabbro (1 sample). Full petrographic descriptions and thin section photos of the samples are available in Appendix 2.

5.3 RESIDUAL PROGRAM DESCRIPTION

The method of residual chemistry calculation presented in this study provides a new method for quantification of chemical changes at the thin section scale. This method is highly dependent on the assumptions outlined above and the boundary conditions set up in the residual progam. These conditions specify parameters such as how points are classified and how residuals are calculated. As a result, it is necessary to explain fully each subroutine in the residual program to better understand how residuals are calculated.

The following sections include detailed explanations of various portions of the residual program (see Appendix 3). Each section corresponds to the main subroutines in the residual program. Visual Basic® syntax is not discussed, however, a more detailed explanation of Visual Basic® code can be found in the Visual Basic® Users Guide. The residual program was run as a macro in Microsoft® Excel® 5.0. A flowchart of the program's operation is given in Figure 5.1.

Figure 5.1 Flowchart of residual program operation. Arrows link operations and Excel® sheets. Major program subroutines are set in bold type. Excel® sheet names are outlined by boxes. Short descriptive explanations of each step are found to the right. See text for explanation.

Start with microprobe data in text file.

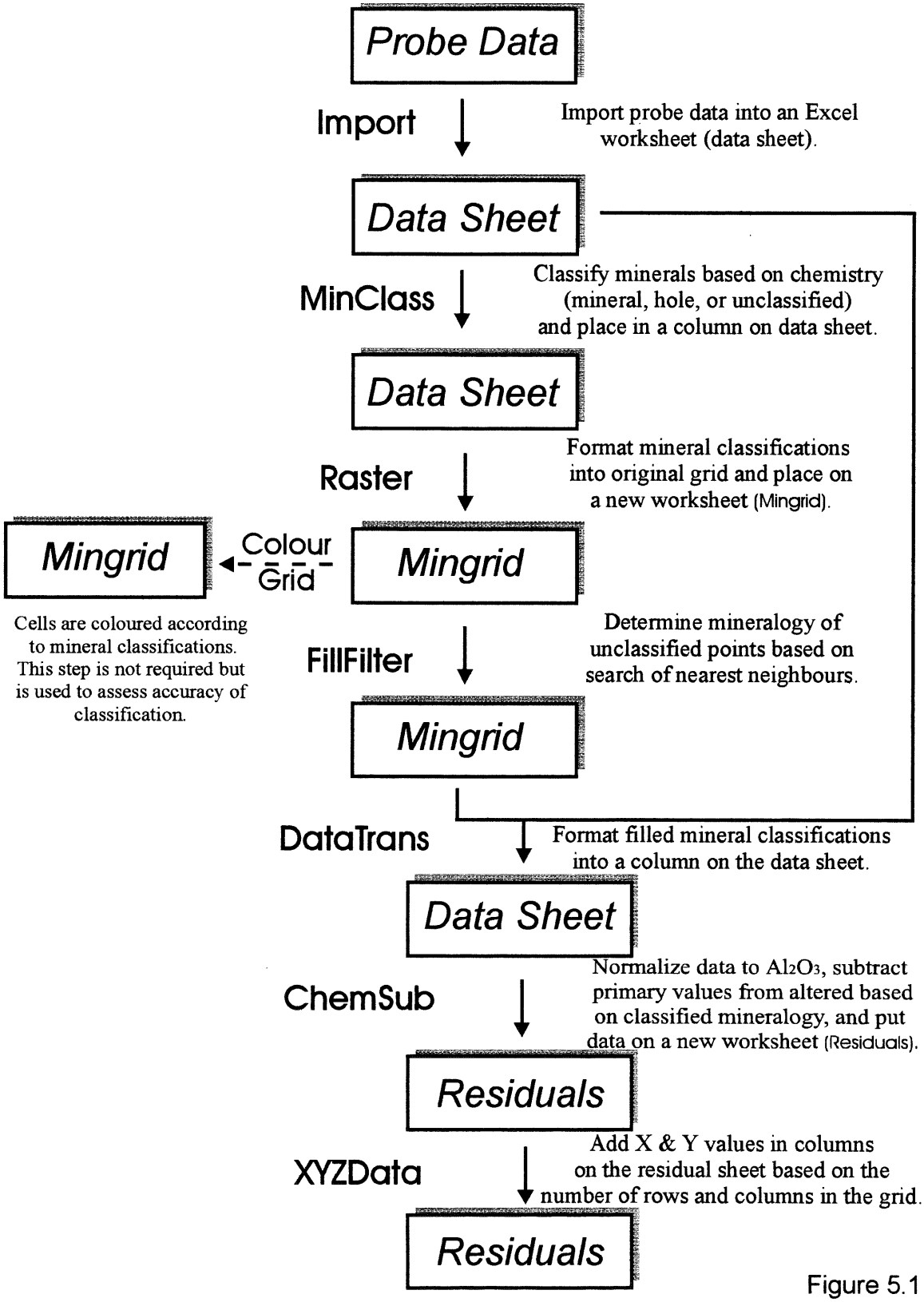

Figure 5.1

5.3.1 Variable Setup

The first section sets up the universal variables used in the program. Brief descriptions of each variable are given in the right column of the code in Appendix 3.

5.3.2 Main Program

The main program (ResidualMap) controls screen updating, execution of subroutines, and allows the user to input parameters which are specific to individual thin sections. This includes the number of points, rows and columns in the microprobe grid. There are seven subroutines, each of which is discussed individually.

5.3.3 Mineral Classification Subroutine

The mineral classification subroutine (MinClass) classifies each grid point based on its overall composition and places the value in a column on the data sheet. There are nine possible classifications: H = hole; Q = quartz; M = magnetite; I = ilmenite; O = olivine; X = clinopyroxene; L = calcic plagioclase; N = sodic plagioclase; A = amphibole; and - = unclassified. The column values in the code (Appendix 3) used for mineral classification correspond to those in Table 5.2. Minerals were classified according to the following criteria:

Hole: total < 70 wt%

Quartz: SiO_2 > 70 wt%

Magnetite: FeO > 70 wt%

Ilmenite: TiO_2 > 30 wt%; SiO_2 < 10 wt%; and FeO > 20 wt%

Olivine: MgO > 25 wt%; and Al_2O_3 < 1 wt%

Clinopyroxene: CaO > 15 wt%; and Al_2O_3 <5 wt%

Calcic Plagioclase: FeO < 2 wt%; Na_2O < 5.5 wt%; and CaO > 10 wt%

Sodic Plagioclase: FeO < 2 wt%; Na_2O > 5 wt%; and CaO < 10 wt%

Amphibole: CaO < 15 wt%; FeO > 5 wt%; MgO > 3 wt%

These classifications were determined by grouping subsets of gridded microprobe analyses, within the host rock, on the basis of mineralogy. Approximately 20 points were used for each mineral. Ranges of element variability were determined from these subsets and used in constructing classification schemes. Each classification scheme was designed to be mutually exclusive in order to be mineral specific. This subroutine behaves such that classification schemes are applied sequentially to each point until the conditions are fulfilled, at which time the program continues to the next point. As a result, minerals which can be most accurately identified appear at the beginning of the list. Classifications were thoroughly tested and reconfirmed by comparison with petrography and reconnaissance microprobe analyses. As a result, the classifications are believed to be very accurate for analyses within the host rock. Analyses within veins are less accurate due to complex mineralogy in many samples. Also, misidentification is possible which would result in an incorrectly calculated residual. All points not meeting any of these criteria are termed unclassified. Points with totals less than 70 wt% are believed to contain questionable data and are classified as holes.

5.3.4 Data Rastering Subroutine

The data rastering subroutine (Raster) reformats the mineral classifications from a column on the data sheet into their original grid. This is based on the number of rows (RowNum) and columns (ColumnNum) specified by the user in the main program. The grid is inserted on a new worksheet called "mingrid".

5.3.5 Mineral Filling Filter Subroutine

The mineral filling filter subroutine (FillFilter) replaces unclassified points on the "mingrid" worksheet with an appropriate mineral classification based on the asumption that a point is likely to be the same mineral as the majority of its nearest neighbours (spatial autocorrelation). Since the thin sections which have been mapped are predominantly from medium- to coarse-grained samples, most minerals contain several points, at 0.5mm spacing. It is also observed that the majority of unclassified points occur at grain

boundaries or in highly altered areas. Unclassified points at grain boundaries are almost certainly similar to their neighbours. Furthermore, points in highly altered areas are classified based on previous classifications which are well constrained.

Reclassification is accomplished through a number of nested subroutines within the FillFilter subroutine. The nine nearest neighbours of unclassified points are searched in a box pattern (BoxFilter) unless the point occurs in a location which does not have nine neighbours. This includes points located in the top row, bottom row, left column, right column, or any corner. In these locations only a subset of the nine nearest neighbours is searched which is determined by a group of subroutines of the same name, such as: TopRow, UpperLeftCorner, etc. (see code for all subroutine names). An example of all subroutine search patterns is shown in Figure 5.2. All neighbouring cells are given equal weighting. The unclassified point is reclassified as the most frequent mineral among the neighbours searched. In the case of a tie, the point is reclassified in the following order: calcic plagioclase → sodic plagioclase → clinopyroxene → amphibole → olivine → ilmenite → magnetite → quartz. This order is based on the modal mineralogy of the samples analyzed, in decreasing abundance.

Once a point has been reclassified, the program searches for the next unclassified point. The search pattern is from left to right, by row, and beginning in the upper left corner. As a result points which are reclassified in previous rows will affect later points. This is necessary to ensure no points will be surrounded by unclassified neighbours. This is not believed to influence the reclassification because of the scarcity of unclassified points surrounded by unclassified neighbours in test runs.

5.3.6 Mineral Grid Colouring Subroutine

The mineral grid colouring subroutine (ColourGrid) was originally written during development of the MinClass and FillFilter subroutines and provides an easy way to assess their accuracy with respect to the observed petrography. This subroutine simply changes the background colour of each cell on the "mingrid" worksheet based on its classification. Adjacent points with the same colour define mineral grains which can be compared with

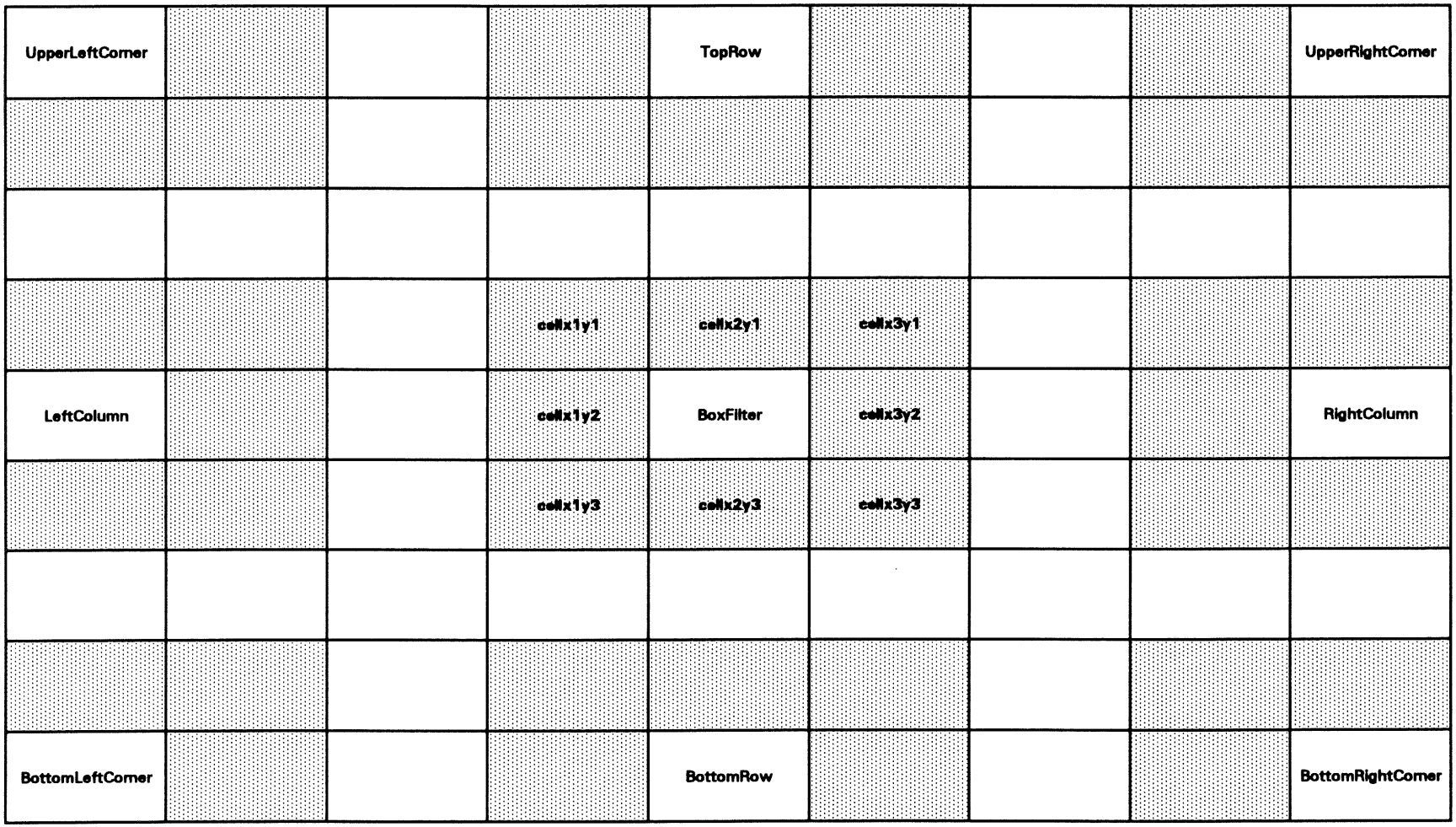

Figure 5.2 Example grid with search patterns from FillFilter subroutine. Search patterns are shaded. The name of the search subroutine is indicated for the point on which it is performed. Cell subroutines are indicated for the BoxFilter search but are the same for all searches.

sketches made from petrographic observations of each thin section. Coloured mingrid sheets (Figures 5.3, 5.6, 5.9, 5.12, and 5.15), thin section photos (Appendix 2), and thin section sketches (Figure 5.4, 5.7, 5.10, 5.13, and 5.16) show very good agreement for the samples analyzed which further supports accurate classification. Although this subroutine does not directly affect the residual calculation, it is included to show that all operations were compared with petrographic observations.

5.3.7 Data Transfer Subroutine

The data transfer subroutine (DataTrans) reformats the filled mineral grid back into a column on the original data sheet. The transferred column is next to the original classification column from the MinClass subroutine which allows quick comparison.

5.3.8 Residual Calculation Subroutine

The residual calculation subroutine (ChemSub) subtracts primary mineral compositions from normalized gridded microprobe data. Minerals which contain Al_2O_3 are normalized to constant Al_2O_3 and minerals which do not contain Al_2O_3 are given a normalization ratio of 1. Primary mineral analyses for both of the represented units, olivine gabbro and oxide olivine gabbro, have been gathered from published data (Hébert *et al.* , 1991; Natland *et al.*, 1991) and averaged (Table 5.1). Analyses of primary ilmenite and magnetite were not available for olivine gabbro samples. Samples from which primary analyses have been used were paired with the appropriate lithology by using the lithostratigraphy of Dick *et al.* (1991). One standard deviation from the mean for each element has been quoted to provide an estimate of chemical variability.

Residuals were calculated using the following formula:

$$(N^P \times X_e^B) - X_e^A = R_e^P \qquad 5.1$$

In this equation, mineral A is altered to mineral B. X_e^z is the weight fraction of element e, expressed in oxide weight percent, for mineral z which is known from chemical analysis.

R_e^p is the residual calculated for element e at point p. N^p is the normalization ratio for point p by which the altered mineral is multiplied to correct for passive accumulation of other elements. In cases where a mineral normally contains Al_2O_3, such as amphibole, clinopyroxene, or plagioclase, N^p is calculated using the following formula:

$$N^p = \frac{X^A_{Al_2O_3}}{X^B_{Al_2O_3}} \qquad 5.2$$

where $Al_2O_3^A$ and $Al_2O_3^B$ are the Al_2O_3 values for primary and altered minerals, respectively, at a given point. When combined, these equations are very similar to Equation 4.3 which was used to calculate element fluxes:

$$\left[\left(\frac{X^A_{Al_2O_3}}{X^B_{Al_2O_3}}\right) \times X_e^B\right] - X_e^A = R_e^p \qquad 5.3$$

Calculation of residuals has been constructed in this manner to allow direct comparison of chemical maps with element-flux calculations.

The ChemSub subroutine places all calculated residuals on a new worksheet called "residuals". The values on this sheet are in the same order as the original data sheet (Table 5.2). In order to calculate residuals, microprobe values less than zero are replaced by zero on the data sheet to avoid negative numbers. This is true for all elements except for Al_2O_3 which is set at 0.01(a small positive number) to avoid division by zero. For minerals classified as amphibole, clinopyroxene, sodic plagioclase, or calcic plagioclase, the normalization ratio is calculated using Equation 5.2. If the calculated value for the normalization ratio is greater than 2, which can occur if the primary Al_2O_3 value is significantly greater than the altered value, the normalization ratio is reset to a value of 1.99. This is necessary to ensure that overly high residuals are not calculated which would otherwise skew the data. For minerals classified as olivine, quartz, ilmenite, or magnetite,

the normalization ratio is set at 1. This is necessary because of the very low values of Al_2O_3 in these minerals. A normalization ratio of 1 was chosen because normalization to another element was not possible. It was necessary to be consistent between oxides, and normalization to 1 does not influence the data. Finally, the residual for each of the eight remaining elements is calculated using Equation 5.1 and the value is placed in the appropriate column on the "residuals" worksheet. Negative residuals represent losses and positive residuals represent gains in the host rock as a result of alteration. Points which have been classified as holes are assumed to contain questionable data which precludes calculation of a residual for that point. In addition, residuals were not calculated for points classified as ilmenite or magnetite in olivine gabbro samples because equivalent analyses of primary minerals were not available. In these cases, a value of zero is substituted for each of the eight oxides, which represents a background value.

5.3.9 Grid Coordinate Subroutine

The XYZData subroutine creates two columns on the "residuals" worksheet containing the X and Y coordinates of each point. Since all of the original microprobe grid files were created using a spacing of 0.5 mm in both the X and Y directions, the X and Y coordinates are simply calculated from the number of rows and columns specified by the user for that sample. The values are calculated in order to be imported into SURFER® for Windows™. As a result, the first point has the largest Y value because SURFER® begins at the lower left corner during creation of grid files.

5.4 RESULTS

Residual chemical maps are plotted in Figures 5.5, 5.8, 5.11, 5.14, and 5.17. Each of these five figures contains residual maps for each of the eight oxides analyzed (labelled a through h). Map areas differ between samples because of differences in thin section sizes and shapes. In each case, the largest area possible was analyzed. The location of the vein in each sample has been indicated in grey. In addition, mineralogy from thin section

sketches has been overlain on each residual map to relate residual chemistry to mineralogy (dashed lines). The location of minerals from thin section sketches is only approximate. Mingrid worksheets (Figures 5.3, 5.6, 5.9, 5.12, and 5.15) and thin section sketches (Figures 5.4, 5.7, 5.10, 5.13, and 5.16) for each sample preceed the residual maps. Some residual maps contain diamond shaped patterns. This pattern is an artifact of the contouring routine and is related to a large contrast in values between adjacent grid nodes. Sample photographs are found in Figure 4.3 and thin section photographs and petrographic descriptions are found in Appendix 2. A brief description of chemical trends for each sample follows.

5.4.1 Sample 31R-3 4-10 cm

SiO_2 residuals exhibit a large range of variability, however, most values range between -5 and 5 wt%. Large, positive SiO_2 residuals (> 20 wt%) observed near the vein represent vein material which has not been adequately included in the thin section sketch. Other areas containing large, positive SiO_2 residuals (> 20 wt%) seem to be associated with amphibole, as identified on the mingrid worksheet (Figure 5.3). Normalization ratios in these areas are large (>1.5), possibly representing Al mobility. Calculated SiO_2 residuals are, therefore, exaggerated and probably reflect gains significantly less than 20 wt% in these areas. Smaller, positive SiO_2 residuals (~5 to 15 wt%) are present in the cores of several cinopyroxene grains, identified from thin section sketches. These positive SiO_2 residuals may represent primary values which are slightly greater than those used for the calculation of residuals. In these cases, SiO_2 residual values are not actual residuals but instead represent primary values.

Large, negative SiO_2 residuals (< -25 to -30 wt%) are isolated and occur predominantly in areas identified as amphibole on the mingrid worksheet (Figure 5.3) and thin section sketch (Figure 5.4). Investigation of original microprobe data in these areas reveals high concentrations of Al_2O_3 (>10 wt%). Detailed petrography suggests these areas resemble replacement by amphibole after olivine, however, the Mg content in microprobe analyses is lower than expected. This has resulted in a classification as

amphibole rather than olivine for these areas. The relatively high Al values suggest that local mobilization of Al probably occurred. Normalization ratios in these areas are very small (< 0.2 to 0.5) which has resulted in exaggerated negative SiO_2 residuals. Actual SiO_2 residuals in these areas are probably significantly less than -30 wt%. SiO_2 residuals do not exhibit any apparent trends with distance from the vein.

FeO residuals are less variable than those for SiO_2 and most values range between -10 and 10 wt %. A single positive residual (~20 wt%) occurs in the top right corner of the map in an area identified as an amphibole on the mingrid worksheet (Figure 5.3). This value is exaggerated in a similar manner to the SiO_2 residuals discussed above. Smaller (~10 wt%) FeO residuals are present at the bottom of the map, near the vein, in an area which was previously identified as possibly exhibiting local Al mobility. These values are most likely also exaggerated. FeO residuals do not exhibit any other apparent trends with either mineralogy or distance from the vein.

CaO residuals range from -20 to 20 wt%. Negative CaO residuals are concentrated near the vein, however, they are also distributed throughout the map. Areas previously identified as amphibole on the mingrid worksheet (Figure 5.3) exhibit negative CaO residuals (-5 to -20 wt%). Residuals in these areas are suspect because the calculated CaO residuals are most likely exaggerated due to local Al mobility. Positive CaO residuals occur in areas identified as the cores of clinopyroxene grains from thin section sketches (Figure 5.4) and are similar in distribution to those identified for SiO_2. CaO residuals do not show any other trends with mineralogy.

MgO residuals range from -20 to 20 wt%. MgO residuals exhibit similar patterns to CaO residuals. For example, negative MgO residuals (~-10 to -20 wt%) occur in similar areas as negative CaO residuals. This includes areas previously identified as amphibole from the mingrid worksheet (Figure 5.3) which possibly exhibit local Al mobility. Positive MgO residuals also occur in similar areas as positive CaO residuals, particularly in the cores of clinopyroxene grains. Positive MgO residuals in the cores of clinopyroxene grains most likely reflect primary variation and not alteration effects.

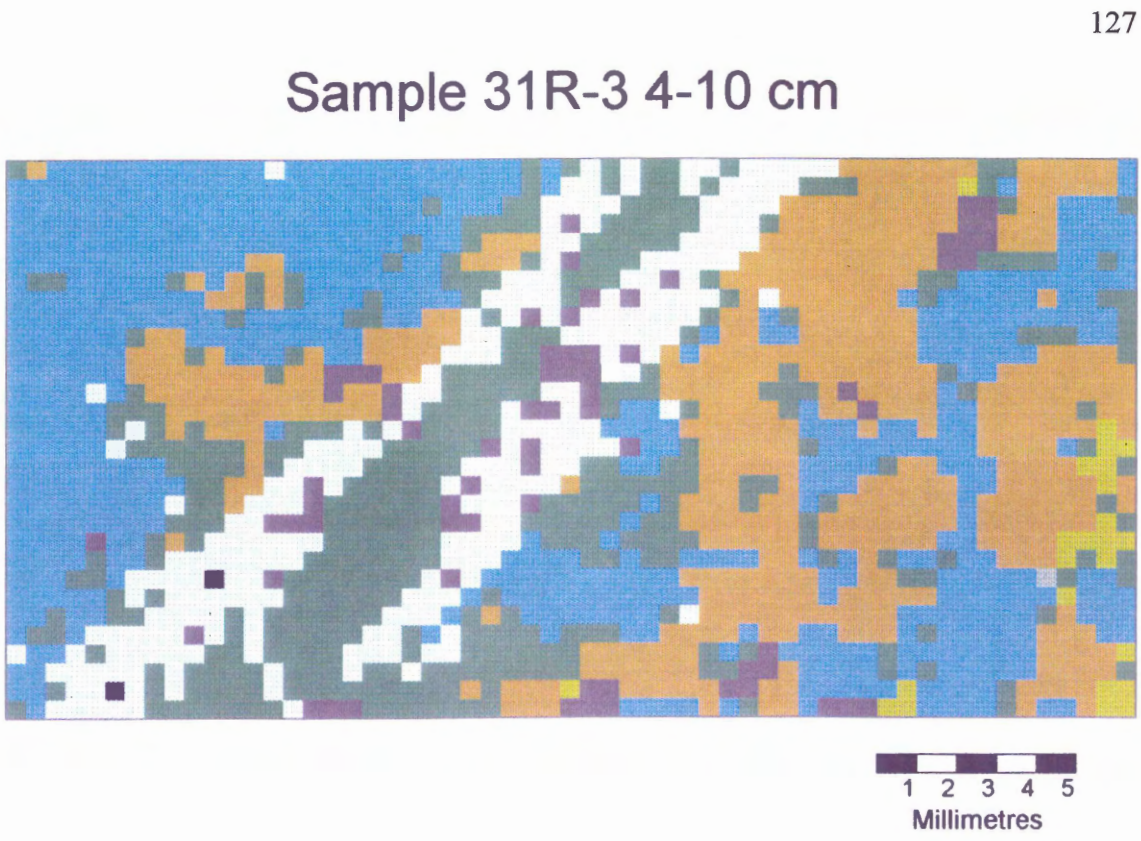

Figure 5.3 Coloured "mingrid" worksheet for sample 31R-3 4-10 cm. Colours represent different minerals. Each coloured cell has dimensions of 0.5 mm square. See text for explanation.

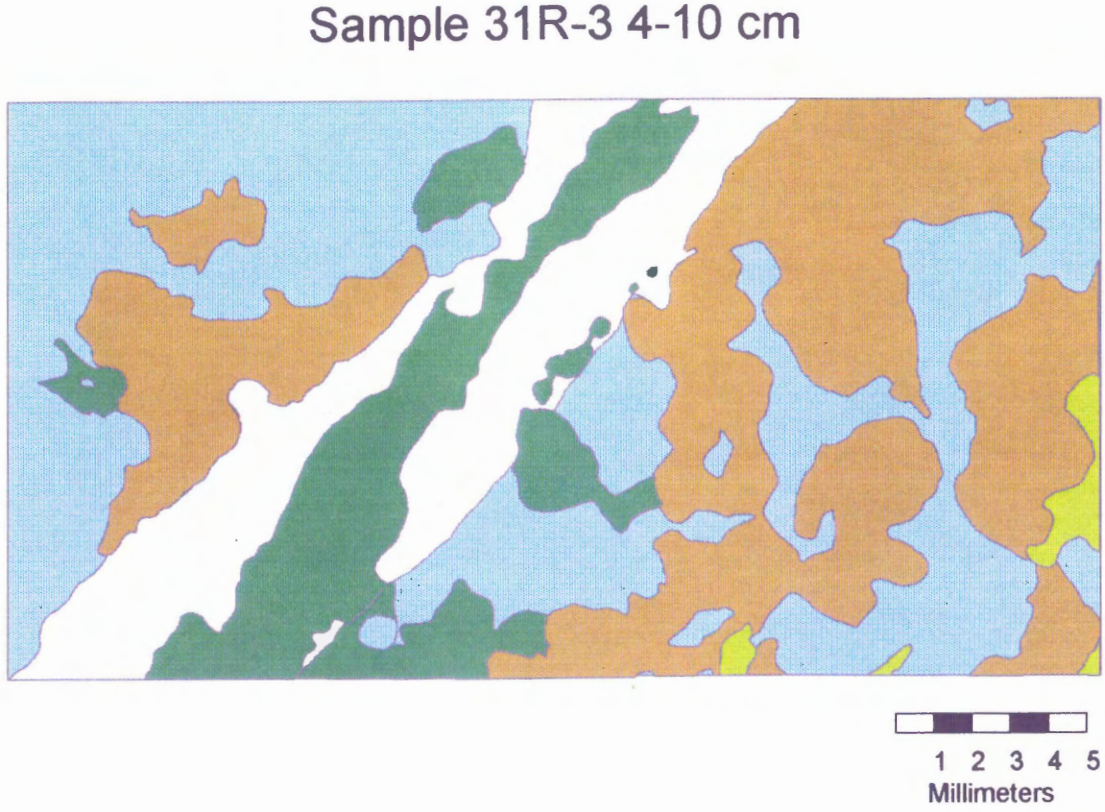

Figure 5.4 Digitized thin section sketch of sample 31R-3 4-10 cm. The thin section was projected onto a screen and traced. The area shown is approximately the same as the area of the chemical map for the sample. Mineralogy is approximate and was confirmed by detailed petrography.

Figure 5.5 Chemical residual maps of SiO_2, FeO, CaO, MgO, Na_2O, K_2O, MnO, and TiO_2 for sample 31R-3 4-10 cm. Negative residuals represent losses and positive residuals represent gains in the host rock as a result of alteration. Contours are drawn at intervals of 5 wt%. Values greater than 50 and less than -50 are grouped into the >50 and <-50 contours, respectively. The vein is indicated in grey and the mineralogy of the sample is indicated by dashed lines. The location of the vein and individual minerals is from Figure 5.4 and is approximate. Scale is in millimeters. See text for explanation.

Sample 31R-3 4-10 cm SiO2

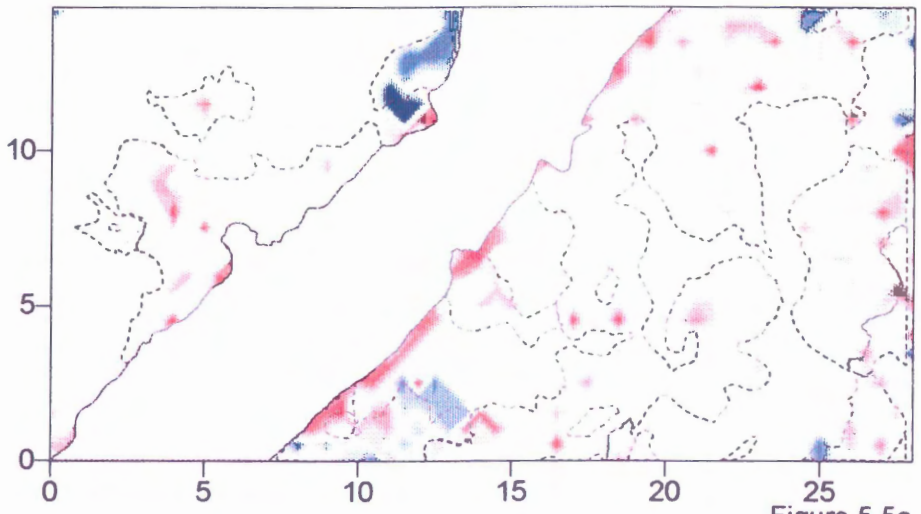

Figure 5.5a

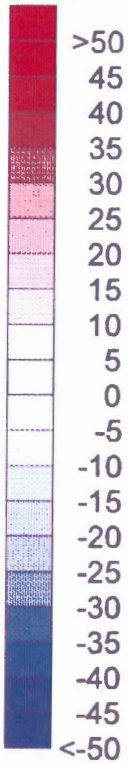

Sample 31R-3 4-10 cm FeO

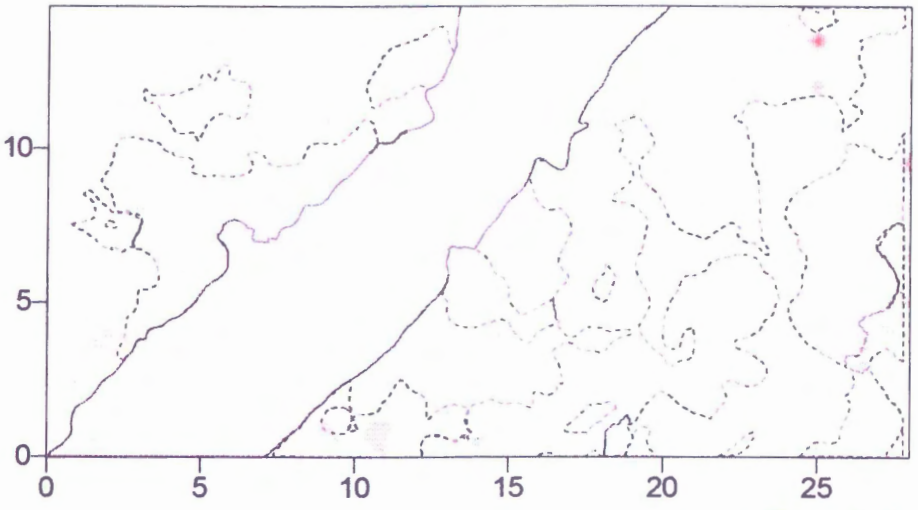

Figure 5.5b

Sample 31R-3 4-10 cm CaO

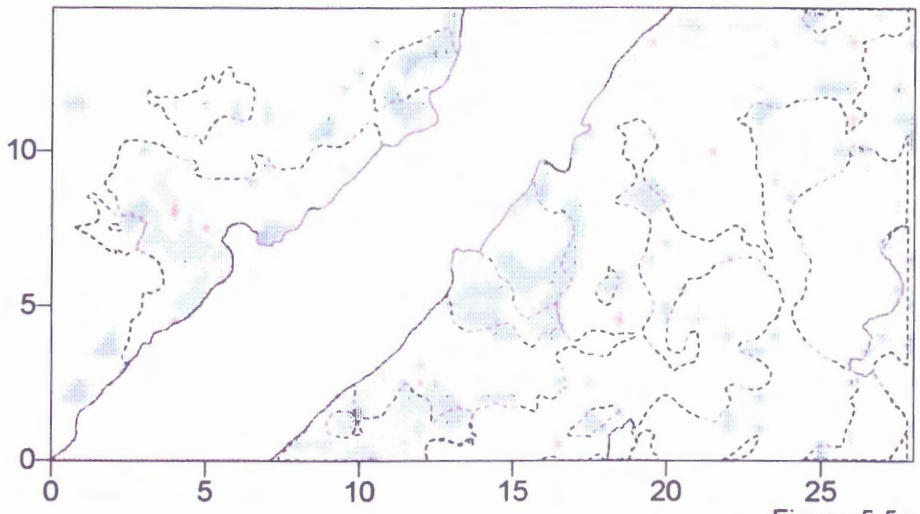

Figure 5.5c

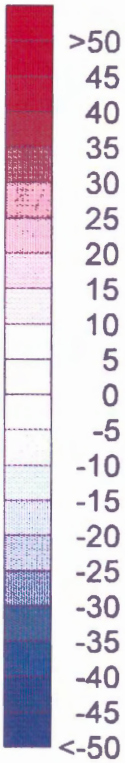

Sample 31R-3 4-10 cm MgO

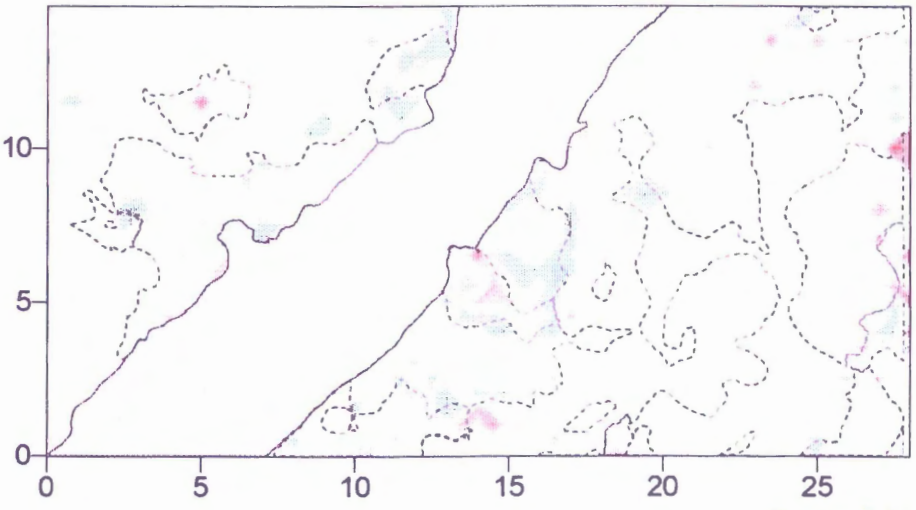

Figure 5.5d

Sample 31R-3 4-10 cm MnO

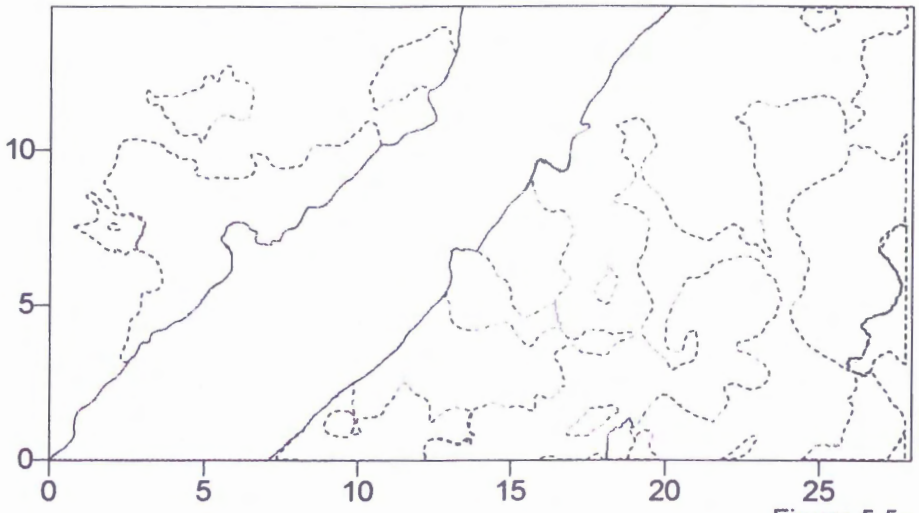

Figure 5.5g

Sample 31R-3 4-10 cm TiO2

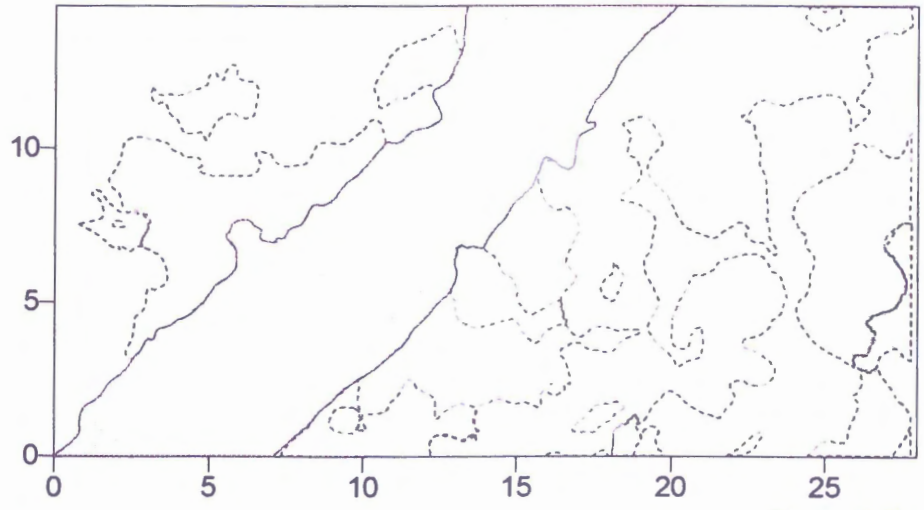

Figure 5.5h

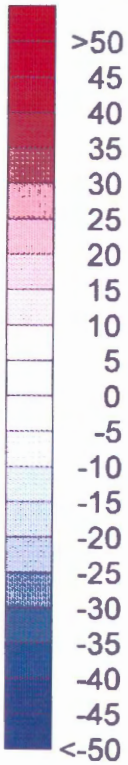

Sample 31R-3 4-10 cm Na2O

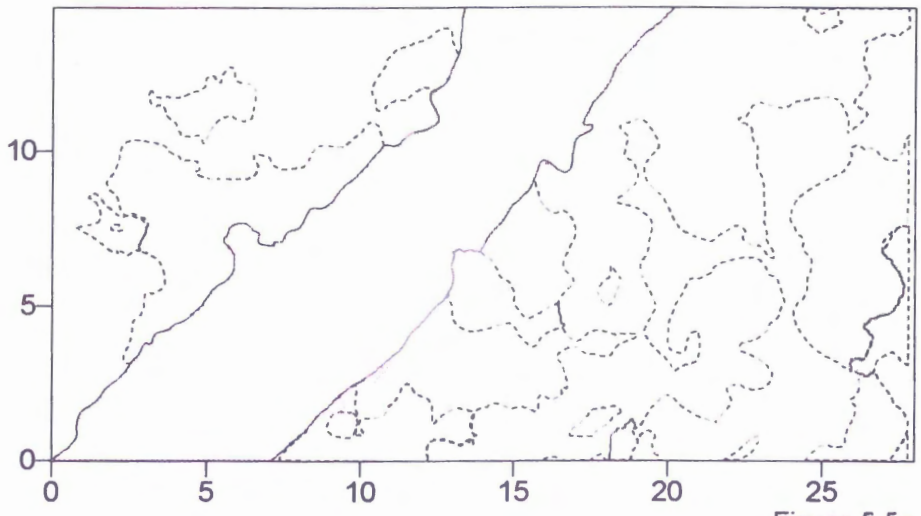

Figure 5.5e

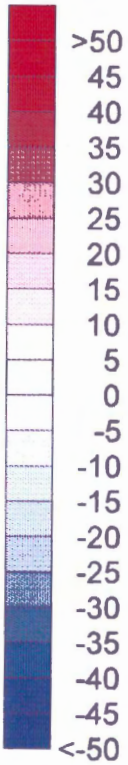

Sample 31R-3 4-10 cm K2O

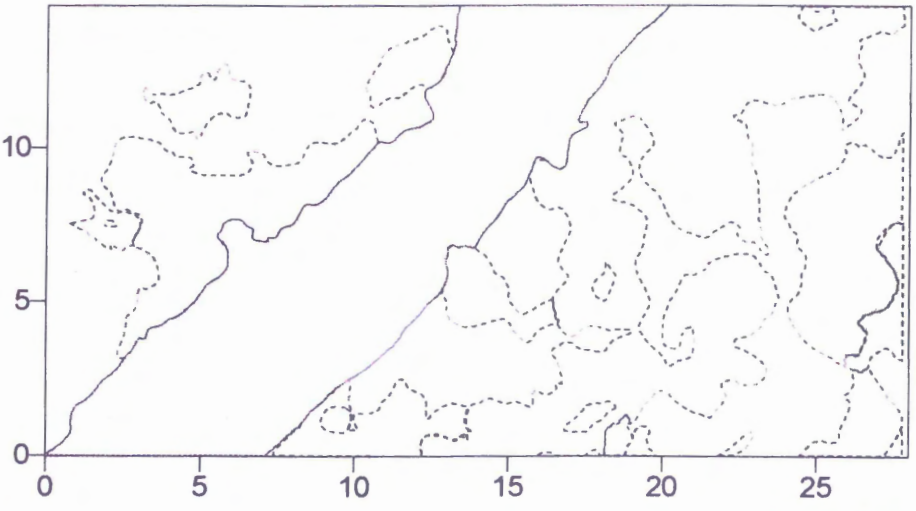

Figure 5.5f

Na_2O, K_2O, MnO, and TiO_2 all exhibit small residual ranges (-5 to 5 wt%). A few larger (~10 to 15 wt%) positive Na_2O residuals are observed near the vein. These positive residuals occur in similar areas as positive SiO_2 residuals which are interpreted to represent vein material which has not been adequately included by the thin section sketch. K_2O residuals seem to be divided into two groups: less than zero, associated with plagioclase, and greater than zero, associated with other minerals (see Figure 5.4). This suggests the primary value of K_2O for plagioclase used in the residual program may be sightly greater than the actual primary value. MnO and TiO_2 show the opposite correlation: values less than zero are associated with clinopyroxene and values greater than zero are associated with plagioclase. Similarly, this suggests the primary values used to calculate residuals for MnO and TiO_2 in clinopyroxene, may be slightly greater than the actual primary value. In these cases, K_2O, MnO, and TiO_2 residual values represent primary variations. Na_2O, K_2O, MnO, an TiO_2 residual maps do not show any variation with distance from the vein.

5.4.2 Sample 35R-4 117-124 cm

SiO_2 residuals exhibit a large range of variability. Areas identified as amphibole, olivine, and sodic plagioclase on the mingrid worksheet (Figure 5.6) exhibit SiO_2 residual values that deviate the most from zero. Large, positive SiO_2 residuals (>20 wt%) occur in areas identified as amphibole on the mingrid worksheet (Figure 5.6). These areas are concentrated around areas identified as olivine and the vein in the thin section sketch (Figure 5.7). Normalization ratios in these areas are greater than 1.5, possibly suggesting Al mobility. Calculated SiO_2 residuals are, therefore, exaggerated in these areas and most likely reflect gains less than 20 wt%. Smaller, positive SiO_2 residuals (5 to 20 wt%) are localized near the vein and values seem to decrease with distance from the vein. These SiO_2 residual values are associated with sodic plagioclase in the mingrid worksheet (Figure 5.6). These values may represent an alteration halo near the vein.

Large, negative SiO_2 residuals (<-25 to -30 wt%) occur in a number of areas identified as amphibole on the mingrid worksheet (Figure 5.6) and thin section sketch

(Figure 5.7). Microprobe analyses in many of these areas reveal high concentrations of Al (>5 to 10 wt%), particularly near olivine identified from the thin section sketch (Figure 5.7). Local Al mobilization likely occured in these areas resulting in very small (<0.2 to 0.5) normalization ratios. Actual SiO_2 residuals in these areas are most likely significantly less than - 30 wt%.

Most FeO residuals range between -5 and 5 wt%. Two large, positive (> 50 wt%) residuals occur in an area identified as amphibole after olivine in the mingrid worksheet (Figure 5.6) and thin section sketch (Figure 5.7). Both of these points have low totals (<90 wt%), very low Al_2O_3 values (<1 wt%), and high normalization ratios (1.99). The assumption that amphibole formed from clinopyroxene does not hold for these points. As a result the calculated residuals are not valid. FeO residuals are most variable in areas identified as amphibole (-20 to 10 wt%). Some of this variation could be due to local Al mobility. FeO residuals do not show any other trends with either mineralogy or distance from the vein.

CaO residuals range from -20 to 20 wt%. Negative CaO residuals (-5 to -20 wt%) are concentrated near the vein and in areas identified as amphibole on the mingrid worksheet (Figure 5.6). As discussed previously, these areas likely exhibit local Al mobility resulting in exaggerated residuals. Positive CaO residuals (~20 wt%) are observed in two points located in the core of a clinopyroxene grain. These values most likely represent primary, rather than secondary, variation. CaO residuals do not show any other trends with mineralogy.

MgO residuals range from -20 to 20 wt%. MgO residuals exhibit similar patterns to those for CaO although the MgO residual map contains relatively less negative residuals and a few more positive residuals. Like CaO, MgO residuals are concentrated near the vein and in areas identified as amphibole on the mingrid worksheet (Figure 5.6), the latter likely exhibiting local Al mobility. Small, positive MgO residuals (~10 wt%) are observed at the same two points in the core of a clinopyroxene grain, previously identified in the CaO residual map, which are also interpreted as resulting from primary rather than secondary variation. MgO residuals do not show any other trends with mineralogy.

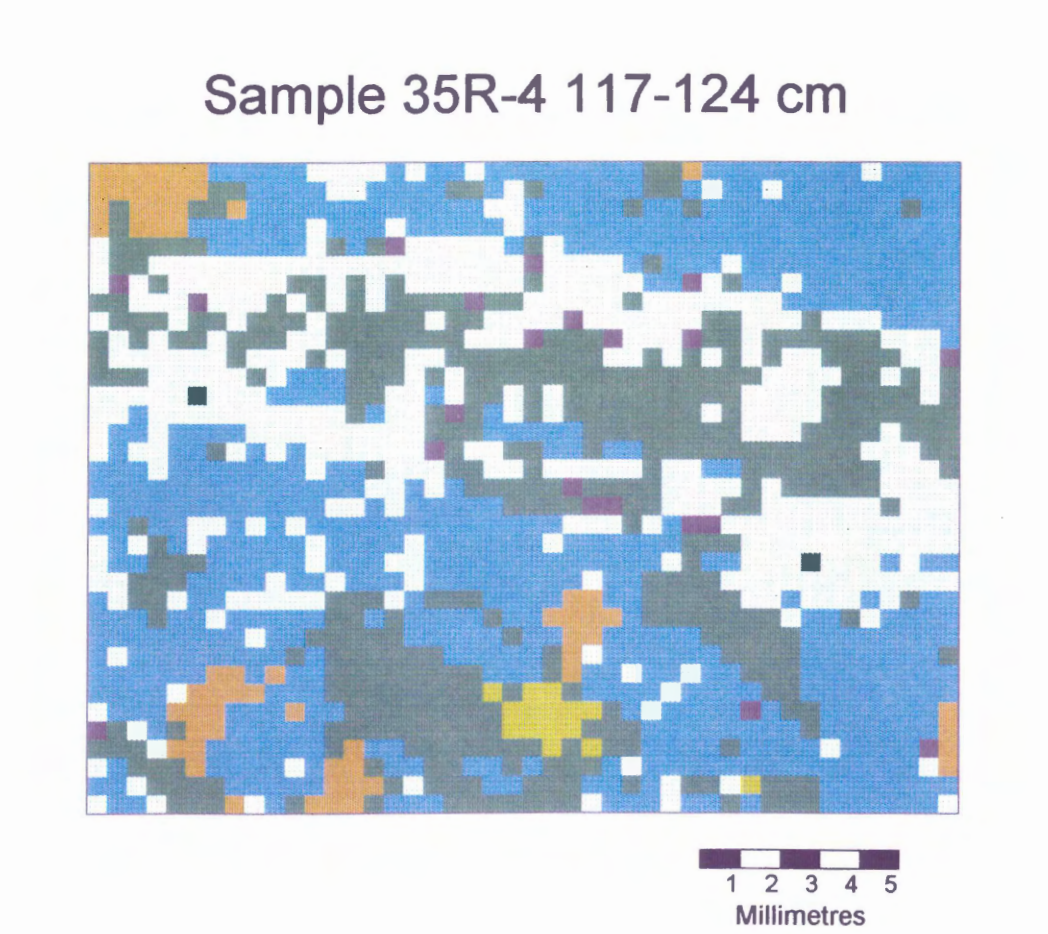

Figure 5.6 Coloured "mingrid" worksheet for sample 35R-4 117-124 cm. Colours represent different minerals. Each coloured cell has dimensions of 0.5 mm square. See text for explanation.

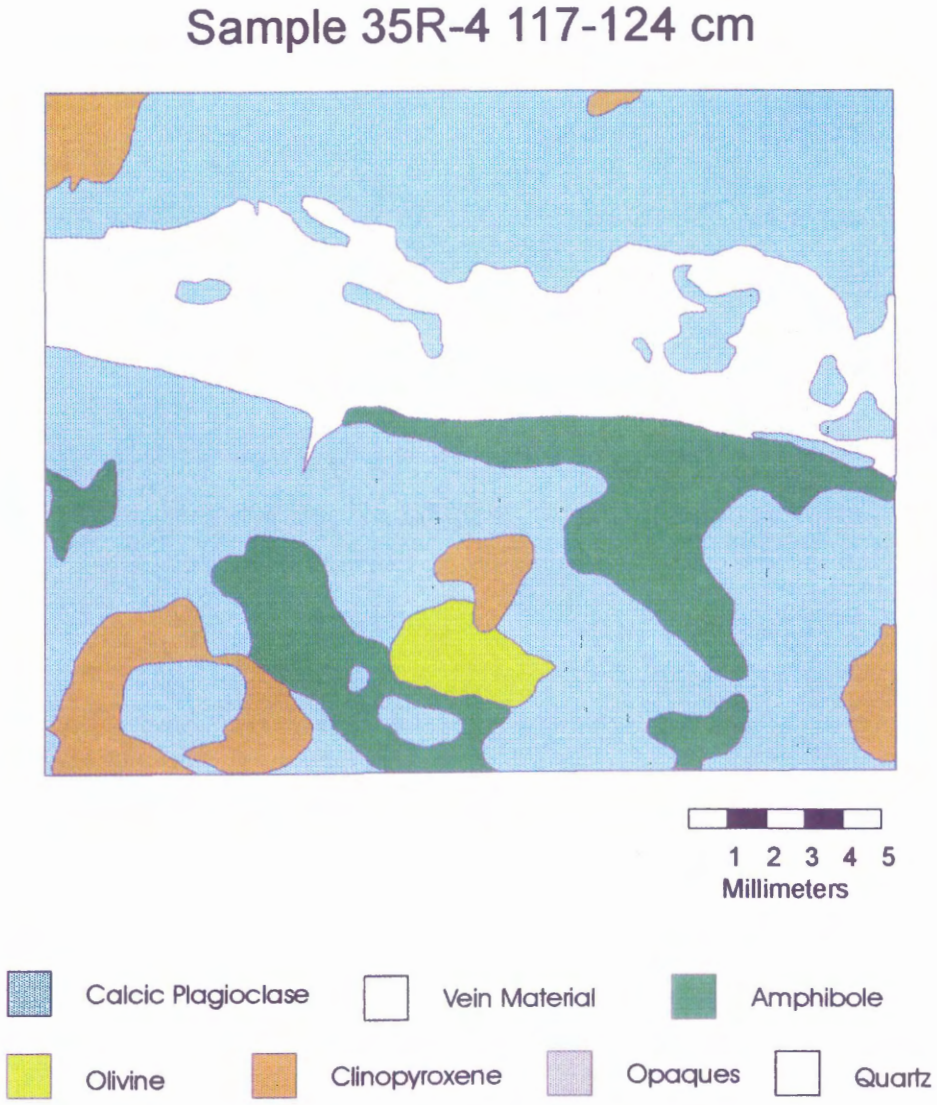

Figure 5.7 Digitized thin section sketch of sample 35R-4 117-124 cm. The thin section was projected onto a screen and traced. The area shown is approximately the same as the area of the chemical map for the sample. Mineralogy is approximate and was confirmed by detailed petrography.

Figure 5.8 Chemical residual maps of SiO_2, FeO, CaO, MgO, Na_2O, K_2O, MnO, and TiO_2 for sample 35R-4 117-124 cm. Negative residuals represent losses and positive residuals represent gains in the host rock as a result of alteration. Contours are drawn at intervals of 5 wt%. Values greater than 50 and less than -50 are grouped into the >50 and <-50 contours, respectively. The vein is indicated in grey and the mineralogy of the sample is indicated by dashed lines. The location of the vein and individual minerals is from Figure 5.7 and is approximate. Scale is in millimeters. See text for explanation.

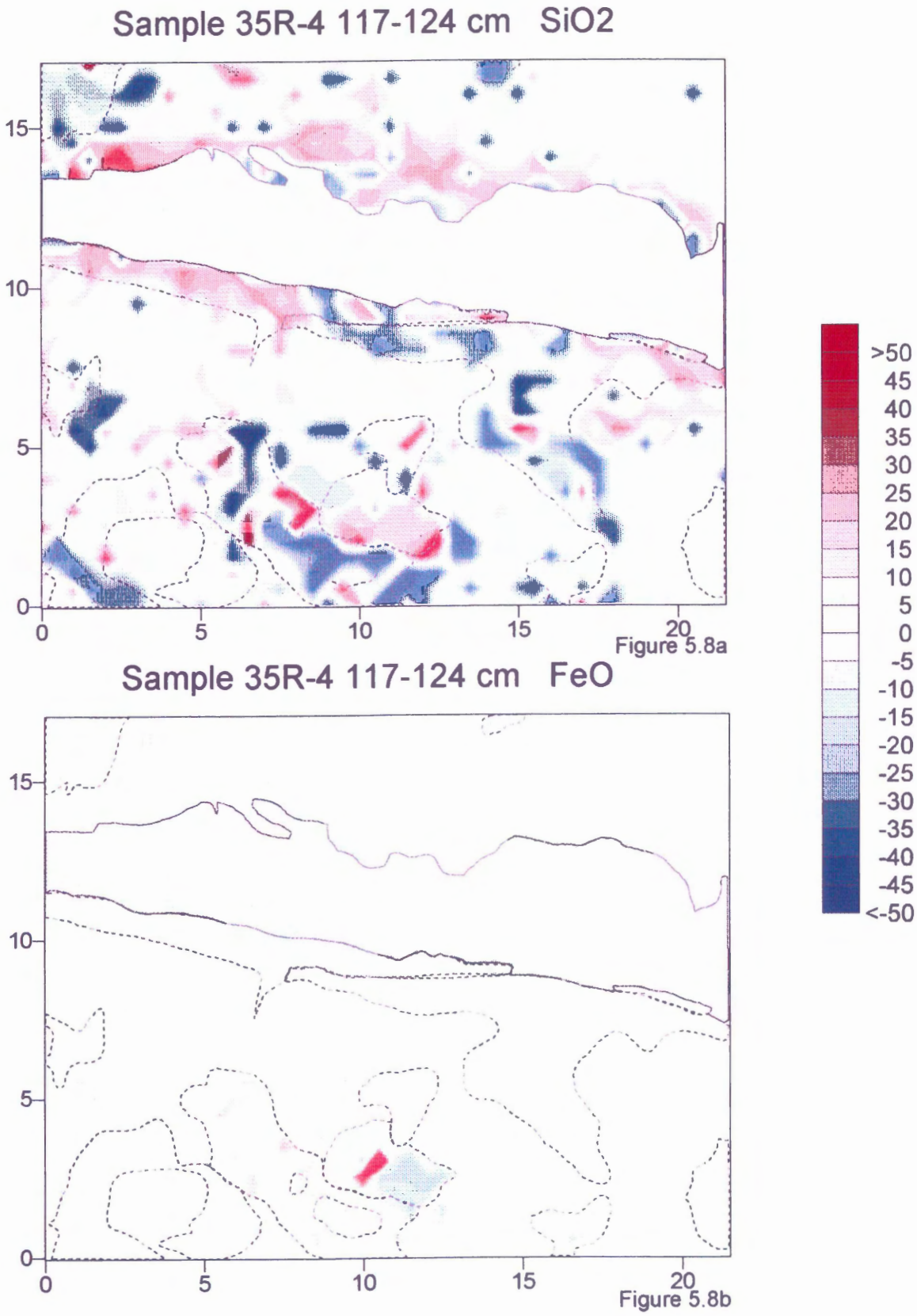

Figure 5.8a

Figure 5.8b

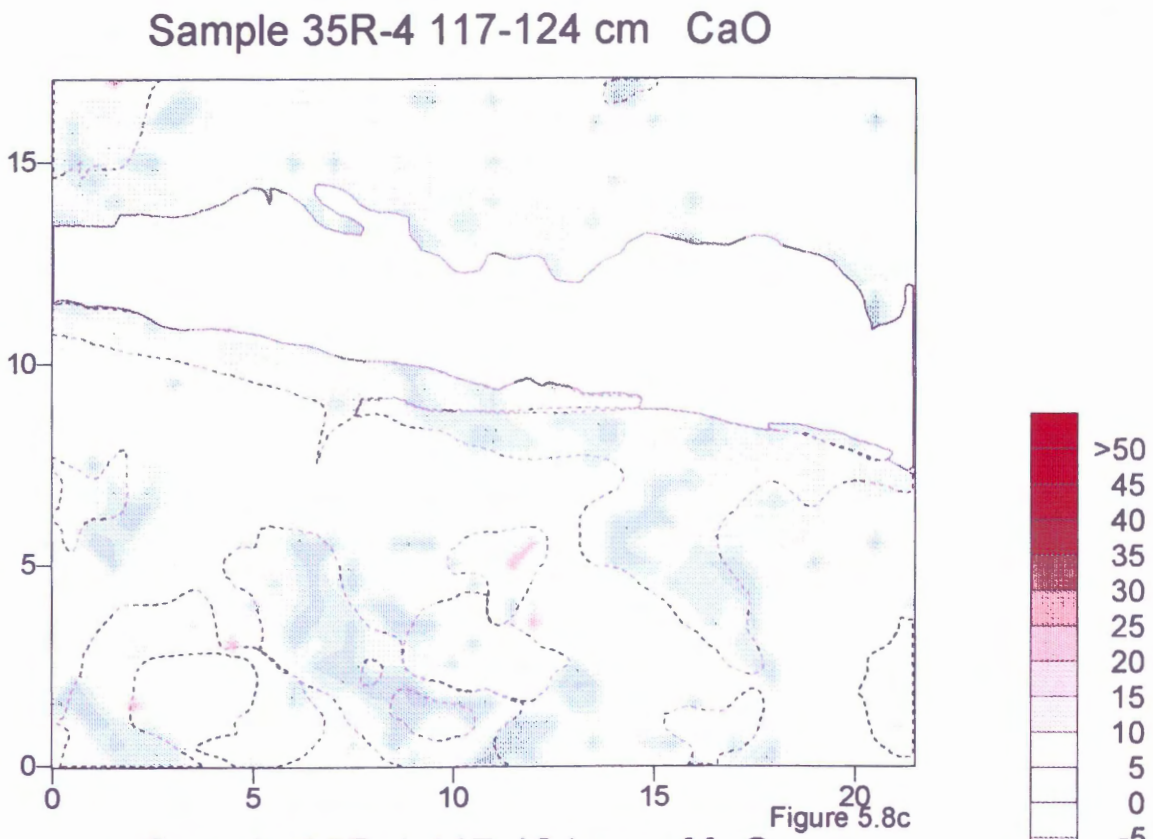

Figure 5.8c

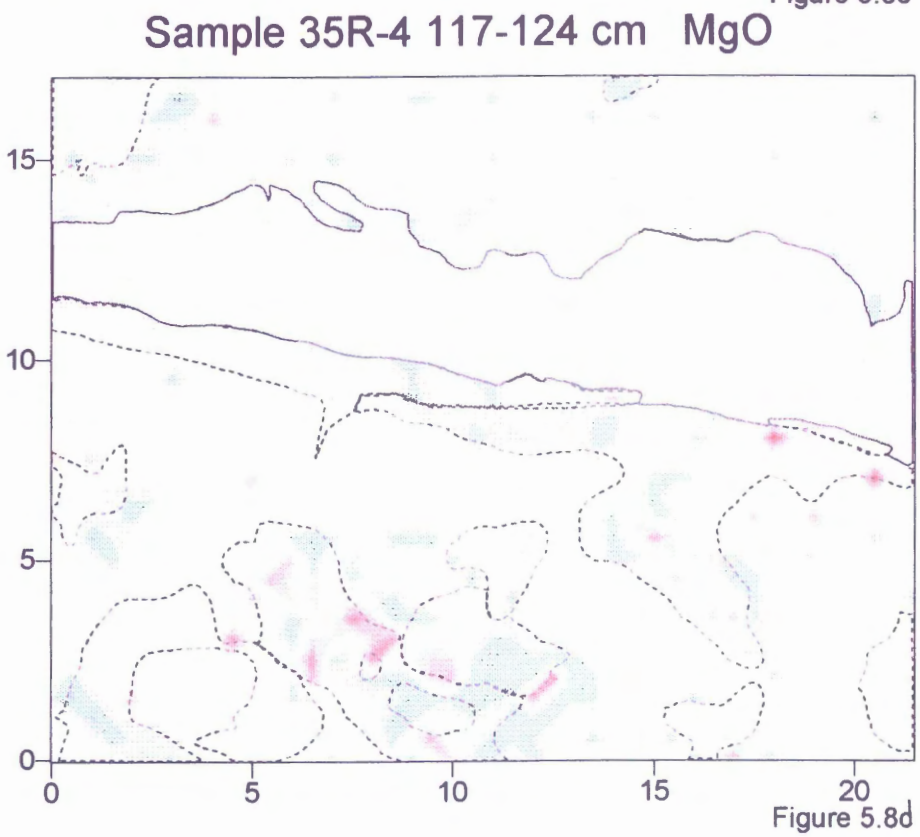

Figure 5.8d

Sample 35R-4 117-124 cm Na2O

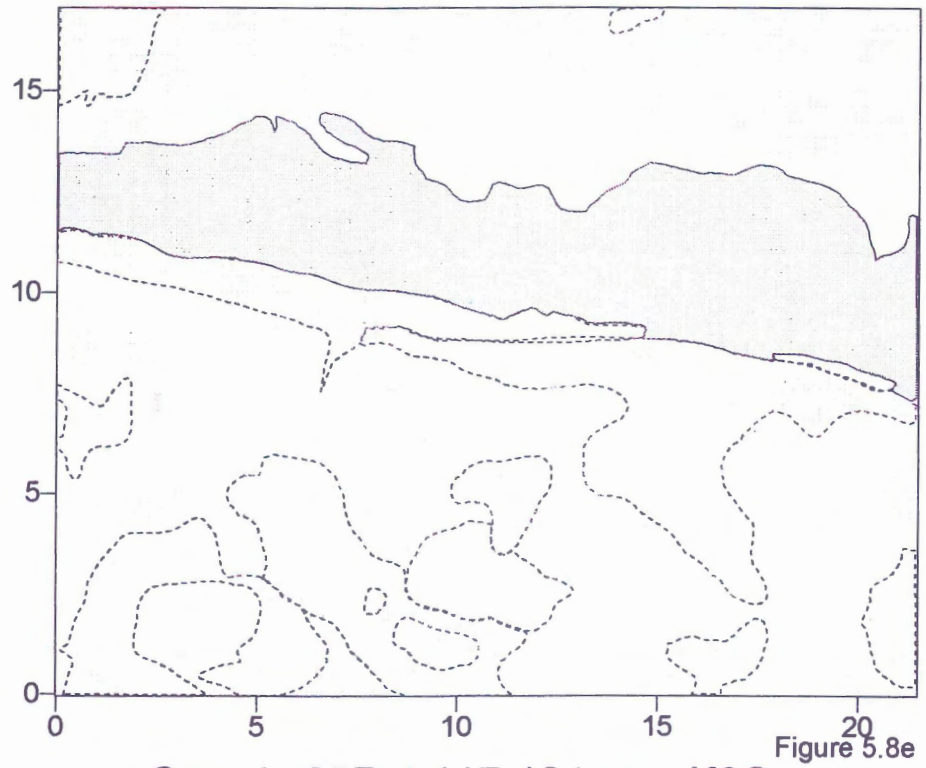

Figure 5.8e

Sample 35R-4 117-124 cm K2O

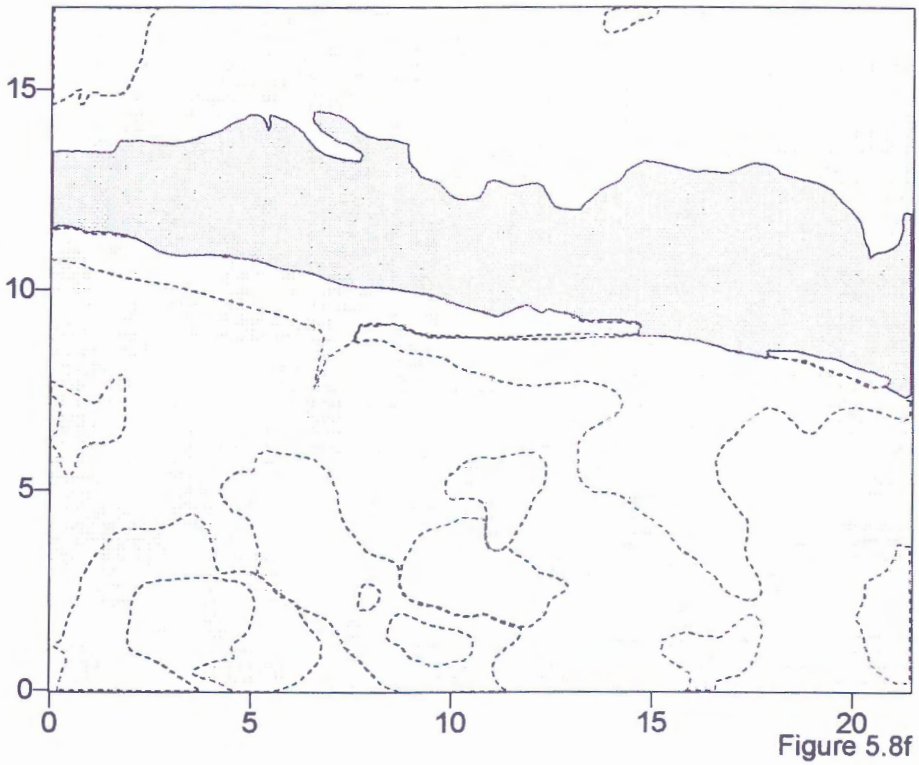

Figure 5.8f

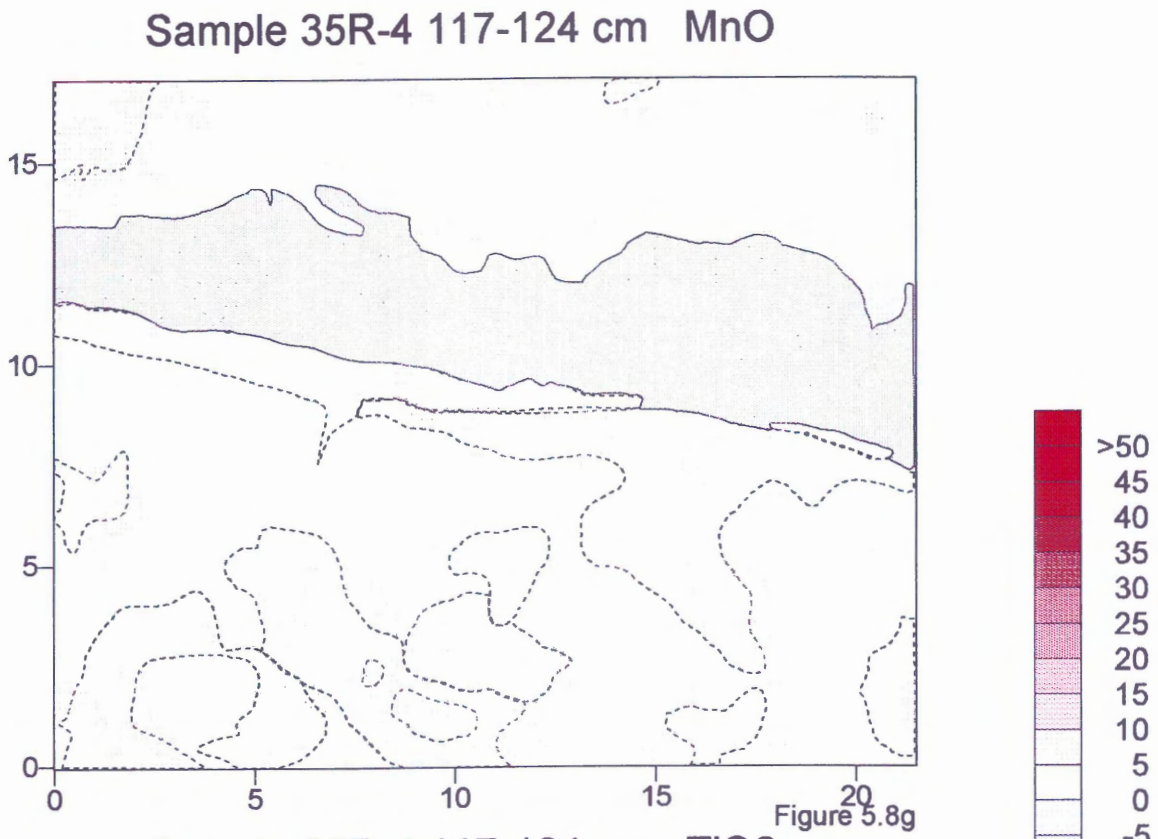

Figure 5.8g

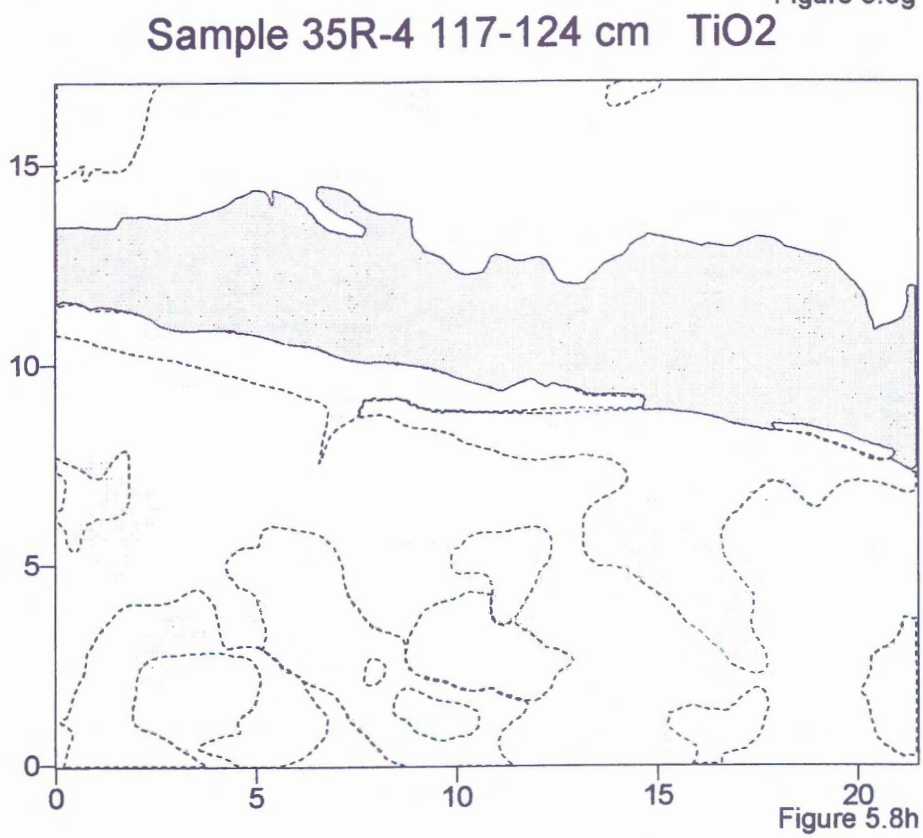

Figure 5.8h

Na_2O, K_2O, MnO, and TiO_2 all exhibit small residual ranges (-5 to 5 wt%). A few larger (<10 wt%) positive Na_2O residuals are observed near the vein. These positive residuals occur in similar areas as positive SiO_2 residuals which are interpreted as an alteration halo near the vein. K_2O residuals seem to be randomly distributed. MnO and TiO_2 show a slight correlation with mineralogy: values less than zero are associated with clinopyroxene and amphibole, and values greater than zero are associated with plagioclase. This suggests the primary values used to calculate residuals for MnO and TiO_2 in clinopyroxene may be slightly greater than the actual primary value. MnO and TiO_2 residual values, therefore, most likely represent primary variations. Na_2O, K_2O, MnO, an TiO_2 residual maps do not show any variation with distance from the vein.

5.4.3 Sample 44R-1 35-47 cm

SiO_2 residuals exhibit a large range of variablity, particularily in areas identified as amphibole, olivine, and sodic plagioclase on the mingrid worksheet (Figure 5.9). Large, positive SiO_2 residuals (> 20 wt%) observed near the vein are identified as sodic plagioclase in the mingrid worksheet (Figure 5.9). These points represent vein material which has not been adequately included by the thin section sketch. Large, positive SiO_2 residuals (> 20 wt%) are also associated with amphibole, identified on the mingrid worksheet (Figure 5.9), after olivine. Normalization ratios in these areas are large (>1.5), possibly representing Al mobilization. Calculated SiO_2 residuals in these areas are exaggerated and probably reflect gains significantly less than 20 wt%. Smaller, positive SiO_2 residuals (~5 to 20 wt%) are observed in areas identified as sodic plagioclase in the mingrid worksheet (Figure 5.9), away from the vein margin, and are likely secondary.

Large, negative SiO_2 residuals (<-30 wt%) occur in a number of areas identified as amphibole on the mingrid worksheet (Figure 5.9) and thin section sketch (Figure 5.10), such as the large area located in the left-central portion of the SiO_2 residual map. Microprobe analyses in this area are characterized by low totals, high concentrations of Al_2O_3 (>10 - 15 wt%), and very small normalization ratios (many < 0.2). Local Al mobilization likely occured in these areas. As a result, SiO_2 residuals are most likely

significantly less than - 30 wt%. One area, in the bottom-central portion of the SiO_2 residual map, appears to contain small, negative residuals surrounded by larger, negative residuals. Closer observation of these values indicates that the central portion actually contains values less than -30 wt%. This is an apparent anomaly in the contouring.

CaO residuals range from -20 to 25 wt%, however, only a few areas have CaO residuals larger than 5 wt%. Negative CaO residuals are concentrated near the vein in areas previously interpreted to represent vein material which has not been adequately included by the thin section sketch. Negative CaO residuals (-5 to -20 wt%) also occur in areas previously identified as amphibole on the mingrid worksheet (Figure 5.9). Residuals in these areas are suspect because the calculated CaO residuals are most likely exaggerated due to local Al mobility. Positive CaO residuals (>25 wt%) occur in a few points, identified as clinopyroxene grains from thin section sketches (Figure 5.10), in the upper-left portion of the CaO residual map. Microprobe values at these points are characterized by low totals (<90 wt%), low Al_2O_3 values (<1.5 wt%), and high normalization ratios (>1.9). This suggests that local mobilization of Al likely occured in these areas. As a result, CaO residuals are exaggerated. CaO residuals do not show any other trends with mineralogy.

MgO residuals exhibit similar patterns to those for CaO and range from -20 to 20 wt%. Like CaO, negative MgO residuals are concentrated in areas identified as amphibole on the mingrid worksheet (Figure 5.9) Small, positive MgO residuals, ranging from 10 to 20 wt%, are also observed at several points identified as amphibole in the mingrid worksheet (Figure 5.9). Both positive and negative residuals, in areas identified as amphibole, are suspect because of possible Al mobility. MgO residuals do not show any other trends with mineralogy.

FeO, Na_2O, K_2O, MnO, and TiO_2 all exhibit small residual ranges (-5 to 5 wt%). A few larger (<10 to 15 wt%) positive Na_2O residuals are observed near the vein. These positive residuals occur in similar areas as positive SiO_2 residuals which are interpreted as vein material which has not been adequately included by the thin section sketch. FeO, Na_2O, MnO, and TiO_2 residuals seem to be randomly distributed, however, K_2O residuals

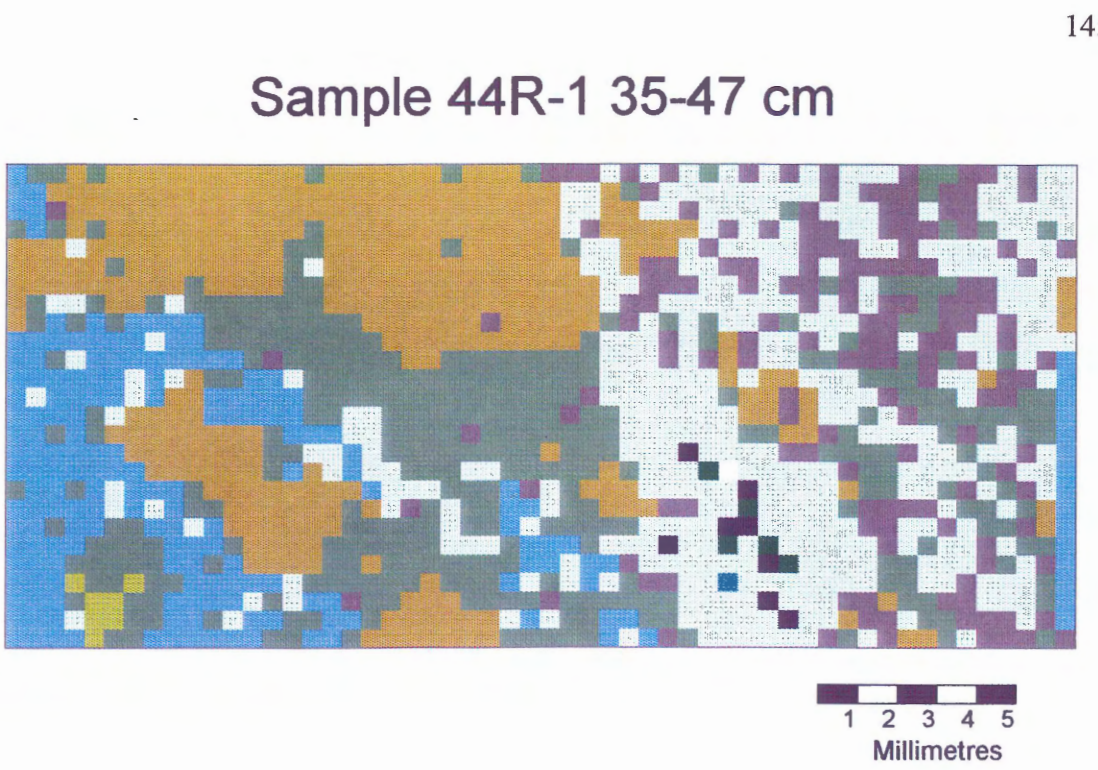

Figure 5.9 Coloured "mingrid" worksheet for sample 44R-1 35-47 cm. Colours represent different minerals. Each coloured cell has dimensions of 0.5 mm square. See text for explanation.

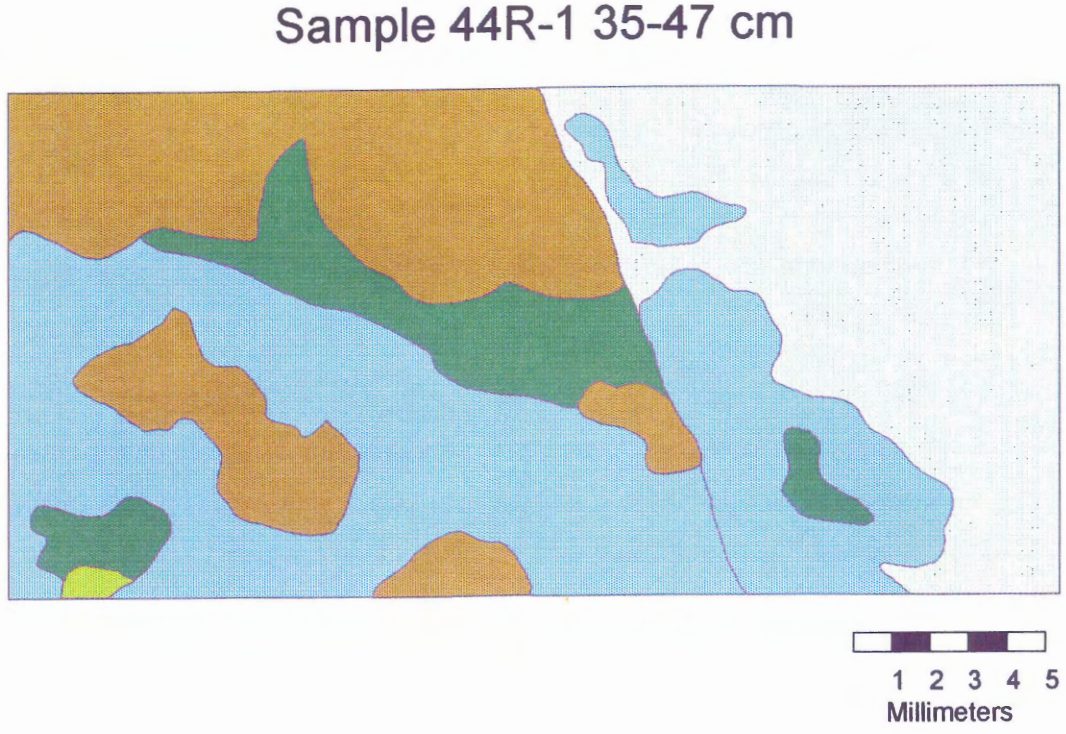

Figure 5.10 Digitized thin section sketch of sample 44R-1 35-47 cm. The thin section was projected onto a screen and traced. The area shown is approximately the same as the area of the chemical map for the sample. Mineralogy is approximate and was confirmed by detailed petrography.

Figure 5.11 Chemical residual maps of SiO_2, FeO, CaO, MgO, Na_2O, K_2O, MnO, and TiO_2 for sample 44R-1 35-47 cm. Negative residuals represent losses and positive residuals represent gains in the host-rock as a result of alteration. Contours are drawn at intervals of 5 wt%. Values greater than 50 and less than -50 are grouped into the >50 and <-50 contours, respectively. The vein is indicated in grey and the mineralogy of the sample is indicated by dashed lines. The location of the vein and individual minerals is from Figure 5.10 and is approximate. Scale is in millimeters. See text for explanation.

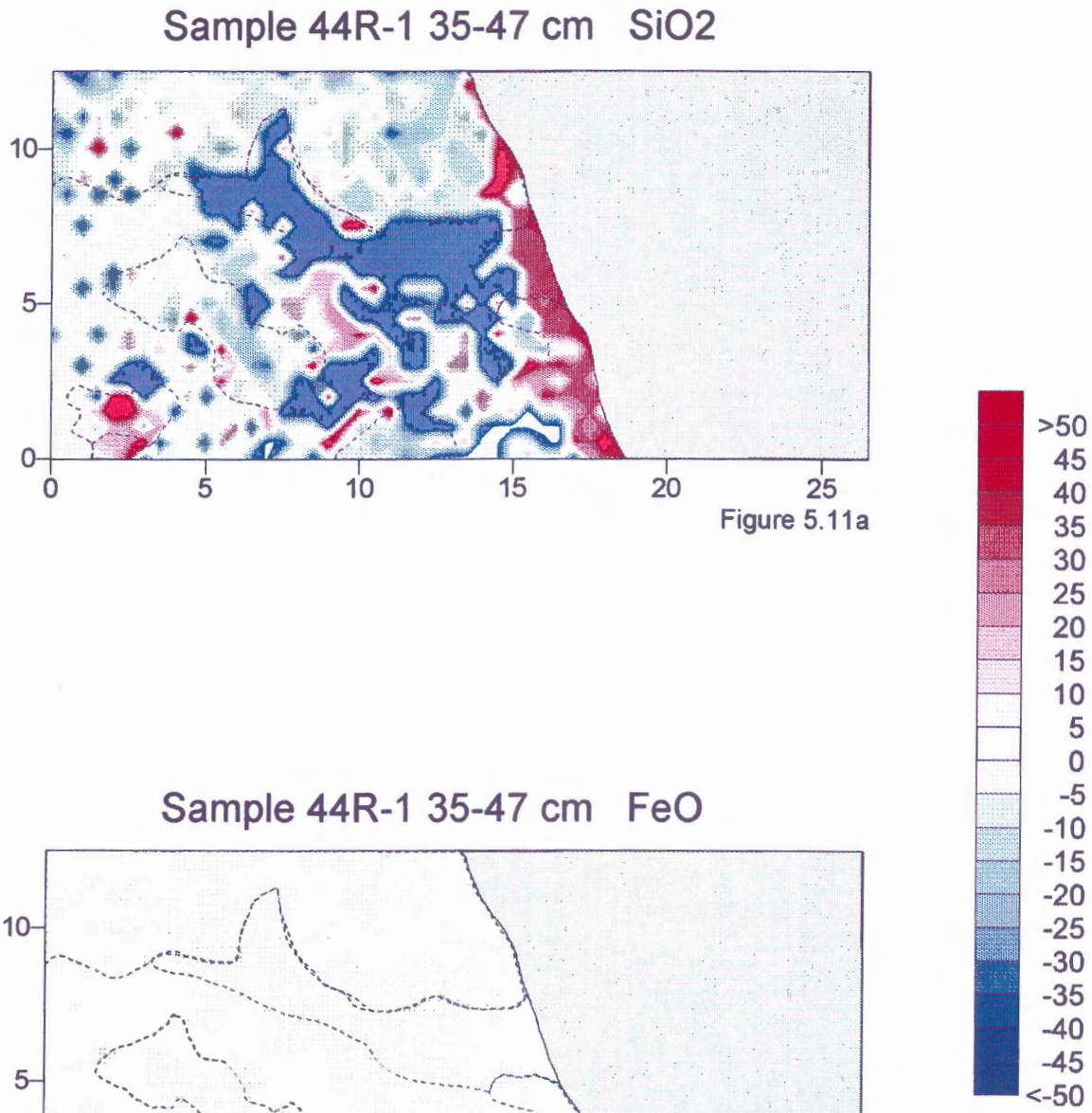

Figure 5.11a

Figure 5.11b

Sample 44R-1 35-47 cm CaO

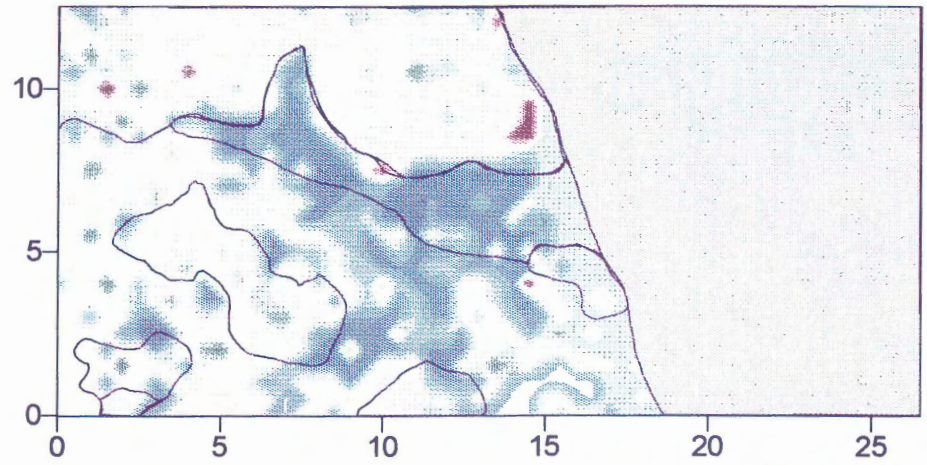

Figure 5.11c

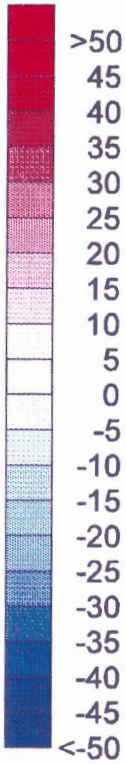

Sample 44R-1 35-47 cm MgO

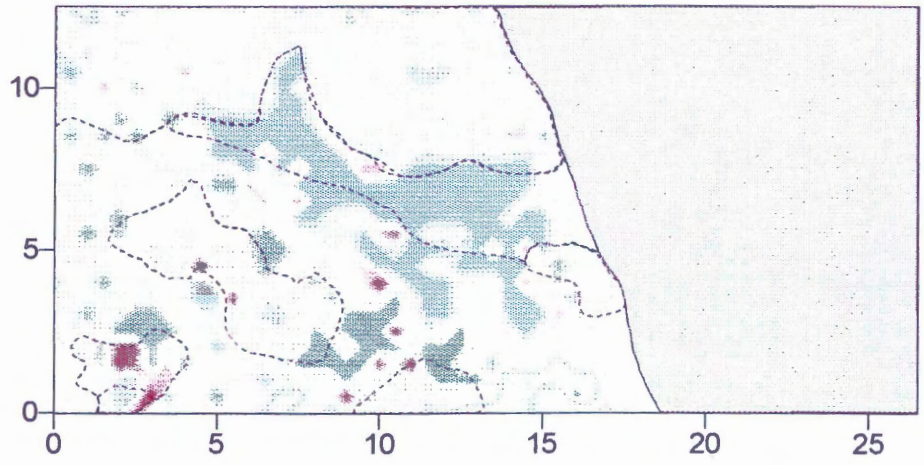

Figure 5.11d

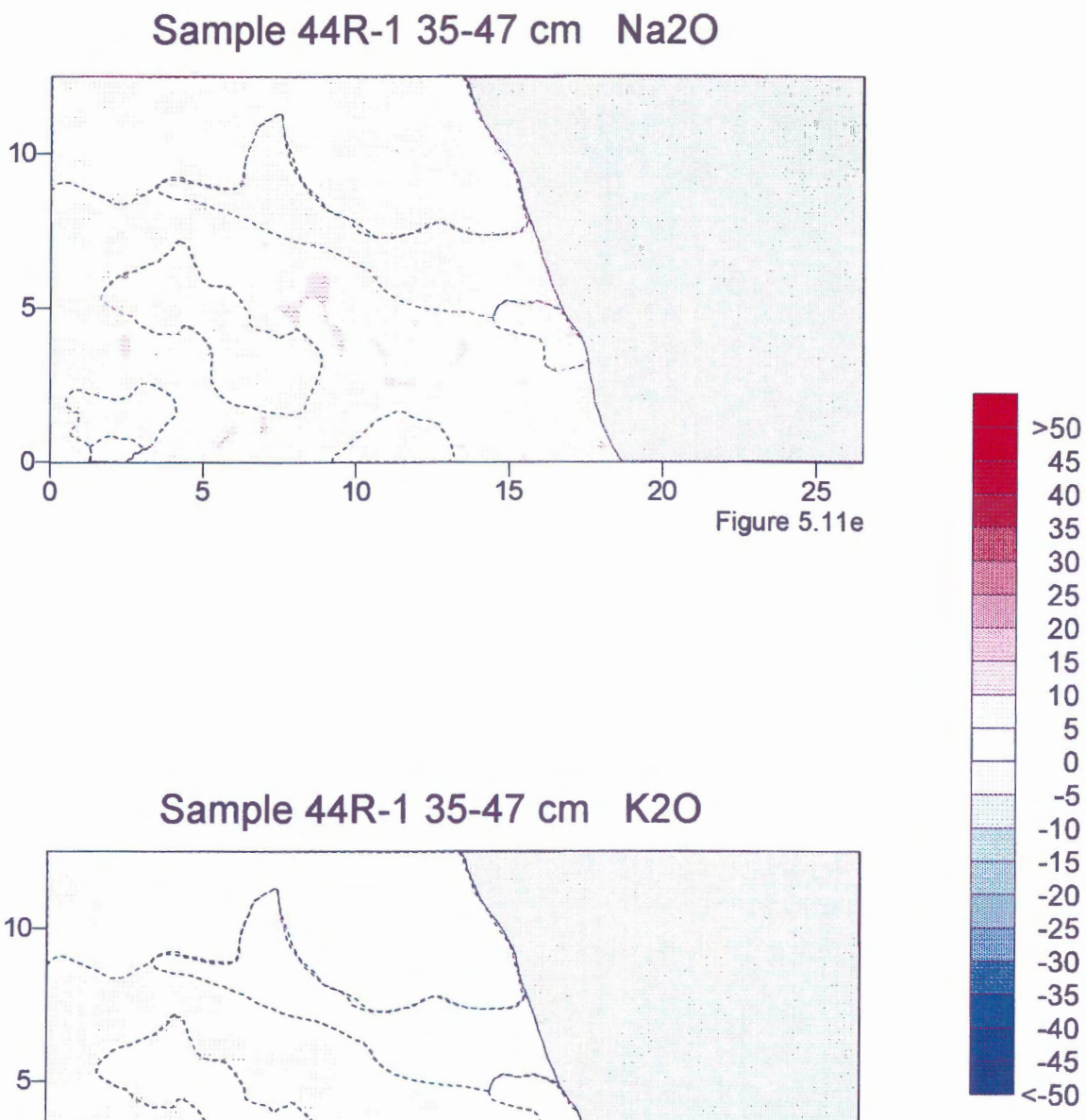

Figure 5.11e

Figure 5.11f

Sample 44R-1 35-47 cm MnO

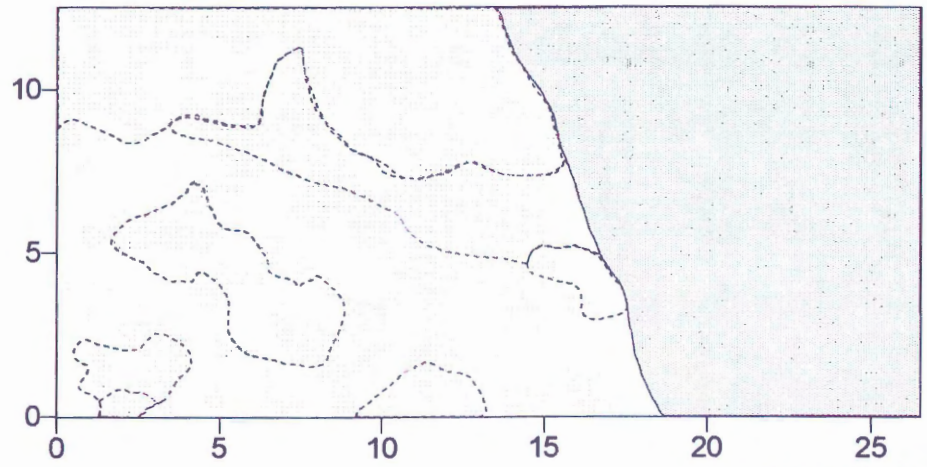

Figure 5.11g

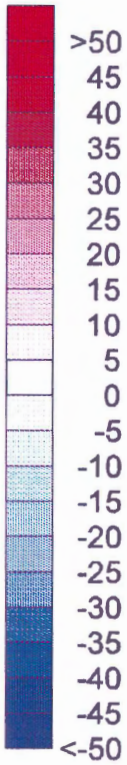

Sample 44R-1 35-47 cm TiO2

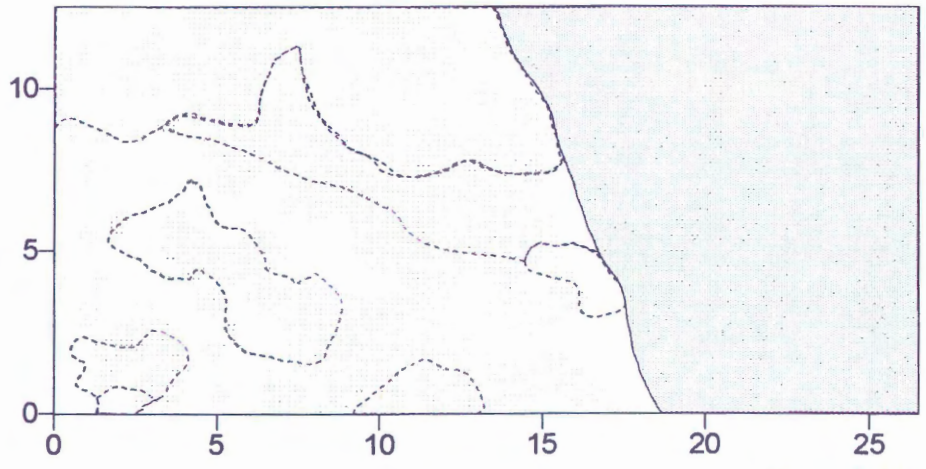

Figure 5.11h

show a slight correlation with mineralogy: values less than zero are associated with plagioclase, and values greater than zero are associated with other minerals. This suggests the primary values used to calculate residuals for K_2O in plagioclase may be slightly greater than the actual primary value. K_2O residuals, therefore, likely reflect primary rather than secondary variations. FeO, K_2O, MnO, an TiO_2 residual maps do not show any variation with distance from the vein.

5.4.4 Sample 54R-4 69-78 cm

SiO_2 residuals exhibit a large range of variablity. Large, positive SiO_2 residuals (20 to >50 wt%) are observed in areas identified as amphibole, and a few areas identified as clinopyroxene, on the mingrid worksheet (Figure 5.12). These areas are characterized by low Al_2O_3 values which have resulted in very large normalization ratios (>1.5), possibly representing mobility of Al. Calculated SiO_2 residuals in these areas are exaggerated and probably reflect gains significantly less than the calculated values. Large, negative SiO_2 residuals (<-30 wt%) also occur in a number of areas identified as amphibole on the mingrid worksheet (Figure 5.12). Several of these areas occur directly beside , or within, large, positive residuals. Microprobe analyses in these areas are characterized by low totals, high concentrations of Al_2O_3 (>10 wt%), and very small normalization ratios (many < 0.5). Local Al mobilization likely occured in these areas and SiO_2 residuals are most likely significantly less than those calculated. In addition, several points which contain residual values significantly different from their neighbours, appear to have been incorrectly classified. Several of these points occur in areas identified as ilmenite and magnetite. Points which were originally left unclassified by the residual program, were later filled as either ilmentite of magnetite in these areas. Microprobe data suggest that these points are silicates which have been incorrectly classified as oxide minerals. This has resulted in incorrect calculation of residuals for these points.

Most FeO residuals range between -10 and 15 wt %, however, a few areas contain large, positive residuals (>40 wt%). These points are identified as an amphibole and clinopyroxene on the mingrid worksheet (Figure 5.12). Each of these points has a high

normalization ratio (>1.9) which has exaggerated the calculated FeO residual values. Two points contain large, negative FeO residuals (<-30 wt%). These points were incorrectly classified and the residuals are, therefore, incorrect. The larger FeO residuals are slightly more common near the vein.

CaO residuals range from -20 to 20 wt%, however, only a few areas have CaO residuals greater than 5 wt%. Negative CaO residuals (-5 to -20 wt%) commonly occur in areas previously identified as amphibole on the mingrid worksheet (Figure 5.12). Residuals in these areas are suspect because the calculated CaO residuals are most likely exaggerated due to local Al mobility. Positive CaO residuals (5 to 20 wt%) occur in a few areas, identified as clinopyroxene grains on the mingrid worksheet (Figure 5.12). Microprobe values in these areas points are characterized by high normalization ratios (>1.9) which suggests that local mobilization of Al likely occured. As a result, CaO residuals in these areas are exaggerated.

MgO residuals exhibit similar patterns to those for CaO and range from -20 to >20 wt%. Like CaO, negative MgO residuals are concentrated in areas identified as amphibole on the mingrid worksheet (Figure 5.12) Small, positive MgO residuals, ranging from 10 to 20 wt%, are also observed in several areas identified as amphibole. Areas identified as clinopyroxene on the mingrid worksheet (Figure 5.12) also exhibit positive residuals. Both positive and negative residuals, in areas identified as amphibole, are suspect because of possible Al mobility. Positive CaO residuals (10 to15 wt%) in areas identified as clinopyroxene are suspect for the same reasons. MgO residuals do not show any trends with distance from the vein.

Na_2O, K_2O, MnO, and TiO_2 all exhibit small residual ranges (-5 to 5 wt%). Two large TiO_2 residuals, one positive and one negative, occur in areas previously identified as being incorrectly classified. Smaller, negative TiO_2 residuals (~-15 wt%) represent losses from ilmentite. Positive MnO residuals (>10 to 15 wt%) occur in areas identified as amphibole on the mingrid worksheet (Figure 5.12). These values are suspect because Al mobility is likely in these areas. Na_2O, K_2O, MnO, and TiO_2 residuals seem to be

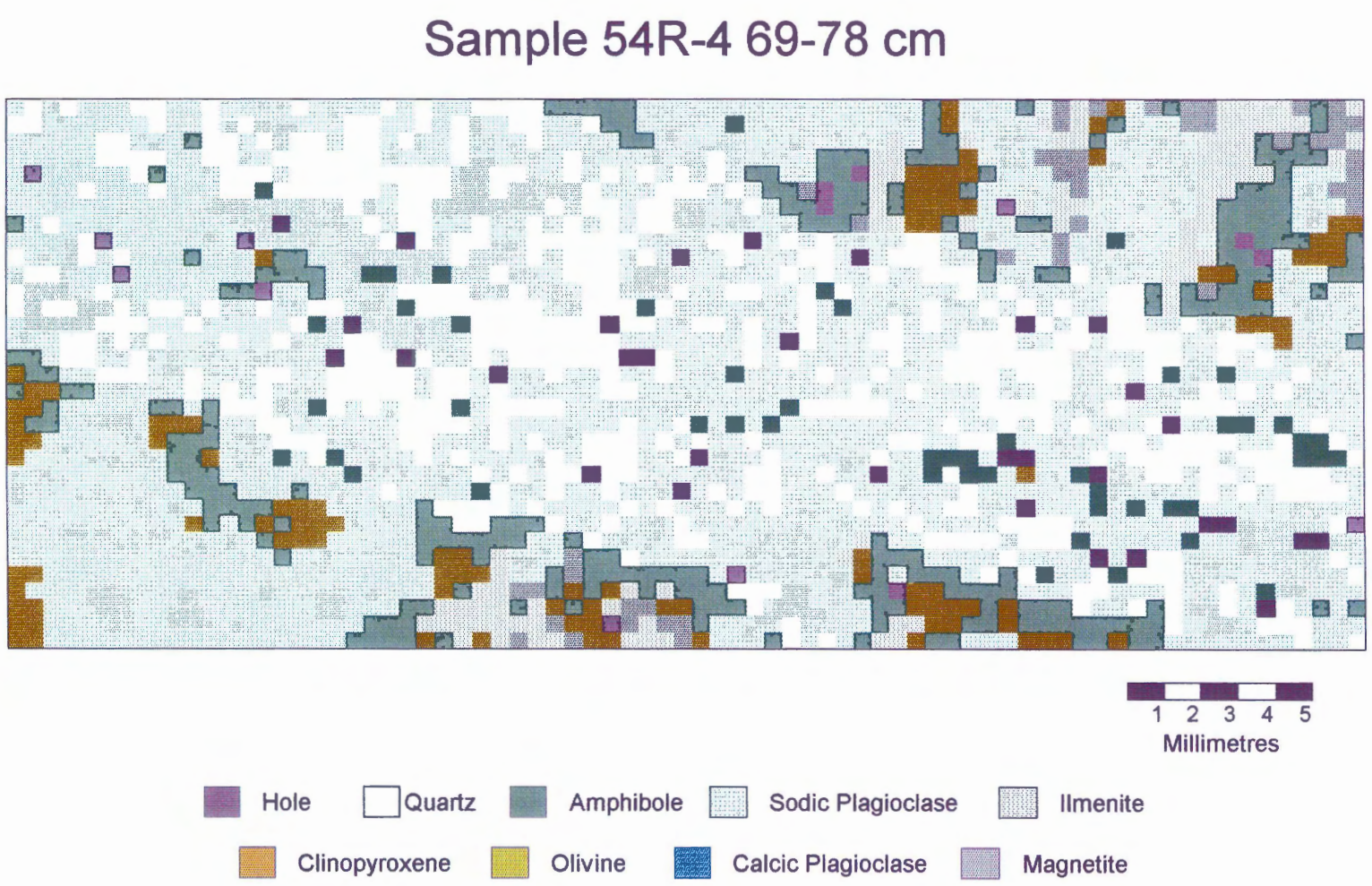

Figure 5.12 Coloured "mingrid" worksheet for sample 54R-4 69-78 cm. Colours represent different minerals Each coloured cell has dimensions of 0.5 mm square. See text for explanation

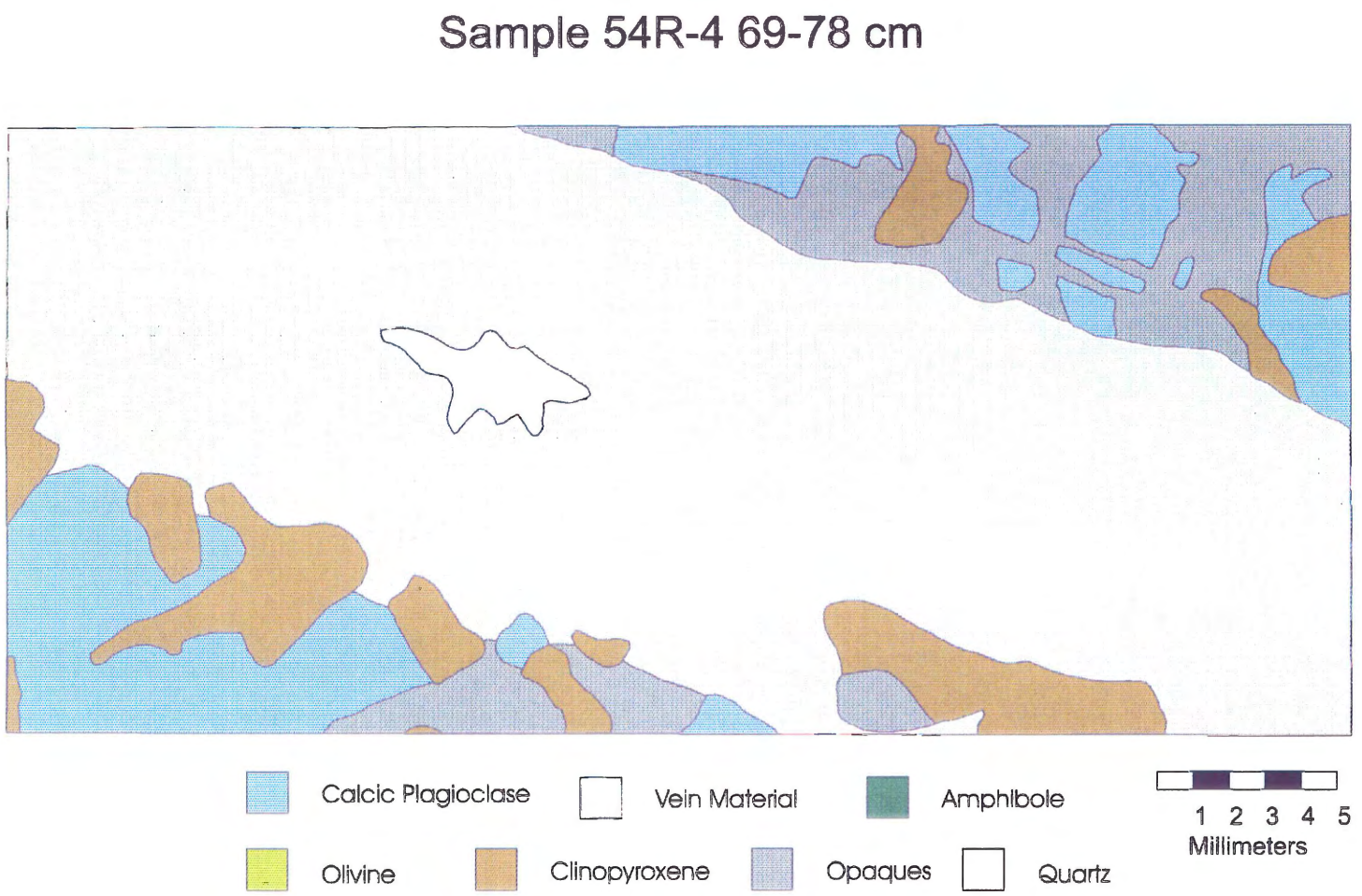

Figure 5.13 Digitized thin section sketch of sample 54R-4 69-78 cm. The thin section was projected onto a screen and traced. The area shown is approximately the same as the area of the chemical map for the sample. Mineralogy is approximate and was confirmed by detailed petrography.

Figure 5.14 Chemical residual maps of SiO_2, FeO, CaO, MgO, Na_2O, K_2O, MnO, and TiO_2 for sample 54R-4 69-78 cm. Negative residuals represent losses and positive residuals represent gains in the host-rock as a result of alteration. Contours are drawn at intervals of 5 wt%. Values greater than 50 and less than -50 are grouped into the >50 and <-50 contours, respectively. The vein is indicated in grey and the mineralogy of the sample is indicated by dashed lines. The location of the vein and individual minerals is from Figure 5.13 and is approximate. Scale is in millimeters. See text for explanation.

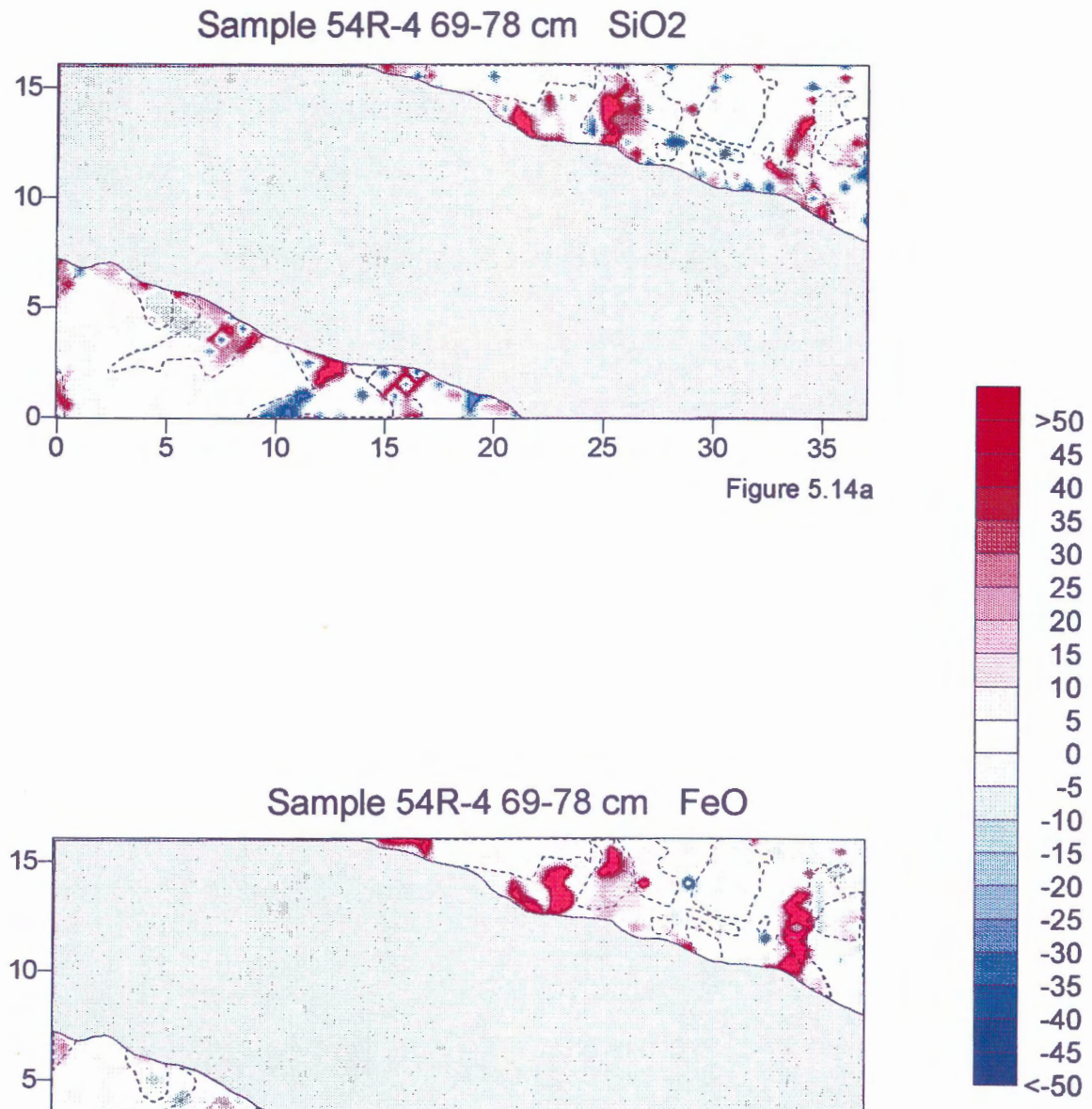

Figure 5.14a

Figure 5.14b

Sample 54R-4 69-78 cm CaO

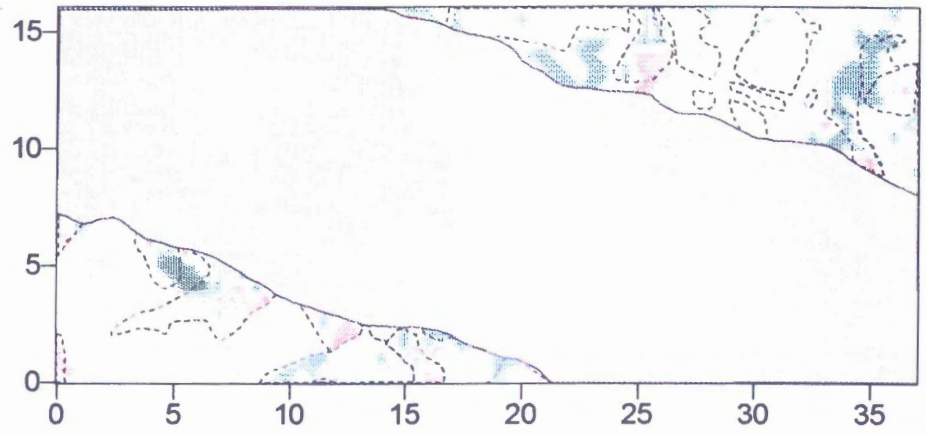

Figure 5.14c

Sample 54R-4 69-78 MgO

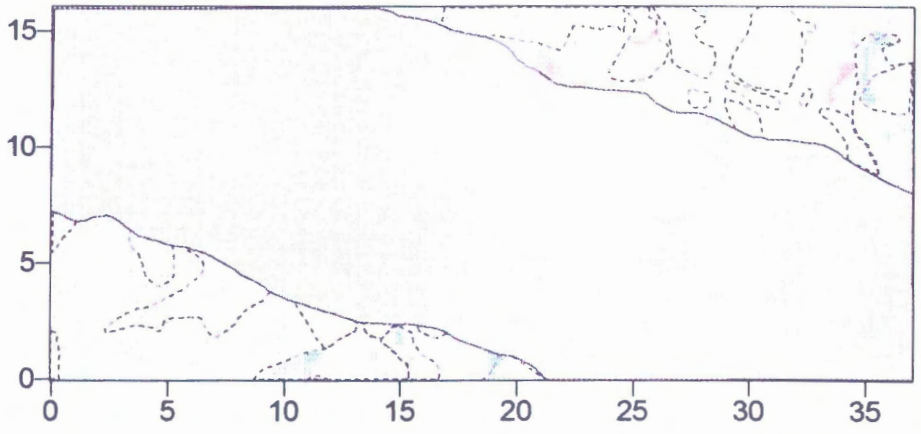

Figure 5.14d

Sample 54R-4 69-78 cm Na2O

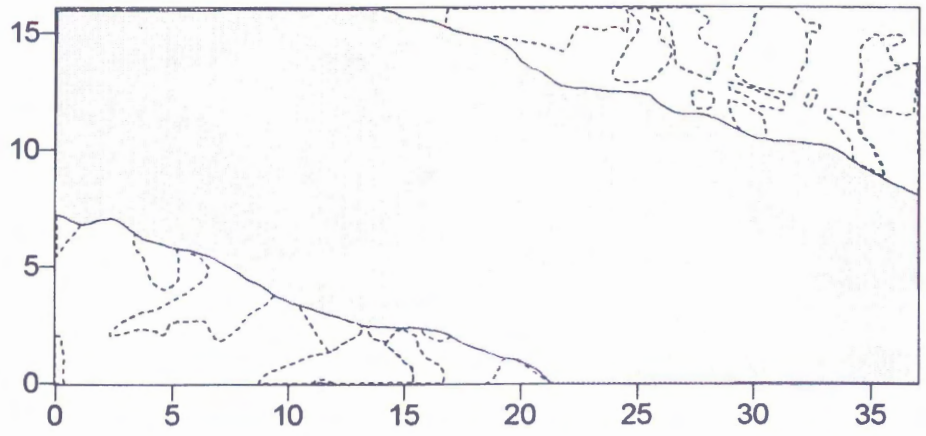

Figure 5.14e

Sample 54R-4 69-78 cm K2O

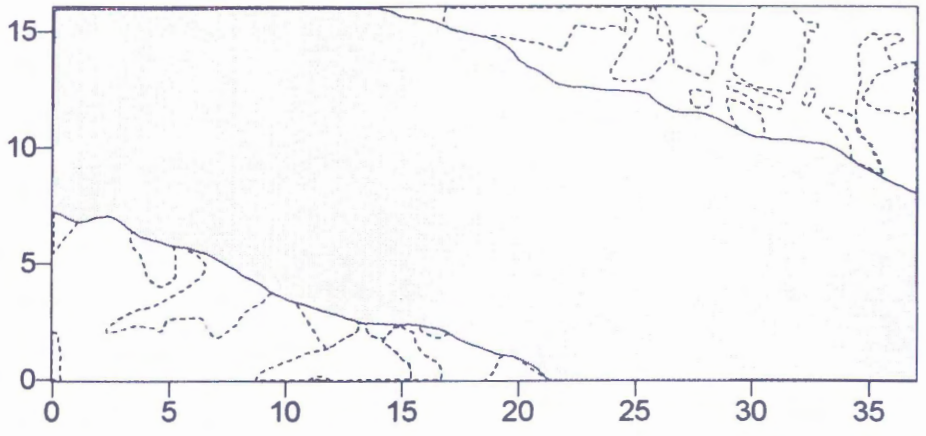

Figure 5.14f

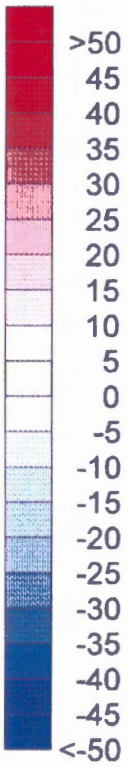

Sample 54R-4 69-78 cm MnO

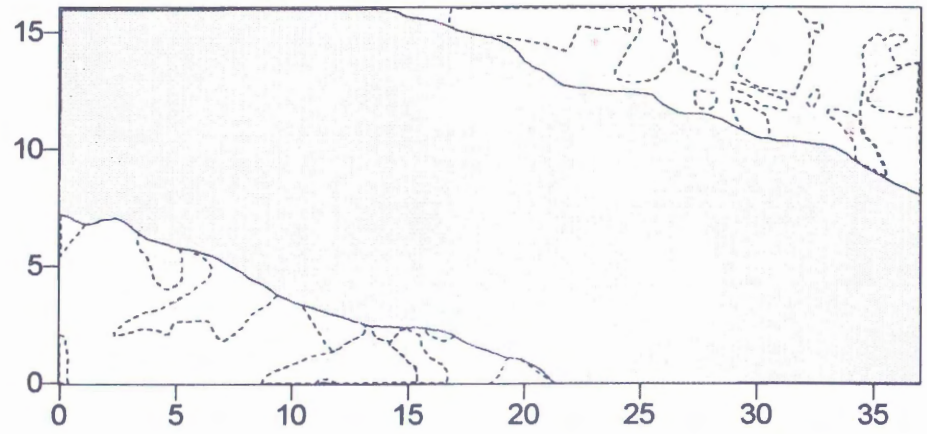

Figure 5.14g

Sample 54R-4 69-78 cm TiO2

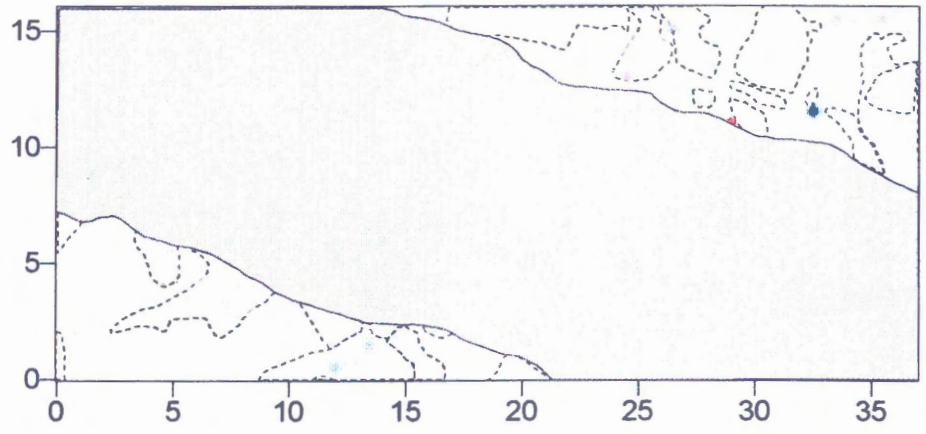

Figure 5.14h

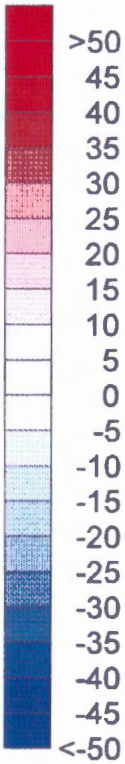

randomly distributed. FeO, K_2O, MnO, an TiO_2 residual maps do not show any variation with distance from the vein.

5.4.5 Sample 58R-3 0-8 cm

SiO_2 residuals exhibit a large range of variablity, particularily in areas identified as amphibole and sodic plagioclase on the mingrid worksheet (Figure 5.15). Large, positive SiO_2 residuals (> 20 wt%) are observed in areas identified as amphibole on the mingrid worksheet (Figure 5.15). Large, positive SiO_2 residuals (>20 wt%) are also observed in areas identified as clinopyroxene. Both of these areas are characterized by low Al_2O_3 values which has resulted in very large normalization ratios (>1.5), possibly representing Al mobilization. Calculated SiO_2 residuals in these areas are exaggerated and probably reflect gains significantly less than 20 wt%. Smaller, positive SiO_2 residuals (~5 to 20 wt%) are observed at a few points, particularly in the top portion of the SiO_2 residual map. Many of these points are identified as sodic plagioclase in the mingrid worksheet (Figure 5.15), and likely represent secondary variation.

Large, negative SiO_2 residuals (<-30 wt%) also occur in a number of areas identified as amphibole on the mingrid worksheet (Figure 5.15) and thin section sketch (Figure 5.16). Several of these areas occur directly beside large, positive residuals. Microprobe analyses in these areas are characterized by low totals, high concentrations of Al_2O_3 (>10 - 15 wt%), and very small normalization ratios (many < 0.2). Local Al mobilization likely occured in these areas and SiO_2 residuals are most likely significantly less than - 30 wt%. One area, in the bottom-right corner of the SiO_2 residual map, appears to contain small, negative residuals surrounded by larger, negative residuals. Closer observation of these values indicates that the central portion actually contains values less than -30 wt%. This is an apparent anomaly in the contouring.

Most FeO residuals range between -5 and 5 wt %, however, a few points contain positive residuals greater than 10 wt%. These points are identified as an amphibole on the mingrid worksheet (Figure 5.15). Each of these points has a correspondingly high normalization ratio (>1.9) which has exaggerated the calculated FeO residual values.

Three negative (~-15 wt%) FeO residuals are present in the top-left corner of the FeO residual map. These points are identified as olivine on the mingrid worksheet (Figure 5.15) and probably reflect secondary variation. FeO residuals do not exhibit any apparent trends with distance from the vein.

CaO residuals range from -20 to 20 wt%, however, only a few areas have CaO residuals greater than 5 wt%. Negative CaO residuals (-5 to -20 wt%) commonly occur in areas previously identified as amphibole on the mingrid worksheet (Figure 5.15). Residuals in these areas are suspect because the calculated CaO residuals are most likely exaggerated due to local Al mobility. Positive CaO residuals (5 to 20 wt%) occur in a few areas, identified as clinopyroxene grains on the mingrid worksheet (Figure 5.15). Microprobe values in these areas are characterized by high normalization ratios (>1.9) which suggests that local mobilization of Al likely occured. As a result, CaO residuals in these areas are exaggerated. Contouring anomalies, similar to those identified for SiO_2, also occur in the CaO residual map. CaO residuals do not show any apparent trends with distance from the vein.

MgO residuals exhibit similar patterns to those for CaO and range from -20 to >20 wt%. Like CaO, negative MgO residuals are concentrated in areas identified as amphibole on the mingrid worksheet (Figure 5.15) Small, positive MgO residuals, ranging from 10 to >20 wt%, are observed in several areas identified as amphibole and clinopyroxene on the mingrid worksheet (Figure 5.15). Both positive and negative residuals, in areas identified as amphibole, are suspect because of possible Al mobility. Positive CaO residuals (>15 wt%) in areas identified as clinopyroxene are suspect for the same reasons. MgO residuals do not show any other trends with mineralogy.

Na_2O, K_2O, MnO, and TiO_2 all exhibit small residual ranges (-5 to 5 wt%). A few larger (10 wt%) positive Na_2O residuals are observed in areas identified as sodic plagioclase on the mingrid worksheet (Figure 5.15). A single, large, positive TiO_2 residual is located in the bottom right corner of the TiO_2 residual map. This point is identified as an amphibole on the mingrid worksheet (Figure 5.15) and is characterized by a large normalization ratio (1.99). This point also has a relatively high value for TiO_2 (28 wt%).

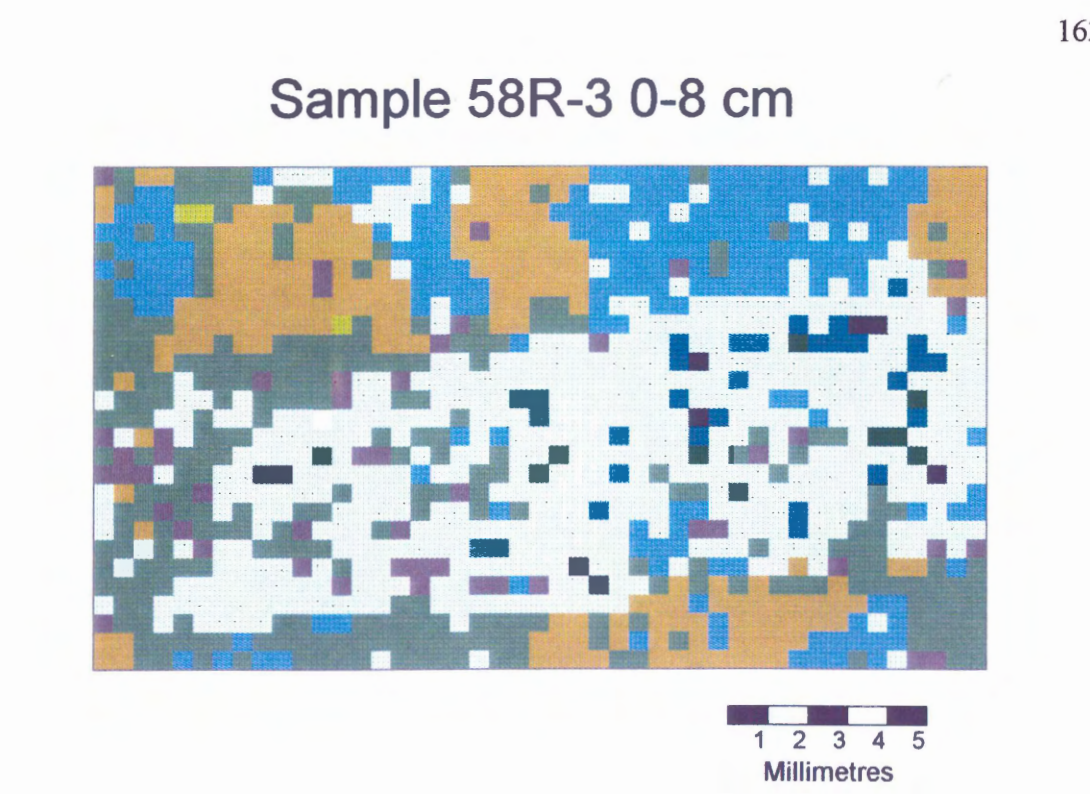

Figure 5.15 Coloured "mingrid" worksheet for sample 58R-3 0-8 cm. Colours represent different minerals. Each coloured cell has dimensions of 0.5 mm square. See text for explanation.

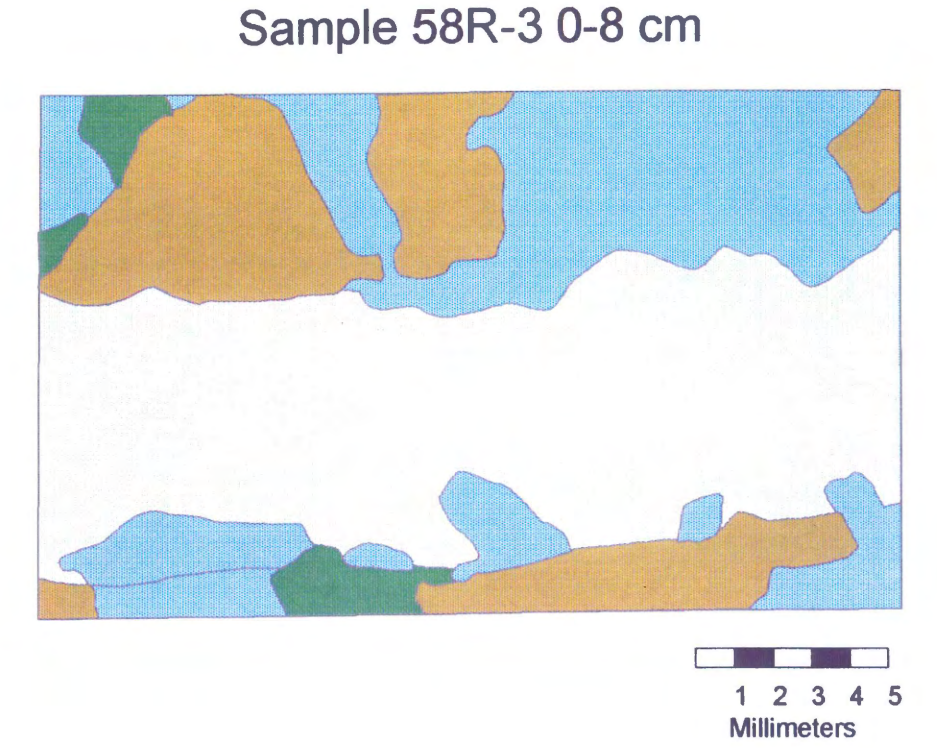

Figure 5.16 Digitized thin section sketch of sample 58R-3 0-8 cm. The thin section was projected onto a screen and traced. The area shown is approximately the same as the area of the chemical map for the sample. Mineralogy is approximate and was confirmed by detailed petrography.

Figure 5.17 Chemical residual maps of SiO_2, FeO, CaO, MgO, Na_2O, K_2O, MnO, and TiO_2 for sample 58R-3 0-8 cm. Negative residuals represent losses and positive residuals represent gains in the host-rock as a result of alteration. Contours are drawn at intervals of 5 wt%. Values greater than 50 and less than -50 are grouped into the >50 and <-50 contours, respectively. The vein is indicated in grey and the mineralogy of the sample is indicated by dashed lines. The location of the vein and individual minerals is from Figure 5.16 and is approximate. Scale is in millimeters. See text for explanation.

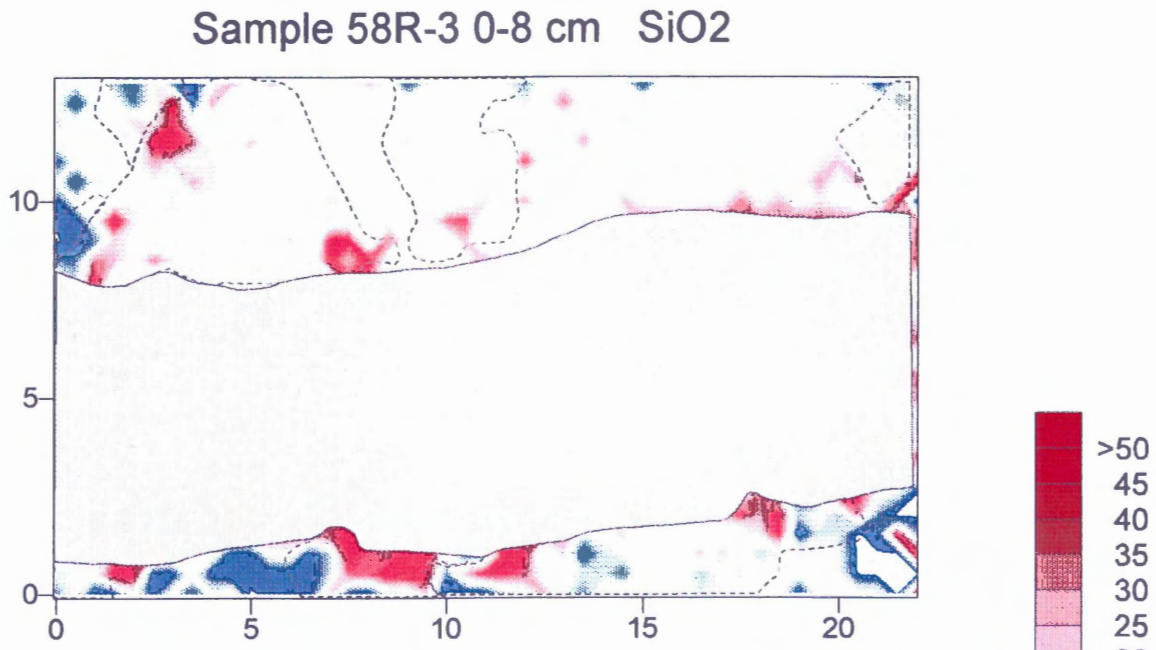

Figure 5.17a

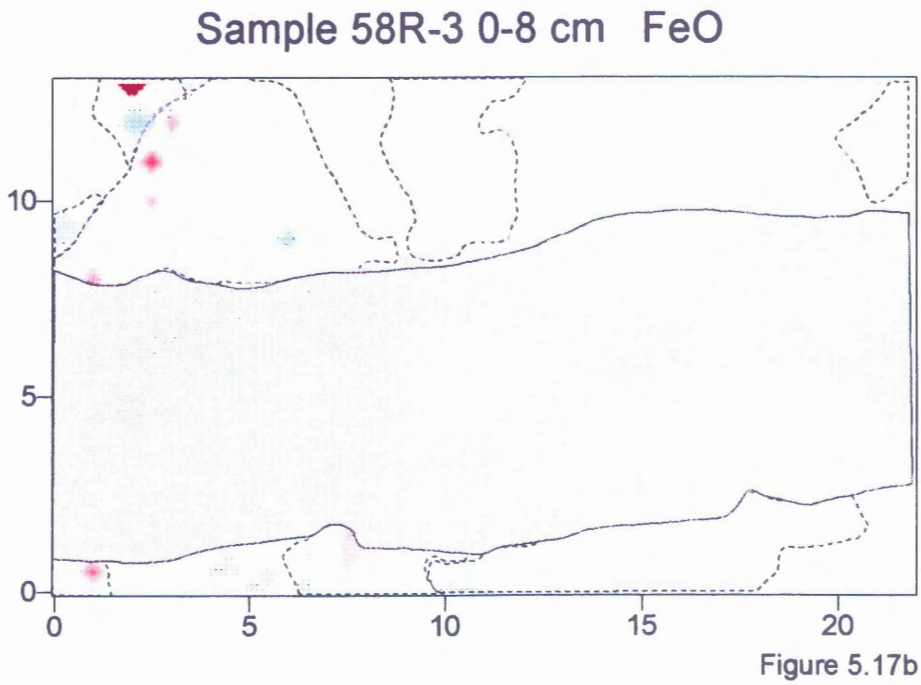

Figure 5.17b

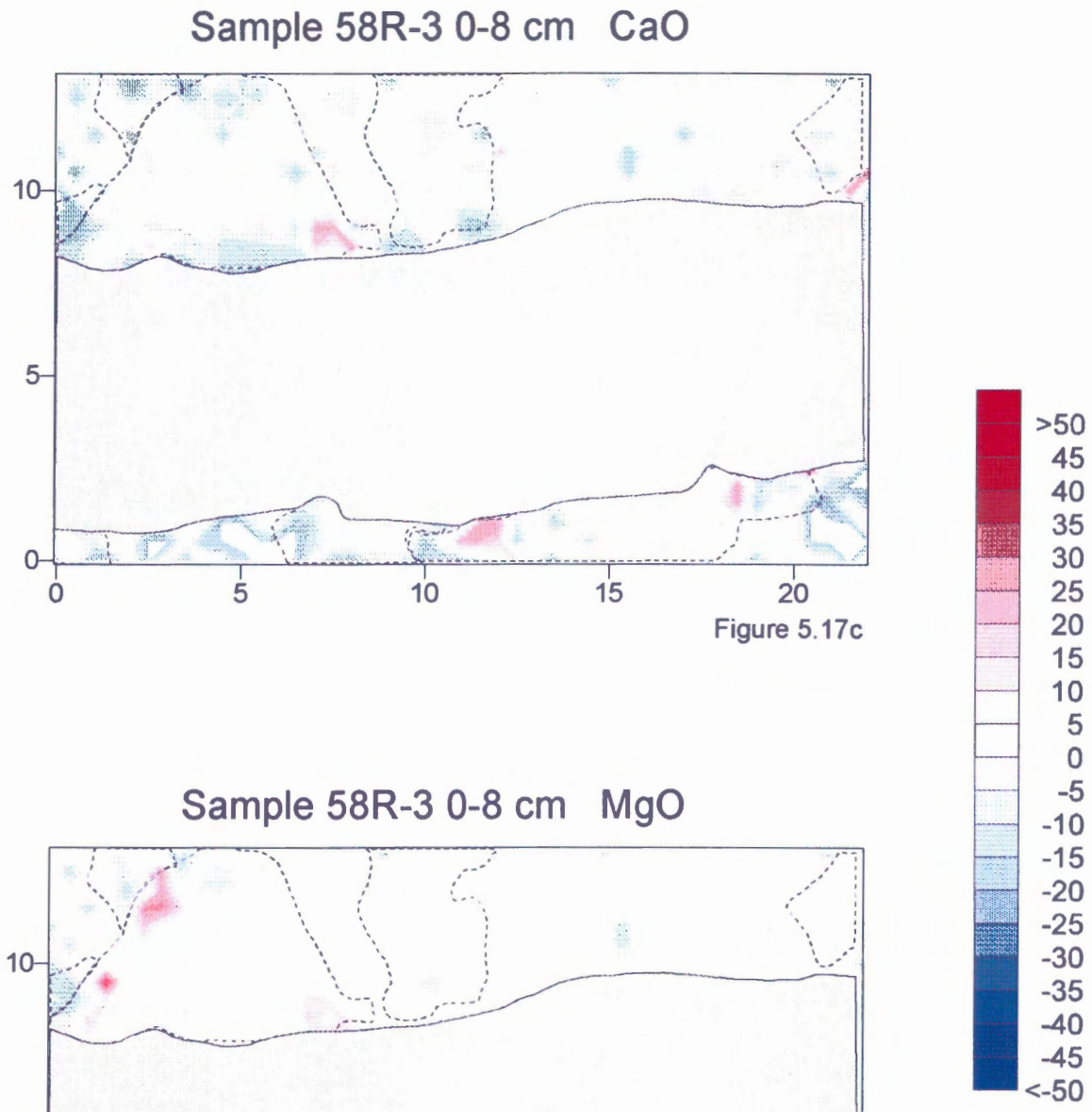

Figure 5.17c

Figure 5.17d

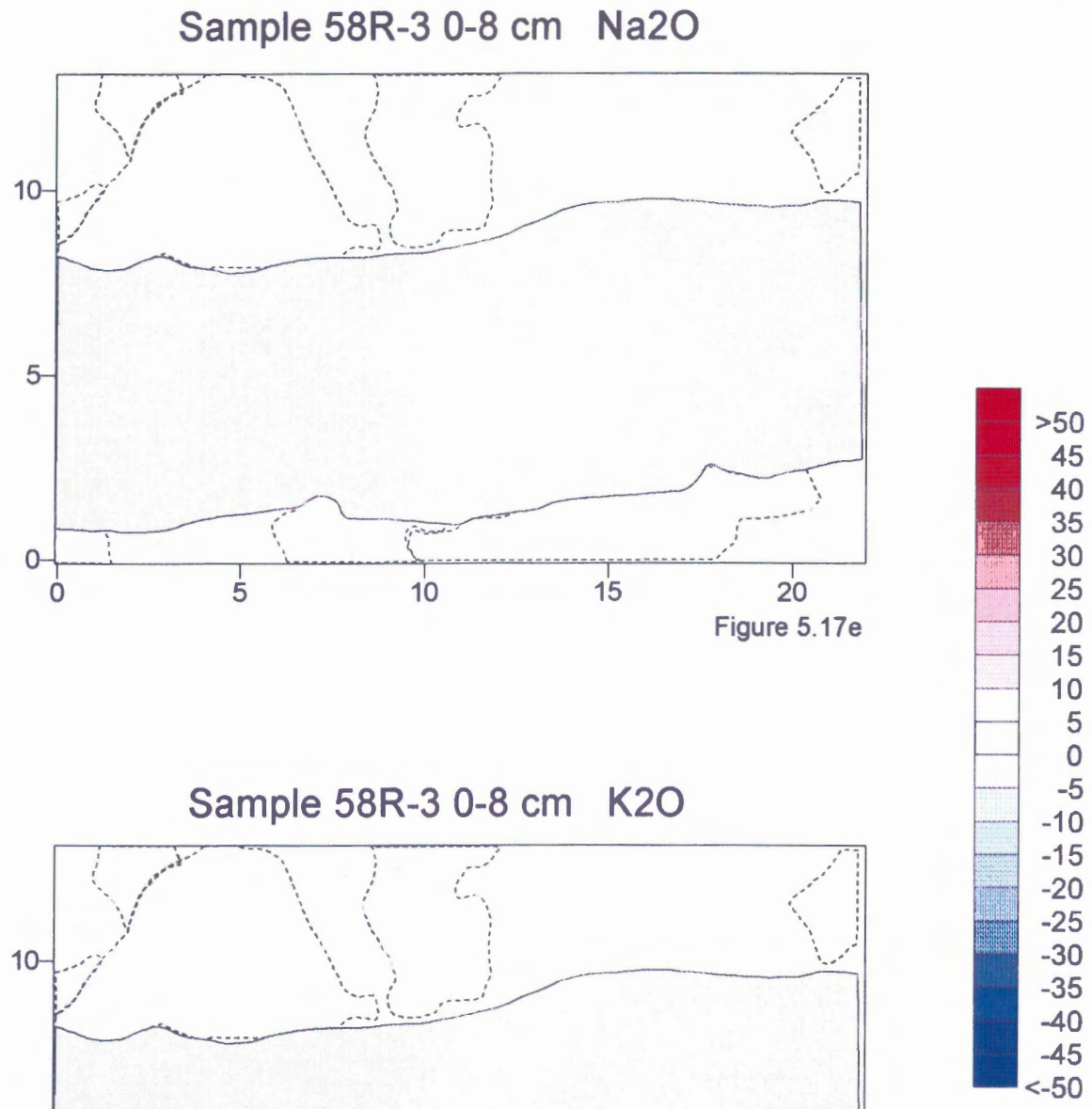

Figure 5.17e

Figure 5.17f

Sample 58R-3 0-8 cm MnO

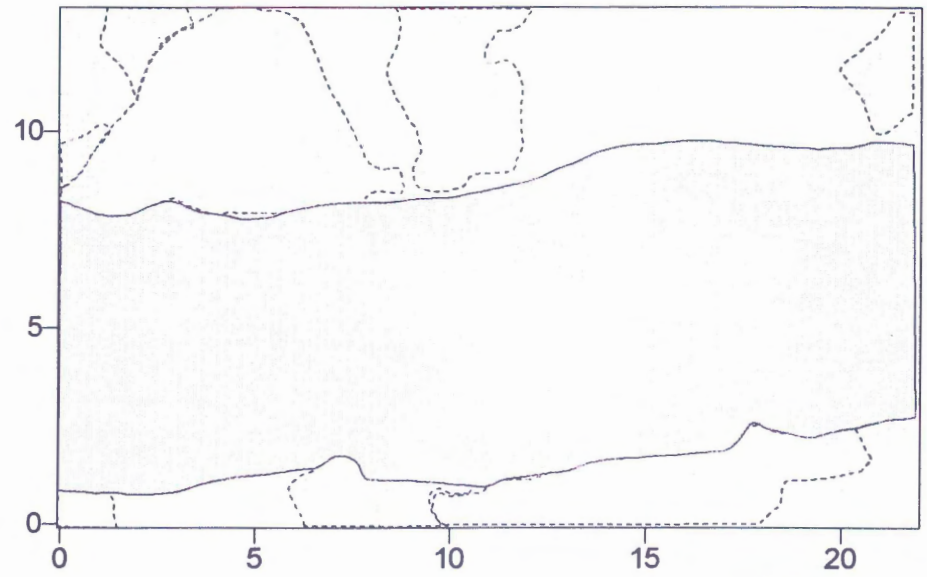

Figure 5.17g

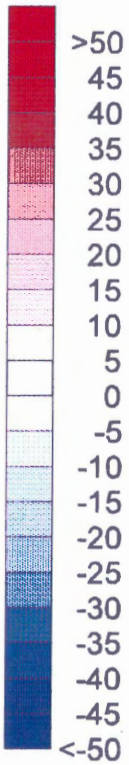

Sample 58R-3 0-8 cm TiO2

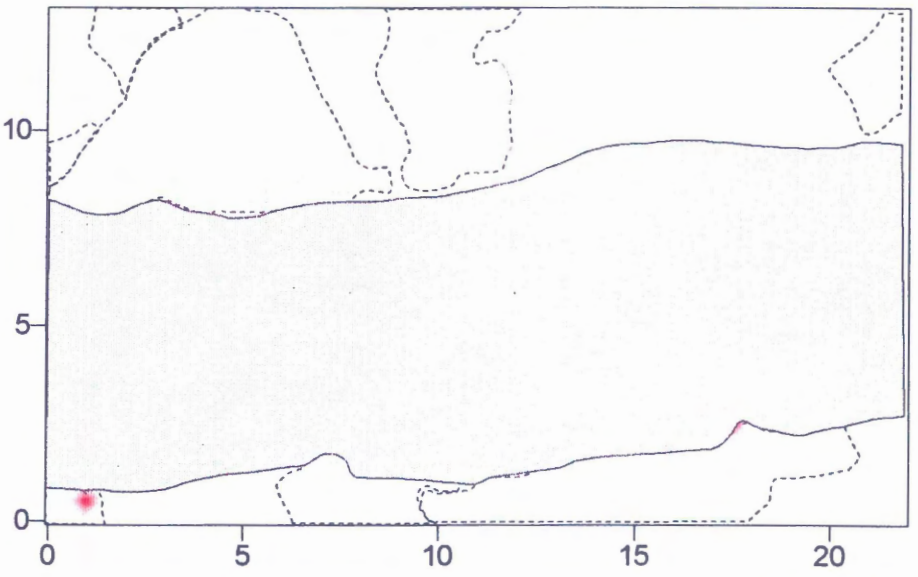

Figure 5.17h

This point is incorrectly classified which has resulted in incorrect residual values. Na_2O, K_2O, MnO, and TiO_2 residuals seem to be randomly distributed. FeO, K_2O, MnO, an TiO_2 residual maps do not show any variation with distance from the vein.

5.5 DISCUSSION

The purpose of creating the residual chemical maps was to determine the chemical effects of alteration in host rock adjacent to hydrothermal veins at the thin section scale. Chemical modification of the host rock is evident in many residual chemical maps that exhibit large residuals proximal to veins. This is particularly evident in the CaO residual map for sample 31R-3 4-10 cm and the SiO_2, CaO and Na_2O residual maps for sample 35R-4 117-124 cm. Residual values also seem to diminish with distance from the vein, suggesting a chemical gradient. These gradients are interpreted to be alteration halos in the host rock resulting from alteration which becomes progressively intense toward the vein. These halos are only evident for certain elements, such as those listed above, which suggests these elements are more mobile. Gradients are only seen within a few millimeters of veins while the host rock often exhibits residuals closer to zero. This suggests that alteration is most intense near veins and only limited chemical modification of the host rock has taken place.

In most cases, residual values which deviate significantly from zero represent the formation of secondary minerals as a result of alteration. In some cases, these secondary minerals have very different chemistry than the minerals from which they formed, including different values for Al_2O_3. In these situations the assumption of constant Al used to calculate residuals likely does not hold true. This is particularly evident in areas displaying alteration after olivine. The calculated normalization ratio can, therefore, have a big effect on the residual value. This is particularly evident in SiO_2, and to a lesser extent CaO and MgO, residual maps which show areas with large positve and negative residuals. SiO_2, CaO, and MgO are particularly susceptible to variations in the normalization ratio because the primary values of these oxides are relatively large (>10

wt%). Many of these areas occupied by amphibole display highly variable Al_2O_3 values relative to primary pyroxene. As a result very large (>1.5) and small (<0.5) normalization ratios are calculated for these points resulting in large SiO_2 residuals (± 20 wt%). Although these residuals may actually represent smaller gains and losses of SiO_2 than those calculated, it was necessary to maintain the assumption of constant Al_2O_3 for consistency and to allow comparison of chemical maps with element-flux calculations.

Areas in which secondary minerals have replaced primary minerals can still be used to qualitatively assess the degree of alteration. For example, many areas identified as amphibole on mingrid worksheets and thin section sketches exhibit chemical gradients, particularly in MgO. These gradients represent gradual changes in chemistry between the primary mineral and the secondary equivalent. Although the calculated MgO residual values in areas identified as amphibole are likely exaggerated, gradual changes in MgO are similar to those obseverd in microprobe traverses (see Chapter 3).

Many of the residual chemical maps show similar features. Similar patterns between samples are seen in residual maps for Na_2O, K_2O, MnO, and TiO_2 which commonly show only small variations in residuals. This is probably because these oxides are found in low concentrations in these rocks and the hydrothermal fluid. Alteration, therefore, does not result in large changes in these oxides. Residual maps for SiO_2, CaO, and MgO show larger variations in residuals for all samples because of their higher concentrations. The large residual values calculated for certain areas identified as amphibole (and sometimes clinopyroxene) are most likely exaggerated due to local Al mobility, as discussed previously. FeO residuals do not exhibit any discernable trend between samples which is probably due to primary variability.

5.5.1 Comparison of Trends in Olivine Gabbro Samples

Four of the five samples from which residual chemical maps have been created are olivine gabbro. Each of the olivine gabbro samples shows similar trends in residual chemistry. Residual maps exibit similar magnitudes of variablity for the same oxide in each of the samples. For example, Na_2O, K_2O, MnO, and TiO_2 all show small residual ranges and

SiO_2, CaO, and MgO all show larger residual ranges. FeO residuals are variable between samples. Residuals for certain minerals are also similar between samples. These trends suggests that alteration in these samples is similar. This is not surprising since each of these samples is from the same lithology and contains veins with similar assemblages (see Table 4.4), suggesting similar initial fluid compositions.

5.5.2 Comparison of Trends Between Lithologies

Only two lithologies were chosen for chemical mapping, olivine gabbro and oxide olivine gabbro (sample 54R-4 69-78 cm). Residual chemical maps for sample 54R-4 69-78 cm show similar trends to the olivine gabbro samples. For example, Na_2O, K_2O, MnO, and TiO_2 all show small residual ranges and SiO_2, CaO, and MgO all show larger residual ranges. FeO is variable in olivine gabbro samples and can not be compared to sample 54R-4 69-78 cm. In addition, areas identified as amphibole on the mingrid worksheet in sample 54R-4 69-78 cm show similarly large positive and negative residuals to those in olivine gabbro samples. This suggests that local Al mobility likely also occured in sample 54R-4 69-78 cm, particularily in areas identified as amphibole. Sample 54R-4 69-78 cm, however, does not exhibit chemical gradients in any of its residual chemical maps. This is likely due to the fact that the plagiogranite vein found in sample 54R-4 69-78 cm (see Appendix 2) has been interpreted to have formed from late magmatic fluids based on previous interpretation of similar veins (Kelley, 1996; Stakes *et al.*, 1991). This may have had a different effect on the host rock than the other veins which contain lower temperature, hydrothermal assemblages.

5.5.3 Comparison of Trends and Mineralogy

The clearest association between residual values and mineralogy is the large residuals associated with amphibole. As discussed above, these large residuals are likely the result of local Al mobilization and not secondary alteration. A similar association is observed in areas identified as clinopyroxene which also exhibit local Al mobilization. Areas identified as sodic plagioclase on mingrid worksheets exhibit small, positive Na_2O residuals (0 to 5

wt%) in samples 35R-4 117-124 cm, 44R-1, 35-47 cm, and 58R-3 0-8 cm. These values are probably due to secondary variation.

Small negative K_2O residuals (-5 to 0 wt%) in samples 31R-3 4-10 cm and 44R-1 35-47 cm appear to be correlated with areas identified as plagioclase on mingrid worksheets and thin section sketches. A similar trend is seen for small negative (-5 to 0 wt%) MnO and TiO_2 residuals in sample 35R-4 117-124 cm which are correlated with areas identified as amphibole and clinopyroxene. These trends likely result from using primary values which are slightly different from actual values to calculate residuals. As a result, these trends likely reflect primary, rather than secondary, variation.

5.5.4 Comparison of Microprobe Traverses and Chemical Maps

Although microprobe traverse data were not normalized to constant Al, comparison of chemical trends between traverses and residual maps can determine if the two trends are similar. Microprobe traverses from primary clinopyroxene to secondary amphibole are characterized mainly by decreases in CaO and variable changes in MgO and FeO within a few millimeters. Very similar trends are seen in residual maps, particularily in CaO. CaO consistently exhibits the greatest variablity (~10 to 15 wt%) in microprobe traverses which is well within the contouring interval used for the residual maps (5 wt%). FeO and MgO exhibit slightly smaller variability (~5 to 10 wt%) which is only marginally above the countouring interval and which could mask the trend. Still, several areas identified as clinopyroxene altered to amphibole (clinopyroxene next to amphibole on mingrid sheets) do show variable FeO and MgO residuals . In additon, certain areas also show the gradual nature of these chemical changes indicated by closely spaced (<1 mm) contours.

One microprobe traverse from primary plagioclase altered to sodic plagioclase is characterized mainly by an increase in SiO_2 and Na_2O and a decrease in CaO. Similar trends are seen in residual maps. SiO_2 and CaO exhibit slightly larger variability in the microprobe traverse than Na_2O. A similar amount of variability is seen in residual maps. These trends are slighlty less gradual that those for alteration of clinopyroxene, however, different contour levels are still apparent, particularily near the vein margin. Alteration of

primary plagioclase to epidote is difficult to determine from residual maps because epidote was not classified on mingrid worksheets and the modal percentage of epidote is small. Mineral traverses were not performed from primary olivine to secondary minerals, however, residual chemical maps indicate limited Al mobility on a millimetre scale in these areas.

5.5.5 Comparison of Element Fluxes and Residual Maps

Normalization of element fluxes and most minerals in residual calculations to constant Al allows direct comparison. Estimates of chemical changes in the host rock from residual maps (by visual estimation) are summarized in Table 5.3. All samples exhibit losses of CaO and MgO, as estimated from residual maps. A similar trend is observed from element-flux calculations, although element fluxes are more variable (Figure 4.7). Limited changes in Na_2O, K_2O, MnO, and TiO_2 are observed for olivine gabbro samples from both element fluxes and residual maps. Other oxides display variable changes in both element fluxes and residual maps.

The similarity between trends in element fluxes and residual maps suggests that the residual maps accurately depict chemical changes in the host rock as a result of alteration. This is what one would expect if the residual maps were created according to the guidelines and assumptions listed in previous sections. However, areas which do not conform to the initial assumptions, such as constant Al in amphibole, have resulted in incorrect residual calculation.

5.6 SUMMARY

Residual chemical maps of eight elements have been created from gridded microprobe data collected from five samples, which represent two lithologies. Gridded microprobe data for nine elements were first collected from five polished sections. Residual chemistry was then calculated using Equation 5.1 by a program written in Visual Basic®. Microprobe data for points identified as amphibole, clinopyroxene, sodic plagioclase, or

Table 5.3 Summary of chemical changes from residual maps

Lithology:	Olivine Gabbro				Oxide Olivine Gabbro
Sample:	31R-3 4-10 cm	35R-4 117-124 cm	44R-1 35-47 cm	58R-3 0-8 cm	54R-4 69-78 cm
SiO_2	nc	+	-	+	+
FeO	-	-	nc	nc	nc
MgO	-	-	-	-	-
CaO	-	-	-	-	-
Na_2O	nc	+	nc	nc	nc
K_2O	nc	nc	nc	nc	nc
MnO	nc	nc	nc	nc	nc
TiO_2	nc	nc	nc	nc	nc

Gains and losses were visually estimated from residual maps. Areas suspected of Al mobility were not included. + = gain; - = loss ; nc = small or no change.

calcic plagioclase were normalized to constant Al before residual calculation. Normalization to constant Al in areas identified as amphibole (and sometimes clinopyroxene) does not seem to be appropriate because of suspected Al mobility on a small scale. Microprobe data for points identified as olivine, quartz, ilmenite, or magnetite were not normalized because of the very low or variable Al_2O_3 content of these minerals. Contour maps, contoured at intervals of 5 wt%, were created in SURFER® for Windows™ for each of the samples. Positive values in residual maps indicate gains and negative values indicate losses as a result of host-rock alteration.

The purpose of creating residual maps was to determine the chemical effect of alteration on the host rock near hydrothermal veins. This is evident in residual maps and is characterized by residual gradients proximal to veins. These gradients are interpreted as alteration halos and indicate that alteration becomes more intense toward the vein. Gradients are only observed in certain oxide residual maps, namely SiO_2, CaO, and Na_2O, suggesting that alteration affected different elements by different amounts. In general, alteration halos are restricted to areas within a few millimeters of veins suggesting limited chemical modification of the host rock. Residual maps show very similar trends to microprobe traverses for alteration of both clinopyroxene and plagioclase. In addition, estimates of chemical changes in the host rock from residual maps (by visual estimation) are almost the same in direction and magnitude as calculated element fluxes for the same samples. However, residual maps also provide spatial information on alteration trends which whole-rock analyses do not.

Residual maps, therefore, provide a new method of quantifying chemical changes at the thin section scale and provide a link between traditional methods of estimating chemical changes due to alteration. Two standard methods, microprobe traverses and element fluxes, have already been described (see Chapters 3 and 4). Residual chemical maps allow investigation at a scale slighlty larger than traverses and slightly smaller that whole-rock analysis, which when combined, provides a more complete picture of the chemical effects of alteration.

Chapter 6

Conclusions

Detailed geochemical analyses document the geochemical effects of alteration on host rock near hydrothermal veins in samples of lower ocean crust from ODP Hole 735B. Veins in these samples contain complex mineral assemblages which record metamorphic conditions ranging from anhydrous granulite facies conditions to lower greenschist and zeolite facies conditions. Progressive alteration under changing conditions is suggested by veins which display sequential mineral assemblages.

Most veins in samples from this study contain mineral assemblages characteristic of amphibolite facies metamorphic conditions, including plagioclase, green and brown amphibole, and minor diopside. Vein amphibole, particularly in samples from the upper portions of the core, contains significant amounts of chlorine (up to a few tenths of a percent) which suggests influence by seawater. Penetration of seawater is believed to have caused cooling from granulite to amphibolite conditions during progressive alteration in Hole 735B rocks.

Alteration halos near veins, documented in residual chemical maps, only penetrate a few millimetres into the host rock. This suggests that alteration has resulted in only limited chemical modification of the host rock. In addition, alteration halos are only observed in certain oxide residual maps, namely SiO_2, CaO, Na_2O, and to a lesser extent MgO, suggesting that these oxides were mobile during alteration. Alteration halos are characterized by gains of SiO_2 and Na_2O and losses of CaO and MgO. These changes are similar to those on a micro-scale seen in microprobe traverses from primary to secondary minerals, which indicate that CaO and MgO were lost, FeO and Na_2O were gained, Al_2O_3 remained relatively constant, and SiO_2 was variable during alteration. Overall, chemical changes in microprobe traverses are abrupt on the scale of a few millimetres. Element fluxes on a hand specimen scale, calculated from whole-rock samples adjacent to hydrothermal veins, indicate that CaO, MgO, TiO_2, Rb, and Nb were lost, SiO_2, Fe_2O_3, Na_2O, K_2O, Sr, Y, and Zr were variable, and MnO and P_2O_5 displayed no change.

The mobility of generally accepted immobile elements is questioned in samples from Hole 735B. Element fluxes in oxide-bearing gabbro indicate that TiO_2 is lost during alteration under amphibolite facies conditions. This apparent mobility is the reverse of what is observed in Layer 2 rocks which display lower temperature greenschist conditions (Gillis, 1986; Alt and Emmermann, 1985; Humphris and Thompson, 1978). TiO_2 may, therefore, be mobile in Ti-rich oceanic rocks during high temperature (600-700^0) alteration. Similarly, local Al mobility is suspected in Hole 735B samples. In residual chemical maps, Al displays limited mobility which is restricted to areas where amphibole replaces olivine. Overall, Al is found to be immobile, like Ti, during alteration under greenschist conditions in Layer 2 ocean rocks (Gillis, 1986; Alt and Emmermann, 1985; Humphris and Thompson, 1978). Similar immobility of Al is indicated by microprobe traverses between primary and secondary minerals (other than olivine to amphibole) in Hole 735B samples.

When considering the chemical changes associated with alteration, it is important to consider the scale at which the changes are observed. CaO and MgO are lost in mineral traverses, chemical maps, and whole-rock element fluxes. These three methods span a range of scales from sub-millimetre to centimetres. The similarity of the observed trends for CaO and MgO at different scales suggests that scale has no effect on the mobility of these oxides in samples from this study. Other oxides, such as Al_2O_3, exhibit different trends with scale. Limited Al mobility in areas exhibiting alteration of olivine to amphibole is indicated in residual chemical maps. Alteration of olivine was not documented in mineral traverses, however, element flux calculations normalized to a variety of least mobile elements suggests that Al is most likely immobile at the hand sample scale. This finding is in agreement with previous studies which have shown that Al is immobile during alteration of mafic rocks by seawater (Gillis, 1986; Alt and Emmermann, 1985; Humphris and Thompson, 1978). Similarly, TiO_2 mobility indicated by element fluxes in oxide-bearing gabbro is not observed in oxide-free lithologies. Olivine gabbro makes up more than 60% of the total core recovered from Hole 735B (Dick *et al.* 1991a). As a result, Ti is most likely not mobile on the scale of the core as a hole. So, although certain elements

may exhibit limited mobility on a small scale, larger scale variations may be significantly different.

Qualitative comparison of element fluxes from Hole 735B samples with equivalent studies of oceanic Layer 2 provides a basis to assess the differences in the chemical effects of alteration in the upper and lower ocean crust (Bach *et al.*, 1996; Bednarz and Schmincke, 1989; Thompson, 1983, Mottl, Holland, and Corr, 1979; Mottl and Holland, 1978; Humphris and Thompson, 1978). Comparison with these studies indicates that element-flux trends for Si and Na appear to be similar. However, Mg and Rb fluxes appear to be opposite in direction. Both Rb and Mg are lost from samples from Hole 735B and gained in samples from Layer 2. The apparent variation in Mg and Rb fluxes between Layers 2 and 3 is most likely the result of different conditions during alteration. Von Damm *et al.* (1985) identified a number of factors that could contribute to the observed variations:

(1) differences in rock type;
(2) differences in temperature of the hydrothermal solutions at depth in the system;
(3) differences in the residence times, or flow rates, of the water in the fissure system;
(4) differences in the depth at which sea water-rock reaction takes place, which affect the path length of the hydrothermal cell; and
(5) differences in the age of the hydrothermal system.

Hydrothermal alteration is a ubiquitous process operating in the ocean crust as a whole. Several of the factors listed above, which influence chemical modification of host rock during hydrothermal alteration, can change substantially at different levels in the ocean crust. For example, volcanic rocks in Layer 2 commonly contain glass which reacts with sea water more rapidly than more crystalline rocks common in Layer 3. In addition, residence times and flow rates most likely vary considerably between Layers 2 and 3. Finally, rocks recovered from Hole 735B represent a unique opportunity to study alteration in Layer 3. Hole 735B samples contain metamorphic assemblages which indicate much higher temperatures during alteration than those in Layer 2 samples. As a

result, differences in chemical changes between various levels in the ocean crust should be expected.

Gains and losses by the host rock in studies of Layer 2 are interpreted to result from the formation of secondary alteration products such as smectite, actinolite-tremolite, talc, sodic feldspar, zeolites, and chlorite (Mottl, Holland, and Corr, 1979; Mottl and Holland, 1978). These minerals characterize greenschist and zeolite facies metamorphism of oceanic basalts. Alteration in Hole 735B samples is characterized by higher temperature, amphibolite facies assemblages in which the dominant secondary mineral is amphibole. The apparent loss of Rb from Hole 735B samples is likely due to the low abundance of clay minerals relative to Layer 2 rocks. Similarly, loss of Mg from olivine during alteration in Hole 735B samples is probably not balanced by the formation of minerals such as Mg-hornblende, talc, and tremolite. This has resulted in the observed loss of MgO from Hole 735B samples. In addition, chlorite and smectite are not as abundant in Hole 735B samples as Layer 2 rocks, possibly reducing further uptake of Mg by the host rock.

Samples used in this study represent some of the most altered portions of the core recovered from Hole 735B. The chemical effects of alteration documented in these samples indicate that alteration in the lower ocean crusts results in only limited chemical modification, even in altered samples adjacent to veins. Alteration is most intense within 1 cm of veins and diminishes with distance from veins. Comparison of chemical changes in samples from Hole 735B with those from Layer 2 suggests that alteration of the ocean crust as a whole is heterogeneous, resulting in differences in style of alteration, degree of alteration, and alteration assemblages. Chemical changes in samples from Hole 735B which appear to be reversed from those observed at higher levels in the ocean crust, therefore, may have a significant impact on calculations of geochemical budgets for seawater and the ocean crust as a whole.

Appendix 1

Analytical Methods

1.1 WHOLE-ROCK ANALYSES

1.1.1 Sample Preparation

Whole-rock powders were prepared from altered host rock adjacent to veins. Care was taken to sample as close to the vein as possible without including vein material. Cut surfaces were abraded with 80 grit silicon carbide on glass. Samples were cleansed in an ultrasound with water and methanol, crushed first in a hydraulic press then in a jaw crusher, and powdered in a tungsten carbide micro ball mill. Final samples ranged from 25 to 50 grams.

1.1.2 Major and Minor Oxides

Major and minor element oxides were analyzed on a Philips PW1400 sequential X-ray flourescence spectrometer using an Rh-anode tube at the Regional Geochemical Facility, Saint Mary's University, Halifax. Fused glass disks were used for major and minor oxide determination. Prior to fusing, 1 gram of each sample was heated for 1.5 hours at 1050 °C in an electric furnace for the determination of Loss on Ignition (LOI). Major and minor element calibrations were obtained using 30 international standards (see Govindaraju, 1989 for recommended values) in addition to 'in house' standards. Analytical precision is better than 1% for major and minor oxide determinations.

1.1.3 Trace elements

Trace elements were analysed at the Department of Earth Sciences, Memorial University of Newfoundland. The analytical procedure involved digestion of a 0.1 gram samplee aliquot in a HF/HNO3 (+ boric and oxalic acids) followed by analysis of the solution by inductively coupled mass spectrometry (ICP-MS) using the method of standard addition to correct for matrix effects (see Jenner et al,. 1990). Any sample material that did not

dissolve in HF/HNO3 was attacked with HCl/HNO3. Geological reference standards and a reagent blank were analysed to measure accuracy and precision. Reagent blank concentrations are insignificant and have not been subtracted from sample concentrations. The precision of the method is better than 7% for trace element determinations.

1.2 MINERAL ANALYSES

Mineral analyses for major and minor oxides were performed on a JEOL 733 electron microprobe equipped with an Oxford Link eXL energy dispersive system at Dalhousie University. The resolution of the energy dispersive detector is 137 ev at 5.9 Kev. An accelerating voltage of 15 Kv was used with a beam current of 15 nA. Probe spot size was approximately 1 micron. Traverse point spectra were accumulated for 40 seconds and chemical map spectra were accumulated for 2 seconds. Raw values were corrected using Link's ZAF matrix correction program. The instrument was calibrated using cobalt metal. Instrument precision is ± 0.5% at 1 standard deviation. Geologic standards were used as controls. Traverse analyses are accurate to ± 1.5 to 2.0% of the value. Chemical map analyses are probably less accurate due to shorter spectrum accumulation.

Appendix 2

Petrographic Descriptions

Samples used in this study follow the sample numbering system used by the Ocean Drilling Program (ODP). For a complete description of the numbering procedure see the Introduction and Explanatory Notes, Shipboard Scientific Party (1989). The samples are from Hole 735B recovered during ODP Leg 118. For this reason, sample numbers do not include the leg and hole number. The depth of each sample in meters below seafloor (mbsf) is indicated in brackets to the right. Rock names and unit classifications follow conventions used in Dick et al. (1991a). The approximate locations of microprobe traverses have been marked on the appropriate sections.

Sample: 22R-1 82-90 cm (95.8 mbsf)

Rock Type: Olivine Gabbro

Unit: II

Coarse-grained subhedral granular olivine gabbro. Olivine is completely replaced by colourless amphibole, chlorite, and secondary magnetite. Clinopyroxene grains are fractured and altered to green amphibole along cleavage traces and at grain boundaries. Plagioclase is cross-cut by numerous amphibole and albite veinlets. Minor alteration filling fractures in plagioclase with yellow-brown clay is evident. The sample is also cut by a 7-10mm wide vein at one end that contains green amphibole and minor fine-grained plagioclase. Plagioclase and clinopyroxene grains are deformed and fractured along the margin of the vein.

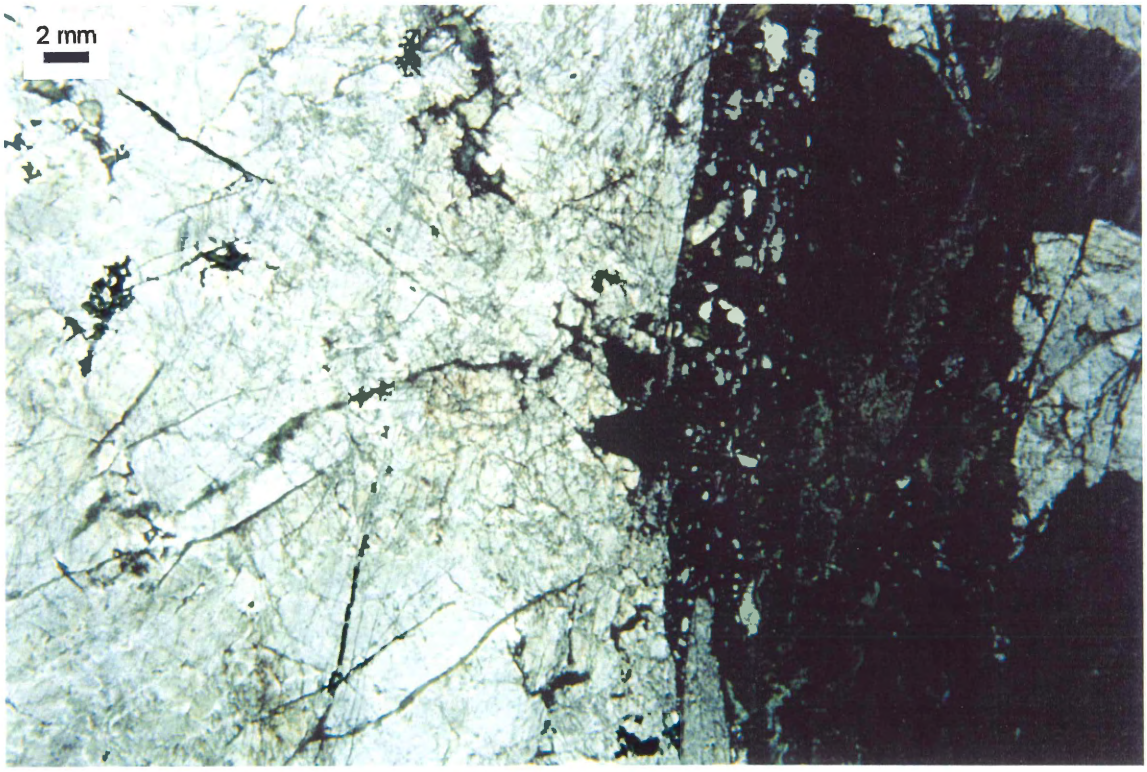

Sample:31R-3 (4-10cm) (146.57 msbf)

Rock Type: Olivine Gabbro

Unit: II

Coarse-grained olivine gabbro displaying anhedral granular and mesocumulate textures. Anhedral olivine grains (3-5mm) are relatively fresh (~ 20% altered) but are rimmed by colourless amphibole and are partly replaced by brown clay, oxides, and minor carbonate along fractures. Coarse-grained subhedral clinopyroxene grains (up to 1cm) display subophitic texture and poikilitically enclose plagioclase. Clinopyroxene is rimmed by green amphibole. The sample is cut by a vein (4-7mm) that contains fine-grained plagioclase at the margins and green amphibole at the centre. Subhedral plagioclase grains are remarkably fresh in the sample with only minor replacement by brown clay along fractures near the vein margin. Clinopyroxene is altered to brown and green amphibole and plagioclase is recrystallized along the vein margin.

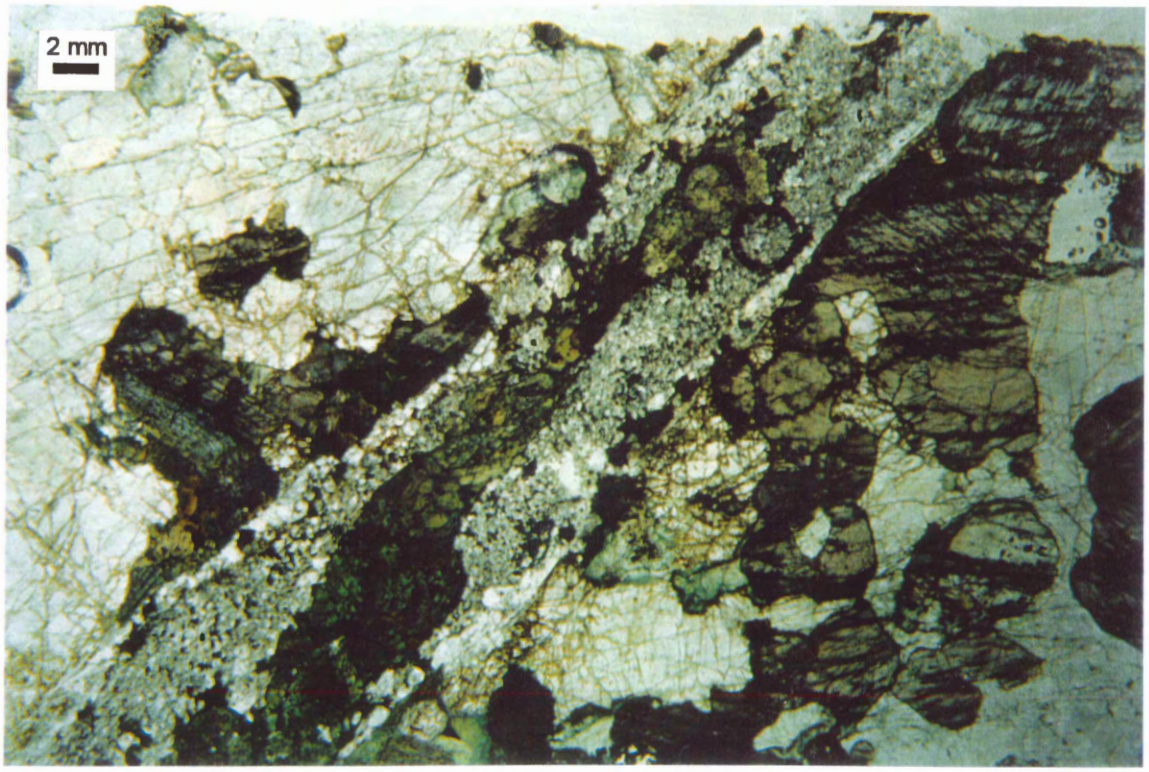

Sample: 32R-2 (86-95cm) (150.5 mbsf)

Rock Type: Olivine Gabbro

Unit: II

Coarse-grained olivine gabbro displaying subhedral granular and mesocumulate textures. Olivine is almost completely replaced by colourless and light green amphibole, opaque minerals, and brown clay. Subhedral clinopyroxene grains (up to 8mm) display subophitic textures and poikilitically enclose plagioclase. Clinopyroxene is altered to green amphibole along fractures and at grain boundaries. Subhedral plagioclase grains (up to 5mm) are cross-cut by fractures and veinlets filled with green amphibole and clay (?). The sample is cut by a 5mm wide vein filled mostly with acicular green amphibole. The host rock along the vein margin has been pervasively altered within a few millimetres of the vein. Plagioclase along the vein contains irregular patches of albite.

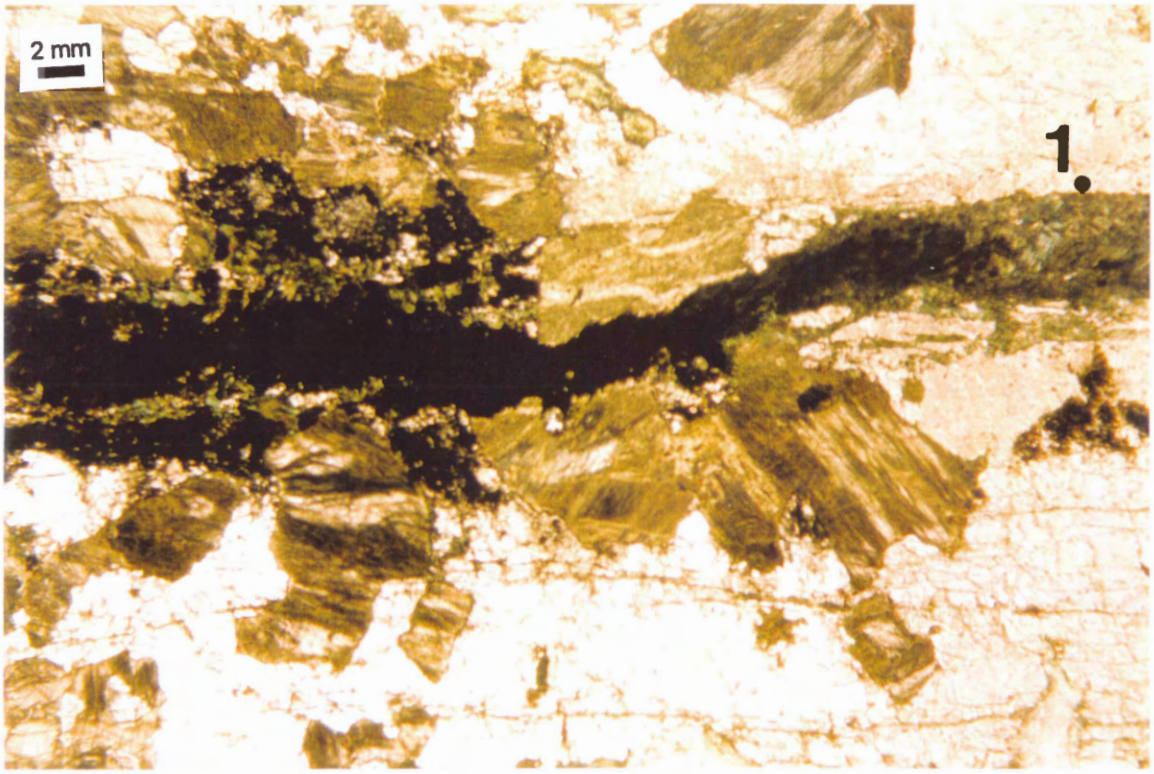

Sample: 35R-4 (117-124cm) (169.21 mbsf)

Rock Type: Olivine Gabbro

Unit: II

Coarse-grained olivine gabbro showing anhedral granular and mesocumulate textures. Subhedral clinopyroxene grains (up to 7mm) display subophitic textures and poikilitically enclose plagioclase. Olivine is completely pseudomorphed by colourless amphibole, brown clay, oxides and chlorite. Clinopyroxene is rimmed by green amphibole. Plagioclase grains (up to 1cm) are cross-cut by tiny fractures filled with brown clay, albite, and minor carbonate. The sample is cut by a narrow veinlet (3-5mm) which contains fine-grained plagioclase, euhedral to anhedral green amphibole (some acicular), and minor albite.

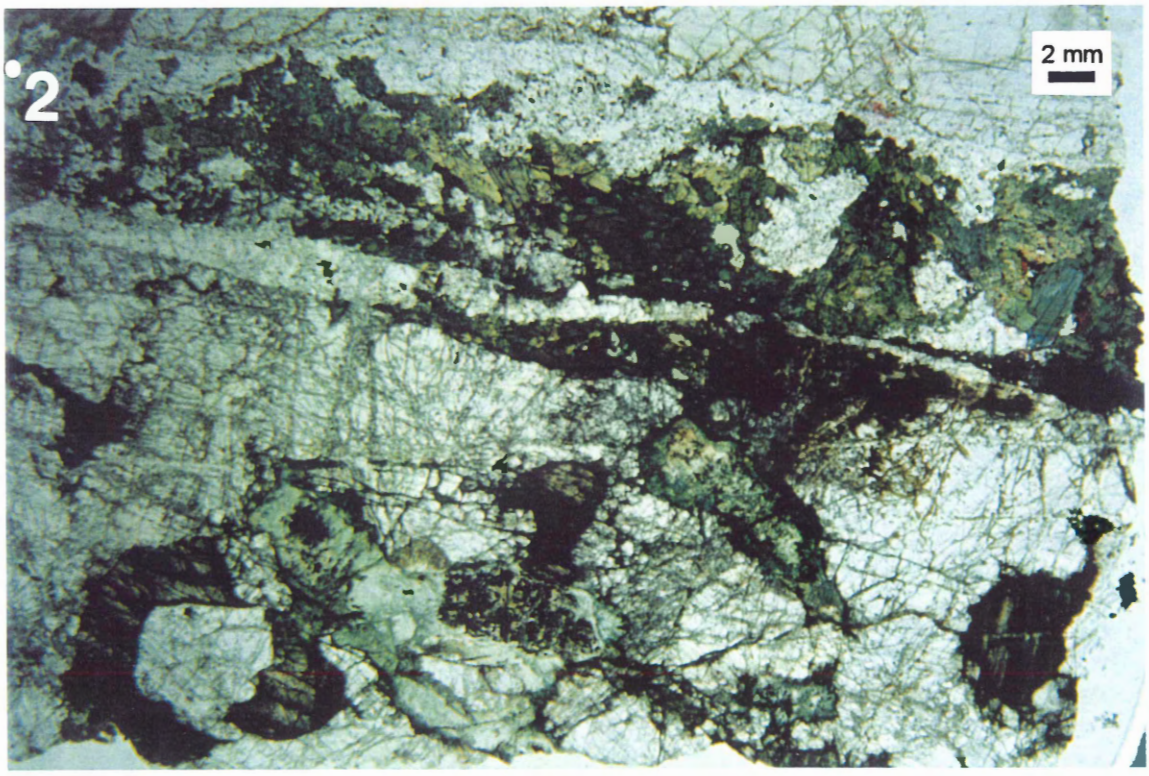

Sample: 41R-1 (26-31cm) (196.28 mbsf)

Rock Type: Disseminated Oxide Olivine Gabbro

Unit: IIIB

Medium-grained, subhedral granular disseminated oxide olivine gabbro. Olivine is completely pseudomorphed by colourless amphibole, oxides, and chlorite. Subhedral clinopyroxene grains (3-5mm) are rimmed by green and brown amphibole. Subhedral plagioclase is cross-cut by numerous tiny veinlets filled with brown clay and chlorite. One side of the sample contains a 1cm wide vein containing fine-grained plagioclase with minor epidote and sphene. The vein also contains green diopside at the margin. Anhedral oxides are found both in the host rock and in the vein.

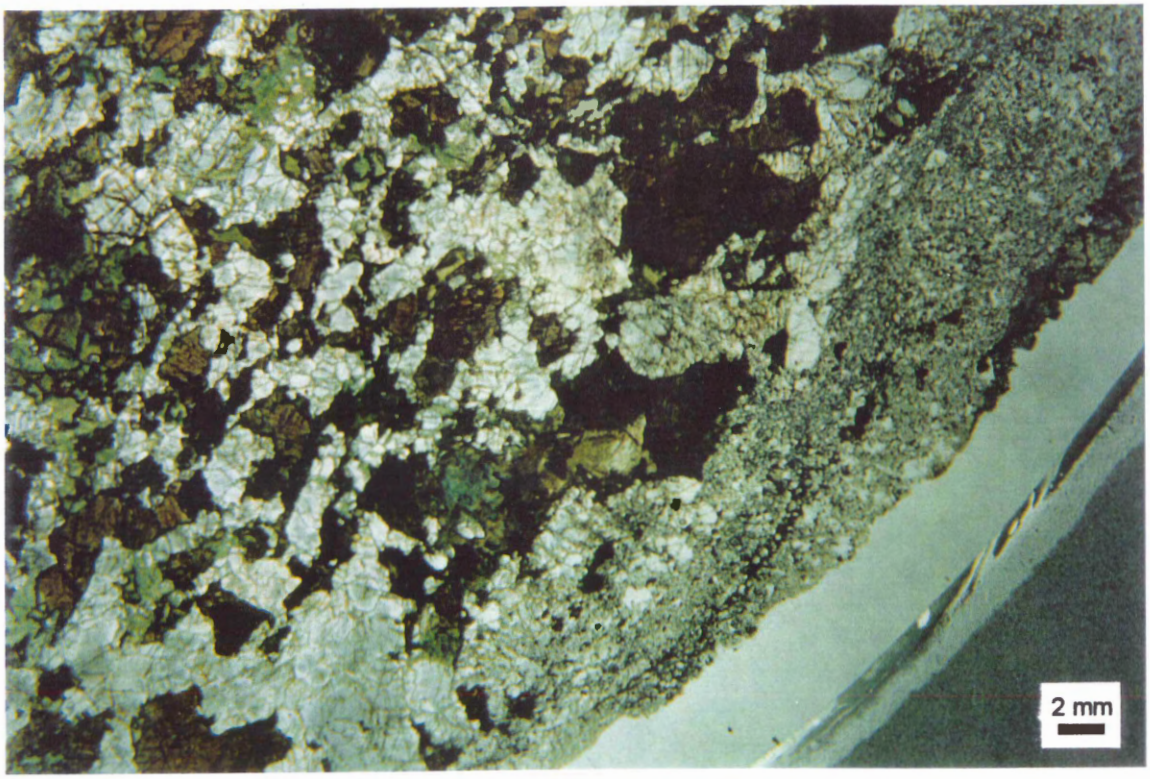

Sample: 41R-3 (43-49cm) (199.46 mbsf)

Rock Type: Disseminated Oxide Olivine Gabbro

Unit: IIIB

Medium grained, subhedral granular disseminated oxide olivine gabbro. Olivine is completely pseudomorphed by colourless amphibole, oxides and chlorite. Subhedral clinopyroxene grains (<1-4mm) are partially replaced along cleavage traces, and are rimmed by, green amphibole. Subhedral plagioclase is cut by numerous tiny veinlets of green clay, chlorite, and albite. Chlorite and green clay also occur at grain boundaries between plagioclase and clinopyroxene and in irregular patches. The sample is cut by an 8mm vein of fine-grained plagioclase, colourless amphibole poikilitically enclosing plagioclase, epidote, and minor clay. Anhedral oxides occur in the host rock and in the vein.

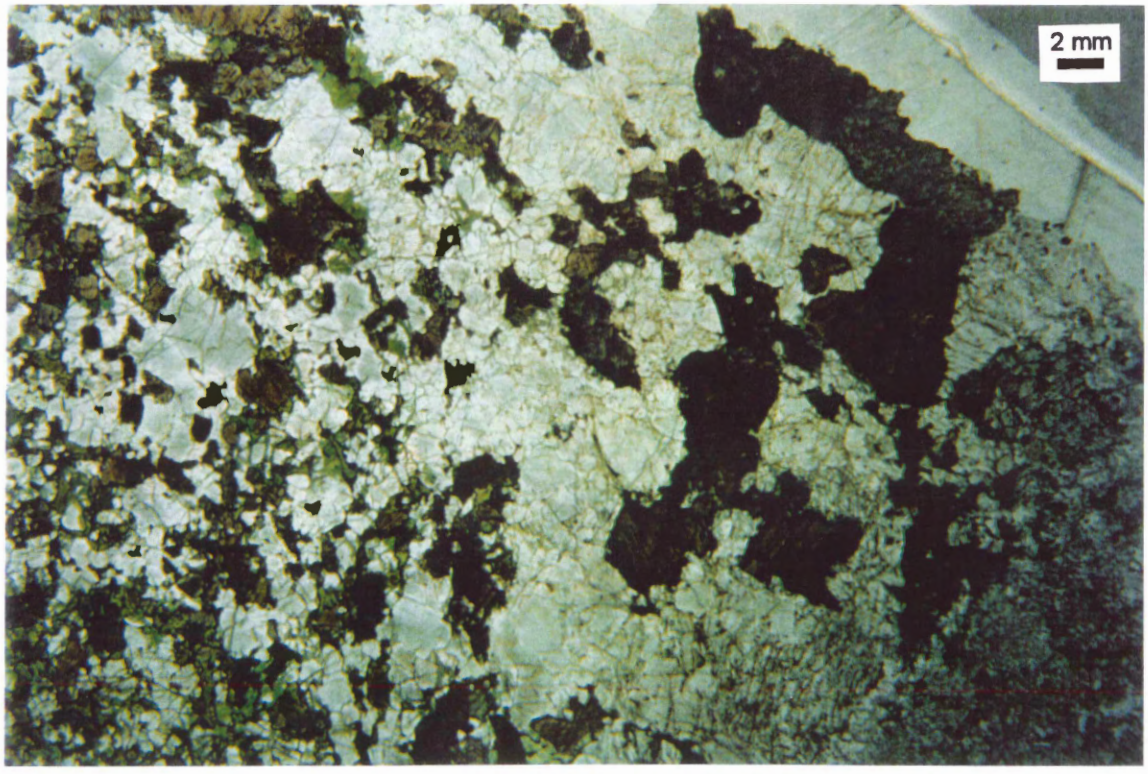

Sample: 44R-1 (35-47cm) (211.41 mbsf)

Rock Type: Olivine Gabbro

Unit: IIIC

Coarse-grained olivine gabbro displaying subhedral granular and mesocumulate textures. Olivine is completely replaced by colourless amphibole, chlorite, and oxides. Coarse-grained (7-10mm) clinopyroxene grains are altered to green and brown amphibole along grain boundaries and cleavage traces. Subhedral plagioclase is pervasively altered along fractures, and cut by veinlets filled with chlorite, clay, albite, and minor epidote. One side of the section is a 15-20mm vein containing recrystallized plagioclase, pale green and colourless amphibole (some acicular), relatively abundant (2-3%) epidote, and brown clay. The vein also contains subhedral grains of colourless to pale green diopside rimmed by green amphibole.

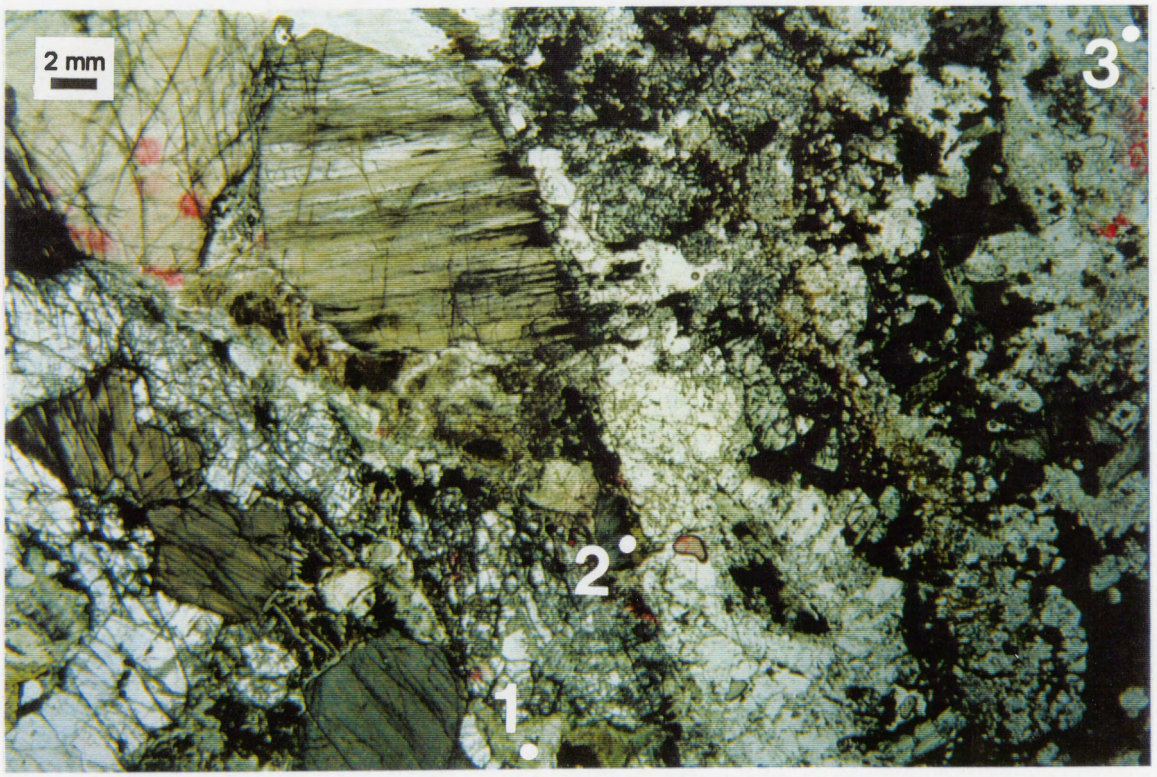

Sample: 54R-4 (69-78cm) (263.24 mbsf)

Rock Type: Oxide Olivine Gabbro

Unit: IV

Note: This section was initially cut for fluid inclusion study and is anomalously thick (~70μm). Some features are therefore difficult to distinguish.

Coarse-grained, subhedral oxide olivine gabbro. Subhedral clinopyroxene is pervasively altered and rimmed by green and brown amphibole. Minor subhedral, pleochroic, pale brown orthopyroxene is rimmed by green amphibole. Plagioclase is cut by abundant fractures and tiny veinlets filled with brown clay. Irregular patches containing chlorite, colourless amphibole, reddish-brown oxides, and minor carbonate (?) are most likely pseudomorphs after olivine. Anhedral oxides are abundant and fill spaces between plagioclase and clinopyroxene. The section is cut by a 10-12mm plagiogranite vein containing quartz, feldspar, brown clay, and pale green amphibole. Unlike other veins, that formed by fractures which broke around mineral grains, this vein truncates all features including opaque minerals.

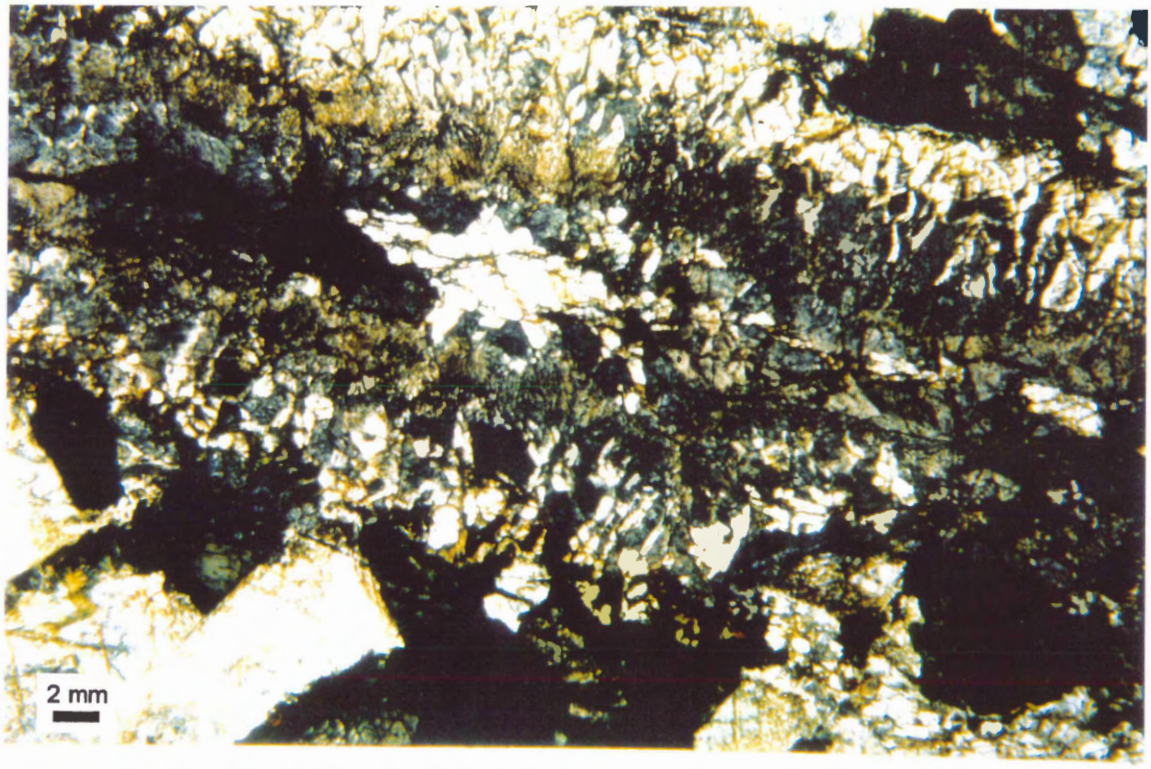

Sample: 58R-3 (0-8cm) (283.54 mbsf)

Rock Type: Olivine Gabbro

Unit: V

Coarse-grained, subhedral granular olivine gabbro. Coarse-grained (4-6mm) irregular patches filled with colourless amphibole, chlorite, brown clay and oxides are most likely pseudomorphs after olivine. Clinopyroxene grains (4-6mm) are altered along cleavage traces and grain boundaries to green and minor brown amphibole. Plagioclase is highly fractured and cut by numerous tiny veinlets filled with brown clay and chlorite. The sample is cut by an 8mm wide vein containing numerous secondary minerals including recrystallized plagioclase, green and brown amphibole (some acicular), chlorite, opaques, brown clay, zeolites, epidote, and minor sphene. Clinopyroxene grains cut by the vein are altered to brown then green amphibole toward the vein centre.

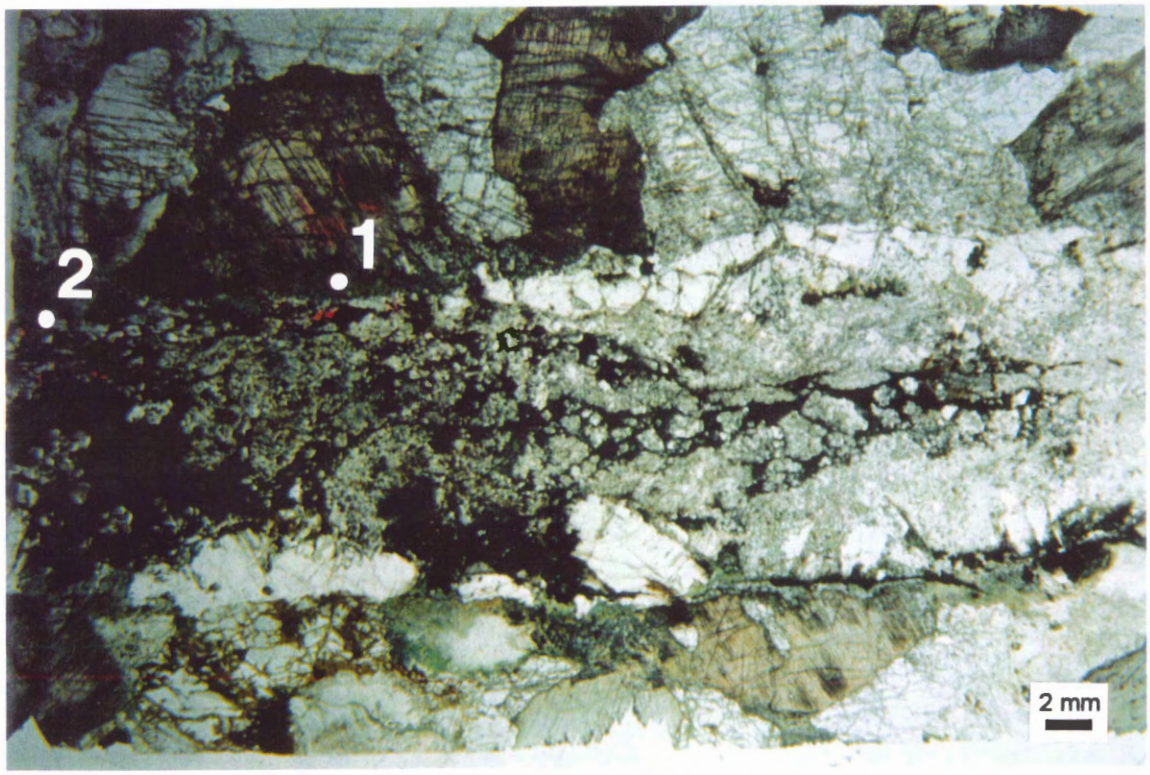

Sample: 60R-4 (112-120cm) (296.16 mbsf)

Rock Type: Olivine Gabbro

Unit: V

Very coarse-grained olivine gabbro displaying subhedral granular and cumulate textures. Olivine is partially replaced by red-brown opaque oxide clots, colourless and light green amphibole, and some clay. Large clinopyroxene grains (up to 1.5 cm) show only slight signs (~ 10%) of alteration to green amphibole along grain boundaries. Subhedral clinopyroxene poikilitically encloses plagioclase laths in a few areas. Subhedral plagioclase grains (4-8mm) are relatively fresh but exhibit signs of alteration to clay along fractures. The sample is cut by a 5mm wide vein containing a number of secondary minerals including recrystallized plagioclase, green and brown amphibole, brown clay, epidote, chlorite, and minor sphene. Clinopyroxene is altered to brown and green amphibole along the vein margin and plagioclase is zoned.

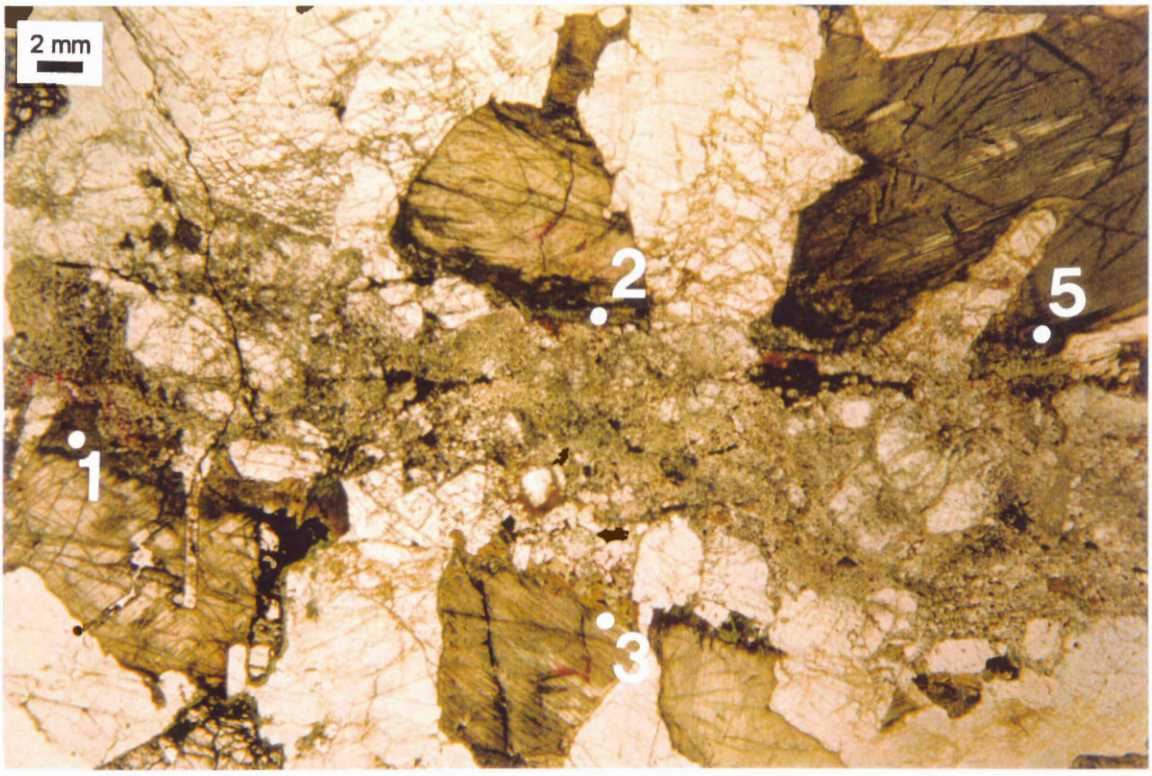

Sample: 63R-6 (98-106cm) (314.02 mbsf)

Rock Type: Olivine Gabbro

Unit: V

Coarse-grained olivine gabbro displaying anhedral to subhedral granular and mesocumulate textures. Olivine is completely replaced by large (some >7mm) red-brown opaque oxide clots, colourless amphibole, and chlorite. Anhedral clinopyroxene grains (up to 7mm) display subophitic textures and poikilitically enclose plagioclase grains. Plagioclase is relatively fresh (~ 10% altered) but is cross-cut by thin fractures and veinlets containing brown clay, chlorite, and albite. One side of the section contains a 6-8mm vein containing recrystallized plagioclase, chlorite, pale green diopside, and minor epidote, sphene and opaque minerals. Alteration decreases markedly away from the vein and is characterized by a decrease in veinlets penetrating the host rock. Thin, (<1mm) late-stage carbonate veins cut the section.

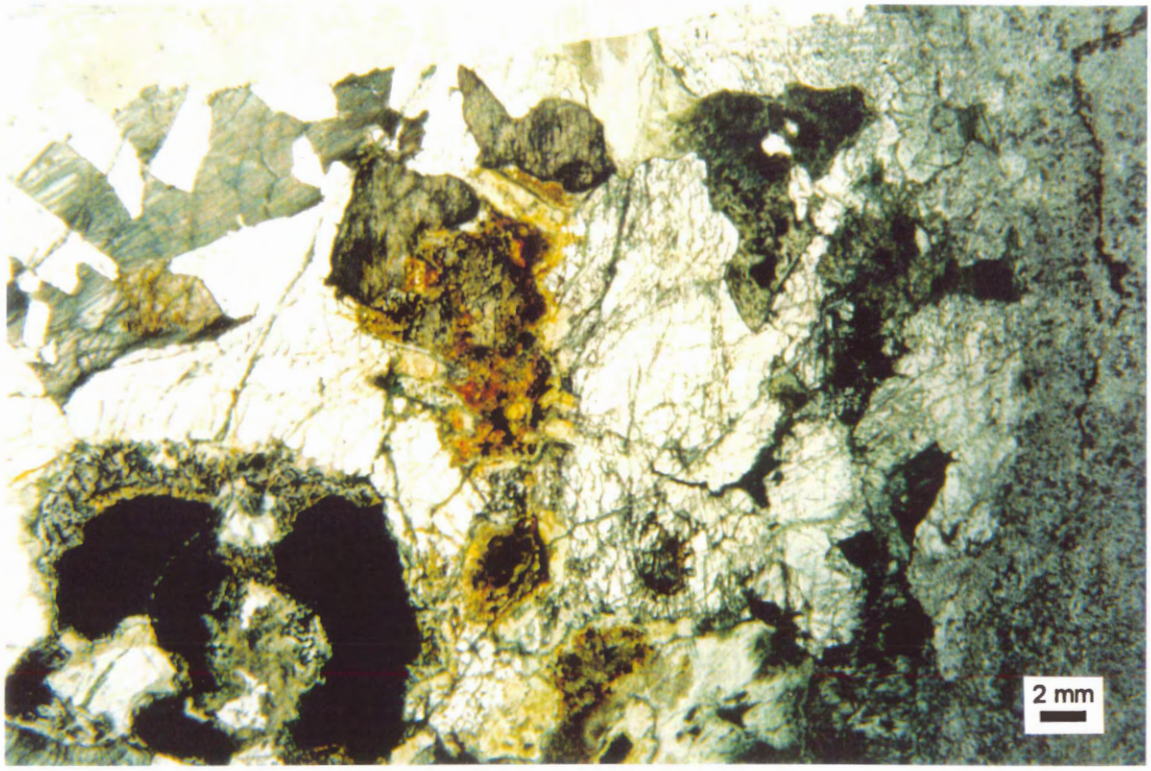

Sample: 68R-2 (68-75cm) (337.22 mbsf)

Rock Type: Olivine Gabbro

Unit: V

Very coarse- to coarse-grained olivine gabbro displaying anhedral to subhedral granular and cumulate textures. Olivine is completely pseudomorphed by brown clay and colourless amphibole. Clinopyroxene grains (>1cm) poikilitically enclose plagioclase laths. Plagioclase is relatively fresh (~ 10% altered) but some alteration to clay along fractures is evident. The section is cross-cut by numerous amphibole veinlets. One side of the section is a 1cm wide vein, containing brown clay, epidote, recrystallized plagioclase, chlorite, and minor diopside. Plagioclase has been recrystallized along the vein margin and altered to epidote.

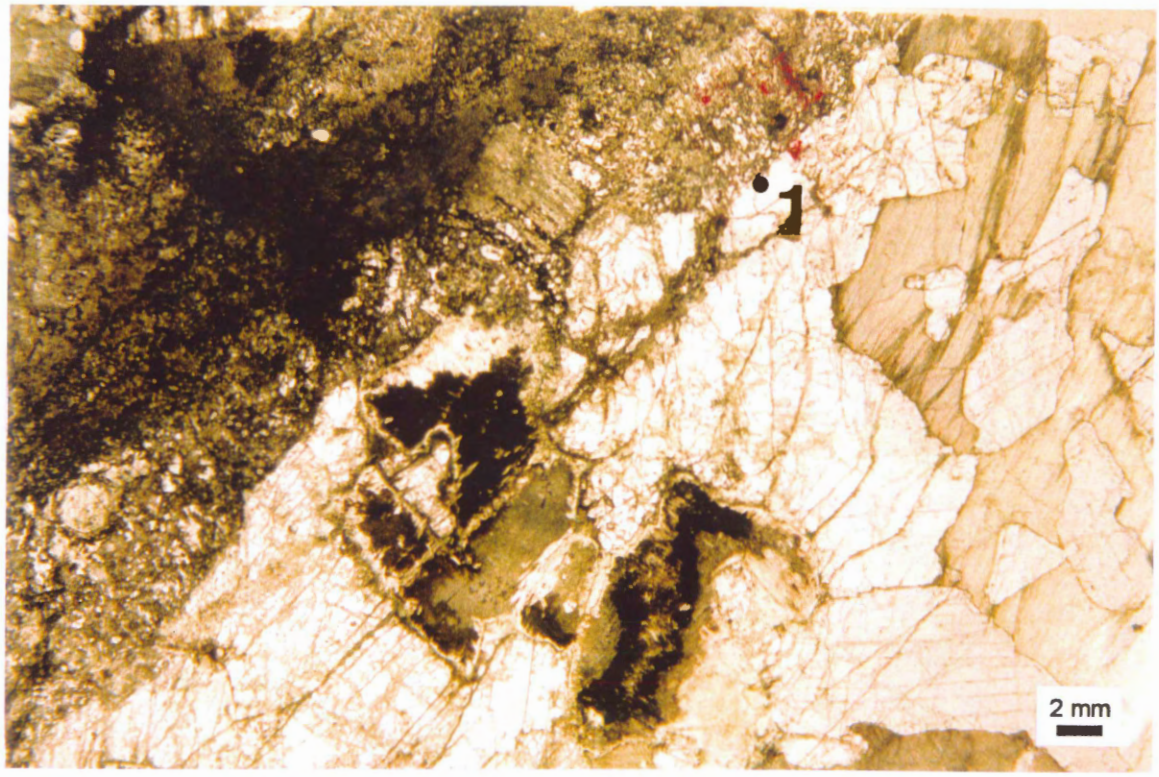

Sample: 72R-3 (10-19cm) (359.15 mbsf)

Rock Type: Olivine Gabbro

Unit: V

Coarse-grained olivine gabbro displaying subhedral granular and mesocumulate textures. Olivine is partially replaced by red-brown opaque oxide clots and is altered along fractures to secondary oxides and clay. Subhedral clinopyroxene grains (up to 5mm) display ophitic to subophitic textures and poikilitically enclose subhedral to euhedral plagioclase laths. Plagioclase is relatively fresh and displays only minor (~ 5-10%) alteration along tiny fractures and veinlets filled with yellow-brown clay. The section is cut by thin (<1mm), late-stage, subparallel carbonate-clay veins.

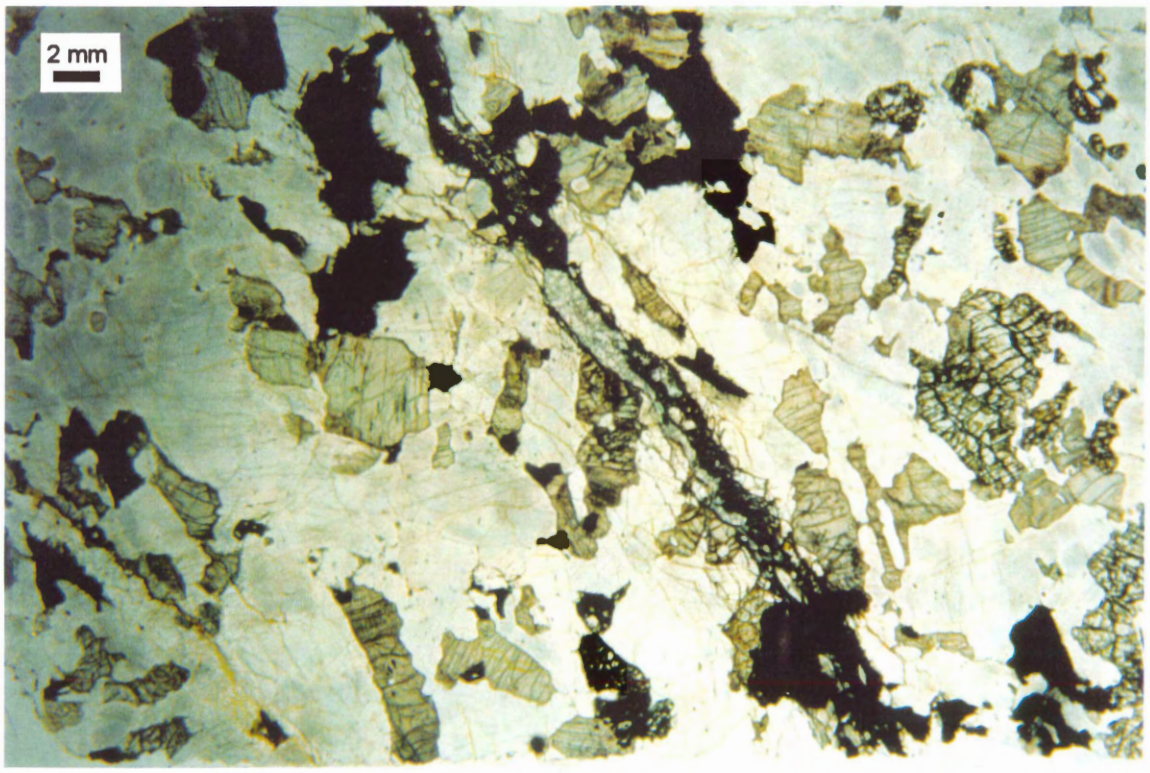

Appendix 3

Residual Program

Residuals were calculated using the following program written in Visual Basic®. Because two different lithologies (olivine gabbro and oxide olivine gabbro) were mapped, two copies of the same program with slight variations were necessary. The program code in this appendix was used to calculate olivine gabbro residuals. Therefore, primary compositions used in this version are for olivine gabbro. Values used to calculate oxide olivine gabbro residuals are indicated by bold italics in the program code. A few comments are found in the code to ease understanding, however, the program is discussed in detail in Chapter 5. Code and comments are set in different typefaces to ease recognition. Line separators are used to distinuish major subroutines. The program was run as a macro in Microsoft® Excel® 5.0. All code is in its original format.

RESIDUAL PROGRAM

```
Dim ColumnPos As Integer          Column Number
Dim xvalue As Variant             Cell X value
Dim yvalue As Variant             Cell Y value
Dim StartCell As Integer          Start cell number
Dim EndCell As Integer            End cell number
Dim PointNum As Variant           Number of Points in Raster
Dim RowNum As Variant             Number of Rows in Raster
Dim ColumnNum As Variant          Number of Columns in Raster
Dim counter As Integer
Dim amph As Integer               Amphibole counter
Dim cpx As Integer                CPX counter
Dim olivine As Integer            Olivine counter
Dim plag As Integer               Calcic Palgioclase counter
Dim NaPlag As Integer             Sodic Plagioclase counter
Dim quartz As Integer             Quartz counter
Dim mag As Integer                Magnetite counter
Dim ilm As Integer                Ilmenite counter
Dim NormRatio As Single           Normalization Ratio based on constant Al2O3
```

```
Sub ResidualMap()

  Sheets(1).Select
  Application.ScreenUpdating = False
  savestatusbar = Application.DisplayStatusBar
  Application.DisplayStatusBar = True
```

```
    MsgBox "Residual Map Program"

    PointNum = InputBox( _
       prompt:="Enter the number of POINTS.", _
       default:=1710)

    RowNum = InputBox( _
       prompt:="Enter the number of ROWS.", _
       default:=30)

    ColumnNum = InputBox( _
       prompt:="Enter the number of COLUMNS.", _
       default:=57)

       MinClass

       Raster

       FillFilter

       ColourGrid

       DataTrans

       ChemSub

       XYZData

    Application.ScreenUpdating = True
    Application.StatusBar = False
    Application.DisplayStatusBar = savestatusbar

End Sub
```

```
Sub MinClass()

    Sheets(1).Select
    StartCell = 2
    EndCell = PointNum + 1

    For I = StartCell To EndCell

       Application.StatusBar = "Classifying cell:   " & I

       If Sheets(1).Cells(I, 11).Value < 70 Then
            Sheets(1).Cells(I, 15).Value = "H"

       ElseIf Sheets(1).Cells(I, 2).Value > 70 Then
            Sheets(1).Cells(I, 15).Value = "Q"
```

```
    ElseIf Sheets(1).Cells(I, 5).Value > 70 Then
        Sheets(1).Cells(I, 15).Value = "M"

    ElseIf Sheets(1).Cells(I, 3).Value > 30 And Sheets(1).Cells(I, 2).Value < 10 _
      And Sheets(1).Cells(I, 5).Value > 20 Then
        Sheets(1).Cells(I, 15).Value = "I"

    ElseIf Sheets(1).Cells(I, 7).Value > 25 And Sheets(1).Cells(I, 4).Value < 1 Then
        Sheets(1).Cells(I, 15).Value = "O"

    ElseIf Sheets(1).Cells(I, 8).Value > 15 And Sheets(1).Cells(I, 4).Value < 5 Then
        Sheets(1).Cells(I, 15).Value = "X"

    ElseIf Sheets(1).Cells(I, 5).Value < 2 And Sheets(1).Cells(I, 9).Value < 5.5 _
      And Sheets(1).Cells(I, 8).Value > 10 Then
        Sheets(1).Cells(I, 15).Value = "L"

    ElseIf Sheets(1).Cells(I, 5).Value < 2 And Sheets(1).Cells(I, 9).Value > 5 _
      And Sheets(1).Cells(I, 8).Value < 10 Then
        Sheets(1).Cells(I, 15).Value = "N"

    ElseIf Sheets(1).Cells(I, 8).Value < 15 And Sheets(1).Cells(I, 5).Value > 5 _
      And Sheets(1).Cells(I, 7).Value > 3 Then
        Sheets(1).Cells(I, 15).Value = "A"

    Else Sheets(1).Cells(I, 15).Value = "-"

    End If

  Next I

End Sub
```

```
Sub Raster()

  Sheets(1).Select
  Sheets.Add
  Sheets(1).Name = "mingrid"

  ColumnPos = 15
  StartCell = 2
  EndCell = ColumnNum + 1
  Y = 1

    For DownRaster = 1 To RowNum

    Application.StatusBar = "Rastering row:  " & DownRaster & "  of:  " & RowNum

      X = 1
```

```
        For I = StartCell To EndCell
          CellValue = Sheets("Sheet1").Cells(I, ColumnPos)
          Sheets("mingrid").Cells(Y, X).Value = CellValue
          X = X + 1
        Next I

        StartCell = StartCell + ColumnNum
        EndCell = EndCell + ColumnNum
        Y = Y + 1

    Next DownRaster

End Sub
```

```
Sub FillFilter ()

  yvalue = 1
  counter = 1

  For DownRow = 1 To RowNum

    xvalue = 1

    For AcrossRow = 1 To ColumnNum

    Application.StatusBar = "Filling cell:   " & counter

      If Sheets(1).Cells(yvalue, xvalue).Value = "-" Then

          amph = 0
          cpx = 0
          olivine = 0
          plag = 0
          NaPlag = 0
          quartz = 0
          mag = 0
          ilm = 0

        If yvalue = 1 And xvalue = 1 Then
          UpperLeftCorner

        ElseIf yvalue = 1 And xvalue = ColumnNum Then
          UpperRightCorner

        ElseIf yvalue = RowNum And xvalue = 1 Then
          BottomLeftCorner

        ElseIf yvalue = RowNum And xvalue = ColumnNum Then
```

```
    BottomRightCorner

ElseIf yvalue = 1 Then
    TopRow

ElseIf yvalue = RowNum Then
    BottomRow

ElseIf xvalue = 1 Then
    LeftColumn

ElseIf xvalue = ColumnNum Then
    RightColumn
Else BoxFilter
End If

If plag >= amph And plag >= olivine And plag >= cpx _
    And plag >= NaPlag And plag >= quartz And plag >= mag _
    And plag >= ilm Then
        Sheets(1).Cells(yvalue, xvalue).Value = "L"

ElseIf NaPlag >= amph And NaPlag >= olivine And NaPlag >= cpx _
    And NaPlag >= plag And NaPlag >= quartz And NaPlag >= mag _
    And NaPlag >= ilm Then
        Sheets(1).Cells(yvalue, xvalue).Value = "N"

ElseIf cpx > amph And cpx >= olivine And cpx >= plag _
    And cpx >= NaPlag And cpx >= quartz And cpx >= mag _
    And cpx >= ilm Then
        Sheets(1).Cells(yvalue, xvalue).Value = "X"

ElseIf amph >= olivine And amph >= cpx And amph >= plag _
    And amph >= NaPlag And amph >= quartz And amph >= mag _
    And amph >= ilm Then
        Sheets(1).Cells(yvalue, xvalue).Value = "A"

ElseIf olivine >= amph And olivine >= cpx And olivine >= plag _
    And olivine >= NaPlag And olivine >= quartz And olivine >= mag _
    And olivine >= ilm Then
        Sheets(1).Cells(yvalue, xvalue).Value = "O"

ElseIf ilm >= amph And ilm >= cpx And ilm >= plag _
    And ilm >= NaPlag And ilm >= quartz And ilm >= mag _
    And ilm >= olivine Then
        Sheets(1).Cells(yvalue, xvalue).Value = "I"

ElseIf mag >= amph And mag >= cpx And mag >= plag _
    And mag >= NaPlag And mag >= quartz And mag >= ilm _
    And mag >= olivine Then
        Sheets(1).Cells(yvalue, xvalue).Value = "M"
```

```
        ElseIf quartz >= amph And quartz >= cpx And quartz >= plag _
          And quartz >= NaPlag And quartz >= ilm And quartz >= mag _
          And quartz >= olivine Then
            Sheets(1).Cells(yvalue, xvalue).Value = "Q"

        End If

      End If

    xvalue = xvalue + 1
    counter = counter + 1

    Next AcrossRow

    yvalue = yvalue + 1

  Next DownRow

End Sub

Sub UpperLeftCorner()
  cellx3y2
  cellx3y3
  cellx2y3
End Sub

Sub UpperRightCorner()
  cellx2y3
  cellx1y3
  cellx1y2
End Sub

Sub BottomLeftCorner()
  cellx2y1
  cellx3y1
  cellx3y2
End Sub

Sub BottomRightCorner()
  cellx1y2
  cellx1y1
  cellx2y1
End Sub

Sub TopRow()
  cellx1y2
  cellx1y3
  cellx2y3
  cellx3y3
  cellx3y2
End Sub
```

```
Sub BottomRow()
   cellx1y2
   cellx1y1
   cellx2y1
   cellx3y1
   cellx3y2
End Sub

Sub LeftColumn()
   cellx2y1
   cellx3y1
   cellx3y2
   cellx3y3
   cellx2y3
End Sub

Sub RightColumn()
   cellx2y1
   cellx1y1
   cellx1y2
   cellx1y3
   cellx2y3
End Sub

Sub BoxFilter()
   cellx1y1
   cellx2y1
   cellx3y1
   cellx3y2
   cellx3y3
   cellx2y3
   cellx1y3
   cellx1y2
End Sub

Sub cellx1y1()
   If Sheets(1).Cells(yvalue - 1, xvalue - 1).Value = "A" Then amph = amph + 1
   ElseIf Sheets(1).Cells(yvalue - 1, xvalue - 1).Value = "O" Then olivine = olivine + 1
   ElseIf Sheets(1).Cells(yvalue - 1, xvalue - 1).Value = "X" Then cpx = cpx + 1
   ElseIf Sheets(1).Cells(yvalue - 1, xvalue - 1).Value = "L" Then plag = plag + 1
   ElseIf Sheets(1).Cells(yvalue - 1, xvalue - 1).Value = "N" Then NaPlag = NaPlag + 1
   ElseIf Sheets(1).Cells(yvalue - 1, xvalue - 1).Value = "Q" Then quartz = quartz + 1
   ElseIf Sheets(1).Cells(yvalue - 1, xvalue - 1).Value = "M" Then mag = mag + 1
   ElseIf Sheets(1).Cells(yvalue - 1, xvalue - 1).Value = "I" Then ilm = ilm + 1
   End If
End Sub

Sub cellx2y1()
   If Sheets(1).Cells(yvalue - 1, xvalue).Value = "A" Then amph = amph + 1
   ElseIf Sheets(1).Cells(yvalue - 1, xvalue).Value = "O" Then olivine = olivine + 1
   ElseIf Sheets(1).Cells(yvalue - 1, xvalue).Value = "X" Then cpx = cpx + 1
```

```
    Elself Sheets(1).Cells(yvalue - 1, xvalue).Value = "L" Then plag = plag + 1
    Elself Sheets(1).Cells(yvalue - 1, xvalue).Value = "N" Then NaPlag = NaPlag + 1
    Elself Sheets(1).Cells(yvalue - 1, xvalue).Value = "Q" Then quartz = quartz + 1
    Elself Sheets(1).Cells(yvalue - 1, xvalue).Value = "M" Then mag = mag + 1
    Elself Sheets(1).Cells(yvalue - 1, xvalue).Value = "I" Then ilm = ilm + 1
    End If
End Sub

Sub cellx3y10
    If Sheets(1).Cells(yvalue - 1, xvalue + 1).Value = "A" Then amph = amph + 1
    Elself Sheets(1).Cells(yvalue - 1, xvalue + 1).Value = "O" Then olivine = olivine + 1
    Elself Sheets(1).Cells(yvalue - 1, xvalue + 1).Value = "X" Then cpx = cpx + 1
    Elself Sheets(1).Cells(yvalue - 1, xvalue + 1).Value = "L" Then plag = plag + 1
    Elself Sheets(1).Cells(yvalue - 1, xvalue + 1).Value = "N" Then NaPlag = NaPlag + 1
    Elself Sheets(1).Cells(yvalue - 1, xvalue + 1).Value = "Q" Then quartz = quartz + 1
    Elself Sheets(1).Cells(yvalue - 1, xvalue + 1).Value = "M" Then mag = mag + 1
    Elself Sheets(1).Cells(yvalue - 1, xvalue + 1).Value = "I" Then ilm = ilm + 1
    End If
End Sub

Sub cellx3y20
    If Sheets(1).Cells(yvalue, xvalue + 1).Value = "A" Then amph = amph + 1
    Elself Sheets(1).Cells(yvalue, xvalue + 1).Value = "O" Then olivine = olivine + 1
    Elself Sheets(1).Cells(yvalue, xvalue + 1).Value = "X" Then cpx = cpx + 1
    Elself Sheets(1).Cells(yvalue, xvalue + 1).Value = "L" Then plag = plag + 1
    Elself Sheets(1).Cells(yvalue, xvalue + 1).Value = "N" Then NaPlag = NaPlag + 1
    Elself Sheets(1).Cells(yvalue, xvalue + 1).Value = "Q" Then quartz = quartz + 1
    Elself Sheets(1).Cells(yvalue, xvalue + 1).Value = "M" Then mag = mag + 1
    Elself Sheets(1).Cells(yvalue, xvalue + 1).Value = "I" Then ilm = ilm + 1
    End If
End Sub

Sub cellx3y30
    If Sheets(1).Cells(yvalue + 1, xvalue + 1).Value = "A" Then amph = amph + 1
    Elself Sheets(1).Cells(yvalue + 1, xvalue + 1).Value = "O" Then olivine = olivine + 1
    Elself Sheets(1).Cells(yvalue + 1, xvalue + 1).Value = "X" Then cpx = cpx + 1
    Elself Sheets(1).Cells(yvalue + 1, xvalue + 1).Value = "L" Then plag = plag + 1
    Elself Sheets(1).Cells(yvalue + 1, xvalue + 1).Value = "N" Then NaPlag = NaPlag + 1
    Elself Sheets(1).Cells(yvalue + 1, xvalue + 1).Value = "Q" Then quartz = quartz + 1
    Elself Sheets(1).Cells(yvalue + 1, xvalue + 1).Value = "M" Then mag = mag + 1
    Elself Sheets(1).Cells(yvalue + 1, xvalue + 1).Value = "I" Then ilm = ilm + 1
    End If
End Sub

Sub cellx2y30
    If Sheets(1).Cells(yvalue + 1, xvalue).Value = "A" Then amph = amph + 1
    Elself Sheets(1).Cells(yvalue + 1, xvalue).Value = "O" Then olivine = olivine + 1
    Elself Sheets(1).Cells(yvalue + 1, xvalue).Value = "X" Then cpx = cpx + 1
    Elself Sheets(1).Cells(yvalue + 1, xvalue).Value = "L" Then plag = plag + 1
    Elself Sheets(1).Cells(yvalue + 1, xvalue).Value = "N" Then NaPlag = NaPlag + 1
    Elself Sheets(1).Cells(yvalue + 1, xvalue).Value = "Q" Then quartz = quartz + 1
```

```
   ElseIf Sheets(1).Cells(yvalue + 1, xvalue).Value = "M" Then mag = mag + 1
   ElseIf Sheets(1).Cells(yvalue + 1, xvalue).Value = "I" Then ilm = ilm + 1
   End If
End Sub

Sub cellx1y30
   If Sheets(1).Cells(yvalue + 1, xvalue - 1).Value = "A" Then amph = amph + 1
   ElseIf Sheets(1).Cells(yvalue + 1, xvalue - 1).Value = "O" Then olivine = olivine + 1
   ElseIf Sheets(1).Cells(yvalue + 1, xvalue - 1).Value = "X" Then cpx = cpx + 1
   ElseIf Sheets(1).Cells(yvalue + 1, xvalue - 1).Value = "L" Then plag = plag + 1
   ElseIf Sheets(1).Cells(yvalue + 1, xvalue - 1).Value = "N" Then NaPlag = NaPlag + 1
   ElseIf Sheets(1).Cells(yvalue + 1, xvalue - 1).Value = "Q" Then quartz = quartz + 1
   ElseIf Sheets(1).Cells(yvalue + 1, xvalue - 1).Value = "M" Then mag = mag + 1
   ElseIf Sheets(1).Cells(yvalue + 1, xvalue - 1).Value = "I" Then ilm = ilm + 1
   End If
End Sub

Sub cellx1y20
   If Sheets(1).Cells(yvalue, xvalue - 1).Value = "A" Then amph = amph + 1
   ElseIf Sheets(1).Cells(yvalue, xvalue - 1).Value = "O" Then olivine = olivine + 1
   ElseIf Sheets(1).Cells(yvalue, xvalue - 1).Value = "X" Then cpx = cpx + 1
   ElseIf Sheets(1).Cells(yvalue, xvalue - 1).Value = "L" Then plag = plag + 1
   ElseIf Sheets(1).Cells(yvalue, xvalue - 1).Value = "N" Then NaPlag = NaPlag + 1
   ElseIf Sheets(1).Cells(yvalue, xvalue - 1).Value = "Q" Then quartz = quartz + 1
   ElseIf Sheets(1).Cells(yvalue, xvalue - 1).Value = "M" Then mag = mag + 1
   ElseIf Sheets(1).Cells(yvalue, xvalue - 1).Value = "I" Then ilm = ilm + 1
   End If
End Sub
```

```
Sub ColourGrid()

   yvalue = 1
   counter = 1

   For DownRow = 1 To RowNum

      xvalue = 1

      For AcrossRow = 1 To ColumnNum

      Application.StatusBar = "Colouring cell:   " & counter & _
                  "  of:  " & PointNum

        If Sheets("mingrid").Cells(yvalue, xvalue).Value = "A" Then
            Cells(yvalue, xvalue).Select
            With Selection.Interior
               .ColorIndex = 51
               .Pattern = xlSolid
            End With
```

```
ElseIf Sheets("mingrid").Cells(yvalue, xvalue).Value = "X" Then
    Cells(yvalue, xvalue).Select
    With Selection.Interior
       .ColorIndex = 45
    .Pattern = xlSolid
    End With

ElseIf Sheets("mingrid").Cells(yvalue, xvalue).Value = "O" Then
    Cells(yvalue, xvalue).Select
    With Selection.Interior
       .ColorIndex = 44
       .Pattern = xlSolid
    End With

ElseIf Sheets("mingrid").Cells(yvalue, xvalue).Value = "L" Then
    Cells(yvalue, xvalue).Select
    With Selection.Interior
       .ColorIndex = 41
       .Pattern = xlSolid
    End With

ElseIf Sheets("mingrid").Cells(yvalue, xvalue).Value = "N" Then
    Cells(yvalue, xvalue).Select
    With Selection.Interior
       .ColorIndex = 34
       .Pattern = xlSolid
    End With

ElseIf Sheets("mingrid").Cells(yvalue, xvalue).Value = "I" Then
    Cells(yvalue, xvalue).Select
    With Selection.Interior
       .ColorIndex = 15
       .Pattern = xlSolid
    End With

ElseIf Sheets("mingrid").Cells(yvalue, xvalue).Value = "M" Then
    Cells(yvalue, xvalue).Select
    With Selection.Interior
       .ColorIndex = 16
       .Pattern = xlSolid
    End With

ElseIf Sheets("mingrid").Cells(yvalue, xvalue).Value = "H" Then
    Cells(yvalue, xvalue).Select
    With Selection.Interior
       .ColorIndex = 1
       .Pattern = xlSolid
    End With

End If
```

```
    xvalue = xvalue + 1
    counter = counter + 1

    Next AcrossRow

    yvalue = yvalue + 1

  Next DownRow

End Sub
```

```
Sub DataTrans()

  yvalue = 1
  counter = 1

  For DownRow = 1 To RowNum

  xvalue = 1

    For AcrossRow = 1 To ColumnNum

    Application.StatusBar = "Transfering cell:   " & counter

    temp = Sheets("mingrid").Cells(yvalue, xvalue)
    Sheets("Sheet1").Cells(counter + 1, 16).Value = temp

    xvalue = xvalue + 1
    counter = counter + 1

    Next AcrossRow

    yvalue = yvalue + 1

  Next DownRow

End Sub
```

```
Sub ChemSub()
```

Note: Primary values used in this subroutine are for olivine gabbro.
Values for oxide olivine gabbro samples appear in ***[brackets]*** when different.

```
  Sheets(1).Select
  Sheets.Add
  Sheets(1).Name = "residuals"
```

```
StartCell = 2
EndCell = PointNum + 1
counter = 1

For I = StartCell To EndCell

  Application.StatusBar = "Calculating residual for cell:  " & counter
```

Note: A value of 0.01 has been substituted for Al_2O_3 in cases where the value is negative to avoid division by zero while normalizing the data.

```
  If Sheets(3).Cells(I, 2).Value < 0 Then Sheets(3).Cells(I, 2) = 0
  If Sheets(3).Cells(I, 3).Value < 0 Then Sheets(3).Cells(I, 3) = 0
  If Sheets(3).Cells(I, 4).Value < 0 Then Sheets(3).Cells(I, 4) = 0.01
  If Sheets(3).Cells(I, 5).Value < 0 Then Sheets(3).Cells(I, 5) = 0
  If Sheets(3).Cells(I, 6).Value < 0 Then Sheets(3).Cells(I, 6) = 0
  If Sheets(3).Cells(I, 7).Value < 0 Then Sheets(3).Cells(I, 7) = 0
  If Sheets(3).Cells(I, 8).Value < 0 Then Sheets(3).Cells(I, 8) = 0
  If Sheets(3).Cells(I, 9).Value < 0 Then Sheets(3).Cells(I, 9) = 0
  If Sheets(3).Cells(I, 10).Value < 0 Then Sheets(3).Cells(I, 10) = 0

  If Sheets(3).Cells(I, 16).Value = "X" _
  Or Sheets(3).Cells(I, 16).Value = "A" Then

    NormRatio = 2.79 / Sheets(3).Cells(I, 4).Value
    (NormRatio = 1.97 / Sheets(3).Cells(I, 4).Value)

    If NormRatio > 2 Then NormRatio = 1.99
```

Note: If the calculated value of the NormRatio is greater than 2 it is reset to a value of 1.99. This is necessary to ensure that overly high residuals are not calculated which would otherwise skew the data.

```
    Sheets(1).Cells(I, 12).Value = NormRatio
    Sheets(1).Cells(I, 13).Value = Sheets(3).Cells(I, 16).Value

    Sheets(1).Cells(I, 1).Value = counter
    Sheets(1).Cells(I, 2).Value = (Sheets(3).Cells(I, 2).Value * NormRatio) - 51.41    (50.72)
    Sheets(1).Cells(I, 3).Value = (Sheets(3).Cells(I, 3).Value * NormRatio) - 0.5      (0.57)
    Sheets(1).Cells(I, 4).Value = (Sheets(3).Cells(I, 4).Value * NormRatio) - 2.79     (1.97)
    Sheets(1).Cells(I, 5).Value = (Sheets(3).Cells(I, 5).Value * NormRatio) - 7.29     (13.25)
    Sheets(1).Cells(I, 6).Value = (Sheets(3).Cells(I, 6).Value * NormRatio) - 0.3      (0.59)
    Sheets(1).Cells(I, 7).Value = (Sheets(3).Cells(I, 7).Value * NormRatio) - 16.72    (13.12)
    Sheets(1).Cells(I, 8).Value = (Sheets(3).Cells(I, 8).Value * NormRatio) - 20.4     (19.32)
    Sheets(1).Cells(I, 9).Value = (Sheets(3).Cells(I, 9).Value * NormRatio) - 0.4      (0.36)
    Sheets(1).Cells(I, 10).Value = (Sheets(3).Cells(I, 10).Value * NormRatio) - 0

  ElseIf Sheets(3).Cells(I, 16).Value = "L" _
  Or Sheets(3).Cells(I, 16).Value = "N" Then

    NormRatio = 30.04 / Sheets(3).Cells(I, 4).Value
```

(NormRatio = 26.06 / Sheets(3).Cells(I, 4).Value)

If NormRatio > 2 Then NormRatio = 1.99

Note: If the calculated value of the NormRatio is greater than 2 it is reset to a value of 1.99. This is necessary to ensure that overly high residuals are not calculated which would otherwise skew the data.

```
Sheets(1).Cells(I, 12).Value = NormRatio
Sheets(1).Cells(I, 13).Value = Sheets(3).Cells(I, 16).Value

Sheets(1).Cells(I, 1).Value = counter
Sheets(1).Cells(I, 2).Value = (Sheets(3).Cells(I, 2).Value * NormRatio) - 52.47    (59.04)
Sheets(1).Cells(I, 3).Value = (Sheets(3).Cells(I, 3).Value * NormRatio) - 0
Sheets(1).Cells(I, 4).Value = (Sheets(3).Cells(I, 4).Value * NormRatio) - 30.04    (26.06)
Sheets(1).Cells(I, 5).Value = (Sheets(3).Cells(I, 5).Value * NormRatio) - 0.22     (0.19)
Sheets(1).Cells(I, 6).Value = (Sheets(3).Cells(I, 6).Value * NormRatio) - 0
Sheets(1).Cells(I, 7).Value = (Sheets(3).Cells(I, 7).Value * NormRatio) - 0.09     (0.03)
Sheets(1).Cells(I, 8).Value = (Sheets(3).Cells(I, 8).Value * NormRatio) - 12.82    (7.6)
Sheets(1).Cells(I, 9).Value = (Sheets(3).Cells(I, 9).Value * NormRatio) - 4.42     (7.36)
Sheets(1).Cells(I, 10).Value = (Sheets(3).Cells(I, 10).Value * NormRatio) - 0.08   (0.12)

Elself Sheets(3).Cells(I, 16).Value = "O" Then

NormRatio = 1
```

Note: For points identified as olivine the normalization ratio is set to 1. This is necessary because of the very low values of Al_2O_3 in olivine.

```
Sheets(1).Cells(I, 12).Value = NormRatio
Sheets(1).Cells(I, 13).Value = Sheets(3).Cells(I, 16).Value

Sheets(1).Cells(I, 1).Value = counter
Sheets(1).Cells(I, 2).Value = (Sheets(3).Cells(I, 2).Value * NormRatio) - 38.14    (34.21)
Sheets(1).Cells(I, 3).Value = (Sheets(3).Cells(I, 3).Value * NormRatio) - 0
Sheets(1).Cells(I, 4).Value = (Sheets(3).Cells(I, 4).Value * NormRatio) - 0.01
Sheets(1).Cells(I, 5).Value = (Sheets(3).Cells(I, 5).Value * NormRatio) - 21.62    (43.21)
Sheets(1).Cells(I, 6).Value = (Sheets(3).Cells(I, 6).Value * NormRatio) - 0.45     (0.9)
Sheets(1).Cells(I, 7).Value = (Sheets(3).Cells(I, 7).Value * NormRatio) - 39.78    (21.64)
Sheets(1).Cells(I, 8).Value = (Sheets(3).Cells(I, 8).Value * NormRatio) - 0.05     (0.06)
Sheets(1).Cells(I, 9).Value = (Sheets(3).Cells(I, 9).Value * NormRatio) - 0
Sheets(1).Cells(I, 10).Value = (Sheets(3).Cells(I, 10).Value * NormRatio) - 0

Elself Sheets(3).Cells(I, 16).Value = "I" Then

NormRatio = 1
```

Note: For points identified as ilmenite the normalization ratio is set to 1. This is necessary because of the very low values of Al_2O_3 in ilmenite.

```
Sheets(1).Cells(I, 12).Value = NormRatio
```

```
Sheets(1).Cells(I, 13).Value = Sheets(3).Cells(I, 16).Value
```

Note: Primary values for ilmenite were not available for olivine gabbro samples. As a result, residual values could not be calculated. A value of zero has been substituted which represents background. Residual values for oxide olivine gabbro samples were calculated in the same manner as other minerals.

```
Sheets(1).Cells(I, 1).Value = counter
Sheets(1).Cells(I, 2).Value = 0   ((Sheets(3).Cells(I, 2).Value * NormRatio) - 0)
Sheets(1).Cells(I, 3).Value = 0   ((Sheets(3).Cells(I, 3).Value * NormRatio) - 50.16)
Sheets(1).Cells(I, 4).Value = 0   ((Sheets(3).Cells(I, 4).Value * NormRatio) - 0.01)
Sheets(1).Cells(I, 5).Value = 0   ((Sheets(3).Cells(I, 5).Value * NormRatio) - 47.28)
Sheets(1).Cells(I, 6).Value = 0   ((Sheets(3).Cells(I, 6).Value * NormRatio) - 1.04)
Sheets(1).Cells(I, 7).Value = 0   ((Sheets(3).Cells(I, 7).Value * NormRatio) - 0.83)
Sheets(1).Cells(I, 8).Value = 0   ((Sheets(3).Cells(I, 8).Value * NormRatio) - 0)
Sheets(1).Cells(I, 9).Value = 0   ((Sheets(3).Cells(I, 9).Value * NormRatio) - 0)
Sheets(1).Cells(I, 10).Value = 0  ((Sheets(3).Cells(I, 10).Value * NormRatio) - 0)
```

```
Elself Sheets(3).Cells(I, 16).Value = "M" Then

  NormRatio = 1
```

Note: For points identified as magnetite the normalization ratio is set to 1. This is necessary because of the variable values of Al_2O_3 in magnetite.

```
Sheets(1).Cells(I, 12).Value = NormRatio
Sheets(1).Cells(I, 13).Value = Sheets(3).Cells(I, 16).Value
```

Note: Primary values for magnetite were not available for olivine gabbro samples. As a result, residual values could not be calculated. A value of zero has been substituted which represents background. Residual values for oxide olivine gabbro samples were calculated in the same manner as other minerals.

```
Sheets(1).Cells(I, 1).Value = counter
Sheets(1).Cells(I, 2).Value = 0   ((Sheets(3).Cells(I, 2).Value * NormRatio) - 0)
Sheets(1).Cells(I, 3).Value = 0   ((Sheets(3).Cells(I, 3).Value * NormRatio) - 5.25)
Sheets(1).Cells(I, 4).Value = 0   ((Sheets(3).Cells(I, 4).Value * NormRatio) - 2.61)
Sheets(1).Cells(I, 5).Value = 0   ((Sheets(3).Cells(I, 5).Value * NormRatio) - 84.63)
Sheets(1).Cells(I, 6).Value = 0   ((Sheets(3).Cells(I, 6).Value * NormRatio) - 0.34)
Sheets(1).Cells(I, 7).Value = 0   ((Sheets(3).Cells(I, 7).Value * NormRatio) - 0.19)
Sheets(1).Cells(I, 8).Value = 0   ((Sheets(3).Cells(I, 8).Value * NormRatio) - 0)
Sheets(1).Cells(I, 9).Value = 0   ((Sheets(3).Cells(I, 9).Value * NormRatio) - 0)
Sheets(1).Cells(I, 10).Value = 0  ((Sheets(3).Cells(I, 10).Value * NormRatio) - 0)
```

```
Elself Sheets(3).Cells(I, 16).Value = "Q" Then

  NormRatio = 1
```

Note: For points identified as quartz the normalization ratio is set to 1.

This is necessary because of the very low values of Al_2O_3 in quartz.

```
        Sheets(1).Cells(I, 12).Value = NormRatio
        Sheets(1).Cells(I, 13).Value = Sheets(3).Cells(I, 16).Value

        Sheets(1).Cells(I, 1).Value = counter
        Sheets(1).Cells(I, 2).Value = (Sheets(3).Cells(I, 2).Value * NormRatio) - 98
        Sheets(1).Cells(I, 3).Value = (Sheets(3).Cells(I, 3).Value * NormRatio) - 0
        Sheets(1).Cells(I, 4).Value = (Sheets(3).Cells(I, 4).Value * NormRatio) - 0.01
        Sheets(1).Cells(I, 5).Value = (Sheets(3).Cells(I, 5).Value * NormRatio) - 0
        Sheets(1).Cells(I, 6).Value = (Sheets(3).Cells(I, 6).Value * NormRatio) - 0
        Sheets(1).Cells(I, 7).Value = (Sheets(3).Cells(I, 7).Value * NormRatio) - 0
        Sheets(1).Cells(I, 8).Value = (Sheets(3).Cells(I, 8).Value * NormRatio) - 0
        Sheets(1).Cells(I, 9).Value = (Sheets(3).Cells(I, 9).Value * NormRatio) - 0
        Sheets(1).Cells(I, 10).Value = (Sheets(3).Cells(I, 10).Value * NormRatio) - 0

      ElseIf Sheets(3).Cells(I, 16).Value = "H" Then

        Sheets(1).Cells(I, 1) = counter
        Sheets(1).Cells(I, 2) = 0
        Sheets(1).Cells(I, 3) = 0
        Sheets(1).Cells(I, 4) = 0
        Sheets(1).Cells(I, 5) = 0
        Sheets(1).Cells(I, 6) = 0
        Sheets(1).Cells(I, 7) = 0
        Sheets(1).Cells(I, 8) = 0
        Sheets(1).Cells(I, 9) = 0
        Sheets(1).Cells(I, 10) = 0

      End If

    counter = counter + 1

    Next I

    Sheets(3).Select
    Range("A1:J1").Select
    Selection.copy
    Sheets("residuals").Select
    Range("A1").Select
    ActiveSheet.Paste
    Application.CutCopyMode = False

End Sub

---

Sub XYZData0

Sheets("residuals").Select
```

```
Columns("A:A").Select
Selection.Insert Shift:=xlToRight
Selection.Insert Shift:=xlToRight
Range("A1").Select
ActiveCell.FormulaR1C1 = "X Data"
Range("B1").Select
ActiveCell.FormulaR1C1 = "Y Data"

StartCell = 1
EndCell = ColumnNum
Y = 2
XData = 0
YData = (RowNum / 2) - 0.5
counter = 1

  For Row = 1 To RowNum

    Application.StatusBar = "Point:  " & counter & "  of:  " & PointNum

      For I = 1 To ColumnNum
        Sheets("residuals").Cells(Y, 1).Value = XData
        Sheets("residuals").Cells(Y, 2).Value = YData
        Y = Y + 1
        XData = XData + 0.5
        counter = counter + 1
      Next I

    XData = 0
    YData = YData - 0.5

  Next Row

End Sub
```

Appendix 4
Microprobe Traverse Data

Analysis	SiO2	TiO2	Al2O3	FeO	MnO	MgO	CaO	Na2O	K2O	Cr2O3	Cl	Total
35R-4 117-124 S2 P1	51.95	0.36	3.30	5.32	0.19	17.22	20.87	0.39	0.00	0.24	0.00	99.85
35R-4 117-124 S2 P2	52.75	0.45	3.01	5.35	0.16	16.38	21.80	0.48	0.00	0.12	0.02	100.51
35R-4 117-124 S2 P3	53.39	0.78	2.58	10.82	0.29	17.62	11.01	1.16	0.13	0.23	0.05	98.05
35R-4 117-124 S2 P4	52.17	0.44	4.15	11.70	0.11	17.31	11.03	1.37	0.06	0.20	0.15	98.70
35R-4 117-124 S2 P5	50.91	0.73	4.79	11.81	0.24	16.56	11.14	1.52	0.14	0.08	0.16	98.08
35R-4 117-124 S2 P6	50.53	0.29	5.81	11.09	0.24	16.75	11.10	1.90	0.08	0.01	0.19	97.99
44R-1 35-47 S1 P1	52.36	0.65	3.24	4.64	0.20	16.35	22.28	0.56	0.04	0.39	0.00	100.71
44R-1 35-47 S1 P2	53.25	0.81	2.59	4.13	0.08	16.70	22.74	0.40	0.01	0.39	0.04	101.14
44R-1 35-47 S1 P3	56.35	0.19	2.24	3.73	0.09	22.91	12.96	0.83	0.00	0.02	0.00	99.33
44R-1 35-47 S1 P4	50.90	0.03	4.28	13.35	0.00	16.04	10.86	0.66	0.03	0.02	0.01	96.18
44R-1 35-47 S1 P5	59.06	0.00	0.08	2.67	0.06	24.30	12.16	0.23	0.04	0.10	0.00	98.69
44R-1 35-47 S1 P6	56.34	0.05	0.59	9.38	0.04	18.82	12.66	0.22	0.02	0.07	0.02	98.22
44R-1 35-47 S2 P1	47.95	1.81	6.14	14.54	0.18	13.62	10.66	2.05	0.27	0.28	0.00	97.50
44R-1 35-47 S2 P2	49.72	1.18	4.82	16.33	0.15	13.67	10.44	1.68	0.19	0.22	0.05	98.44
44R-1 35-47 S2 P3	41.69	0.12	0.34	5.45	0.09	8.98	23.03	0.19	0.00	0.21	0.01	80.11
44R-1 35-47 S2 P4	51.71	0.63	4.39	5.24	0.23	16.32	20.82	0.98	0.06	0.54	0.00	100.92
44R-1 35-47 S2 P5	52.34	0.51	3.28	4.64	0.10	16.31	21.98	0.52	0.00	0.34	0.02	100.04
44R-1 35-47 S3 P1	53.25	0.55	3.06	4.52	0.17	16.62	22.09	0.54	0.03	0.23	0.04	101.10
44R-1 35-47 S3 P2	54.69	0.19	0.23	7.02	0.27	15.36	23.35	0.44	0.00	0.12	0.00	101.68
44R-1 35-47 S3 P3	54.94	0.34	1.49	12.53	0.17	16.81	11.27	0.81	0.07	0.17	0.05	98.65
44R-1 35-47 S3 P4	49.17	0.50	5.70	18.52	0.15	11.20	11.95	1.42	0.01	0.11	0.01	98.74
44R-1 35-47 S3 P5	44.07	0.32	7.62	15.61	0.14	9.92	10.47	1.42	0.04	0.07	0.03	89.71
58R-3 0-8 S1 P1	54.06	0.20	1.49	6.25	0.13	14.41	24.28	0.47	0.00	0.20	0.01	101.50
58R-3 0-8 S1 P2	52.17	1.03	5.03	8.44	0.19	18.77	11.84	1.55	0.16	0.16	0.00	99.35
58R-3 0-8 S1 P3	52.93	0.38	3.12	11.16	0.21	17.15	12.14	0.87	0.08	0.28	0.04	98.36
58R-3 0-8 S1 P4	51.60	0.59	4.41	12.79	0.11	16.76	10.40	1.67	0.04	0.23	0.06	98.65
58R-3 0-8 S1 P5	52.08	0.17	4.49	13.88	0.09	14.38	12.38	0.63	0.06	0.08	0.00	98.24
58R-3 0-8 S1 P6	54.99	0.10	2.76	9.40	0.10	18.08	12.61	0.43	0.00	0.00	0.00	98.47
58R-3 0-8 S2 P1	53.85	0.07	1.28	8.11	0.17	14.20	23.01	0.76	0.02	0.16	0.00	101.63
58R-3 0-8 S2 P2	50.20	0.17	5.21	17.56	0.19	12.16	12.10	0.96	0.05	0.34	0.00	98.94
58R-3 0-8 S2 P3	51.27	0.15	4.31	17.55	0.17	12.29	12.14	0.87	0.02	0.09	0.02	98.88
58R-3 0-8 S2 P4	50.08	0.05	5.77	16.96	0.02	12.47	12.35	1.00	0.03	0.07	0.00	98.80
58R-3 0-8 S2 P5	53.13	0.17	3.81	9.69	0.01	17.94	12.36	1.00	0.00	0.00	0.01	98.12
58R-3 0-8 S2 P6	55.27	0.26	1.52	11.31	0.15	17.81	11.75	0.60	0.00	0.07	0.00	98.74
58R-3 0-8 S2 P7	50.77	0.16	4.15	15.07	0.28	13.37	11.04	0.67	0.02	0.07	0.00	95.61

Sample numbers follow the sample numbering system used by the ocean drilling program. S = spot; P = point.

Appendix 4 (continued)

Analysis	SiO2	TiO2	Al2O3	FeO	MnO	MgO	CaO	Na2O	K2O	Cr2O3	Cl	Total
60R-4 112-120 S1 P1	50.42	0.59	3.89	6.24	0.11	17.82	19.67	0.50	0.00	0.26	0.04	99.53
60R-4 112-120 S1 P2	49.48	1.19	6.52	9.70	0.19	16.51	13.28	1.83	0.24	0.26	0.05	99.25
60R-4 112-120 S1 P3	48.52	1.48	5.92	13.54	0.32	15.31	10.49	2.10	0.18	0.08	0.01	97.94
60R-4 112-120 S1 P4	52.95	0.36	2.64	12.37	0.19	17.13	11.20	1.02	0.07	0.02	0.08	98.03
60R-4 112-120 S1 P5	49.00	0.23	6.60	15.77	0.19	13.02	12.06	1.26	0.06	0.06	0.03	98.28
60R-4 112-120 S2 P1	53.12	0.69	3.21	4.92	0.09	16.24	21.79	0.58	0.00	0.22	0.00	100.86
60R-4 112-120 S2 P2	52.15	0.57	3.78	5.52	0.08	18.15	19.72	0.63	0.00	0.24	0.00	100.85
60R-4 112-120 S2 P3	53.03	0.39	2.35	9.16	0.33	15.26	18.98	1.01	0.04	0.12	0.00	100.66
60R-4 112-120 S2 P4	48.51	1.65	6.33	13.08	0.45	15.43	10.52	2.12	0.16	0.00	0.00	98.25
60R-4 112-120 S2 P5	48.34	1.52	6.10	13.53	0.26	15.23	10.33	2.09	0.23	0.07	0.00	97.71
60R-4 112-120 S3 P1	51.36	0.67	4.04	5.34	0.11	16.78	20.53	0.65	0.00	0.30	0.01	99.77
60R-4 112-120 S3 P2	52.02	0.90	4.12	5.92	0.08	16.08	21.49	0.75	0.00	0.25	0.00	101.60
60R-4 112-120 S3 P3	51.51	0.61	3.64	12.81	0.27	16.47	11.00	1.36	0.25	0.21	0.08	98.21
60R-4 112-120 S3 P4	51.46	0.85	3.72	12.98	0.46	16.49	10.90	1.40	0.12	0.06	0.01	98.45
60R-4 112-120 S3 P5	51.96	0.44	3.43	16.16	0.00	13.38	11.69	0.66	0.01	0.03	0.00	97.77
60R-4 112-120 S5 P1	49.84	3.30	2.63	8.58	0.40	15.59	18.94	0.73	0.00	0.25	0.03	100.28
60R-4 112-120 S5 P2	51.97	1.12	3.00	6.72	0.12	15.40	21.07	0.88	0.00	0.26	0.01	100.57
60R-4 112-120 S5 P3	44.71	0.09	4.52	10.33	0.21	14.71	9.23	0.46	0.07	0.09	0.04	84.45
60R-4 112-120 S5 P4	55.72	0.18	2.18	6.71	0.06	20.54	12.86	0.60	0.01	0.13	0.03	99.01
60R-4 112-120 S5 P5	54.55	0.07	2.71	10.63	0.00	17.45	12.89	0.35	0.00	0.00	0.02	98.68
32R-2 86-95 S1 P1	51.20	0.02	31.82	0.01	0.02	0.06	14.14	3.67	0.03	0.09	0.02	101.09
32R-2 86-95 S1 P2	63.34	0.00	23.74	0.07	0.14	0.00	4.65	8.44	0.03	0.00	0.01	100.42
32R-2 86-95 S1 P3	62.84	0.00	24.11	0.04	0.09	0.00	5.23	8.07	0.02	0.04	0.00	100.43
32R-2 86-95 S1 P4	62.14	0.02	24.82	0.13	0.00	0.07	5.71	7.73	0.03	0.00	0.00	100.65
68R-2 68-75 S1 P1	54.39	0.18	29.67	0.23	0.01	0.01	11.81	4.91	0.06	0.05	0.01	101.33
68R-2 68-75 S1 P2	54.03	0.00	29.81	0.19	0.00	0.04	11.88	4.69	0.05	0.03	0.01	100.76
68R-2 68-75 S1 P3	41.19	0.19	28.25	5.21	0.16	0.07	21.83	0.94	0.08	0.05	0.00	97.99
68R-2 68-75 S1 P4	39.06	0.19	29.66	5.53	0.25	0.11	23.32	0.08	0.00	0.00	0.02	98.22
68R-2 68-75 S1 P5	39.32	0.00	29.01	5.96	0.00	0.12	23.42	0.08	0.00	0.00	0.05	97.97

Sample numbers follow the sample numbering system used by the ocean drilling program. S = spot; P = point.

Appendix 5
Recalculated Amphibole Analyses from Microprobe Traverses

Sample number:	35R-4 117-124 cm				44R-1 35-47 cm									58R-3 0-8 cm						
Spot:	2	2	2	2	1	1	1	1	2	2	3	3	3	1	1	1	1	1	2	2
Point:	3	4	5	6	3	4	5	6	1	2	3	4	5	2	3	4	5	6	2	3
SiO2	53.39	52.17	50.91	50.53	56.35	50.90	59.06	56.34	47.95	49.72	54.94	49.17	44.07	52.17	52.93	51.60	52.08	54.99	50.20	51.27
TiO2	0.78	0.44	0.73	0.29	0.19	0.03	0.00	0.05	1.81	1.18	0.34	0.50	0.32	1.03	0.38	0.59	0.17	0.10	0.17	0.15
Al2O3	2.58	4.15	4.79	5.81	2.24	4.28	0.08	0.59	6.14	4.82	1.49	5.70	7.62	5.03	3.12	4.41	4.49	2.76	5.21	4.31
FeO	10.82	11.70	11.81	11.09	3.73	13.35	2.67	9.38	14.54	16.33	12.53	18.52	15.61	8.44	11.16	12.79	13.88	9.40	17.56	17.55
Cr2O3	0.23	0.20	0.08	0.01	0.02	0.02	0.10	0.07	0.28	0.22	0.17	0.11	0.07	0.16	0.28	0.23	0.08	0.00	0.34	0.09
MnO	0.29	0.11	0.24	0.24	0.09	0.00	0.06	0.04	0.18	0.15	0.17	0.15	0.14	0.19	0.21	0.11	0.09	0.10	0.19	0.17
MgO	17.62	17.31	16.56	16.75	22.91	16.04	24.30	18.82	13.62	13.67	16.81	11.20	9.92	18.77	17.15	16.76	14.38	18.08	12.16	12.29
CaO	11.01	11.03	11.14	11.10	12.96	10.86	12.16	12.66	10.66	10.44	11.27	11.95	10.47	11.84	12.14	10.40	12.38	12.61	12.10	12.14
Na2O	1.16	1.37	1.52	1.90	0.83	0.66	0.23	0.22	2.05	1.68	0.81	1.42	1.42	1.55	0.87	1.67	0.63	0.43	0.96	0.87
K2O	0.13	0.06	0.14	0.08	0.00	0.03	0.04	0.02	0.27	0.19	0.07	0.01	0.04	0.16	0.08	0.04	0.06	0.00	0.05	0.02
Cl	0.05	0.15	0.16	0.19	0.00	0.01	0.00	0.02	0.00	0.05	0.05	0.01	0.03	0.00	0.04	0.06	0.00	0.00	0.00	0.02
Total	98.05	98.70	98.08	97.99	99.33	96.18	98.69	98.22	97.50	98.44	98.65	98.74	89.71	99.35	98.36	98.65	98.24	98.47	98.94	98.88
O = Cl	0.01	0.03	0.04	0.04	0.00	0.00	0.00	0.00	0.00	0.01	0.01	0.00	0.01	0.00	0.01	0.01	0.00	0.00	0.00	0.01
Total	98.00	98.55	97.92	97.80	99.33	96.16	98.69	98.20	97.50	98.39	98.60	98.74	89.68	99.35	98.32	98.59	98.24	98.47	98.94	98.86
Recalculation Method	13ECNK	13ECNK	13ECNK	13ECNK	15ENK	13ECNK	15EK	13ECNK	13ECNK	13ECNK	13ECNK	13ECNK	13ECNK	13ECNK	13ECNK	13ECNK	13ECNK	13ECNK	13ECNK	13ECNK
Si	7.48	7.27	7.20	7.14	7.66	7.27	7.97	7.87	6.97	7.13	7.70	7.21	7.05	7.20	7.46	7.20	7.47	7.67	7.28	7.43
Al	0.43	0.68	0.80	0.86	0.34	0.72	0.01	0.10	1.03	0.81	0.25	0.79	0.95	0.80	0.52	0.72	0.53	0.33	0.73	0.57
Fe3	0.09	0.04	0.00	0.00	0.00	0.01	0.02	0.03	0.00	0.05	0.06	0.00	0.00	0.00	0.02	0.08	0.00	0.00	0.00	0.00
Sum in T	8.00	8.00	8.00	8.00	8.00	8.00	8.00	8.00	8.00	8.00	8.00	8.00	8.00	8.00	8.00	8.00	8.00	8.00	8.00	8.00
Al	0.00	0.00	0.00	0.10	0.02	0.00	0.00	0.00	0.03	0.00	0.00	0.20	0.48	0.02	0.00	0.00	0.22	0.12	0.16	0.17
Cr	0.03	0.02	0.01	0.00	0.00	0.00	0.01	0.01	0.03	0.03	0.02	0.01	0.01	0.02	0.03	0.03	0.01	0.00	0.04	0.01
Fe3	0.68	0.94	0.82	0.80	0.07	1.21	0.08	0.26	0.62	0.87	0.60	0.31	0.35	0.60	0.51	1.09	0.28	0.30	0.45	0.33
Ti	0.08	0.05	0.08	0.03	0.02	0.00	0.00	0.01	0.20	0.13	0.04	0.06	0.04	0.11	0.04	0.06	0.02	0.01	0.02	0.02
Mg	3.68	3.60	3.49	3.53	4.64	3.41	4.89	3.92	2.95	2.92	3.51	2.45	2.36	3.86	3.60	3.49	3.07	3.76	2.63	2.66
Fe2	0.49	0.39	0.58	0.51	0.26	0.37	0.03	0.81	1.15	1.03	0.82	1.96	1.74	0.37	0.79	0.33	1.39	0.80	1.68	1.79
Mn	0.03	0.01	0.03	0.03	0.00	0.00	0.00	0.01	0.02	0.02	0.02	0.02	0.02	0.02	0.03	0.01	0.01	0.01	0.02	0.02
Ca	0.00	0.00	0.00	0.00	0.00	0.00	0.00	0.00	0.00	0.00	0.00	0.00	0.00	0.00	0.00	0.00	0.00	0.00	0.00	0.00
Sum in C	5.00	5.00	5.00	5.00	5.00	5.00	5.00	5.00	5.00	5.00	5.00	5.00	5.00	5.00	5.00	5.00	5.00	5.00	5.00	5.00
Fe2	0.00	0.00	0.00	0.00	0.10	0.00	0.18	0.00	0.00	0.00	0.00	0.00	0.00	0.00	0.00	0.00	0.00	0.00	0.00	0.00
Mn	0.00	0.00	0.00	0.00	0.01	0.00	0.01	0.00	0.00	0.00	0.00	0.00	0.00	0.00	0.00	0.00	0.00	0.00	0.00	0.00
Ca	1.65	1.65	1.69	1.68	1.89	1.66	1.76	1.90	1.66	1.61	1.69	1.88	1.80	1.75	1.83	1.56	1.90	1.89	1.88	1.89
Na	0.32	0.35	0.31	0.32	0.00	0.18	0.06	0.06	0.34	0.40	0.22	0.12	0.21	0.25	0.17	0.45	0.10	0.12	0.12	0.11
Sum in B	1.97	2.00	2.00	2.00	2.00	1.84	2.00	1.96	2.00	2.00	1.91	2.00	2.00	2.00	2.00	2.00	2.00	2.00	2.00	2.00
Ca	0.00	0.00	0.00	0.00	0.00	0.00	0.00	0.00	0.00	0.00	0.00	0.00	0.00	0.00	0.00	0.00	0.00	0.00	0.00	0.00
Na	0.00	0.02	0.11	0.20	0.22	0.00	0.00	0.00	0.24	0.07	0.00	0.28	0.24	0.17	0.07	0.01	0.08	0.00	0.15	0.13
K	0.02	0.01	0.03	0.02	0.00	0.01	0.01	0.00	0.05	0.04	0.01	0.00	0.01	0.03	0.01	0.01	0.01	0.00	0.01	0.00
Sum in A	0.02	0.03	0.13	0.22	0.22	0.01	0.01	0.00	0.29	0.11	0.01	0.28	0.24	0.20	0.09	0.01	0.09	0.00	0.16	0.14
Sum cations	14.99	15.03	15.13	15.22	15.22	14.85	15.01	14.96	15.29	15.11	14.93	15.28	15.24	15.20	15.09	15.01	15.09	15.00	15.16	15.14
Cl	0.01	0.04	0.04	0.05	0.00	0.00	0.00	0.00	0.00	0.01	0.01	0.00	0.01	0.00	0.01	0.01	0.00	0.00	0.00	0.01
Sum_oxy	23.00	23.00	23.00	23.00	23.00	23.00	23.00	23.00	23.00	23.00	23.00	23.00	23.00	23.00	23.00	23.00	23.00	23.00	23.00	23.00

Appendix 5 (continued)

Sample number:	58R-3 0-8 cm				60R-4 112-120 cm											
Spot:	2	2	2	2	1	1	1	1	2	2	3	3	3	5	5	5
Point:	4	5	6	7	2	3	4	5	4	5	3	4	5	3	4	5
SiO2	50.08	53.13	55.27	50.77	49.48	48.52	52.95	49.00	48.51	48.34	51.51	51.46	51.96	44.71	55.72	54.55
TiO2	0.05	0.17	0.26	0.16	1.19	1.48	0.36	0.23	1.65	1.52	0.61	0.85	0.44	0.09	0.18	0.07
Al2O3	5.77	3.81	1.52	4.15	6.52	5.92	2.64	6.60	6.33	6.10	3.64	3.72	3.43	4.52	2.18	2.71
FeO	16.96	9.69	11.31	15.07	9.70	13.54	12.37	15.77	13.08	13.53	12.81	12.98	16.16	10.33	6.71	10.63
Cr2O3	0.07	0.00	0.07	0.07	0.26	0.08	0.02	0.06	0.00	0.07	0.21	0.06	0.03	0.09	0.13	0.00
MnO	0.02	0.01	0.15	0.28	0.19	0.32	0.19	0.19	0.45	0.26	0.27	0.46	0.00	0.21	0.06	0.00
MgO	12.47	17.94	17.81	13.37	16.51	15.31	17.13	13.02	15.43	15.23	16.47	16.49	13.38	14.71	20.54	17.45
CaO	12.35	12.36	11.75	11.04	13.28	10.49	11.20	12.06	10.52	10.33	11.00	10.90	11.69	9.23	12.86	12.89
Na2O	1.00	1.00	0.60	0.67	1.83	2.10	1.02	1.26	2.12	2.09	1.36	1.40	0.66	0.46	0.60	0.35
K2O	0.03	0.00	0.00	0.02	0.24	0.18	0.07	0.06	0.16	0.23	0.25	0.12	0.01	0.07	0.01	0.00
Cl	0.00	0.01	0.00	0.00	0.05	0.01	0.08	0.03	0.00	0.00	0.08	0.01	0.00	0.04	0.03	0.02
Total	98.80	98.12	98.74	95.61	99.25	97.94	98.03	98.28	98.25	97.71	98.21	98.45	97.77	84.45	99.01	98.68
O = Cl	0.00	0.00	0.00	0.00	0.01	0.00	0.02	0.01	0.00	0.00	0.02	0.00	0.00	0.01	0.01	0.01
Total	98.80	98.11	98.74	95.61	99.20	97.94	97.95	98.24	98.25	97.71	98.12	98.43	97.77	84.41	98.98	98.65
Recalculation Method	13ECNK	13ECNK	13ECNK	13ECNK	13ENK	13ECNK	13ECNK	13ECNK	13ECNK	13ECNK	13ECNK	13ECNK	13ECNK	15ENK	13ECNK	13ECNK
Si	7.25	7.46	7.69	7.45	7.04	6.93	7.45	7.10	6.89	6.91	7.29	7.24	7.52	7.39	7.64	7.65
Al	0.75	0.54	0.25	0.55	0.96	1.00	0.44	0.90	1.06	1.03	0.61	0.62	0.48	0.62	0.35	0.35
Fe3	0.00	0.00	0.06	0.00	0.00	0.08	0.11	0.00	0.05	0.07	0.11	0.14	0.00	0.00	0.01	0.00
Sum in T	8.00	8.00	8.00	8.00	8.00	8.00	8.00	8.00	8.00	8.00	8.00	8.00	8.00	8.00	8.00	8.00
Al	0.24	0.09	0.00	0.17	0.14	0.00	0.00	0.22	0.00	0.00	0.00	0.00	0.10	0.27	0.00	0.10
Cr	0.01	0.00	0.01	0.01	0.03	0.01	0.00	0.01	0.00	0.01	0.02	0.01	0.00	0.01	0.01	0.00
Fe3	0.37	0.43	0.58	0.68	0.00	0.93	0.80	0.51	0.95	0.97	0.81	0.88	0.46	0.15	0.37	0.27
Ti	0.01	0.02	0.03	0.02	0.13	0.16	0.04	0.03	0.18	0.16	0.07	0.09	0.05	0.01	0.02	0.01
Mg	2.69	3.75	3.69	2.92	3.50	3.26	3.59	2.81	3.27	3.25	3.47	3.46	2.89	3.62	4.20	3.65
Fe2	1.68	0.71	0.67	1.17	1.16	0.61	0.54	1.40	0.56	0.58	0.60	0.51	1.50	0.94	0.40	0.98
Mn	0.00	0.00	0.02	0.04	0.02	0.04	0.02	0.02	0.05	0.03	0.03	0.05	0.00	0.00	0.01	0.00
Ca	0.00	0.00	0.00	0.00	0.03	0.00	0.00	0.00	0.00	0.00	0.00	0.00	0.00	0.00	0.00	0.00
Sum in C	5.00	5.00	5.00	5.00	5.00	5.00	5.00	5.00	5.00	5.00	5.00	5.00	5.00	5.00	5.00	5.00
Fe2	0.00	0.00	0.00	0.00	0.00	0.00	0.00	0.00	0.00	0.00	0.00	0.00	0.00	0.34	0.00	0.00
Mn	0.00	0.00	0.00	0.00	0.00	0.00	0.00	0.00	0.00	0.00	0.00	0.00	0.00	0.03	0.00	0.00
Ca	1.92	1.86	1.75	1.74	2.00	1.60	1.69	1.87	1.60	1.58	1.67	1.64	1.81	1.63	1.89	1.94
Na	0.08	0.14	0.16	0.19	0.00	0.40	0.28	0.13	0.40	0.42	0.33	0.36	0.19	0.00	0.11	0.06
Sum in B	2.00	2.00	1.91	1.93	2.00	2.00	1.97	2.00	2.00	2.00	2.00	2.00	2.00	2.00	2.00	2.00
Ca	0.00	0.00	0.00	0.00	0.00	0.00	0.00	0.00	0.00	0.00	0.00	0.00	0.00	0.00	0.00	0.00
Na	0.20	0.13	0.00	0.00	0.51	0.18	0.00	0.23	0.18	0.16	0.04	0.03	0.00	0.15	0.05	0.03
K	0.01	0.00	0.00	0.01	0.04	0.03	0.01	0.01	0.03	0.04	0.05	0.02	0.00	0.02	0.00	0.00
Sum in A	0.20	0.13	0.00	0.01	0.55	0.22	0.01	0.24	0.21	0.20	0.09	0.05	0.00	0.16	0.05	0.03
Sum cations	15.20	15.13	14.91	14.93	15.55	15.22	14.98	15.24	15.21	15.20	15.09	15.05	15.00	15.16	15.05	15.03
Cl	0.00	0.00	0.00	0.00	0.01	0.00	0.02	0.01	0.00	0.00	0.02	0.00	0.00	0.01	0.01	0.01
Sum_oxy	23.00	23.00	23.00	23.00	23.00	23.00	23.00	23.00	23.00	23.00	23.00	23.00	23.00	23.00	23.00	23.00

References

Alt, J.C. and Emmermann, R. 1985. Geochmistry of hydrothermally altered basalts: Deep Sea Drilling Project Hole 504B, Leg 83. In Anderson, R.N., Honnorez, J., Becker, K., et al., Initial Reports DSDP, 83: Washington (U.S. Govt. Printing Office), p. 249-262.

Anderson, G.M. & Burnham, C.W., 1983. Feldspar solubility and the transport of aluminum under metamorphic conditions. Am. J. of Sci., 283-A, p. 283-297.

Appleyard, E.C., 1980. Mass balance computations in metasomatism: metagabbro / nepheline syenite pegmatite interaction in northern Norway. Contrib. Mineral. Petrol., 73, p. 131-144.

Bai, W.-J., Zhou, M.-F., and Robinson, P.T., 1993. Possibly diamond-bearing mantle peridotites and podiform chromites in the Luobusa and Donqiao ophiolites, Tibet. Can. J. Earth Sci., 30, p. 1650-1659.

Baumgartner, L.P. & Eugster, H.P., 1988. Experimental determination of corundum solubility and Al-speciation in supercritical H_2O-HCl solutions. Geological Soc. of Am. Abst. Prog., 20, p. A191.

Bird, D.K., Rogers, R.D., and Manning, C.E., 1988. Hydrothermal alteration of Tertiary layered gabros. Am. J. Sci., 288, p. 405-457.

Bednarz, U. and Schmincke, H.-U., 1989. Mass transfer during sub-seafloor alteration of the upper Troodos crust (Cyprus). Contrib. Mineral. Petrol., 102, p. 93-101.

Cannat, M., 1991. Plastic deformation at an oceanic spreading ridge: a microstructural study of Site 735 gabbros (southwest Indian Ocean). In Von Herzen, R.P, Robinson, P.T., et al., Proc. ODP, Sci. Results, 118: College Station, TX (Ocean Drilling Program), p. 399-408.

Cannat, M., Mével, C., and Stakes, D., 1991. Normal ductile shear zones at an oceanic spreading ridge: tectonic evolution of Site 735 gabbros (southwest Indian Ocean). In Von Herzen, R.P, Robinson, P.T., et al., Proc. ODP, Sci. Results, 118: College Station, TX (Ocean Drilling Program), p. 415-430.

Cronan, D.S., 1992. Marine minerals in exclusive economic zones. New York: Chapman & Hall, 209 p.

Deer, W.A., Howie, R.A., and Zussman, J., 1992. An introduction to the rock-forming minerals. New York: John Wiley & Sons, 696p.

Delaney, J.R., McDuff, R.E., and Lupton, J.E., 1984., Hydrothermal fluid temperatures of 400°C on the Endeavour Segment, northern Juan de Fuca. Eos Trans., AGU, 65, p. 973.

Detrick, R.S., Buhl, P., Vera, E., Mutter, J., Orcutt, J., Madsen, J., and Brocher, T., 1987. Multichannel seismic imaging of a crustal magma chamber along the East Pacific Rise. Nature, 326, p. 35-41.

Detrick, R.S. and Purdy. G.M., 1980. The crustal structure of the Kane Fracture Zone from seismic refraction studies. J. Geophys. Res., 85, p. 3759-3777.

Dick, H.B.J., Meyer, P.S., Bloomer, S., Kirby, S., Stakes, D., and Mawer, C., 1991a. Lithostratigraphic evolution of an *in-situ* section of oceanic layer 3. In Von Herzen, R.P, Robinson, P.T., et al., Proc. ODP, Sci. Results, 118: College Station, TX (Ocean Drilling Program), p. 439-538.

Dick, H.B.J., Schouten, H., Meyer, P.S., Gallo, D.G., Berg, H., Tyce, R., Patriat, P., Johnson, K.T.M., Snow, J., and Fisher, A., 1991b. Tectonic evolution of the Atlantis II Fracture Zone. In Von Herzen, R.P, Robinson, P.T., et al., Proc. ODP, Sci. Results, 118: College Station, TX (Ocean Drilling Program), p. 359-398.

Dick, H.B.J., Robinson, P.T., and Meyer, P.S., 1992. The plutonic foundation of a slow-spreading ridge. AGU, Geophys. Monograph 70, p. 1-39.

Dipple, G.M., Wintsch, R.P., and Andrews, M.S., 1990. Identification of tthe scales of differential element mobility in a ductile fault zone. J. Metamorphic Geol., 8, p 645-661.

Fox, P.J. and Stroup, J.B., 1981. The plutonic foundation of the oceanic crust. In Emiliani, C., ed., The Sea, 7, New York: Wiley, p. 119-218.

Fox, P.J., Detrick, R.S., and Purdy, G.M., 1980. Evidence for crustal thinning near fracture zones: Implications for ophiolites. In A. Panayiotou (ed.), Ophiolites: Proc. Int. Ophiolite Symp. Cyprus 1979: Cyprus (Geological Survey Dept.), 161-168.

Gillis, K.M., 1986. Multistage alteration of the extrusive sequence, Troodos ophiolite, Cyprus. Ph.D. dissertation, Dalhousie University, 384 p.

Gillis, K.M. and Robinson, P.T., 1988. Distribution of alteration zones in the upper oceanic crust. Geology, 16, p. 262-266.

_____, 1985. Low-temperature alteration of the extusive sequence, Troodos ophiolite. Cyprus, Can. Mineral., 23, p. 431-441.

Gillis, K.M., Thompson, G., and Kelley, D.S., 1993. A view of the lower crustal component of hydrothermal systems at the Mid-Atlantic ridge. J. Geophys. Res., 98, p. 19,597-19,619.

Gorvindaraju, K., 1989. Compilation of working values and sample description for 272 geostandards. Geostandards Newsletter, 23, 113 p.

Greenough, J.D., Fryer, B.J., and Robinson, P.T., 1990. Geochemical effects of alteration on mafic rocks from Indian Ocean Site 706. In Duncan, R.A., Backman, J., Peterson, L.C., et al., Proc. ODP, Sci. Results, 115: College Station, TX (Ocean Drilling Program), p. 85-92.

Gresens, R.L., 1967. Composition-volume relationships of metasomatism. Chem. Geol., 2, p. 47-65.

Hébert, R., Constantin, M., and Robinson, P.T., 1991. Primary mineralogy of Leg 118 gabbroic rocks and their place in the spectrum of oceanic mafic igneous rocks. In Von Herzen, R.P, Robinson, P.T., et al., Proc. ODP, Sci. Results, 118: College Station, TX (Ocean Drilling Program), p. 3-20.

Humphris, S.E. and Thompson, G., 1978. Hydrothermal alteration of oceanic basalts by seawater. Geochim. Cosmochim. Acta, 42, p. 107-125.

Ito, E. and Anderson, A.T., Jr., 1983. Submarine metamorphism of gabbros from the Mid-Cayman Rise: Petrographic and mineralogic constraints on hydrothermal processes at slow-spreading ridges. Contrib. Min. Petrol., 82, p. 371-388.

Kelley, D.S., and Delaney, J.R., 1987. Two phase separation and fracturing in mid-ocean ridge gabbros at temperatures greater than 700°C. Earth Planet. Sci. Lett., 83, p. 53-66.

Kelley, D.S., Gillis, K.M., and Thompson, G., 1993. Fluid evolution in submarine magma-hydrothermal systems at the Mid-Atlantic ridge. J. Geophys. Res., 98, p. 19,579-19,596.

Kelley, D.S., Hoering, T., and Frantz, J.D., 1994. Methane-rich fluids in gabbroic rocks from the Southwest Indian Ridge: results from mass spectrometric analyses. EOS Trans. AGU, 75, p. 657.

Kelley, D.S., 1996. Methane-rich fluids in the oceanic crust. J. Geophys. Res., 101, p. 2943-2962.

Kristmannsdottir, H., 1979. Alteration of basaltic rocks by hydrothermal activity at 100-300°C. Proc. 6th Int. Clay Conf., p. 359-367.

Madge, L.S., Dick, H.J.B., and Hart, S.R., 1995. Tectonics, alteration and the fractal distribution of hydrothermal veins in the lower ocean crust. Earth and Planetary Science Letters, 129, p. 103-119.

Mével, C., 1988. Metamorphism in oceanic layer 3, Gorridge Bank, Eastern Atlantic. Contrib. Mineral. Petrol., 100, p. 496-509.

_____, 1987. Evolution of oceanic gabbros from DSDP Leg 82: influence of the fluid phase on metamorphic crystallizations. Earth Planet. Sci. Lett., 83, p. 67-79.

Miyashiro, A., 1973. The Troodos ophiolite complex was probably formed in an island arc. Earth Planet. Sci. Letters. 19, p. 218-224.

Mottl, M.J., Holland, H.D., and Corr, R.F., 1979. Chemical exchange during hydrothermal alteration of basalt by seawater - II. Experimental results for Fe, Mn, and sulfur species. Geochim.Cosmochim. Acta, 43, p. 869-884.

Mottl, M.J. and Holland, H.D., 1978. Chemical exchange during hydrothermal alteration of basalt by seawater - I. Experimental results from major and minor components of seawater. Geochim.Cosmochim. Acta, 42, p. 1103-1115.

Muehlenbachs, K., 1986. In Valley, J.W., et al., eds., Stable Isotopes in high temperature geological processes. Rev. in Min., v. 16, Min. Soc. Amer., p. 425-443.

Natland, J.H., Meyer, P.S., Dick, H.J.B., and Bloomer, S.H., 1991. Magmatic oxides and sulfides in gabbroic rocks from Hole 735B and the later development of the liquid line of descent. In Von Herzen, R.P, Robinson, P.T., et al., Proc. ODP, Sci. Results, 118: College Station, TX (Ocean Drilling Program), p. 75-112.

Robinson, P., Spear, F.S., Schumacher, J.C., Laird, J., Klein, C., Evans, B.W., and Doolan, B.L., 1982. Phase relations of metamorphic amphiboles: natural occurrence and theory. In Veblen, D.R. and Ribbe, P.H. (eds.), Amphiboles:

Petrology and Experimental Phase Relations. Rev. Mineral., 9B: Washington (Mineral. Soc. Am.), p. 1-227.

Robinson, P.T., Dick, H.J.B., and Von Herzen, R., 1991. Metamorphism and alteration in oceanic layer 3: Hole 735B. In Von Herzen, R.P, Robinson, P.T., et al., Proc. ODP, Sci. Results, 118: College Station, TX (Ocean Drilling Program), p. 541-552.

Robinson, P.T., Melson, W.G., O'Hearn, T., and Schmincke, H.-U., 1983. Volcanic glass compositions of the Troodos ophiolite, Cyprus. Geology, 11, p. 400-404.

_____, 1984. Fluid Inclusions, Rev. in Min., v. 12, Min. Soc. Amer., 644 p.

Rona, P.A., Klinkhammer, G., Nelson,T.A., Trefrey, J.H., and Elderfield, H., 1986. Black smokers, massive sulfides and vent biota at the Mid-Atlantic Ridge. Nature, 321, p. 33-57.

Scott, S.D., 1992. Polymetallic sulfide riches from the deep: Fact or fallacy? In Use and misuse of the seafloor. K.J. Hsü and J. Thiede eds., John Wiley & Sons Ltd., p. 87-115.

_____, 1987. Seafloor Polymetallic sulfides: scientific curiosities or mines of the future? In P.G. Telki, M.R. Dobson, J.R. Moore, and U. von Stackelberg, eds., Marine Minerals, Dordrecht: D. Riedel, p. 277-300.

Shipboard Scientific Party, 1989. Site 735. In Robinson, P.T., Von Herzen R.P., et al., Proc. ODP, Init. Repts., 118: College Station, TX (Ocean Drilling Program), p. 89-222.

Stakes, D., Mével, C., Cannat, M., and Chaput, T., 1991. Metamorphic stratigraphy of Hole 735B. In Von Herzen, R.P, Robinson, P.T., et al., Proc. ODP, Sci. Results, 118: College Station, TX (Ocean Drilling Program), p. 153-179.

Stakes, D.S. and O'Neil, J.R., 1982. Mineralogy and stable isotope geochemistry of hydrothermally altered oceanic rocks. Earth Sci. Planet. Lett., 57, p. 285-304.

Thompson, G., 1983. Basalt-seawater interaction. In Rona, P.A., Bostrom, K., Laubieer, L. and Smith, K.L., (eds.), Hydrothermal processes at seafloor spreading centers. Plenum Press, New York, 255-278.

Vanko, D.A., 1988. Temperature, pressure, and composition of hydrothermal fluids, with their bearing on the magnitude of tectonic uplift at mid-ocean ridges, inferred from fluid inclusions in oceanic layer 3 rocks. J. Geophys. Res., 93, p. 4595-4611.

_____, 1986. High-chlorine amphiboles from oceanic rocks: Product of highly saline hydrothermal fluids? Am. Mineral., 71, p. 51-59.

Vanko, D.A. and Stakes, D.S., 1991. Fluids in oceanic layer 3: evidence from veined rocks. Hole 735B, Southwest Indian Ridge, In Von Herzen, R.P, Robinson, P.T. et al., Proc. ODP, Sci. Results, 118: College Station, TX (Ocean Drilling Program), p. 181-215.

Von Damm, K. L., Edmond, J.M., Grant, B., Measures, C.I., Walden, B., and Weiss, R.F., 1985. Chemistry of submarine hydrothermal solutions at 21^{0}N, East Pacific Rise. Geochim. Cosmochim. Acta, 49, p. 2221-2237.

Von Damm, K.L., 1988. Systematics and postulated controls on submarine hydrothermal solution chemistry. J. Geophys. Res., 93, p. 4551-4561.